SPACECRAFT ATTITUDE RESOURCE SHARING

By

SHAWN C. JOHNSON

A DISSERTATION PRESENTED TO THE GRADUATE SCHOOL
OF THE UNIVERSITY OF FLORIDA IN PARTIAL FULFILLMENT
OF THE REQUIREMENTS FOR THE DEGREE OF
DOCTOR OF PHILOSOPHY

UNIVERSITY OF FLORIDA

2013

In loving memory of my mother, Carole Cushman Johnson

ACKNOWLEDGMENTS

I met my advisor and committee chair, Dr. Norman G. Fitz-Coy, first as the professor of my undergraduate Astrodynamics course. At that time, he impressed upon me the importance of fundamentals and the perils of taking shortcuts. Throughout my doctoral studies I have not only learned from his experience, but also from his superb integrity and character. These are traits that I will aim to share with those that I mentor and I am very thankful for his tireless support. I also would like to thank, Drs. Prabir Barooah, Warren Dixon, Seth Lacy, and Janise McNair, for supporting and fostering my research ideas and serving as members on my supervisory committee. I am particularly grateful to Dr. Seth Lacy for providing the catalyst to this research, as my mentor at the Air Force Research Laboratory, and the plethora of discussions along the way.

In addition, there are many individuals that have given me strength throughout this endeavor. I would like to thank the past and present members of the Space Systems Group for their camaraderie, as well as many engaging research discussions over the years. Of this group, I am particularly thankful to Dr. Josue Muñoz for providing me motivation since our first year in college. I am also thankful to my friends and family for their love and encouragement. Particularly, I am indebted to my parents for helping me navigate life's many choices, providing guidance when asked upon, but never attempting to control my path – the GNC of life. To my Papa; the original Gator in our family; thank you for instilling in me a passion and enthusiasm for learning. To my grandmother, thank you for being an example of positivity, patience, and love; and for putting that Tangram set in my hands when I was three. I am grateful to my siblings for teaching me more than I could ever learn in a classroom, I will always look up to you. Finally, I would like to thank my wife for her enduring love and support. Everyday I am humbled by her caring nature and ability to bring out the best in others.

TABLE OF CONTENTS

page

ACKNOWLEDGMENTS 4

LIST OF TABLES 9

LIST OF FIGURES 10

ABSTRACT 13

CHAPTER

1 INTRODUCTION 15

1.1 Resource Sharing 18
1.2 Relevant Missions 22
1.2.1 Rendezvous and Docking Missions 22
1.2.2 Space-based Interferometry 24
1.2.3 Satellite Networks 25
1.2.4 System F6 25
1.3 Problem Statements 26
1.3.1 Problem 1: Inertial Attitude Estimation in a Disaggregated System 28
1.3.2 Problem 2: Attitude Data Fusion 29
1.3.3 Problem 3: Sensor Tasking 30
1.4 Thesis Statements 31
1.4.1 Thesis 1: On Inertial Attitude Estimation for Disaggregated Systems 31
1.4.2 Thesis 2: On Minimal Attitude Parameterization Data Fusion 31
1.4.3 Thesis 3: On Sensor Tasking for Attitude Resource Distribution . . 31
1.5 Dissertation Organization 32

2 SYSTEM DYNAMICS AND CONTROL 34

2.1 General Nomenclature 34
2.2 Rigid Body Kinematics 34
2.3 Coordinate Frames 35
2.3.1 Earth-Centered Inertial (ECI) 36
2.3.2 Earth-Centered Earth-Fixed (ECF) 36
2.3.3 Hill (LVLH) 36
2.3.4 Perifocal (PQW) 36
2.3.5 Body Frame (B) 37
2.4 Attitude Parameterizations and Kinematics 37
2.4.1 Attitude Matrix 39
2.4.2 Euler Angles 42
2.4.3 Axis-Angle 43
2.4.4 Euler Symmetric Parameters (Unit Quaternions) 45
2.4.5 Classic Rodrigues Parameters (CRPs) 46

2.4.6 Modified Rodrigues Parameters (MRPs) . . . 46
2.4.7 Stereographic Orientation Projections (SOPs) . . . 47
2.4.8 Generalized Cayley Transformation . . . 49
2.4.9 Vectorial Attitude Parameterizations . . . 50
2.5 Summary of Attitude Parameterizations . . . 53
2.6 Attitude Dynamics . . . 55
2.7 Attitude Tracking Control . . . 56
2.7.1 Desired Coordinate Frames . . . 56
2.7.1.1 Relative spacecraft sharing frame (SH) . . . 57
2.7.1.2 Ground target frame (T) . . . 57
2.7.2 Desired Quaternion Kinematics . . . 59
2.7.2.1 Relative spacecraft sharing frame kinematics . . . 59
2.7.2.2 Ground target frame kinematics . . . 60
2.7.3 Clohessy-Wiltshire-Hill (CWH) Equations . . . 61
2.7.4 Attitude Tracking Controller Derivation . . . 63
2.8 Summary . . . 65

3 DISAGGREGATED ATTITUDE ESTIMATION . . . 67

3.1 General Nomenclature . . . 67
3.2 Inertial Attitude Sensors . . . 68
3.2.1 Sun Sensors . . . 69
3.2.2 Magnetometers . . . 69
3.2.3 Star Trackers . . . 71
3.2.4 Rate Gyroscope . . . 73
3.3 Deterministic Attitude Determination . . . 74
3.3.1 q-algorithm . . . 76
3.3.2 Other Attitude Determination Algorithms . . . 78
3.4 Kalman Filter Review . . . 79
3.5 Extended Kalman Filter . . . 84
3.6 Extended Kalman Filter for Inertial Attitude Estimation . . . 85
3.6.1 Sensitivity Matrix Derivation . . . 86
3.6.2 Discrete Propagation Derivation . . . 88
3.6.3 Example Inertial Attitude EKF with a Magnetometer and Sun Sensors for Low Precision Pointing . . . 89
3.6.4 Example Inertial Attitude EKF with a Star Tracker for High Precision Pointing . . . 91
3.7 Relative Attitude Sensors . . . 94
3.8 Deterministic Relative Attitude Determination . . . 97
3.9 Inertial Attitude Estimation in a Disaggregated System . . . 98
3.9.1 Sensitivity Matrix Derivation . . . 98
3.9.2 Discrete Propagation Derivation . . . 101
3.9.3 Notes on Disaggregated Attitude Estimation . . . 104
3.10 Summary . . . 104

4 ATTITUDE DATA FUSION 105

4.1 Data Fusion Overview 105
4.2 Data Fusion Review 106
4.3 Data Fusion and the Error State 108
4.3.1 Euclidean Fusion Error State 108
4.3.2 Attitude Fusion Error State 110
4.4 Unknown Cross-Correlation Data Fusion Algorithms 112
4.4.1 Covariance Intersection 113
4.4.2 Ellipsoid Intersection 115
4.4.3 Summary of Data Fusion Laws for Attitude States 117
4.5 Review of the Unit Quaternion for Data Fusion 118
4.6 Vectorial Attitude Parameterization 119
4.7 Parameterized Attitude Error Vector 120
4.7.1 First-Order Model of Attitude Error Vector 121
4.7.2 Data Fusion Jacobian 122
4.7.3 Attitude Error Vector Approximation Accuracy 123
4.7.4 Unit Quaternion Transformation 128
4.8 Minimal Attitude Parameterization Data Fusion 128
4.8.1 Shadow Switching Data Fusion Process 129
4.8.2 Example: FRP Covariance Intersection with Shadow Switching . . 131
4.9 Vectorial Attitude Data Fusion with the Local Error Approach 131
4.10 Comments on Attitude Data Fusion 134
4.10.1 A Note on MRP Singularities and Shadow Switching 135
4.10.2 A Note on the Minimization Criterion for the CI Attitude Fusion Law 136
4.10.3 A Note on Covariance Intersection and Ellipsoidal Intersection . . . 137
4.10.4 A Note on Attitude Data Fusion with Appended State Vectors . . . 138
4.11 Two Star Tracker Data Fusion Example 138
4.12 Summary 141

5 STOCHASTIC GREEDY SENSOR TASKING 143

5.1 Sensor Tasking Overview 143
5.2 Tasking Problem Statement 145
5.3 Tasking Solution Methodology 146
5.4 Resource Sharing Assumption on Dynamics Time Constants 147
5.5 Tasking 148
5.5.1 Baseline Tasking 148
5.5.2 Greedy Tasking 149
5.6 Performance Metrics 151
5.6.1 Trace 152
5.6.2 Matrix Norms 152
5.6.3 Differential Entropy 154
5.7 Simulations 155
5.7.1 Perfect Relative Attitude Sensor Assumption 156
5.7.2 Simulation Initialization 156

5.7.3 Single-run Results . . . 158
5.7.4 Monte Carlo Analysis . . . 162
5.7.5 A Note on the Trace Performance Metric . . . 165
5.8 Summary . . . 165

6 SPACECRAFT ATTITUDE RESOURCE SHARING SIMULATIONS . . . 167

6.1 Simulation Initializations . . . 167
6.2 Two Spacecraft Attitude Resource Sharing . . . 168
6.2.1 Two Spacecraft with Star Trackers Scenario . . . 169
6.2.2 Two Spacecraft with Coarse Deputy Sensors Scenario . . . 170
6.3 Three Spacecraft Attitude Resource Sharing . . . 172
6.3.1 Three Spacecraft with Star Trackers Scenario . . . 174
6.3.2 Three Spacecraft with Coarse Deputy-1 Sensors Scenario . . . 175
6.4 Tasking Algorithm Comparison for Attitude Estimate Resource Sharing with Data Fusion . . . 178
6.5 Observations on Spacecraft Attitude Estimate Resource Sharing . . . 181
6.6 Summary . . . 184

7 Conclusions . . . 185

7.1 Revisiting the Research Questions and Thesis Statements . . . 185
7.2 Future Work . . . 186

REFERENCES . . . 188

BIOGRAPHICAL SKETCH . . . 199

LIST OF TABLES

Table page

1-1 Resource sharing technologies for the spacecraft subsystems 21

2-1 Several generating functions and the vectorial parameterization of $SO(3)$ . . . 52

2-2 Inverse kinematics Jacobian for several vectorial attitude parameterizations . . 54

2-3 Properties comparison of several attitude parameterizations 54

3-1 Assumptions for application of the Kalman filter 80

3-2 Discrete Kalman filter 84

3-3 List of modifications to the Kalman filter for the extended Kalman filter 85

3-4 Inertial attitude extended Kalman filter 90

3-5 State initializations for coarse sensor inertial attitude simulations 90

3-6 Time parameters for coarse sensor inertial attitude simulations 90

3-7 State estimate initializations and sensor characteristics for coarse sensor inertial attitude simulations 91

3-8 State initializations for fine precision inertial attitude simulations 93

3-9 State estimate initializations for fine precision inertial attitude simulations . . . 93

3-10 Extended Kalman filter for inertial attitude estimation in a disaggregated system 103

4-1 Resource sharing data fusion and system architecture taxonomy 106

4-2 Transformations for vectorial attitude parameterizations and the unit quaternion 128

5-1 State initializations for tasking simulations 157

5-2 Control and time parameters for tasking simulations 157

5-3 Sensor characteristics for tasking simulations 158

5-4 State estimate initializations for tasking simulations 158

5-5 Aggregated Tasking Performance Comparison (Relative Sensor 10° FOV) RMS Error (arcsec) 161

5-6 Tasking performance comparison (relative sensor with 60° FOV) RMS error (arcsec) 162

6-1 Sensor characteristics used in attitude estimate resource sharing simulations . 168

LIST OF FIGURES

Figure page

1-1 Fractionated elements technology readiness level 19

1-2 Potential benefit of the reduction in mass of a small satellite 20

1-3 Illustration of the Orbital Express rendezvous and docking mission 24

1-4 Resource sharing in communications networks 25

1-5 Illustration of System F6 cluster-level fault tolerance 26

1-6 Fundamental functions for the attitude resource sharing process 28

1-7 Attitude resource-sharing architecture 29

2-1 Common coordinate frames 37

2-2 Relative attitude compositions 40

2-3 Stereographic projections 48

2-4 Common stereographic projections 49

2-5 Tracking coordinate frames 58

3-1 Description of a typical star tracker 71

3-2 Description of the geometry of focal-plane measurements using a virtual CCD 74

3-3 Magnetic field and sun vector collinearity for an example inertial attitude EKF with a magnetometer and sun sensors 91

3-4 True body angular velocity for an example inertial attitude EKF with a magnetometer and sun sensors 92

3-5 Quaternion error for an example inertial attitude EKF with a magnetometer and sun sensors 92

3-6 Available star vectors for an example inertial attitude EKF with a star tracker . . 93

3-7 Quaternion error for an example inertial attitude EKF with a star tracker 94

3-8 Notional depiction of a VISNAV measurement 95

3-9 Description of the VISNAV sensor geometry 96

4-1 Star graph representation for attitude resource sharing 106

4-2 Notional covariance intersection uncertainty ellipse comparison 113

4-3 Notional ellipsoidal intersection uncertainty ellipse comparison 115
4-4 Linearity of several orders of the higher-order Rodrigues parameters 124
4-5 Attitude error vector approximation accuracy for the MRPs and FRPs 126
4-6 Attitude error vector approximation accuracy for the MRPs and FRPs using the local error representation 133
4-7 Attitude error vector approximation accuracy with the CRPs using the local error representation 134
4-8 Justification for data fusion at the quaternion unit sphere using the shadow parameterizations 136
4-9 Example two star tracker data fusion using the FRPs and shadow parameters . 139
4-10 Pointing error comparison of two star trackers with and without data fusion . . . 140
4-11 Comparison of star tracker data fusion with MRP shadow parameter and local error representation 140
5-1 Stochastic tasking greedy control problem 146
5-2 Resource sharing process 147
5-3 Relative position in the Hill frame 159
5-4 RMS error tasking performance comparison (relative sensor 10° FOV) 160
5-5 RMS error tasking performance comparison (relative sensor 60° FOV) 163
5-6 Monte Carlo attitude error trajectories for a 10° FOV relative attitude sensor using the trace metric 164
5-7 Monte Carlo sample data comparison of the RMS error 165
6-1 Angular velocity resulting from torque-free motion for the deputies in all simulated scenarios 169
6-2 Local and fused quaternion error for the two spacecraft star tracker scenario . 170
6-3 Chief attitude control for the two spacecraft star tracker scenario 171
6-4 Covariance intersection weights for the two spacecraft star tracker scenario . . 171
6-5 Two spacecraft local and fused quaternion error with coarse deputy attitude sensing 172
6-6 Chief attitude control for the two spacecraft coarse deputy attitude sensing scenario 173

6-7 Covariance intersection weights for the two spacecraft coarse deputy attitude sensing scenario . . . 173
6-8 Effects observed at the onset of data fusion with precise and coarse sensors . 174
6-9 Local and fused quaternion error for the three spacecraft star tracker scenario 176
6-10 Chief attitude control for the three spacecraft star tracker scenario . . . 177
6-11 Covariance intersection weights for the three spacecraft star tracker scenario . 177
6-12 Local and fused quaternion error for the three spacecraft scenario with coarse Deputy-1 sensing . . . 178
6-13 Chief attitude control for the three spacecraft scenario with coarse Deputy-1 sensing . . . 179
6-14 Covariance intersection weights for the three spacecraft scenario with coarse Deputy-1 sensing . . . 179
6-15 Affect of tasking algorithm choice on the error bounds of a three spacecraft scenario with fine precision sensing . . . 181
6-16 Affect of tasking algorithm choice on the error bounds of a three spacecraft scenario with coarse Deputy-2 attitude sensing . . . 182
6-17 Effect of tasking on the Chief boresight attitude accuracy . . . 183
6-18 Chief attitude control for the three spacecraft scenario with coarse Deputy-1 sensing using Round-robin tasking . . . 183

Abstract of Dissertation Presented to the Graduate School
of the University of Florida in Partial Fulfillment of the
Requirements for the Degree of Doctor of Philosophy

SPACECRAFT ATTITUDE RESOURCE SHARING

By

Shawn C. Johnson

August 2013

Chair: Norman G. Fitz-Coy
Major: Aerospace Engineering

Disaggregated spacecraft systems distribute the functionality of traditional monolithic spacecraft across several platforms. This dissertation addresses some of the technical challenges associated with a disaggregated attitude determination system (ADS), where the disaggregated ADS is defined by a chief spacecraft, with relative and inertial attitude sensors, and multiple deputy spacecraft, with only inertial attitude sensors or no sensors at all.

A tracking controller and reference signal kinematics are developed for the chief to track the deputies and measure their relative attitude states. These measurements are used in the formulation of a disaggregated implementation of the extended Kalman filter (EKF) for inertial attitude estimation. The disaggregated EKF produces multiple inertial attitude state estimates of the chief and deputies. Euclidean state and attitude state data fusion are reviewed and used to develop a generalized attitude data fusion law based on the attitude error vector. To avoid numerical complexities associated with constrained attitude parameterizations, minimal vectorial attitude parameterizations are investigated for data fusion. The accuracy of the vectorial parameterizations is assessed, and it is shown that the classical Rodrigues parameters are a sufficient parameterization for minimal attitude data fusion, but that higher-order Rodrigues parameters can be used to improve the accuracy. The minimal parameterizations are applied to data fusion laws

using the shadow parameters of the vectorial parameterizations, as well as a local error representation.

A greedy tasking algorithm is also developed. This algorithm makes use of the current covariance information of the deputies to task the chief to track deputies and measure their relative states. Characterizations of the size of the state-error covariance matrix are investigated in simulation based on the trace, matrix norms, and differential entropy. Simulation results show that for measurement sharing, greedy tasking can improve upon the accuracy of the chief and deputies using a fixed tasking strategy. Furthermore, Monte Carlo results show that the greedy tasking algorithm is mostly insensitive to the covariance metric.

This manuscript concludes with numerical simulations of two attitude resource sharing scenarios: (i) between a chief and a single deputy and (ii) between a chief and two deputies. These simulations demonstrate that attitude resource sharing can be used to increase the attitude knowledge of a deputy equipped with low performance attitude sensors and also improve the accuracy of the attitude knowledge of all spacecraft (including the chief) when all spacecraft are equipped with similar sensors.

CHAPTER 1
INTRODUCTION

Spacecraft design is primarily driven by the time, cost, and risk to launch mass to orbit and the cost of developing sophisticated spacecraft and payloads that must survive and operate within the harsh orbital environment. In 2002, this cost averaged between $5000/lb to $10000/lb for launch to low Earth orbit (LEO) [1]. Due to these factors, spacecraft can cost upwards of several billions of dollars and take years to develop. As a result, traditional monolithic spacecraft are designed to be risk averse. For the purpose of this discussion, risk is defined as the product of the probability of a failure occurring and the loss in value if a failure occurs. Since the cost of monolithic spacecraft is implicitly high, they are conservatively designed in order to minimize the probability of failure. Reducing the probability of failure is accomplished by incorporating redundancies and over-engineering at the system and subsystem level. Additionally, the cost and time necessary to develop traditional spacecraft can be prohibitive for responsive missions, where to objective is to respond to a changing mission demand as fast as possible. However, recent research and development of small spacecraft technology and disaggregated space architectures are addressing the challenges of timely and cost-effective mission development. These smaller spacecraft cannot replace all of the capability of monolithic spacecraft, but they do have the potential to complement their larger counterparts and provide new capability.

Small spacecraft definitions vary based on size, weight, and power (SWaP) as well as cost [2]. In the context of this paper, small spacecraft are classified based on mass. Mass is a good surrogate description because it inherently drives the spacecraft form factor, available power, and cost. Small spacecraft typically vary from mini-satellites ($<$ 500 kg) down to pico-satellites ($<$ 1 kg). However, recent research is further pushing mass boundaries into the femto-satellite regime ($<$ 100 g) sometimes referred to as a “satellite-on-a-chip” [3], as well as all the way down to spacecraft with dimensions as

fine as interplanetary dust and mass on the order of milligrams [4]. All classes of small spacecraft are being investigated for their potential for shorter development times and improved capability over traditional spacecraft for certain mission types – commonly, distributed sensing.

Complementing small spacecraft technology is the advent of disaggregated spacecraft architectures. These architectures make use of several smaller spacecraft to produce a capability traditionally provided by a monolithic spacecraft. The disaggregated spacecraft is an evolution of the fractionated spacecraft, which spatially distributes some or all of the spacecraft bus elements that are physically connected within a traditional monolithic spacecraft in order to achieve a new capability. The difference in disaggregation and fractionation is subtle, in that the individual nodes in a disaggregated architecture contain all of the spacecraft bus elements, but instead distribute the spacecraft to achieve a capability. Whereas, the fractionated spacecraft spatially distributes a traditional spacecraft's bus elements. Although this difference exists, many of the benefits of fractionated spacecraft are equivalent to those for disaggregated spacecraft. It is important to note that the disaggregated concept is newer than the fractionated concept, and thus there is less information available than for fractionated systems. The fractionated literature is reviewed below, but is introduced with the intention to motivate a disaggregated approach. As such, fractionated and disaggregated spacecraft will be used interchangeably for the remainder of this work.

The first benefit to be studied for fractionated space architectures, and thus disaggregated architectures, was flexibility [5]. Flexibility is defined as the "ability of the system to be modified to do jobs not originally included in the requirements definition" and the conclusion of that study was that if flexibility is valued high enough, then a fractionated system may be preferred over a traditional monolithic system. Other properties that demonstrate the benefits of fractionated architectures are responsiveness, maintainability, and scalability. Responsiveness is the "ability to

meet changing requirements or conditions quickly, which corresponds in the framework to a short- or medium-term adaptation to any change in requirements or conditions", maintainability is the "ability of a system to be kept in an appropriate operating condition", and scalability is the "ability of a system to maintain its performance and function, and retain all its desired properties when its scale is increased greatly without having a corresponding increase in the system's complexity" [6]. However, the conclusion of Mathieu's thesis was that industry had no incentive to pursue fractionated space architectures. Hence, the first customer would have to be the government. Subsequently, in 2007 the Defense Advanced Research Projects Agency (DARPA) began investigating fractionated space architectures. At DARPA, Brown [7, 8] used a value-centric design methodology to quantitatively demonstrate the benefits of fractionated systems for robustness to subsystem failures, and responsiveness and adaptability to evolving mission requirements. However, to date, zero fractionated spacecraft missions have flown and several challenges exist in the development of the necessary capability before the first missions can be flown. More recently, disaggregated spacecraft have been under investigation by the United States Air Force with all of these potential benefits in mind for the space-acquisition process [9].

Disaggregated spacecraft systems, like fractionated spacecraft, rely on resource sharing, inter-satellite network protocols and communication, cluster flying, and distributed computing [10]. In this context, a resource is defined as any element or capability that can be transferred from one spacecraft to another. The possible sharable resources correspond directly with the spacecraft's subsystems and payload. The relevant subsystems include, power generation and distribution, attitude determination and control, orbit determination and control, communications, thermal management, and command and data handling. Mission specific payload resource examples include, observational sensors and high-bandwidth downlink communications. Resource sharing is the act of transferring resources between spacecraft and is the focus of this research.

1.1 Resource Sharing

Resource sharing creates several new challenges with respect to traditional self-contained space systems. Specifically, monolithic space assets contain subsystems that are physically connected and that can perform all necessary functions directly on-board. Therefore, an optimized set of hardware and software are on-board to meet the mission requirements. For example, a mission that needs precision pointing will be met with a spacecraft design that has an on-board sensor suite to determine attitude and actuators for controlling attitude. However, when resource sharing is required, either by hardware and software failure or by design, the spacecraft must still be able to generate the necessary resources, exchange those resources and coordinate the actions of the disaggregated capability to respond to mission requirements. These functional requirements motivate the need for hardware that can facilitate the sharing of resources and algorithms that can efficiently coordinate the spacecraft to allocate and distribute the resources to accomplish the required tasking.

Guo conducted a survey of the current state-of-the-art in fractionated space resource sharing for several of the bus elements [11]. This survey focused on architectures, networking, wireless communication, distributed computing, and wireless power transfer. The fractionated architecture for mission planning and system capability has been analyzed using value-centric design tools [8] as well as agent-based systems theory [12]. The technology readiness level (TRL) for many of the bus elements are shown in Figure 1-1A. Space-based wireless communication and networking have the highest TRL, which is intuitive as these two elements are the most fundamental to fractionated spacecraft, because they are required for every other capability. Intra-spacecraft wireless communication, taking place between components within a spacecraft, has been demonstrated on orbit with the Space Shuttle and International Space Station at bandwidths up to 900 MHz. Inter-spacecraft wireless communication, taking place between spacecraft in a network, has been demonstrated with radio frequency (RF) as

well as LASER. LASER has the advantage of being lower power and high bandwidth, and in 2008 was used on the TerraSAR-X spacecraft to transmit at a data-rate of 5.6 Gbps. The case for wireless power transfer for fractionated space systems was presented by Turner [13]. Since then, the technology for wireless power transfer has been under development and the efficiency of these systems, specifically through microwave beaming, is proving the viability of power resource sharing [14]. However, wireless power transfer has only been demonstrated on the ground.

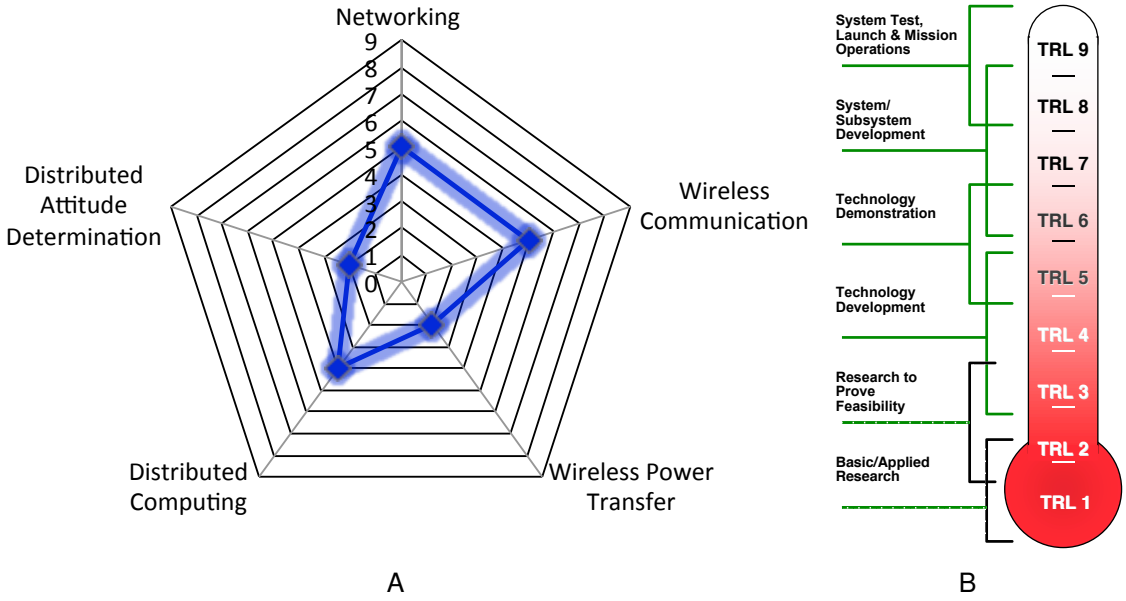

Figure 1-1. Fractionated elements technology readiness level. A) TRL radargram (adapted from [11]). B) NASA technology readiness level [15].

Some spacecraft bus elements were absent from Guo's survey, as they are less mature. For example, actuation is also a viable resource to share. In the past decade, active magnetic control has been under investigation for formation flying missions using Coulomb forces [16] and active magnets [17, 18], and has has also been studied in the context of resource sharing [19]. This technology is still at the theoretical level.

The last bus element of interest, and the focus of this research, is the sharing of sensor measurements for distributed attitude determination and control systems. O'Neill performed high level analysis on the effect of fractionation on pointing-intensive missions

to show that decoupling pointing-intensive subsystems from the other subsystems could reduce mass and cost [20]. This reduction in mass can also potentially improve the attitude maneuverability of a spacecraft as shown in Figure 1-2. This figure shows an example spacecraft with a fixed actuator that is typical in size for a nano-satellite. As the sensor-to-vehicle mass fraction is reduced, the slew rate can potentially be increased while consuming the same power. Due to physical constraints imposed by the optical bench of many attitude sensors, the mass fraction of these sensors is greater for smaller spacecraft than for traditional monolithic spacecraft. That is, for a monolithic spacecraft a star tracker is relatively small, however for a small satellite, such as a 1U CubeSat, a star tracker can take up considerable mass and volume [21]. A similar increase in slewing performance could be seen by increasing the size of the actuators, but at the expense of increased inertia. The point remains that there may be benefit from an attitude control perspective. However, the theory and implementation for resource sharing are still at a low TRL. A summary of the resource sharing elements with key technologies is provided in Table 1-1.

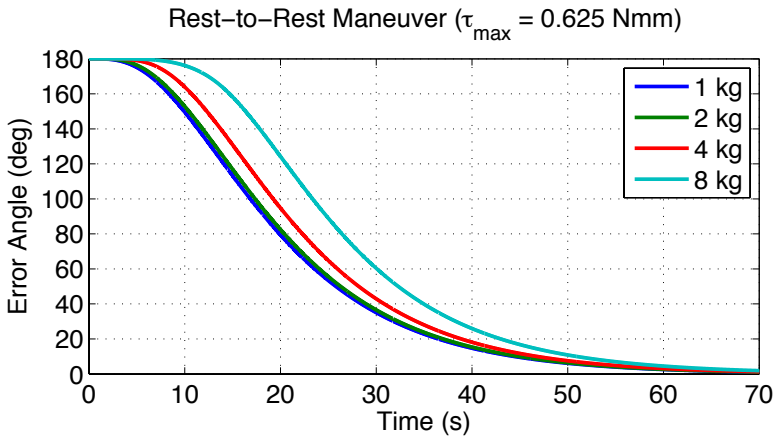

Figure 1-2. Potential benefit of the reduction in mass of a small satellite

Terminology for attitude is now introduced. The terms “inertial”, “absolute”, “relative”, “external”, and “internal” are often associated with attitude. In the context of this research, *inertial attitude* refers to the orientation of a spacecraft with respect to

Table 1-1. Resource sharing technologies for the spacecraft subsystems

Subsystem	Technologies	Functions
Communications	wireless-link, networking	transmitting and receiving data
Electronic Power System	microwave beaming	transmitting and receiving power
Attitude Determination	relative attitude sensors	attitude estimation and data fusion
Propulsion	coulomb control	orbital maneuvering
Command and Data Handling	parallel computing, client-server	information processing

an inertial reference. Sensors that provide information about inertial attitude are referred to as inertial attitude sensors, in which examples include sun sensors, magnetometers, and star trackers. *Relative attitude* refers to the orientation of a spacecraft with respect to another spacecraft or non-inertial reference. Similarly, sensors that provide information about relative attitude are referred to as relative attitude sensors, in which examples include radio frequency, vision-based sensors, and laser communication. One last sensor that deserves attention is the rate gyroscope, which is an inertial sensor that measures the angular velocity in body coordinates.

Resources can also be differentiated by their finiteness. A finite resource is defined as any resource that when transferred is changed on both the sharing and receiving spacecraft. Examples of finite resources include power, communications downlink, and position and attitude actuation. Studies have examined finite resources in fractionated spacecraft from an agent-based perspective [22] and applied game theory [12] to the resource allocation problem. On the other hand, a non-finite resource is defined as any resource that when transferred to a receiving spacecraft remains unchanged on the sharing spacecraft. Examples of non-finite resources include sensor measurements or other data. It is important to note that the transfer of non-finite resources may require the utilization of finite resources, such as power or fuel. An illustrative example is resource sharing of sensor measurements. Depending on the hardware utilized, sensor measurements may require changes in attitude or position (relying on power and/or propellant) as well as inter-satellite communications, which consume power.

Attitude sensor measurements are a non-finite resource that are necessary to determine and control the spacecraft's attitude. It has been shown that in disaggregated

systems there is a confluence of navigation, communications, and control for position control [23]. This same confluence naturally extends to disaggregated attitude determination systems (ADSs). Additionally, Blackmore proved that observability in a distributed attitude determination system requires a relative sensor path from the spacecraft back to an absolute sensor [24]. Therefore, in order to share inertial attitude, relative attitude sensors are necessary to create the relative state path from an inertial attitude sensor. Missions with relevancy to relative state sensing and resource sharing are detailed in the following section.

1.2 Relevant Missions

There are two predominant hardware technologies that must exist to enable on-orbit attitude resource sharing. The first is an inter-satellite communications link. This communications link enables coordination and data-sharing within the network. The second enabling hardware is relative state sensors. Relative state sensors have heritage in missions ranging from rendezvous and docking to space-based interferometry, and although these mission types do not require resource sharing, they provide valuable insight into the resource sharing mechanism. Relevant missions for relative state sensing technologies in flight demonstration, as well as proposed fractionated systems, are discussed in Subsections 1.2.1–1.2.4

1.2.1 Rendezvous and Docking Missions

Rendezvous and docking (RND) involves the far and close approach from one spacecraft to another, as well as the physical linking of the two spacecraft. RND missions rely heavily on the determination of relative attitude and position states for the approach trajectory and docking pose [25]. The sensors utilized for RND missions are only applicable to proximity operations. For example, at larger distances radio frequency (RF) sensors are too noisy to be utilized for high accuracy attitude knowledge. Similarly, vision-based sensors suffer at large distances, because the incident light will coalesce and the object will appear as a single point.

Early systems, such as the Russian *Kurs*, utilized RF signals in a target-chaser configuration to perform RND [26]. More recent missions have used visible spectrum signals measurements for relative state sensing. The *Spacecraft for the Universal Modification of Orbits/Front-end Robotics Enabling Near-term Demonstration (SUMO/FREND)* was a technology demonstration spacecraft designed to service or modify the orbits of other spacecraft. The *FREND* package utilized computer vision and pose estimation techniques for autonomous RND [27]. *XSS-10* [28] and *XSS-11* [29] were spacecraft designed to perform resident space object (RSO) inspection and rendezvous maneuvers using relative navigation sensors. *XSS-10* utilized the visible camera system (VCS) for relative state sensing. *XSS-11* combined an active LIDAR sensor with a visible camera and star tracker system. The *DART* spacecraft was designed to use the advanced video guidance sensor (AVGS) for RND. The AVGS was designed to track retro-reflector fiducials on another spacecraft for relative state sensing, but suffered a ‘’soft-collision‘’ that resulted in a depletion of all of its propellant and was unable to demonstrate the mission objectives [30]. *Orbital Express* was the follow-on to *DART* and consisted of two spacecraft, ASTRO and NextSat. The spacecraft utilized the AVGS and successfully demonstrated RND maneuvers [26]. The *Autonomous Transfer Vehicle (ATV)* was a European Space Agency (ESA) designed spacecraft that used videometer and telegoniometer as relative state sensors to dock and resupply the International Space Station (ISS) [31]. The *formation autonomy spacecraft with thrust, relnav, attitude, and crosslink (FASTRAC)* used relative global position signal (GPS) measurements for relative navigation [32].

Several spacecraft have demonstrated relative attitude and position measurements through a variety of sensors in close proximity. These missions have helped pave the way for disaggregated attitude determination systems, because they provide the requisite relative state sensing path. However, these technologies must be matured or extended to provide the necessary relative state precision to be suitable for resource

sharing missions. It is assumed that this technology will continue to mature and ultimately complement this research for practical implementation.

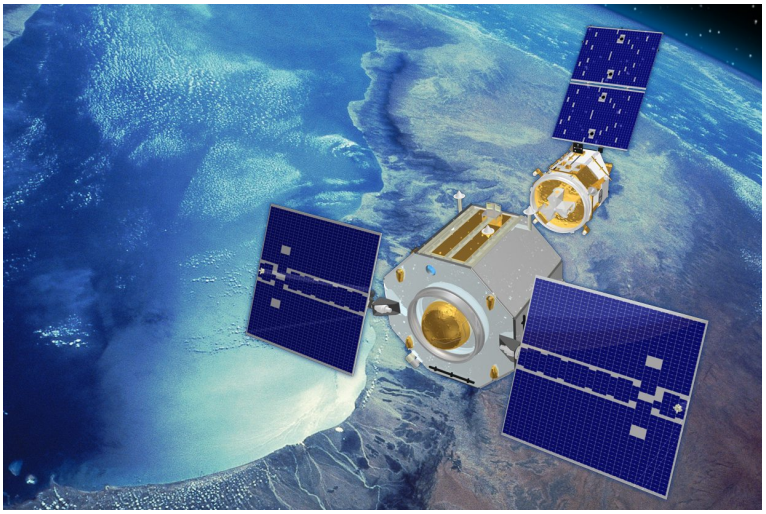

Figure 1-3. Illustration of the Orbital Express rendezvous and docking mission [33]

1.2.2 Space-based Interferometry

The *StarLight* mission is a proximity formation flying interferometry mission that makes use of the Autonomous Formation Flying (AFF) sensor [34]. Similar to the Russian Kurs proximity sensor, the AFF utilizes RF signals to measure relative states to moderate precision. A laser metrology system takes over for the AFF to yield the precision necessary for interferometry.

The proposed *Laser Interferometer Space Antenna (LISA)* mission uses a distributed spacecraft platform to create a large aperture antenna for sensing gravitational waves at low frequencies [35]. Specifically, three identical spacecraft form a 5 million *km* equilateral triangle formation with stringent requirements on relative position and attitude. Due to the large astronomical distances involved, LISA requires inter-satellite communication with the Deep Space Network (DSN) and precise relative state knowledge and control between the interferometer platforms. For this mission, star trackers are not accurate enough to maintain relative attitude to the required precision. LISA utilizes quad laser detectors for direction sensing to the other spacecraft in the

formation. This laser is used as a tracking input for the controller in order to maintain precise relative attitude.

1.2.3 Satellite Networks

Existing satellite networks have already demonstrated inter-satellite networking and communication. These capabilities are the most fundamental to disaggregated spacecraft architectures, as all other disaggregated capabilities rely on them. Two examples of resource sharing in communications networks are the *Tracking and Data Relay Satellite System (TDRSS)* [36] shown in Fig. 1-4A and *Iridium constellation* [37] shown in Fig. 1-4B. These systems were designed to relay data via inter-link communications to other spacecraft and the ground and have established heritage in wirelessly connected satellite constellations and basic data sharing.

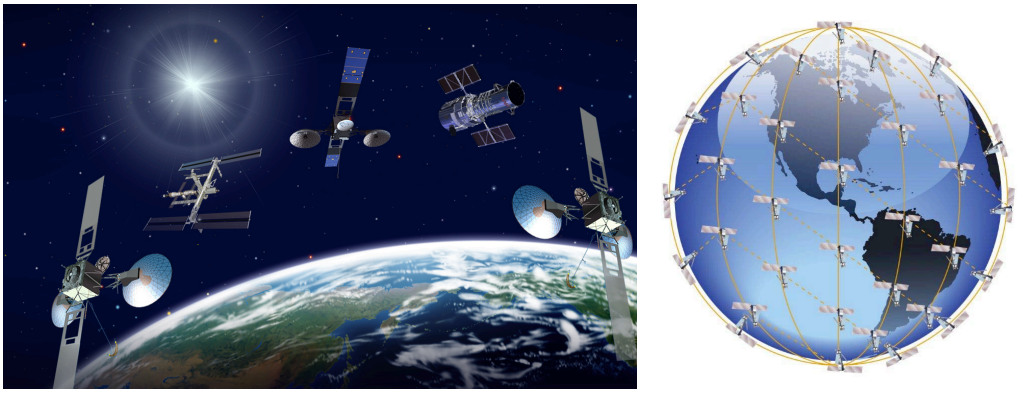

A B

Figure 1-4. Resource sharing in communications networks. A) Illustration of the TDRSS constellation [38]. B) Illustration of the Iridium constellation [39]

1.2.4 System F6

A fractionated mission that was pursued by the Defense Advanced Research Projects Agency (DARPA) is System F6 (Future, Fast, Flexible, Fractionated, Free-Flying Spacecraft). The value-case for fractionated space architectures was made by Brown in 2006 [10]. Subsequently, in 2007, DARPA began pursuing fractionated space architectures through System F6. System F6 is an instantiation of the fractionated spacecraft architecture paradigm shift proposed by Brown, with the goal to provide

evidence of the value of fractionation through flight demonstration of multiple fractionated capabilities. Of particular interest to this research, is the idea of a fractionated attitude determination system. Fractionated attitude has been suggested as a mechanism for increased robustness without requiring significant addition in hardware. Shown in Figure 1-5, fractionated attitude was identified as a demo mission for System F6 fault tolerance at the cluster level, where if a star tracker fails in the network it may be replaced through resource sharing [40]. As part of the DARPA System F6 project,

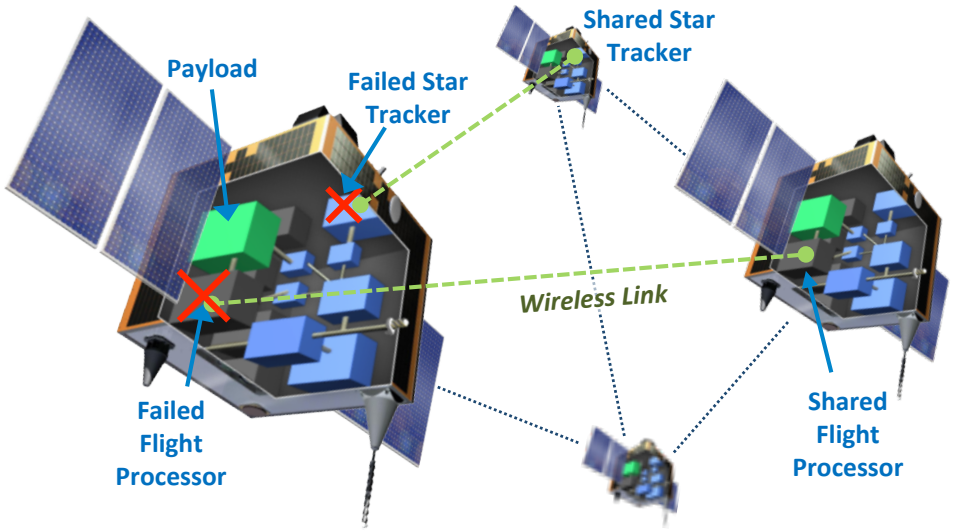

Figure 1-5. Illustration of System F6 cluster-level fault tolerance [40]

Orbital Sciences Corporation developed Pleiades [41], which was a pilot study for a notional fractionated spacecraft system. The system architecture for this mission was a LEO Earth-observation science mission with distributed imagers. The system was fractionated at multiple levels including the imager, communications downlink, data storage, and data processing.

1.3 Problem Statements

Resource sharing has been identified as a critical capability necessary for disaggregated spacecraft systems. At a high level, this is a localization problem, as studied in the simultaneous localization and mapping literature [42], and more recently

using relative attitude localization [43, 44]. The objective of any attitude determination system is to estimate the attitude of the spacecraft as accurately as possible. As a result, a natural attitude-based objective for the disaggregated system is to minimize the uncertainty in the attitude estimation, summed across the network. That is,

$$min \sum_{i=1}^{n} \left(\int_0^T \|\boldsymbol{e}_i\| dt \right), \tag{1–1}$$

where $\boldsymbol{e}_i$ is the attitude state error for the i^{th} spacecraft, n is the total number of spacecraft, and T is the time-horizon of interest.

The resource sharing process is summarized in Figure 1-6, where the control of information is sought. Specifically, information is generated through sensing and incorporated to the state knowledge through estimation. All information sources are then combined to improve knowledge across the disaggregated system. Finally, the next information source is chosen. This process relies on four key functions, including:

1. Inter-satellite communication
2. Estimation of inertial attitude using relative attitude sensor measurements
3. Fusion of multiple information sources
4. Decision algorithms for distribution of attitude resources

Of these four challenges, inter-satellite communication is assumed to exist. The last three are addressed in this work (see: Section 1.4).

Two definitions for the attitude resource are explored in this research:

1. Attitude measurements originating from the chief's sensors, which are shared directly with the deputies
2. Processed attitude estimates, which are shared between the chief and deputies

When processed estimates are shared, data fusion is the tool used for combining multiple sources of information.

Consider the general spacecraft network shown in Figure 1-7, where the chief represents a node with a relative attitude sensor and the deputies are nodes in the

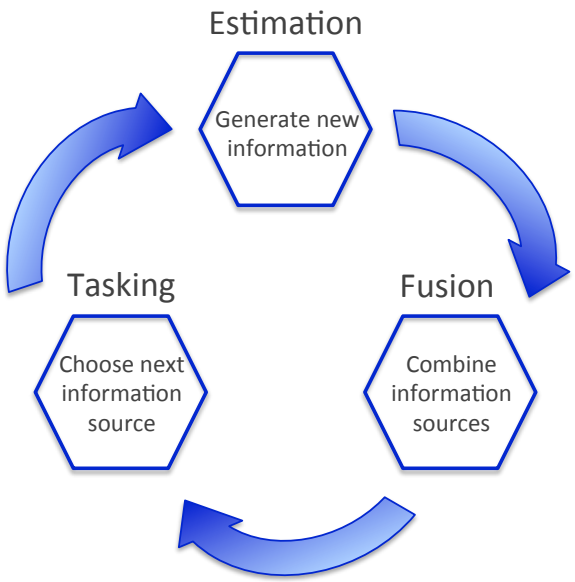

Figure 1-6. Fundamental functions for the attitude resource sharing process

network without relative attitude sensing, and potentially without attitude sensing, altogether. This network can either describe a formation-flying system, where the relative position and attitude of the spacecraft are to be controlled, or a constellation, where the spacecraft have some common objective, but do not rely on maintaining their relative states. The challenges in estimation, data fusion, and sensor tasking for attitude resource sharing are now focused into three problem statements with related research questions.

1.3.1 Problem 1: Inertial Attitude Estimation in a Disaggregated System

Relative attitude sensors are used to directly estimate the relative attitude between a chief and its deputies [45, 46]. The inertial attitude of a deputy can be produced by local inertial sensors. Alternatively, the composition of relative attitude of the deputy with respect to the chief and inertial attitude of the chief can be used to generate new knowledge about the deputies inertial attitude. Taking this into consideration, a relevant research question is, “how can inertial attitude be estimated in a disaggregated system through the use of relative and inertial attitude sensors?”

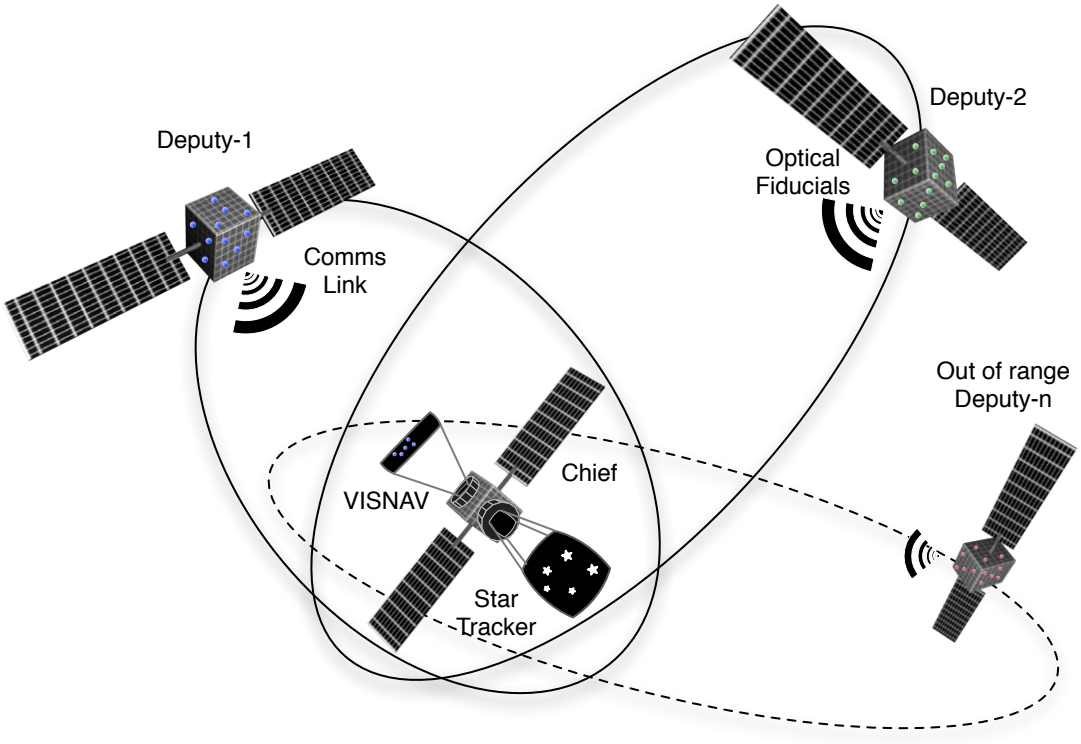

Figure 1-7. Attitude resource-sharing architecture

1.3.2 Problem 2: Attitude Data Fusion

Information transfer between the chief and deputies is accomplished via the wireless link in Figure 1-7. Attitude resource sharing requires that attitude measurements or estimate be shared between spacecraft through this link. In the case of shared attitude estimates, multiple sources of the same information are generated, as relative and inertial attitude can be composed to describe the inertial attitude of another spacecraft. Data fusion seeks an optimal combination of information to produce a best estimate when information dependency is uncertain, as is the case with covariance intersection [47, 48], or dependency is known, as in the case of correlated track fusion [49]. To generate a fused estimate, data fusion algorithms optimize the combination of multi-sensor information by minimizing a cost function, which is a problem dependent

measure of the error between the state estimates and the fused state. For typical applications, the fusion error is a measure of the Euclidean distance. However attitude belongs to the space of special orthogonal matrices, $SO(3)$, which describes the relative orientation between two coordinate systems, and thus a Euclidean distance error is inappropriate for attitude. Therefore, the problem of fusing multiple attitude information sources requires an alternative definition of the fusion error. Two research questions that are addressed in this research are:

1. How can existing data fusion algorithms be extended to attitude states?
2. What is a fast and accurate attitude parameterization for data fusion?

1.3.3 Problem 3: Sensor Tasking

The third objective of this research is to develop algorithms for tasking sensors to allocate and distribute attitude resources within a spacecraft network. The primary focus of this objective is to investigate networks consisting of fractionated ADS distributed across a chief spacecraft and multiple deputies. To achieve the best performance, for a particular cost function, the sensor will ideally be tasked for the infinite horizon. The resulting tasking is the solution to a stochastic optimal control problem.

A well known stochastic optimal control problem is the Linear Quadratic Gaussian (LQG) controller. The LQG controller has a closed-form solution due to the properties of separation and certainty equivalence. The separation property states that the optimal controller and estimator are solved separately [50, 51]. That is, the criterion for determining the control is independent of the estimation and vice versa. Certainty equivalence states that an optimal deterministic controller is equivalent to the same control law replaced by optimal estimated states [52]. For example, under very specific assumptions, the Linear Quadratic Gaussian (LQG) control law solves the deterministic Linear Quadratic Regulator (LQR) and optimal Linear Quadratic Estimator (LQE) independently via their corresponding Riccati equations [53]. However, for dynamic attitude sensor tasking, where the objective is to minimize the pointing error in the

system, the controller actions are based on sensing objectives. This leads to the dual effect where control not only affects the states but also the uncertainty in the states. This is the converse of typical feedback control laws where sensor measurements are based on controller objectives that only affect the state. Control for sensing is nontrivial and results in an absence of the certainty equivalence property and a lack in separation of estimation and control.

Due to a lack in separation and control, optimal solutions are computationally expensive and do not scale well with larger networks (curse of dimensionality). Therefore, the research question for sensor tasking is, "how can a sensor be tasked to minimize the total attitude error in a disaggregated attitude determination system, while also being computationally inexpensive, and scaling well with larger networks?"

1.4 Thesis Statements

To address the research questions presented in Section 1.3, the following describes the thesis statements for estimation, data fusion, and sensor tasking as applied to attitude resource sharing.

1.4.1 Thesis 1: On Inertial Attitude Estimation for Disaggregated Systems

Given inter-satellite communication, an extended Kalman filter for estimating inertial attitude from relative and inertial attitude sensors in a disaggregated system can be utilized while the linearization remains valid.

1.4.2 Thesis 2: On Minimal Attitude Parameterization Data Fusion

Existing data fusion methods on Euclidean state spaces can be extended to the attitude state spaces of $SO(3)$ using the parameterization independent attitude error vector. Proper choice of a minimal attitude parameterization can lead to an unconstrained, global, and nonsingular data fusion process.

1.4.3 Thesis 3: On Sensor Tasking for Attitude Resource Distribution

Greedy sensor tasking is robust for attitude resource distribution in disaggregated spacecraft networks, as it avoids the planning process and the issues with separation in

estimation and control. The primary factors to consider for the greedy decision algorithm are the relative states with constraints and their respective uncertainties.

1.5 Dissertation Organization

This dissertation is divided into seven chapters and proceeds with the following organization.

Chapter 2 introduces the fundamental spacecraft attitude parameterizations and kinematics. Then attitude dynamics and control are introduced in the context of the tracking problem to distribute resources. This chapter lays the groundwork for the remainder of the dissertation.

Chapter 3 summarizes existing attitude sensors and attitude determination and estimation results for inertial and relative attitude. This chapter concludes with the development of an inertial attitude estimator for the chief to estimate the deputies inertial attitude states via the relative attitude sensor. Using these results, the chief and deputies produce multiple estimates of each spacecraft's inertial attitude. This leads to the next chapter on efficient methods of combining multiple sources of information – data fusion.

Chapter 4 reviews existing attitude data fusion techniques and provides a general framework for extending the theory of data fusion for Euclidean state spaces to attitude states on $SO(3)$. Minimal attitude parameterizations, namely the vectorial sets introduced in Chapter 2, are developed to provide a global nonsingular unconstrained parameterization for attitude data fusion. The accuracy of the minimal parameterizations for data fusion are compared. This chapter concludes with a notional two-star-tracker data fusion problem to provide further evidence for the first thesis statement on minimal attitude parameterizations for data fusion.

Chapter 5 introduces the problem of sensor tasking for attitude resource sharing. A greedy tasking algorithm for the capturing of relative state measurements from the chief to the deputies is developed that addresses the issues of uncertainty

minimization, computational tractability, and architecture scalability. The content of this chapter supports the second thesis statement on sensor tasking for attitude resource sharing.This chapter concludes with a four-spacecraft sensor tasking example to verify the approach.

Chapter 6 presents an example resource sharing architecture, which combines the results of Chapter 4 and Chapter 5. Particularly, two and three spacecraft formation flying networks are simulated. Resource sharing is investigated for cases with coarse and fine precision inertial attitude sensors with a high precision relative link. Data fusion is based on the fourth-order Rodrigues parameters and the sensor tasking algorithm are applied. Results are provided that indicate the validity of the approach and provide the final evidence for the thesis of this dissertation.

Chapter 7 draws conclusions from the preceding chapters and makes recommendations for future research.

CHAPTER 2
SYSTEM DYNAMICS AND CONTROL

Attitude resource sharing in a disaggregated spacecraft system is based on the rotational motion of each spacecraft and also on the parameterization used to describe that motion. Resource sharing also relies on the composition of relative and inertial attitude measurements. Therefore, an antecedent to resource sharing and sensor tasking is a fundamental knowledge of inertial and relative attitude dynamics and attitude parameterizations.

2.1 General Nomenclature

Scalars, vectors, and matrices on $\mathbb{R}^n$ are ubiquitously used throughout this work. The nomenclature for these quantities is provided for clarity to the reader. Scalars are written as lowercase letters (e.g., a). Vectors and column matrix representations of vectors will be written in lowercase bold font (e.g., $\boldsymbol{a}$). General matrices are written in upper-case letters (e.g., A). Finally, the quaternions are written as the lowercase, q.

2.2 Rigid Body Kinematics

The motion of a single spacecraft can be treated as a rigid body, where the mutual distance between the particles making up the spacecraft are invariable with a finite mass. A single rigid spacecraft has six degrees-of-freedom – three for translation and three for rotation. Note that non-rigid motion, by means of flexible or articulating members, create additional degrees-of-freedom, but will not be investigated in this research. From Chasle's theorem, the most general displacement of a rigid body is the translation along a line coupled with a rotation about that line [54]. It is thus pertinent to define what is meant by translation and rotation.

Translational motion occurs when the displacement of all particles in the rigid body follow parallel paths. Whereas, rotational motion occurs when there is a nonparallel path followed by some particles in the rigid body. Therefore, at minimum, six coordinates

are necessary to describe the motion of a spacecraft, that is, three coordinates for the translation and three coordinates for the rotation.

For attitude applications there are two concepts which have many definitions in the literature, and thus a clear definition is necessary in the context of this discussion – that of the frame of reference, and the coordinate frame. The frame of reference is where all distances and time are measured for the application of Newtonian and Eulerian dynamics. As such, the frame of reference is non-accelerating and said to be inertial. In practice, defining an exact frame of reference with physical significance for measurements is impossible. Therefore, the frame of reference is chosen that is approximately inertial with respect to the time horizon of interest and the distances expected, such as to maintain the non-acceleration requirement. The second definition is in regard to the coordinate frame. A coordinate frame is a set of basis vectors defined by a plane and a direction in that plane, where the second direction is orthogonal to the plane and the third direction follows from the right-hand rule; forming an orthonormal set.

The definition of attitude is based in the representation of unit vectors defined by coordinate frames. Attitude involves the description of the rotational degrees-of-freedom of a rigid body and is defined as the *relative orientation between two coordinate fames, one of which is typically fixed to the rigid body*. When dealing with spacecraft, of primary concern is the orientation of a coordinate frame fixed to the rigid spacecraft with respect to some other coordinate frame. Several of these coordinate frames are described in the following section.

2.3 Coordinate Frames

As attitude describes the relative orientation between coordinate frames, it is important to understand the definition of the frames that are typically encountered in spacecraft applications. Starting with an inertial coordinate frame where the fundamental laws of dynamics hold, the coordinate frames will be defined in the

sequence originating with the inertial frame of reference and ending with the body, whose motion is of interest.

2.3.1 Earth-Centered Inertial (ECI)

For Earth orbiting applications, a common inertial frame is the ECI frame. The frame ($\mathscr{F}_I$), shown in Figure 2-1A, is defined by the orthonormal basis vectors $\{\boldsymbol{X}_I, \boldsymbol{Y}_I, \boldsymbol{Z}_I\}$. These directions are assumed to be fixed. However, due to the nutation of the Earth, a direction specified to an inertial point in space (such as a star) will accelerate as the originating point of the direction is fixed to the Earth. To rectify this invalidation of the assumption, the J2000 frame considers the reference directions at a specific instance in time. Specifically, the J2000 frame is defined by the equatorial plane, in which $\boldsymbol{X}_I$ lies in the plane and points in the direction from the center of the Earth to the first point of Aries on January 1, 2000.

2.3.2 Earth-Centered Earth-Fixed (ECF)

The ECF frame is fixed to the Earth and is used to describe the rotation of the Earth with respect to the ECI frame, given that the Earth rotates with an angular velocity $\boldsymbol{\omega}^{E/F} = \omega \boldsymbol{Z}_F$, where $\omega = 7.292115 \times 10^{-5} rad/s$ [55]. The ECF frame ($\mathscr{F}_F$), shown in Figure 2-1A, is defined by the orthonormal basis vectors $\{\boldsymbol{X}_F, \boldsymbol{Y}_F, \boldsymbol{Z}_F\}$, where the $\boldsymbol{X}_F$ lies in the equatorial plane is measured by the Earth hour angle (EHA) relative to $\boldsymbol{X}_I$.

2.3.3 Hill (LVLH)

The Hill frame ($\mathscr{F}_H$), shown in Figure 2-1B, is an example of a local-vertical-local-horizontal (LVLH) frame. It is the basis typically used for relative translational motion of multiple spacecraft. It is defined by the orthonormal basis vectors, $\boldsymbol{X}_H = \frac{\boldsymbol{r}}{\|\boldsymbol{r}\|}$, $\boldsymbol{Z}_H = \frac{\boldsymbol{h}}{\|\boldsymbol{h}\|}$ and $\boldsymbol{Y}_H = \boldsymbol{Z}_H \times \boldsymbol{X}_H$, where $\boldsymbol{r}$ is the position vector from the center of the earth to the center of mass of the spacecraft and $\boldsymbol{h}$ is the angular momentum vector of the orbit.

2.3.4 Perifocal (PQW)

The Perifocal frame ($\mathscr{F}_P$), shown in Figure 2-1B, is commonly used at an inertial frame of reference for Earth orbital applications. It has has origin at the occupied focus

of the conic section describing the orbital motion and is defined by the orthonormal basis vectors $\boldsymbol{P} = \frac{\boldsymbol{e}}{\|\boldsymbol{e}\|}$, $\boldsymbol{W} = \frac{\boldsymbol{h}}{\|\boldsymbol{h}\|}$, and $\boldsymbol{Q} = \boldsymbol{W} \times \boldsymbol{P}$, where $\boldsymbol{e}$ is the eccentricity vector.

2.3.5 Body Frame (B)

The Body frame ($\mathscr{F}_B$), is defined by orthonormal basis vectors, $\{\boldsymbol{X}_B, \boldsymbol{Y}_B, \boldsymbol{Z}_B\}$. This frame is fixed to the spacecraft and used to describe the attitude of the spacecraft with respect to the other coordinate frames described in this section. Typically, the frame will originate at the center of mass of the spacecraft, which is convenient for attitude dynamics. For the remainder of the discussion to follow, a star tracker is assumed to be aligned with $\boldsymbol{Z}_B$ and a relative attitude sensor is aligned with $\boldsymbol{X}_B$.

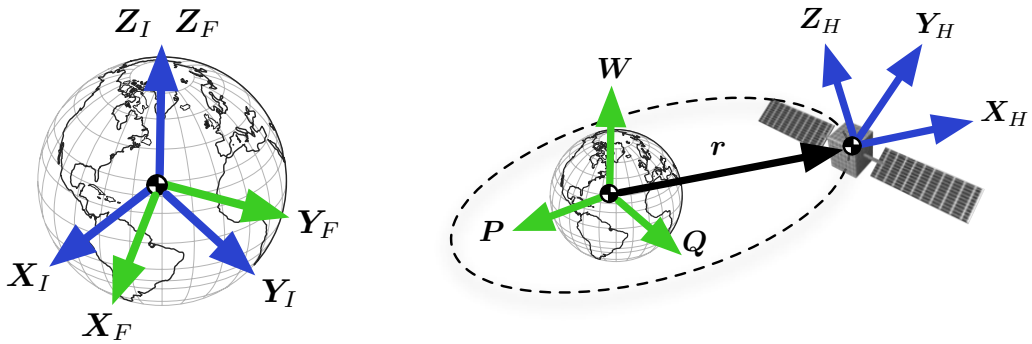

A B

Figure 2-1. Common coordinate frames. A) Inertial and Earth-fixed frames. B) Hill and perifocal frames.

2.4 Attitude Parameterizations and Kinematics

Attitude can be defined as the mapping of vectors in one basis to another, such that

$$\boldsymbol{x}' = R\boldsymbol{x},$$

where $\boldsymbol{x}'$ is a column matrix of the a vector represented in $\mathscr{F}_{E'}$ coordinates, $\boldsymbol{x}$ is the column matrix of that same vector represented in $\mathscr{F}_E$ coordinates, and $R \in SO(3) \subseteq \mathbb{R}^{3\times3}$ maps vectors from $\mathscr{F}_E$ to $\mathscr{F}_{E'}$. The parameterization of $SO(3)$ is a classical problem. Since attitude describes the three degrees-of-freedom of the spacecraft's

rotational motion, there are a minimum of three parameters that are necessary to describe the spacecraft's attitude. However, in general, the attitude matrix that describes the mapping between two basis is non-Euclidean, belonging to the group of special orthogonal matrices denoted by $SO(3)$. There are a number of non-Euclidean representations that parameterize the attitude. Through use of Brouwer's theorem on invariance of domain, Stuelpnagel showed that all minimal attitude parameterizations contain singularities [56]. In fact, it was shown that it takes, at minimum, five parameters to 1-to-1 globally parameterize $SO(3)$. A solution to the existence of singularities is to use redundant representations or ensure that that the minimal parameterization singularity is outside of the attitude region of interest.

Since the choice of attitude parameters is non-unique, many attitude parameterizations have been developed, each with specific advantages and disadvantages. An often cited survey of the attitude parameterizations by Shuster is contained in Reference [57], which was current up to 1993. A survey of those contained in Shuster's paper, as well as a description of more recent attitude parameterizations found by stereographic projections, higher order Cayley transforms is described in Reference [58]. Finally, a generalization of axis-angle derived parameterized, termed the vectorial attitude parameterizations, as described in Reference [59]. A brief summary of the results from the literature is provided in Sections 2.4.1–2.4.8.

There are many important characteristics to consider when choosing a parameterization, such as the presence of singularities, number of parameters and imposed constraints, computation of transcendental functions, and kinematic linearity. Ideally, a parameterization should be globally-singularity free, minimal in number of parameters and constraints, and linear without transcendental functions. However, since all minimal parameterizations are singular, either singularities will be encountered with a finite rotation, or redundant parameters must be utilized. The choice of parameterization is critical for the effectiveness of attitude control, estimation, and data fusion algorithms, as are discussed in this work.

The following subsections review several attitude parameterization with their first-order kinematics and composition laws. Additionally, the second-order kinematics are provided for the unit quaternion parameterizations, which is necessary for the attitude tracking control law that enables the one spacecraft to track another.

2.4.1 Attitude Matrix

The foundation of attitude originates with a vector, $\boldsymbol{x}$, expressed in two different coordinate frames. Each coordinate frame is described by the orthonormal basis vectors, such that $\mathscr{F}_E = \boldsymbol{e}_1, \boldsymbol{e}_2, \boldsymbol{e}_3$ and $\mathscr{F}_{E'} = \boldsymbol{e}'_1, \boldsymbol{e}'_2, \boldsymbol{e}'_3$. The vector, $\boldsymbol{x}$, represented in each basis is

$$\boldsymbol{x} = x_1\boldsymbol{e}_1 + x_2\boldsymbol{e}_2 + x_3\boldsymbol{e}_3 = x'_1\boldsymbol{e}'_1 + x'_2\boldsymbol{e}'_2 + x'_3\boldsymbol{e}'_3$$

Therefore, in order to transform from basis $\mathscr{F}_E$ to $\mathscr{F}_{E'}$, the direction cosines defined by the components

$$R_{ij} = \boldsymbol{e}'_i \cdot \boldsymbol{e}_j,$$

parameterize the matrix, R. The column matrix representation of the vector $\boldsymbol{x}$ in $\mathscr{F}_{E'}$, as denoted by $\boldsymbol{x}'$ is computed through

$$\boldsymbol{x}' = R\boldsymbol{x}.$$

The direction cosine matrix is equivalently termed the attitude matrix when discussing the general proper orthogonal matrix [57]. Mathematically, this matrix is an orthogonal transformation, belonging to the group $SO(3)$. This transformation is preserving of the vector's length and orientation, that is,

$$RR^T = I_{3\times 3},$$

where $I_{3\times 3}$ is the identity matrix of appropriate dimension. Based on this defintion, $R^{-1} = R^T$. It is also proper, satisfying $\det(R) = +1$. There are nine parameters necessary to describe the attitude matrix, and hence, R contains six constraints. As a result, there is a large redundancy in R, which comes at the cost of higher computational burden.

However, the redundancy in R has the advantage of forming a globally unique and singularity-free attitude parameterization that can be used for continuous singularity-free control laws [60].

The composition of two sequential rotations R_1 followed by R_2 is,

$$R = R_2 R_1. \tag{2–1}$$

Rotations do not commute. As a convention, *inertial attitude* is termed to describe the orientation between a rigid body and an inertial coordinate system. Whereas, *relative attitude* is termed to describe the orientation between two non-inertial coordinate frames. The relative attitude between two rigid bodies can be described through the above attitude composition law as shown in Figure 2-2.

The rotations A and B represent the inertial attitude of $\mathcal{F}_A$ and $\mathcal{F}_B$ with respect to the inertial reference, $\mathcal{F}_I$, respectively. Observing the direction of the rotations, the relative attitude from $\mathcal{F}_B$ to $\mathcal{F}_A$, is denoted by C and is equivalent to $A^T B$, as seen in Figure 2-2A. Whereas, Figure 2-2B depicts the relative attitude from $\mathcal{F}_A$ to $\mathcal{F}_B$, and is equivalent to $C^T = B^T A$. Therefore, the relative attitude is defined through attitude compositions.

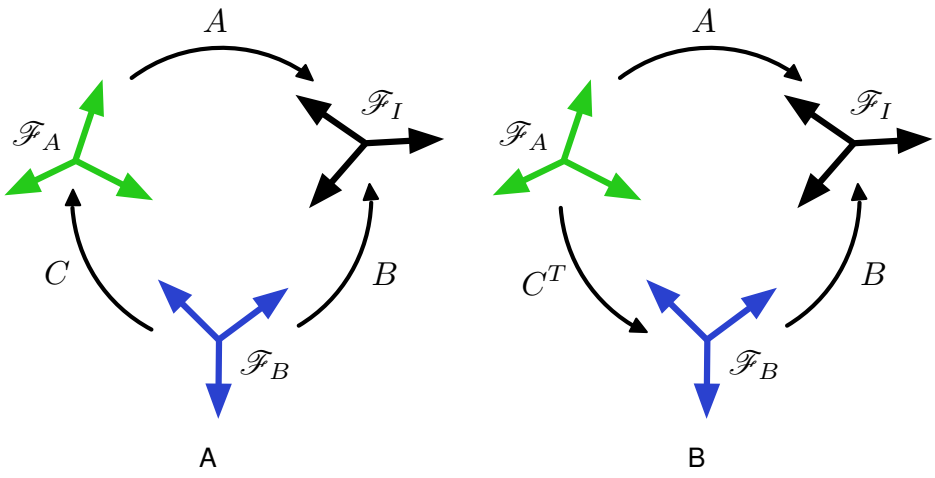

Figure 2-2. Relative attitude compositions. A) $\mathcal{F}_B$ to $\mathcal{F}_A$. B) $\mathcal{F}_A$ to $\mathcal{F}_B$.

Another important fact, is that infinitesimal rotations are characterized by the matrix

$$\Delta R = I_{3\times 3} - [\Delta\phi \boldsymbol{n}\times], \tag{2–2}$$

where $\boldsymbol{n}$ is the axis of rotation, $\Delta\phi$ is an infinitesimal rotation about that axis. Note that the $[\boldsymbol{n}\times]$ notation represents the skew-symmetric matrix equivalent of the cross-product operator, such that

$$[\boldsymbol{n}\times] = \begin{bmatrix} 0 & -n_3 & n_2 \\ n_3 & 0 & -n_1 \\ -n_2 & n_1 & 0 \end{bmatrix}.$$

This fact will be exploited for the developments in Chapter 4 on data fusion. Using the definition of the derivative and making use of the composition of rotations and the definition of an infinitesimal rotation, the skew-symmetric matrix that is parameterized by the angular velocity vector of the rotated frame with respect to the original frame in rotated coordinates is

$$[\omega\times] = R\dot{R}^T. \tag{2–3}$$

Alternatively, given knowledge of the angular velocity, the attitude matrix kinematics are given by

$$\dot{R} = -[\omega\times] R,$$

which can be integrated to yield the attitude over time. Due to numerical truncation, six constraints must be imposed to ensure $R \in SO(3)$.

The second derivative of the attitude matrix is

$$\ddot{R} = -([\dot{\omega}\times] - [\omega\times][\omega\times]) R,$$

or alternatively the skew-symmetric matrix parameterized by the angular acceleration is

$$[\dot{\omega}\times] = -\ddot{R}R^T + [\omega\times][\omega\times].$$

The second derivatives are developed for the attitude matrix and the unit quaternion in anticipation of the the tracking controller described Section 2.7.

2.4.2 Euler Angles

A maximum of three angles is necessary to describe the attitude between two arbitrary coordinate frames, $\mathscr{F}_E$ and $\mathscr{F}_{E'}$. The Euler angles are the angles through which three consecutive rotations are made in sequence that form the composite rotation describing the attitude between the two bases. Consider Euler angles, $\{\theta_1, \theta_2, \theta_3\}$, where the fundamental rotations about directions $\{\mathbf{1}, \mathbf{2}, \mathbf{3}\}$ are described by

$$R(\mathbf{1}, \theta_1) = \begin{bmatrix} 1 & 0 & 0 \\ 0 & \cos\theta_1 & \sin\theta_1 \\ 0 & -\sin\theta_1 & \cos\theta_1 \end{bmatrix}, \; R(\mathbf{2}, \theta_2) = \begin{bmatrix} \cos\theta_2 & 0 & -\sin\theta_2 \\ 0 & 1 & 0 \\ \sin\theta_2 & 0 & \cos\theta_2 \end{bmatrix},$$

$$R(\mathbf{3}, \theta_3) = \begin{bmatrix} \cos\theta_3 & \sin\theta_3 & 0 \\ -\sin\theta_3 & \cos\theta_3 & 0 \\ 0 & 0 & 1 \end{bmatrix}.$$

Euler angle sequences are non-unique and can be categorized as symmetric and asymmetric. Symmetric sequences, such as 3-1-3, have singularities at $\theta_2 = \pm n\pi$ ($n = 1, 2, 3, ...$). Whereas, the asymmetric sequences, such as 3-2-1, have singularities at $\theta_2 = \pm n\pi/2$ ($n = 1, 3, 5, ...$).

The attitude matrix parameterized by the 3-2-1 sequence of Euler angles is

$$R_{321}(\theta_1, \theta_2, \theta_3) = \begin{bmatrix} c\theta_1 c\theta_2 & s\theta_1 c\theta_2 & -s\theta_2 \\ c\theta_1 s\theta_2 s\theta_3 - s\theta_1 c\theta_3 & s\theta_1 s\theta_2 s\theta_3 + c\theta_1 c\theta_3 & c\theta_3 s\theta_3 \\ c\theta_1 s\theta_2 c\theta_3 + s\theta_1 s\theta_3 & s\theta_1 s\theta_2 c\theta_3 - c\theta_1 s\theta_3 & c\theta_2 c\theta_3 \end{bmatrix},$$

where $c\theta \triangleq \cos\theta$ and $s\theta \triangleq \sin\theta$.

Once again, considering the 3-2-1 sequence of Euler angles, the kinematics are

$$\begin{bmatrix} \dot{\theta}_1 \\ \dot{\theta}_2 \\ \dot{\theta}_3 \end{bmatrix} = \frac{1}{c\theta_2} \begin{bmatrix} 0 & s\theta_3 & c\theta_3 \\ 0 & c\theta_2 c\theta_3 & -c\theta_2 s\theta_3 \\ c\theta_2 & s\theta_2 s\theta_3 & s\theta_2 c\theta_3 \end{bmatrix} \boldsymbol{\omega}$$

with inverse kinematics given by

$$\boldsymbol{\omega} = \begin{bmatrix} -s\theta_2 & 0 & 1 \\ c\theta_2 s\theta_3 & c\theta_3 & 0 \\ c\theta_2 c\theta_3 & -s\theta_3 & 0 \end{bmatrix} \begin{bmatrix} \dot{\theta}_1 \\ \dot{\theta}_2 \\ \dot{\theta}_3 \end{bmatrix}.$$

Clearly, the singularity manifests in the kinematics at $\theta_2 = \pm n\pi/2$ ($n = 1, 3, 5, ...$). This fact holds for all asymmetric sequences. Although it was not explicitly shown, all symmetric sequences have kinematic singularities at $\theta_2 = \pm n\pi$ ($n = 1, 3, 5, ...$).

Euler angles form a minimal attitude parameterization and are amenable to rapid computation with the caveat that transcendental functions, in the form of sines and cosines, must be computed. However, they also suffer from singularities. Singularities can be avoided by switching between symmetric and asymmetric Euler angle sequences, but other minimal parameterizations exist that can also avoid singularities, but without the transcendental functions required by the Euler angles.

2.4.3 Axis-Angle

Euler's rotation theorem states, "a rotation about a point is always equivalent to a rotation about a line through the point" [54]. Following from this theorem and the previous development of the attitude matrix, the attitude matrix can be parameterized by an axis and angle decomposition. Given a unit vector, $\boldsymbol{n}$, directed along the axis of rotation, and an angle ϕ through which the body is rotated, the attitude matrix can be parameterized by an axis and the angle of rotation about that axis, which is expressed

through the Euler-Rodrigues formula as

$$R(\boldsymbol{n}, \phi) = \cos\phi I_{3\times 3} + (1 - \cos\phi)\boldsymbol{n}\boldsymbol{n}^T + \sin\phi[\boldsymbol{n}\times]. \tag{2–4}$$

The axis-angle representation is a 4-parameter set that requires the computation of transcendental functions. Additionally, this representation has a 2-to-1 correspondence with the elements of the attitude matrix and is thus non-unique; that is, $R(\boldsymbol{n}, \phi) = R(-\boldsymbol{n}, -\phi)$. Using Eq. 2–3, the kinematics for the axis-angle representation are

$$\begin{aligned} \dot{\boldsymbol{n}} &= \frac{1}{2}\left(I_{3\times 3} - \cot\frac{\phi}{2}[\boldsymbol{n}\times]\right)[\boldsymbol{n}\times]\,\boldsymbol{\omega} \\ \dot{\phi} &= \boldsymbol{n}^T\boldsymbol{\omega} \end{aligned} \tag{2–5}$$

The inverse kinematics are given by

$$\boldsymbol{\omega} = \dot{\phi}\boldsymbol{n} + \sin\phi\dot{\boldsymbol{n}} - (1 - \cos\phi)\,[\boldsymbol{n}\times]\,\dot{\boldsymbol{n}}.$$

There is a singularity at $\phi = 0$ and $\phi = \pm 2\pi$. However, all singularities lie at the null rotation state, which can be accounted for in the representation. This fact does pose problems for stabilizing controllers, as the *cotangent* function is ill-conditioned near the singularity points, which are the typical desired equilibria of a stabilizing controller. (FIND REFERENCE)

The second order kinematics are

$$\begin{aligned} \ddot{\boldsymbol{n}} &= \left(\frac{1}{2}[\dot{\boldsymbol{n}}\times] + \frac{1}{4}\csc^2\frac{\phi}{2}\left(\boldsymbol{n}\boldsymbol{n}^T - \boldsymbol{n}^T\boldsymbol{n}I_{3\times 3}\right)\right)\boldsymbol{\omega} - \frac{1}{2}\cot\frac{\phi}{2}\left(\boldsymbol{n}\boldsymbol{n}^T - \boldsymbol{n}^T\boldsymbol{n}I_{3\times 3}\right)\dot{\boldsymbol{\omega}} \\ \ddot{\phi} &= \dot{\boldsymbol{n}}^T\boldsymbol{\omega} + \boldsymbol{n}^T\dot{\boldsymbol{\omega}}, \end{aligned} \tag{2–6}$$

and the second order inverse kinematics are

$$\dot{\boldsymbol{\omega}} = \ddot{\phi}\boldsymbol{n} + \dot{\phi}\left[(1 - \cos\phi)\,I_{3\times 3} - \sin\phi\,[\boldsymbol{n}\times]\right]\dot{\boldsymbol{n}} + \left[\sin\phi I_{3\times 3} - (1 - \cos\phi)\,[\boldsymbol{n}\times]\right]\ddot{\boldsymbol{n}}$$

2.4.4 Euler Symmetric Parameters (Unit Quaternions)

An extension to the axis-angle representation is made by defining $\boldsymbol{q} \triangleq \sin\frac{\phi}{2}\boldsymbol{n}$ and $q_4 \triangleq \cos\frac{\phi}{2}$. These new parameters make up a four-parameter set which have equivalent algebra to Hamilton's quaternion. The unit quaternion, $q = [\boldsymbol{q}^T, q_4]^T$ is a once redundant parameterization that must satisfy the constraint

$$\boldsymbol{q}^T\boldsymbol{q} + q_4^2 = 1.$$

The unit quaternion parameterizes the attitude matrix as

$$R(q) = (q_4^2 - \boldsymbol{q}^T\boldsymbol{q})I_{3\times 3} + 2\boldsymbol{q}\boldsymbol{q}^T - 2q_4[\boldsymbol{q}\times]. \tag{2–7}$$

The kinematics of the unit quaternion are bilinear such that

$$\dot{q} = \frac{1}{2}\Xi(q)\omega = \frac{1}{2}\Omega(\omega)q$$

where

$$\Xi(q) = \begin{bmatrix} q_4 I_{3\times 3} + [\boldsymbol{q}\times] \\ -\boldsymbol{q}^T \end{bmatrix}, \quad \Omega(\omega) = \begin{bmatrix} -[\omega\times] & \omega \\ -\omega^T & 0 \end{bmatrix}$$

The inverse kinematics are nonlinear and given by

$$\omega = 2\Xi^T(q)\dot{q}$$

The unit quaternion eliminates the transcendental functions found in the axis-angle representation and results in a singularity-free and bilinear kinematic description. As a result the unit quaternion is the parameterization of choice for many modern attitude estimation and control algorithms. However, the unit quaternion is preserving of the 2-to-1 nature of the axis-angle representation and is thus subject to issues such as "wind-up" in feedback controllers. Therefore, care must be taken in application of the unit quaternion [60].

2.4.5 Classic Rodrigues Parameters (CRPs)

The parameters of the Euler symmetric parameters can be combined to form the classic Rodrigues parameters (CRPs), also known as the Gibbs vector, which are defined by

$$\boldsymbol{\rho} \triangleq \frac{\boldsymbol{q}}{q_4} = \tan\frac{\phi}{2}\boldsymbol{n}.$$

This combining of parameters is analogous to a projection of the quaternion 4-sphere onto a 3-dimensional hyperplane as discussed in Subsection 2.4.7. The attitude matrix parameterized by the CRPs is

$$R(\boldsymbol{\rho}) = \frac{1}{1+\boldsymbol{\rho}^T\boldsymbol{\rho}}\{(1-\boldsymbol{\rho}^T\boldsymbol{\rho})I_{3\times3} + 2\boldsymbol{\rho}\boldsymbol{\rho}^T - 2[\boldsymbol{\rho}\times]\}$$

The kinematics for the CRPs are given by

$$\dot{\boldsymbol{\rho}} = \frac{1}{2}\left(I_{3\times3} + [\boldsymbol{\rho}\times] + \boldsymbol{\rho}\boldsymbol{\rho}^T\right)\boldsymbol{\omega}$$

and the inverse kinematics by

$$\boldsymbol{\omega} = \frac{2}{1+\boldsymbol{\rho}^T\boldsymbol{\rho}}\left(I_{3\times3} - [\boldsymbol{\rho}\times]\right)\dot{\boldsymbol{\rho}}$$

The CRPs are an unconstrained minimal parameterization that avoid the computation of transcendental functions, but also introduce a singularity at $\phi = \pm\pi$. In addition, the CRPs are 1-to-1 for $\phi \in (-\pi, +\pi)$. However, this nonsingular range is quite limiting for unconstrained rotations and there is no escaping the singularities due to their 1-to-1 nature.

2.4.6 Modified Rodrigues Parameters (MRPs)

For many applications, a singularity at $\phi = \pm\pi$, as present with the CRPs, may not be acceptable. The modified Rodrigues parameters (MRPs) shift this singularity to $\phi = \pm 2\pi$, by defining

$$\boldsymbol{\sigma} \triangleq \frac{\boldsymbol{q}}{1+q_4} = \tan\frac{\phi}{4}\boldsymbol{n}$$

The attitude matrix expressed with the MRPs is

$$R(\sigma) = I_{3\times3} + \frac{8[\sigma\times]^2 - 4(1-\sigma^T\sigma)[\sigma\times]}{(1+\sigma^T\sigma)^2}$$

The kinematics for the MRPS are given by

$$\dot{\sigma} = \frac{1}{4}\left[\left(1-\sigma^T\sigma\right) I_{3\times3} + 2\left[\sigma\times\right] + 2\sigma\sigma^T\right]\omega$$

and inverse kinematics are

$$\omega = \frac{4}{\left(1+\sigma^T\sigma\right)^2}\left[\left(1-\sigma^T\sigma\right) I_{3\times3} - 2\left[\sigma\times\right] + 2\sigma\sigma^T\right]$$

The mathematical singularities present in the MRPs can be overcome by switching to the shadow set, defined by

$$\sigma_s \triangleq \frac{-\boldsymbol{q}}{1-q_4},$$

when a singularity is near. The shadow set results from the 2-to-1 non-uniqueness of the MRP representation. That is, the MRPs and their shadow set represent the same attitude, but encounter singularities at different orientations, where the MRP is valid for $\phi \in (-2\pi, +2\pi)$ and the shadow set for $\phi \in (0, +4\pi)$.

2.4.7 Stereographic Orientation Projections (SOPs)

Stereographic projections are a geometric technique for projecting a unit sphere onto a plane. A projection point is chosen on the surface of the unit sphere as well as a projection plane. All points on the unit sphere are then mapped to this plane. This idea has been extended to develop new attitude parameterizations by projection of the 4-dimensional sphere that is formed by the constraint surface of the unit quaternion, onto the 3-dimensional hyperplane. This concept was first used by Marandi and Modi to develop the MRPs [61] as seen in Figure 2-4B. Schaub extended this work to develop the symmetric stereographic orientation parameters (SSOPs) and asymmetric

stereographic orientation parameters (ASOPs) [62]. The SSOPs are defined by

$$\zeta = \frac{\boldsymbol{q}}{q_4 - a},$$

where the constant, a, dictates the location of the singularity and is defined by

$$a = \cos\frac{\phi_s}{2}.$$

The ASOPs do not have such a compact form, as the geometric singularity depends on both the axis and angle.

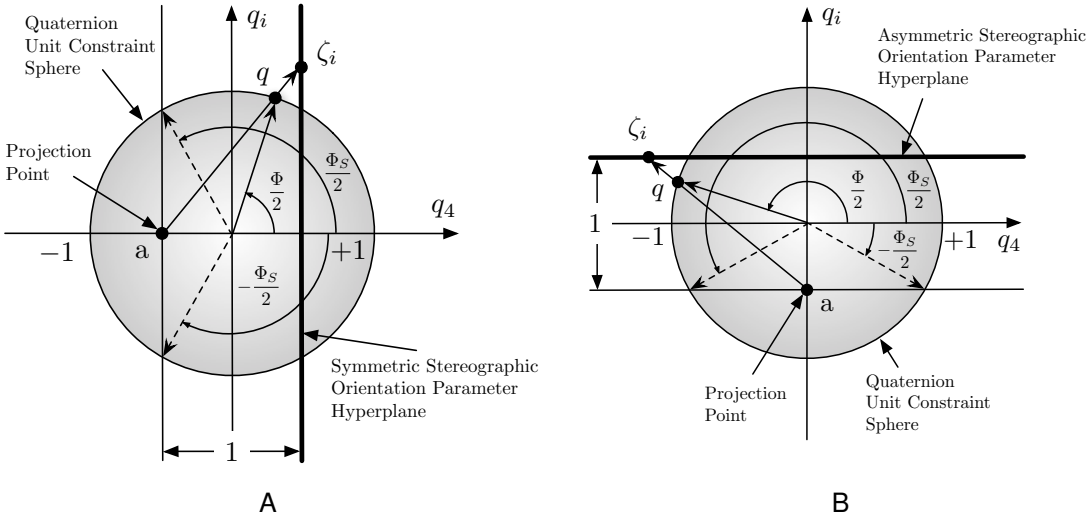

Figure 2-3. Stereographic projections (adapted from [62]). A) Symmetric stereographic projections. B) Asymmetric stereographic projections.

The CRPs and MRPs are subsets of SSOPs having a projection point along the q_4 axis. It is clear from Figure 2-4A that the CRPs are singular at $\Phi = \pm\pi$, where the projection of point $q = [0, 0, 0, -1]^T$ on the three-sphere representing the quaternion unity constraint is at infinity on the CRP hyperplane. Similarly, from Figure 2-4B, it is clear that the MRP is singular at $\Phi = \pm 2\pi$. Other parameters can be developed using stereographic projections

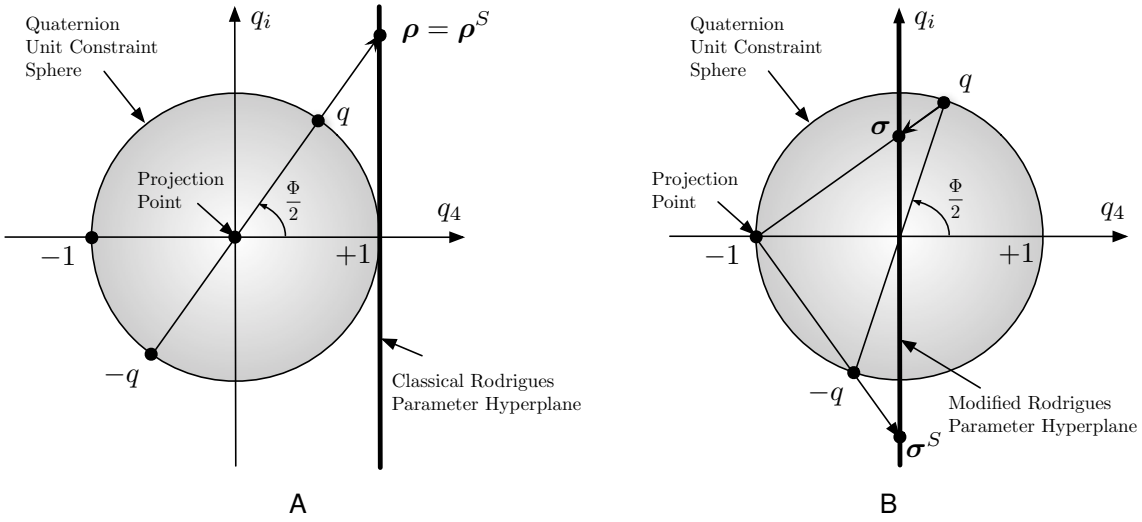

Figure 2-4. Common stereographic projections (adapted from [58]). A) Stereographic projection of CRPs. B) Stereographic projection of MRPs.

2.4.8 Generalized Cayley Transformation

The Cayley transform provides a mapping from the group of skew-symmetric matrices, $so(3)$, to the special orthogonal matrices, $SO(3)$. As the attitude matrix belongs to $SO(3)$, this mapping has significance for attitude representations. The Cayley transform is defined as

$$R(Q) = (I_{3\times3} - Q)(I_{3\times3} + Q)^{-1} = (I_{3\times3} - Q)^{-1}(I_{3\times3} + Q),$$

where Q is a skew-symmetric matrix. By letting $Q = [\boldsymbol{\rho}\times]$, the Cayley transform generates the CRPs. From this observation and the development of the MRPs, Tsiotras used complex analysis with conformal mappings to motivate the extension of the Cayley transform to higher orders with the generalized Cayley transform, given in Eq. 2–8 [63]. These higher order transforms were shown to parameterize the attitude matrix and expand the singularity-free region of applicability of the CRP and MRP attitude parameterizations.

$$R(Q) = (I_{3\times3} - Q)^n(I_{3\times3} + Q)^{-n}$$

Therefore, the second order Cayley transform ($n = 2$) with $Q = [\boldsymbol{\sigma}\times]$ yields the MRPs. An example higher-order parameterization was developed with the 4^{th} order Cayley transform ($n = 4$) using $Q = [\boldsymbol{\tau}\times]$, where

$$\boldsymbol{\tau} \triangleq \frac{\boldsymbol{q}}{1 + q_4 \pm \sqrt{2(1 + q_4)}} = \tan\frac{\phi}{8}\boldsymbol{n}.$$

This fourth order parameterization places the singularities at $\pm 4\pi$. However, Cayley-based parameterizations of order $n \geq 3$ have disadvantages in the kinematical description, where the differential equation is no longer defined by a second-order polynomial expression, as is the case with the CRPs and MRPs.

2.4.9 Vectorial Attitude Parameterizations

Recently, the family of minimal attitude parameterizations known as the vectorial attitude parameterizations [59] were introduced and subsequently characterized with respect to a nonlinearity and singularity index [64]. This generalization of minimal attitude parameterization was used to generate a family of attitude control laws to shape the transient performance of the nonlinear attitude dynamics [65]. With the exception of the Euler angles, all of the minimal parameterizations reviewed in this section belong to a larger class of attitude parameters known as the vectorial attitude parameterizations. The vectorial attitude parameterizations follow from Euler's rotation theorem and have the form,

$$\boldsymbol{r} = r(\phi)\,\boldsymbol{n}, \tag{2–8}$$

which map the axis of rotation, $\boldsymbol{n}$, and angle of rotation, ϕ, through the generating function, $r(\phi)$, to construct a family of minimal attitude parameterizations. Two important families of vectorial attitude parameterizations are the sine and tangent families, defined as

$$\boldsymbol{r}_{s,m} = k_s \sin\frac{\phi}{2m} \tag{2–9}$$

and

$$\boldsymbol{r}_{t,m} = k_t \tan \frac{\phi}{2m}, \tag{2–10}$$

respectively, where k_s and k_t are scaling coefficients and m is the order. All orders of the Rodrigues parameters belong to the tangent family, such that the higher-order Rodrigues parameters are defined by Eq. 2–10 when $k_t = 1$. Whereas the higher-order sine parameters (HOSPs) are defined by Eq. 2–9 when $k_s = 1$. However, an arbitrary number of vectorial parameterizations exist – of which, examples based on higher-order azimuthal projections were defined in Reference [64].

As described in [64], the generating function $r(\phi)$ will produce attitude parameterizations belonging to two singularity classes based on whether the generating function is locally bi-Lipschitz continuous within $\phi \in [-\pi, +\pi]$. Class I parameterizations are not locally bi-Lipschitz continuous within $\phi \in [-\pi, +\pi]$ and thus have unavoidable kinematic singularities within $\phi \in [-2\pi, +2\pi]$. These parameterizations are the most prohibitive for control, estimation, and data fusion when unconstrained motion is encountered. Classic examples of Class I parameterizations are the first-order sine and tangent vectorial parameterizations, which for $k_s, k_t = 1$ are referred to as the orthographic parameters (OPs) and classical Rodrigues parameters (CRPs), respectively. Class II parameterizations are locally bi-Lipschitz continuous within $\phi \in [-\pi, +\pi]$ and thus have avoidable singularities for all rotation angles through use of the shadow parameterizations. Shadow parameterizations are constructed through the projections based on the two-to-one nature of the quaternion. The use of the shadows produces a globally-singularity free parameterization. Examples of Class II parameterizations are the second-order sine and tangent parameterizations, which for $k_s, k_t = 1$ are known as the Lambert parameters (LPs) and modified Rodrigues parameters (MRPs), respectively. One other parameterization of note is the rotation vector, also known as

the equidistant orientation parameters (EOPs), which is a parameterization defined $\forall \phi \in \mathbb{R} - \{0\}$ (i.e., all points on the real line except zero).

A summary of several vectorial attitude parameterizations is given in Table 2-1, with definitions for the generating function and associated parameterization of the attitude matrix and singularity class. In this table, the fourth-order Rodrigues parameters (FRPs) are an example of the general HORPs.

Table 2-1. Several generating functions and the vectorial parameterization of $SO(3)$

Name	$\boldsymbol{r}$	$r(\phi)$	$R(\boldsymbol{r})$
EOPs	$\boldsymbol{\phi}$	ϕ	$\cos\phi I_{3\times3} - \frac{\sin\phi}{\phi}[\boldsymbol{\phi}\times] + \frac{(\cos\phi-1)}{\phi^2}\boldsymbol{\phi}\boldsymbol{\phi}^T$
CRPs	$\boldsymbol{\rho}$	$\tan\frac{\phi}{2}$	$\frac{1}{(1+\rho^2)}\left(\left(1-\rho^2\right)I_{3\times3} - 2[\boldsymbol{\rho}\times] + 2\boldsymbol{\rho}\boldsymbol{\rho}^T\right)$
MRPs	$\boldsymbol{\sigma}$	$\tan\frac{\phi}{4}$	$\frac{1}{\left(1+\sigma^2\right)^2}\left(\left(1-6\sigma^2+\sigma^4\right)I_{3\times3} - 4\left(1-\sigma^2\right)[\boldsymbol{\sigma}\times] + 8\boldsymbol{\sigma}\boldsymbol{\sigma}^T\right)$
FRPs	$\boldsymbol{\tau}$	$\tan\frac{\phi}{8}$	$\frac{\left\{\left[\left(1+\tau^2\right)^4 - 32(1-\tau^2)^2\tau^2\right]I_{3\times3} - 8\left(1-\tau^2\right)\left(1-6\tau^2+\tau^4\right)[\boldsymbol{\tau}\times] + 32\left(1-\tau^2\right)^2\boldsymbol{\tau}\boldsymbol{\tau}^T\right\}}{\left(1+\tau^2\right)^4}$
HORPs	$\boldsymbol{\rho}_m$	$\tan\frac{\phi}{2m}$	$\left(I_{3\times3} - [\boldsymbol{\rho}_m\times]\right)^m\left(I_{3\times3} + [\boldsymbol{\rho}_m\times]\right)^{-m},\ (m>2)$
OPs	$\boldsymbol{\eta}$	$\sin\frac{\phi}{2}$	$\left(1-2\eta^2\right)I_{3\times3} - 2\left(1-\eta^2\right)^{\frac{1}{2}}[\boldsymbol{\eta}\times] + 2\boldsymbol{\eta}\boldsymbol{\eta}^T$
LPs	$\boldsymbol{\lambda}$	$\sin\frac{\phi}{4}$	$\left(1-8\lambda^2+8\lambda^4\right)I_{3\times3} - 4\left(1-2\lambda^2\right)\left(1-\lambda^2\right)^{\frac{1}{2}}[\boldsymbol{\lambda}\times] + 8\left(1-\lambda^2\right)\boldsymbol{\lambda}\boldsymbol{\lambda}^T$

Description of the shadow parameterizations resulting from stereographic projections of the unit quaternion onto the tangent plane have been discussed in detail in [62, 63]. These results were generalized for the vectorial attitude parameterization by Tanygin [64], in which the left shadow parameters are defined by $r(\phi + 2\pi)$ and the right shadows by $r(\phi - 2\pi)$. Furthermore, using these shadows, a global nonsingular attitude representation, $\tilde{\boldsymbol{r}}$ is defined by

$$\tilde{\boldsymbol{r}} = \begin{cases} r(\phi+2\pi)\boldsymbol{n}, & \phi \in (\pi, 2\pi] \\ r(\phi)\boldsymbol{n}, & \phi \in [-\pi, +\pi] \\ r(\phi-2\pi)\boldsymbol{n}, & \phi \in [-2\pi, -\pi) \end{cases} \tag{2–11}$$

It is important to note that although the higher-order Rodrigues parameters and higher-order sine parameters will have further bifurcations leading to many shadow sets, only the shadows described above are necessary as they span $\phi \in [-2\pi, +2\pi]$, which is all that is necessary due to the periodic invariance of attitude.

Taking the time-derivative of Eq. 2–8 yields

$$\dot{\boldsymbol{r}} = \dot{r}(\phi)\boldsymbol{n} + r(\phi)\dot{\boldsymbol{n}}, \tag{2–12}$$

where $\dot{r}(\phi) = (\partial r/\partial\phi)\dot{\phi}$. Applying the known relationships for the axis-angle representation time-derivatives, $\dot{\phi}$ and $\dot{\boldsymbol{n}}$ [57], to Eq. 2–12, leads to the forward kinematics form

$$\dot{\boldsymbol{r}} = G(\boldsymbol{r})\omega, \tag{2–13}$$

where $G(\boldsymbol{r})$ is the forward kinematical Jacobian, which is in general a nonlinear function of $\boldsymbol{r}$. A table of several forward kinematical Jacobian matrices are provided in Reference [64]. However, for data fusion, the inverse kinematics Jacobian is of interest, which relates the angular velocity to the time-derivative of the parameterization through

$$\omega = H(\boldsymbol{r})\dot{\boldsymbol{r}}$$

where $H(\boldsymbol{r}) = G^{-1}(\boldsymbol{r})$ is the inverse kinematical Jacobian. The kinematics and inverse kinematics for various orders of the Rodrigues parameters have already been summarized in Sections 2.4.5-2.4.8.

Table 2-2 provides a summary of the inverse kinematical Jacobian for all of the vectorial attitude parameterizations described in Table 2-1. This table will be extensively used in the developments in Chapter 4, where proper choice of attitude parameterization for data fusion is based on the linearity of the inverse kinematics Jacobian.

2.5 Summary of Attitude Parameterizations

Table 2-3 summarizes the properties of the attitude parameterizations presented in Section 2.4. The properties of interest are whether the parameterization is global, unique, constrained, nonlinear, or contains singularities. Global refers to its ability to describe all attitudes and related kinematic conditions and is directly tied to the presence of singularities. Uniqueness refers to whether the parameterization is 1-to-1

Table 2-2. Inverse kinematics Jacobian for several vectorial attitude parameterizations

Name	$\boldsymbol{r}$	$H(\boldsymbol{r})$
EOPs	ϕ	$\frac{\sin\phi}{\phi} I_{3\times3} - \frac{(1-\cos\phi)}{\phi^2}[\phi\times] + \frac{1}{\phi^2}\left[1 - \frac{\sin\phi}{\phi}\right]\phi\phi^T$
CRPs	ρ	$\frac{2}{(1+\rho^2)}(I_{3\times3} - [\rho\times])$
MRPs	σ	$\frac{4}{(1+\sigma^2)^2}\left[(1-\sigma^2) I_{3\times3} - 2[\sigma\times] + 2\sigma\sigma^T\right]$
FRPs	τ	$\frac{8}{(1+\tau^2)^4}\left[(1-\tau^2)(1-6\tau^2+\tau^4) I_{3\times3} - 4(1-\tau^2)[\tau\times] + 2(5-2\tau^2+\tau^4)\tau\tau^T\right]$
HORPs	ρ_m	$\frac{2\rho}{\rho_m(1+\rho^2)} I_{3\times3} - \frac{2\rho^2}{\rho_m^2(1+\rho^2)}[\rho_m\times] + \left[\frac{2m}{\rho_m^2(1+\rho_m^2)} - \frac{2\rho}{\rho_m^3(1+\rho^2)}\right]\rho_m\rho_m^T$
OPs	η	$\frac{2}{(1-\eta^2)^{\frac{1}{2}}}\left[(1-\eta^2) I_{3\times3} - (1-\eta^2)^{\frac{1}{2}}[\eta\times] + \eta\eta^T\right]$
LPs	λ	$\frac{4}{(1-\lambda^2)^{\frac{1}{2}}}\left[(1-2\lambda^2)(1-\lambda^2) I_{3\times3} - 2(1-\lambda^2)^{\frac{3}{2}}[\lambda\times] + (3-2\lambda^2)\lambda\lambda^T\right]$

with attitude matrix. Constraints refer to the redundancy in the parameterization with respect to the rotational degrees-of-freedom. Nonlinearity describes the form of the kinematical differential equations, where “Transc.” refers to transcendental functions and “Poly.” refers to polynomials of at least order two. Finally, singularity refers to the type of singularity, where “Geo.” refers to the singularity being of geometric origin, in which not all attitudes can be described by the parameterization, “Kin.” refers to kinematic singularities, in which the parameterization or angular velocity escapes to infinity in finite time at certain attitudes, and “Null state” refers to singularities where the null state does not exist for the parameterization.

Table 2-3. Properties comparison of several attitude parameterizations

Name	Symbol	Global	Unique	Const.	Nonlinearity	Singularity
Attitude Matrix	R	Yes	Yes	6	Linear	Nonsingular
Euler Angles	$(\theta_1, \theta_2, \theta_3)$	No	No	0	Transc.	Kin.
Axis-Angle	$(\boldsymbol{n}, \phi)$	No	No	1	Transc.	Null state
Quaternions	q	Yes	No	1	Linear	Nonsingular
EOPs	ϕ	No	No	1	Transc.	Null state
CRPs	ρ	No	Yes	0	Poly.	Geo./Kin.
MRPs	σ	No	No	0	Poly.	Geo./Kin.
FRPs	τ	No	No	0	Poly.	Geo./Kin.
HORPs	ρ_m	No	No	0	Poly.	Geo./Kin.
OPs	η	No	Yes	0	Poly.	Geo./Kin.
LPs	λ	No	No	0	Poly.	Geo./Kin.
HOSPs	η_m	No	No	0	Poly.	Geo./Kin.

The attitude matrix is the only unique global nonsingular description of attitude. However, nine parameters are necessary in its description. The unit quaternion reduces

the number of parameters down to four and is still globally nonsingular with linear kinematics. However, it still requires a single constraint and is non-unique. The unit quaternion properties are sufficient for many applications in attitude estimation and control as described in Section 2.7 and Chapter 3, respectively. However, in Chapter 4, minimal parameterizations will be utilized for fast and efficient attitude data fusion algorithm development, due to their unconstrained nature.

2.6 Attitude Dynamics

Focus is now turned towards attitude dynamics and control. The rotational motion of rigid spacecraft is governed by Euler's Second Law of Motion. This law states that the time-rate-of-change of the angular momentum of a rigid body, $\boldsymbol{H}$, about the center of mass (or an inertial point), point c, is equivalent to the net external torque, τ, acting on the body. That is,

$$\dot{\boldsymbol{H}}_c = \tau \tag{2–14}$$

In general, the external torque in orbit will consist of the control input, as well as disturbance torques originating from environmental factors and non-environmental factors. Examples of environmental factors solar pressure, aerodynamic drag, magnetic interactions, and inertia-induced gravity gradients. An example non-environmental factor is mass ejection [66].

Equation 2–14 is a vector expression. When the vectors are represented in body coordinates, the attitude dynamics equations are

$$J\dot{\omega} = \tau - [\omega\times]J\omega$$

where J is the constant inertia matrix, ω is the angular velocity of the body relative to the inertial frame, and $[\omega\times]J\omega$ is referred to as the gyroscopic torque.

Given knowledge of the spacecraft inertia as well as the environmental effects, the attitude dynamics can be used as a plant model for the design of a control input to affect

the attitude motion. Designing a control input to track another spacecraft for attitude resource sharing is the focus of Section 2.7.

2.7 Attitude Tracking Control

Up to this point in the discussion, attitude parameterizations have been reviewed that describe the relative orientation of a coordinate frame fixed to a spacecraft with respect to another frame of interest. Additionally, attitude dynamics have been reviewed that describe the evolution of the spacecraft's rotational motion. Utilizing these results, the next section is concerned with controlling the rotational motion of a spacecraft to accomplish some mission specific objective. Specifically, attitude control is necessary for attitude resource sharing, as it allows one spacecraft to point a sensor at another spacecraft to capture measurements about the observed spacecraft's states. In the discussion that follows, coordinate frames are developed to describe a desired orientation for resource sharing and a nonlinear control law is developed to ensure that the desired signal is tracked.

2.7.1 Desired Coordinate Frames

An attitude tracking controller requires knowledge of the kinematics of a reference quaternion trajectory with derivatives up to second order. The following section defines several important reference vectors and their associated natural coordinate system. The reference vectors are then used to derive an associated coordinate frame. Finally, the kinematic relationships for each of these coordinate frames are developed. Unless otherwise specified, it is assumed that the primary pointing direction is aligned with the $\boldsymbol{X}_B$ and, if necessary, a secondary pointing direction is aligned with the $\boldsymbol{Z}_B$. Additionally, unless otherwise specified, all derivatives, denoted by $\dot{(\,)}$ are assumed to be inertial. This assumption is valid in most cases, as most reference vectors are known in inertial coordinates and therefore can be differentiated directly without the need to introduce further coordinate transformations.

2.7.1.1 Relative spacecraft sharing frame (SH)

The primary objective of attitude resource sharing is transform of attitude information between two spacecraft. Therefore, the objective is to track an attitude trajectory that points the chief's relative attitude sensor at a neighboring deputy to capture relative attitude information. This pointing direction is defined by the relative position vector. In the context of this section, the relative position vector is denoted by ρ, which is a standard convention. However, it should not be confused with the CRPs in the broader discussions in other chapters. To uniquely define the basis triad, a secondary pointing vector will remain general and is denoted by $\boldsymbol{\Lambda}$. Projections ensure the orthogonality of this basis. For example, the primary goal is to sense another spacecraft, but the secondary objective may be to have an orthogonal face of the spacecraft that is sun-pointing. In that case, if $\boldsymbol{\Lambda}$ is defined as the position vector from the body to the sun, $\boldsymbol{r}_{B/\odot}$, then the $\boldsymbol{Z}_{sh}$ will be as close to sun-pointing while pursuing the primary objective which is defined by the $\boldsymbol{X}_{sh}$ pointing along the relative position vector. This definition also maintains the orthogonality of the bases vectors. Therefore, the sharing frame, shown in Figure 2-5A, is defined by the orthonormal basis vectors, $\{\boldsymbol{X}_{sh}, \boldsymbol{Y}_{sh}, \boldsymbol{Z}_{sh}\}$, where

$$\boldsymbol{X}_{sh} = \frac{\rho}{\|\rho\|}, \quad \boldsymbol{Y}_{sh} = \frac{\boldsymbol{\Lambda} \times \boldsymbol{X}_{sh}}{\|\boldsymbol{\Lambda} \times \boldsymbol{X}_{sh}\|}, \quad \boldsymbol{Z}_{sh} = \boldsymbol{X}_{sh} \times \boldsymbol{Y}_{sh}.$$

2.7.1.2 Ground target frame (T)

The ground target frame ($\mathcal{F}_T$), shown in Figure 2-5B, is defined by the orthonormal basis vectors, $\{\boldsymbol{X}_t, \boldsymbol{Y}_t, \boldsymbol{Z}_t\}$. A Cartesian coordinate system is attached to T and aligned with the basis vectors defined by

$$\boldsymbol{Z}_t = \frac{\upsilon}{\|\upsilon\|}, \quad \boldsymbol{Y}_t = \frac{\boldsymbol{Z}_t \times \boldsymbol{\Lambda}}{\|\boldsymbol{Z}_t \times \boldsymbol{\Lambda}\|}, \quad \boldsymbol{X}_t = \boldsymbol{Y}_t \times \boldsymbol{Z}_t \tag{2–15}$$

where υ is the position vector from the center of mass of the chief to the ground target point. If the mission of the spacecraft is to track ground targets but periodically share

measurements with another spacecraft flying in formation, then choosing $\boldsymbol{\Lambda} = \boldsymbol{\rho}$, ensures the chief's attitude is as near to the secondary sharing objective as possible, while satisfying the primary objective.

Recall from Eq. 2–15 that the target quaternion is defined by the relative target vector $\boldsymbol{\upsilon}$ and a mission-dependent vector that closes the triad. By choosing the mission-dependent vector to be the relative position vector from chief to deputy, $\boldsymbol{\rho}$, the spacecraft will track the target while also minimizing the slew to share. Since $\boldsymbol{\upsilon}$ is measured in inertial coordinates, the matrix

$$R_t = [\boldsymbol{X}_t \ \boldsymbol{Y}_t \ \boldsymbol{Z}_t]^T. \tag{2–16}$$

defines the attitude matrix from the inertial coordinates to the target coordinates. The process outlined in Reference [57] is used for converting the attitude matrix in Eq. 2–16 to the quaternion relating the target frame to the inertial frame. Therefore, the target quaternion, q_t, is known.

The reference attitude trajectory is defined by the basis vectors

$$\boldsymbol{Z}_t = \frac{\boldsymbol{\upsilon}}{(\boldsymbol{\upsilon}^T\boldsymbol{\upsilon})^{1/2}}, \quad \boldsymbol{Y}_t = \frac{[\boldsymbol{Z}_t\times]\,\boldsymbol{\rho}}{(([\boldsymbol{Z}_t\times]\,\boldsymbol{\rho})^T([\boldsymbol{Z}_t\times]\,\boldsymbol{\rho}))^{1/2}}, \quad \boldsymbol{X}_t = [\boldsymbol{Y}_t\times]\,\boldsymbol{Z}_t$$

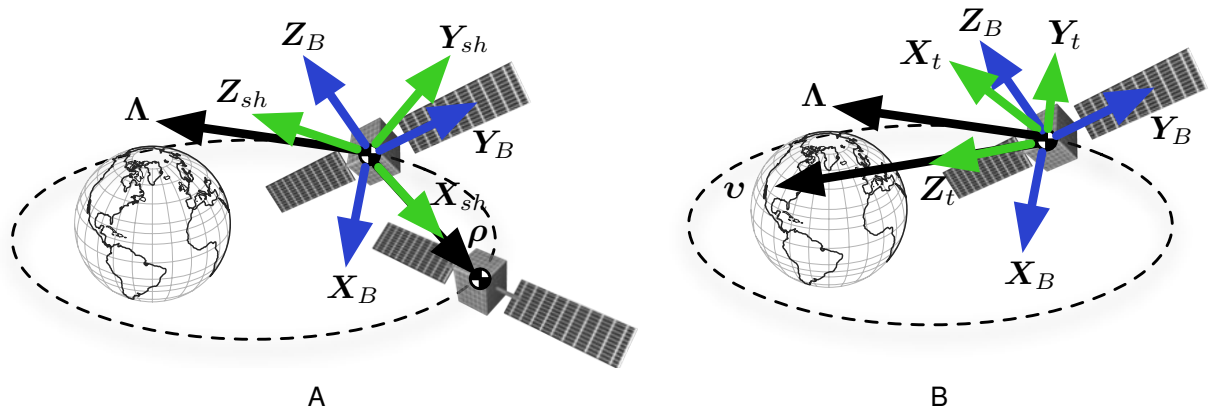

Figure 2-5. Tracking coordinate frames. A) Body and sharing frames. B) Body and target frames.

2.7.2 Desired Quaternion Kinematics

The attitude matrix was constructed from a set of time-varying basis vectors. By differentiating these vectors, the derivatives of the attitude matrix can be constructed. Then, the derivatives of the attitude parameterization of interest can be backed out and used in the controller synthesis.

2.7.2.1 Relative spacecraft sharing frame kinematics

It assumed that all unit vectors and their derivatives are known in inertial coordinates. If this is not the natural description, then transformations must be substituted into these expressions. Therefore, the sharing frame basis vectors are

$$\boldsymbol{X}_{sh} = \frac{\boldsymbol{\rho}}{\left(\boldsymbol{\rho}^T\boldsymbol{\rho}\right)^{1/2}},\ \boldsymbol{Y}_{sh} = \frac{\left[\boldsymbol{\Lambda}\times\right]\boldsymbol{X}_{sh}}{\left(\left(\left[\boldsymbol{\Lambda}\times\right]\boldsymbol{X}_{sh}\right)^T\left(\left[\boldsymbol{\Lambda}\times\right]\boldsymbol{X}_{sh}\right)\right)^{1/2}},\ \boldsymbol{Z}_{sh} = \left[\boldsymbol{X}_{sh}\times\right]\boldsymbol{Y}_{sh}.$$

Since the unit vectors are represented in inertial coordinates and define by desired coordinate frame, they naturally form the attitude matrix defined by

$$R_{sh} = \left[\boldsymbol{X}_{sh}\ \boldsymbol{Y}_{sh}\ \boldsymbol{Z}_{sh}\right]^T,$$

which transforms vectors represented in inertial coordinates to sharing frame coordinates.

Taking the time-derivative of the basis vectors yields

$$\dot{\boldsymbol{X}}_{sh} = \left(\frac{\dot{\boldsymbol{\rho}}\boldsymbol{\rho}^T - \boldsymbol{\rho}\dot{\boldsymbol{\rho}}^T}{\boldsymbol{\rho}^T\boldsymbol{\rho}}\right)\boldsymbol{X}_{sh}$$

$$\dot{\boldsymbol{Y}}_{sh} = \left[\frac{\left(\left[\dot{\boldsymbol{\Lambda}}\times\right]\boldsymbol{X}_{sh} + \left[\boldsymbol{\Lambda}\times\right]\dot{\boldsymbol{X}}_{sh}\right)\left(\left[\boldsymbol{\Lambda}\times\right]\boldsymbol{X}_{sh}\right)^T - \left(\left[\boldsymbol{\Lambda}\times\right]\boldsymbol{X}_{sh}\right)\left(\left[\dot{\boldsymbol{\Lambda}}\times\right]\boldsymbol{X}_{sh} + \left[\boldsymbol{\Lambda}\times\right]\dot{\boldsymbol{X}}_{sh}\right)^T}{\left(\left[\boldsymbol{\Lambda}\times\right]\boldsymbol{X}_{sh}\right)^T\left(\left[\boldsymbol{\Lambda}\times\right]\boldsymbol{X}_{sh}\right)}\right]\boldsymbol{Y}_{sh}$$

$$\dot{\boldsymbol{Z}}_{sh} = \left[\dot{\boldsymbol{X}}_{sh}\times\right]\boldsymbol{Y}_{sh} + \left[\boldsymbol{X}_{sh}\times\right]\dot{\boldsymbol{Y}}_{sh},$$

which can be used to produce the derivative of the attitude matrix. Taking the second derivative of the unit vectors leads to

$$\ddot{\boldsymbol{X}}_{sh} = \left(\frac{\dot{\rho}\rho^T - \rho\dot{\rho}^T - 2\dot{\rho}^T\rho I_{3x3}}{\rho^T\rho} \right) \dot{\boldsymbol{X}}_{sh} + \left(\frac{\ddot{\rho}\rho^T - \rho\ddot{\rho}^T}{\rho^T\rho} \right) \boldsymbol{X}_{sh}$$

$$\ddot{\boldsymbol{Y}}_{sh} = \frac{1}{([\boldsymbol{\Lambda}\times]\boldsymbol{X}_{sh})^T([\boldsymbol{\Lambda}\times]\boldsymbol{X}_{sh})} \left\{ \left[\left(\left[\dot{\boldsymbol{\Lambda}}\times\right]\boldsymbol{X}_{sh} + [\boldsymbol{\Lambda}\times]\dot{\boldsymbol{X}}_{sh} \right)([\boldsymbol{\Lambda}\times]\boldsymbol{X}_{sh})^T - ([\boldsymbol{\Lambda}\times]\boldsymbol{X}_{sh}) \left(\left[\dot{\boldsymbol{\Lambda}}\times\right]\boldsymbol{X}_{sh} \right.\right.\right.$$
$$\left. + [\boldsymbol{\Lambda}\times]\dot{\boldsymbol{X}}_{sh} \right)^T - 2 \left(\left[\dot{\boldsymbol{\Lambda}}\times\right]\boldsymbol{X}_{sh} + [\boldsymbol{\Lambda}\times]\dot{\boldsymbol{X}}_{sh} \right)^T ([\boldsymbol{\Lambda}\times]\boldsymbol{X}_{sh}) I_{3x3} \Big] \dot{\boldsymbol{Y}}_{sh} + \Big[\left(\left[\ddot{\boldsymbol{\Lambda}}\times\right]\boldsymbol{X}_{sh} + 2\left[\dot{\boldsymbol{\Lambda}}\times\right]\dot{\boldsymbol{X}}_{sh} \right.$$
$$\left.\left. + [\boldsymbol{\Lambda}\times]\ddot{\boldsymbol{X}}_{sh} \right)([\boldsymbol{\Lambda}\times]\boldsymbol{X}_{sh})^T - ([\boldsymbol{\Lambda}\times]\boldsymbol{X}_{sh}) \left(\left[\ddot{\boldsymbol{\Lambda}}\times\right]\boldsymbol{X}_{sh} + 2\left[\dot{\boldsymbol{\Lambda}}\times\right]\dot{\boldsymbol{X}}_{sh} + [\boldsymbol{\Lambda}\times]\ddot{\boldsymbol{X}}_{sh} \right)^T \Big] \boldsymbol{Y}_{sh} \right\}$$

$$\ddot{\boldsymbol{Z}}_{sh} = \left[\ddot{\boldsymbol{X}}_{sh}\times\right]\boldsymbol{Y}_{sh} + 2\left[\dot{\boldsymbol{X}}_{sh}\times\right]\dot{\boldsymbol{Y}}_{sh} + [\boldsymbol{X}_{sh}\times]\ddot{\boldsymbol{Y}}_{sh},$$

which can be used to construct the second derivative of the attitude matrix.

2.7.2.2 Ground target frame kinematics

Note: If the relative position vector is measured directly, it will be known in body coordinates. In this case, the relative position vector must be transformed to inertial coordinates for this analysis. Alternatively, if differences in inertial position are utilized, no additional modification is necessary. Also, the target vector, υ, is derived from a given target position in inertial coordinates and the absolute position of the spacecraft, known inertially. Therefore, the target vector and its derivatives are all known in inertial coordinates. Using this knowledge, the inertial derivatives are formulated as

$$\dot{\boldsymbol{Z}}_t = \left(\frac{\dot{\upsilon}\upsilon^T - \upsilon\dot{\upsilon}^T}{\upsilon^T\upsilon} \right) \boldsymbol{Z}_t$$

$$\dot{\boldsymbol{Y}}_t = \left[\frac{([\dot{\boldsymbol{Z}}_t\times]\rho + [\boldsymbol{Z}_t\times]\dot{\rho})([\boldsymbol{Z}_t\times]\rho)^T - ([\boldsymbol{Z}_t\times]\rho)([\dot{\boldsymbol{Z}}_t\times]\rho + [\boldsymbol{Z}_t\times]\dot{\rho})^T}{([\boldsymbol{Z}_t\times]\rho)^T([\boldsymbol{Z}_t\times]\rho)} \right] \boldsymbol{Y}_t$$

$$\dot{\boldsymbol{X}}_t = \left[\dot{\boldsymbol{Y}}_t\times\right]\boldsymbol{Z}_t + [\boldsymbol{Y}_t\times]\dot{\boldsymbol{Z}}_t$$

and the derivative of the attitude matrix is

$$\dot{R}_t = [\dot{\boldsymbol{X}}_t \;\; \dot{\boldsymbol{Y}}_t \;\; \dot{\boldsymbol{Z}}_t]^T.$$

The second derivative of the bases vectors is

$$\ddot{\boldsymbol{Z}}_t = \left(\frac{\dot{\upsilon}\upsilon^T - \upsilon\dot{\upsilon}^T - 2\dot{\upsilon}^T\upsilon I_{3x3}}{\upsilon^T\upsilon}\right)\dot{\boldsymbol{Z}}_t + \left(\frac{\ddot{\upsilon}\upsilon^T - \upsilon\ddot{\upsilon}^T}{\upsilon^T\upsilon}\right)\boldsymbol{Z}_t$$

$$\begin{aligned}\ddot{\boldsymbol{Y}}_t = \frac{1}{([\boldsymbol{Z}_t\times]\,\rho)^T([\boldsymbol{Z}_t\times]\,\rho)}\Big\{&\left[(\left[\dot{\boldsymbol{Z}}_t\times\right]\rho + [\boldsymbol{Z}_t\times]\,\dot{\rho})([\boldsymbol{Z}_t\times]\,\rho)^T - ([\boldsymbol{Z}_t\times]\,\rho)(\left[\dot{\boldsymbol{Z}}_t\times\right]\rho + [\boldsymbol{Z}_t\times]\,\dot{\rho})^T\right.\\ &- 2(\left[\dot{\boldsymbol{Z}}_t\times\right]\rho + [\boldsymbol{Z}_t\times]\,\dot{\rho})^T([\boldsymbol{Z}_t\times]\,\rho)I_{3x3}\Big]\,\dot{\boldsymbol{Y}}_t + \Big[(\left[\ddot{\boldsymbol{Z}}_t\times\right]\rho + 2\left[\dot{\boldsymbol{Z}}_t\times\right]\dot{\rho} + [\boldsymbol{Z}_t\times]\,\ddot{\rho})([\boldsymbol{Z}_t\times]\,\rho)^T\\ &- \left([\boldsymbol{Z}_t\times]\,\rho\right)(\left[\ddot{\boldsymbol{Z}}_t\times\right]\rho + 2\left[\dot{\boldsymbol{Z}}_t\times\right]\dot{\rho} + [\boldsymbol{Z}_t\times]\,\ddot{\rho})^T\Big]\,\boldsymbol{Y}_t\Big\}\end{aligned}$$

$$\ddot{\boldsymbol{X}}_t = \left[\ddot{\boldsymbol{Y}}_t\times\right]\boldsymbol{Z}_t + 2\left[\dot{\boldsymbol{Y}}_t\times\right]\dot{\boldsymbol{Z}}_t + [\boldsymbol{Y}_t\times]\,\ddot{\boldsymbol{Z}}_t$$

and the second derivative of the attitude matrix is

$$\ddot{R}_t = [\ddot{\boldsymbol{X}}_t\ \ddot{\boldsymbol{Y}}_t\ \ddot{\boldsymbol{Z}}_t]^T.$$

Recall that the second derivative of ρ can be computed from the Clohessy-Wiltshire-Hill (CWH) equations and transformed to inertial coordinates. A brief review of the CWH equations is given in Section 2.7.3.

Using attitude matrix and its derivatives, the corresponding angular velocity and derivative of angular velocity for the target, required by the controller, can be computed as

$$[\omega_d\times] = -\dot{R}_t R_t^T$$

$$[\dot{\omega}_d\times] = -\ddot{R}_t R_t^T - \dot{R}_t\dot{R}_t^T$$

2.7.3 Clohessy-Wiltshire-Hill (CWH) Equations

Since the tracking signal for resource distribution utilizes information about the relative position vector, this section reviews the description of relative position. Determining the relative motion and its derivatives when both satellites have knowledge of their inertial position and derivatives results from a differencing in their respective states. However, if relative position is measured onboard the spacecraft, then the description of motion takes place in a non-inertial coordinate system. Under these

conditions, there are many relative motion formulations, which make varying assumptions. The most common relative motion equations are the Clohessy-Wiltshire-Hill (CWH) equations [67, 68]. The CWH equations assume that the one spacecraft is bounded to a circular orbit and that all other spacecraft are in close proximity with respect to their distance from the Earth. Other relative motion formulations exists that relax the circular orbit requirements. The most studied is the Tschauner-Hempel equations [68, 69]. That formulation, however makes use of the true-anomaly domain to obtain closed-form solutions. In practice, the true anomaly must still be mapped to the time domain solving Kepler's Equation, which has no closed-form solution [70]. The assumptions for the CWH equations to hold will always be valid for the interest of this research, but the circular assumption can be relaxed to make use of the results for general elliptical motion of the chief.

Given the chief follows a circular orbit and the deputies are in close proximity to the chief, the CWH equations describes the motion of the relative position vector in LVLH coordinates. The CWH equations are shown in state-space form, in Eq. (2–17),

$$\begin{bmatrix} \dot{x} \\ \dot{y} \\ \dot{z} \\ \ddot{x} \\ \ddot{y} \\ \ddot{z} \end{bmatrix} = \begin{bmatrix} 0 & 0 & 0 & 1 & 0 & 0 \\ 0 & 0 & 0 & 0 & 1 & 0 \\ 0 & 0 & 0 & 0 & 0 & 1 \\ 3n^2 & 0 & 0 & 0 & 2n & 0 \\ 0 & 0 & 0 & -2n & 0 & 0 \\ 0 & 0 & -n^2 & 0 & 0 & 0 \end{bmatrix} \begin{bmatrix} x \\ y \\ z \\ \dot{x} \\ \dot{y} \\ \dot{z} \end{bmatrix} \tag{2–17}$$

The state transition matrix (STM) of the CWH equations has an analytic form, due to its linear time-invariant structure, and is expressed as

$$\Phi(t,t_0)=\begin{bmatrix} 4-3c_{nt} & 0 & 0 & s_{nt}/n & 2(1-c_{nt})/n & 0 \\ -6(nt-s_{nt}) & 1 & 0 & -2(1-c_{nt})/n & 4s_{nt}/n-3t & 0 \\ 0 & 0 & c_{nt} & 0 & 0 & s_{nt}/n \\ 3ns_{nt} & 0 & 0 & c_{nt} & 2s_{nt} & 0 \\ -6n(1-c_{nt}) & 0 & 0 & -2s_{nt} & -3+4c_{nt} & 0 \\ 0 & 0 & -ns_{nt} & 0 & 0 & c_{nt} \end{bmatrix},$$

where n is the mean motion of the chief orbit, and $c_{nt} \triangleq cos(nt)$ and $s_{nt} \triangleq sin(nt)$. The state transition matrix representation of the CWH equations is

$$\boldsymbol{x}(t)=\Phi(t,t_0)\boldsymbol{x}_0=\Phi(t-t_0)\boldsymbol{x}_0$$

given the initial state $\boldsymbol{x}_0=[x_0,y_0,z_0,\dot{x}_0,\dot{y}_0,\dot{z}_0]^T$.

If using the CWH equations, the relative position vector expressed in LVLH coordinates must be transformed to inertial coordinates and differentiated accordingly. Therefore, the attitude matrix from LVLH to inertial coordinates and its derivatives will enter into the desired kinematical representation.

After transforming the relative position and its derivatives into inertial coordinates, substitution into the desired attitude kinematic expressions yields a trajectory that can be tracked to point a relative sensor along the relative position vector.

2.7.4 Attitude Tracking Controller Derivation

The primary objective of the chief is to point its relative attitude sensor along the relative position vector joining itself with the deputy. This objective is satisfied when the body frame is aligned with the desired frame with zero relative angular velocity. Therefore the control objective is to drive the error quaternion, $q_e=[\boldsymbol{q}_e^T,q_{4e}]^T$, defined by Eq. 2–18, to the identity quaternion $[0,0,0,1]^T$ and the error angular velocity, defined by

Eq. 2–19, to zero.

$$q_e = q \otimes q_d^{-1} \tag{2–18}$$
$$= \left[\Xi(q_d^{-1})\ q_d^{-1}\right] q$$

$$\omega_e = \omega - R_{B/D}\omega_d, \tag{2–19}$$

The error states require q_d, which is the quaternion used to represent a desired orientation, ω_d, which is the desired angular velocity, and $R_{B/D}$, which is the attitude matrix from desired to body coordinates.

The attitude tracking controller must generate a stabilizing control input that drives the error quaternion and error angular velocity, asymptotically to the identity quaternion and zero, respectively. Given a state $\boldsymbol{x}$, Lyapunov's second method, also known as the "direct method", states that the existence of a Lyapunov candidate function (LCF) satisfying the following conditions

1. $V(\mathbf{0}) = 0$
2. $\lim_{\|\boldsymbol{x}\|\to\infty} V(\boldsymbol{x}) = \infty$
3. $V(\boldsymbol{x}) > 0,\ \forall\ \boldsymbol{x} - \{\mathbf{0}\}$
4. $\dot{V}(\boldsymbol{x}) < 0\ \forall\ \boldsymbol{x} - \{\mathbf{0}\}$

is sufficient to prove global asymptotic stability (GAS) to the equilibrium state, provided only one equilibrium state exists. Due to the 2-to-1 nature of the quaternions, MRPs, and other non-unique attitude parameterizations, the attitude tracking feedback controller using these representations can only be locally asymptotically stable (LAS). That is, there are two equilibria for the system. Additionally, attitude states are bounded and thus the Lyapunov function cannot be radially unbounded. However, due to the persistence of excitation, the trajectory will never remain trapped in the undesired

equilibrium state and all other attitude initial conditions will asymptotically approach the desired equilibrium.

A LCF is constructed in Eq. 2–20 that is both positive definite and radially unbounded. The choice of K as a scalar multiple of inertia matrix follows from the discussion in Reference [71].

$$V = \frac{1}{2}\omega_e^T K^{-1} J \omega_e + (1 - q_{4_e}^2), \ (\forall K > 0) \tag{2–20}$$

By taking the inertial derivative of V in Eq. 2–20, the Lyapunov derivative,

$$\dot{V} = \omega_e^T K^{-1} (\tau - [\omega\times] J\omega - J\dot{R}_{B/D}\omega_d - JR_{B/D}\dot{\omega}_d + Kq_{4e}\boldsymbol{q}_e) \tag{2–21}$$

can be shown to be negative definite with the control input

$$\tau = [\omega\times] J\omega + J\dot{R}_{B/D}\omega_d + JR_{B/D}\dot{\omega}_d - Kq_{4e}\boldsymbol{q}_e - C\omega_e, \ (\forall C > 0). \tag{2–22}$$

Therefore, the controller in Eq. 2–22 ensures that all of the sufficient conditions for Lyapunov stability [72] are met and the system is asymptotically stable except for the special case when $\omega_e = \mathbf{0}$ and $q_{4e} = 1$. Although the special case is unlikely due to perturbations, causing a persistence of excitation, the quaternion feedback control input is non-unique and provisions should be made when using this controller if that case is expected. Also, note that this control law requires that the desired quaternion is twice differentiable.

2.8 Summary

The requisite theory for attitude parameterizations, kinematics, dynamics, and control were developed in this chapter. The attitude parameterizations were compared based on their advantages and disadvantages with respect to several important properties. Specifically, the attitude matrix was shown to be without any deficiency in uniqueness or singularity, but at the expense of high redundancy and number of constraints. The quaternion is highly regarded due to its linearity and lack of singularity

and single redundancy. However, caution must be given to its non-uniqueness and proneness to wind-up in attitude control, as well as enforcement of its constraint. Finally, the vectorial attitude parameterizations were reviewed, as they are unconstrained and can be made to be globally nonsingular through use of their shadow sets.

Attitude resource sharing requires the chief to point a relative attitude sensor at its deputies to measure their relative states. In order to accomplish this objective, the second-order kinematics of the desired attitude were formulated to generate a reference trajectory for tracking control. A nonlinear tracking controller was derived through Lyapunov's direct method that made use of the unit quaternion parameterization and attitude matrix. These results are critical for sharing attitude information between the chief and deputies.

CHAPTER 3
DISAGGREGATED ATTITUDE ESTIMATION

The goal of inertial attitude estimation in a disaggregated system is for each spacecraft in the network to estimate the entire state of the network using only local information. In the disaggregated estimation scheme, the chief makes use of the relative attitude sensor to capture vector measurements to the deputy of interest. In addition, the chief estimates its inertial attitude. This chapter develops the theory for the chief to estimate a deputy's inertial attitude. In addition, the theory is presented for the deputy to estimate its inertial attitude, but using an augmented state vector to account for the other spacecraft in the network. Thus, the chief and deputies use the same state vector and the attitude estimation for the disaggregated system yields multiple estimates of the inertial states of the chief and each deputy, along with their cross-correlations. This method is beneficial when all information is combined through data fusion.

This chapter first reviews basic results in estimation and Kalman filtering. The remainder of the chapter is divided into two main sections. In the first of these sections, inertial attitude sensors and estimation are surveyed and reviewed. In the second of these sections, the extended Kalman filter equations for the disaggregated attitude estimation scheme are derived.

3.1 General Nomenclature

In this chapter, compact notation is needed to describe the measurement quantities and the state estimates. Particularly, unit vectors describing a direction are the primary measurements necessary for attitude systems, where the direction is specified by a line segment connecting two points. The frame in which those points are known is important as well as the basis in which that vector is represented. The notation for vector measurements is ${}^{A}\tilde{\boldsymbol{a}}_{B/A,i}|_{k}$, where $\boldsymbol{a}$ is the vector, the tilde represents a measured quantity, the left superscript denotes the frame that a is represented, and the right subscript states that the i^{th}-vector originates from a point fixed in in $\mathscr{F}_A$ and

ends in a point fixed in $\mathscr{F}_B$ at time index k. For parameterized attitude states, the notation is $\hat{x}^-_{B/A}|_k$, where x is the attitude state, the hat designates the quantity is a state estimate, the right superscript denotes the pre- or post-update status, and the right subscript states that the attitude is from $\mathscr{F}_B$ to $\mathscr{F}_A$ at time index k. The time index is often dropped, but included when relevant to the discussion. For the attitude matrix, the notation is $R_{B/A}$, where the right subscript states that R transforms vectors represented in $\mathscr{F}_A$ to $\mathscr{F}_B$. Finally, the following equivalency will be used extensively,

$$R_{B/A} = R(\hat{x}^-_{B/A}).$$

3.2 Inertial Attitude Sensors

Attitude sensors are devices that measure quantities used to determine attitude. Inertial attitude sensors measure vectors represented in the body frame, which with mathematical models of the vectors represented in the inertial frame are related through the inertial attitude matrix. Most attitude sensors measure angles that are used to determine a direction, and thus these sensors produce unit vector measurements. However, there are sensors that measure full vector information, that is, magnitude and direction. Also note, without loss of generality, the sensor frame and body frame are assumed to be aligned.

In the following section, measurement models, inertial reference models, and error sources are described for three typical inertial attitude sensors. Sun sensors and magnetometers are typically small, low power, sensors used for low precision attitude measurements. These sensors will be referred to as coarse attitude sensors. It is important to note that higher accuracy versions of these sensors exist, but typically at the expense of large SWaP. Star trackers are fine precision attitude sensors, which are typically higher in SWaP than the coarse sensors. Therefore, star trackers are ideally suited for attitude resource sharing in precision pointing applications.

3.2.1 Sun Sensors

Let the direction from the spacecraft to the sun be denoted by $\boldsymbol{s}$, and referred to as the sun vector. Sun sensors measure the sun vector with respect to the body frame, ${}^{B}\boldsymbol{s}$. Given a mathematical model of the inertially represented sun vector, ${}^{I}\boldsymbol{s}$, the inertial attitude matrix relates the measured and modeled sun vector through

$$ {}^{B}\boldsymbol{s} = R_{B/I}\,{}^{I}\boldsymbol{s}. $$

A sun sensor measures the sun vector with a measurement model given by

$$ {}^{B}\check{\boldsymbol{s}} = R_{B/I}\,{}^{I}\boldsymbol{s} + \eta_s, $$

where η_s is white zero-mean Gaussian noise. The random noise in a sun sensor is a result of several factors such as, Earth and Lunar albedo, reflections, surface area deviations, and temporal variations in the sun's electromagnetic radiation output [73, 74].

The inertial model for the sun vector is given as a function of the Julian date, which specifies the ecliptic longitude of the sun, λ_e and the obliquity of the ecliptic, ε [55]. The inertial sun vector is given by

$$ {}^{I}\boldsymbol{s} = \begin{bmatrix} \cos\lambda_e \\ \cos\epsilon \sin\lambda_e \\ \sin\epsilon \sin\lambda_e \end{bmatrix}. $$

3.2.2 Magnetometers

Let the magnetic field vector at a particular position be denoted by $\boldsymbol{m}$. Unlike the sun vector direction, which is a unit vector, the measured magnetic field vector is a true vector with magnitude and direction and must be normalized, which yields ${}^{B}\boldsymbol{m}$. Given a mathematical model of the normalized inertially represented magnetic field vector, ${}^{I}\boldsymbol{m}$, the inertial attitude matrix relates the measured and modeled magnetic field vector

through

$$^{B}\boldsymbol{m} = R_{B/I}\,{}^{I}\boldsymbol{m}.$$

A three-axis magnetometer (TAM) measures the magnetic field vector with a measurement model given by

$$^{B}\tilde{\boldsymbol{m}} = R_{B/I}\,{}^{I}\boldsymbol{m} + \eta_m,$$

where η_m is white zero-mean Gaussian noise. The random noise in the TAM is a result of internal magnetic and electric fields. In addition, errors that exist in the inertial model can be included in the measured noise. The presence of internal fields typically limits the use of magnetometers to lower orbits, as the strength of the field follows an inverse cube law with distance from the source. Systematic error sources such as sensor misalignment can exist, but can be accounted for through calibration.

Several inertial magnetic models exists, ranging from a low-order magnetic dipole model to high-order spherical harmonics models. One example is the World Magnetic Model (WMM) [75]. The WMM is a 12^{th}-order spherical harmonics model that includes core and surface effects as well as linear secular variations. The magnetic dipole model is given by

$$^{I}\boldsymbol{m} = \frac{R_{\oplus}^{3} H_0}{r^3}\left[\frac{3\left(\boldsymbol{d}^{T}\boldsymbol{r}\right)\boldsymbol{r}}{r^2} - \boldsymbol{d}\right],$$

where $R_{\oplus}$ is the radius of the Earth, H_0 is the magnetic field intensity computed from the first order coefficients of the WMM at the date and time of interest, $\boldsymbol{r}$ is the orbital position vector in inertial coordinates, and $\boldsymbol{d}$ is the direction of the dipole axis in inertial coordinates. The magnetic dipole mode is used as the inertial reference for all magnetic field vector simulations in this work.

3.2.3 Star Trackers

Star trackers, like sun sensors, measure directions to inertially known points. However, measurements of stars differ from the sun in that they can be approximated as inertially fixed points in space. Thus, the inertial representation star directions are independent of the spacecraft position.

Star trackers are highly accurate inertial attitude measuring devices, capable of sub-arcsec accuracies. Unlike sun sensors and magnetometers, star trackers can measure more than one reference vector. Star trackers take focal-plane measurements with a photovoltaic sensor, and map those measurements to the inertial location contained in an on-board star catalog. An example star tracker is shown in Figure 3-1A. Figure 3-1B shows a pin-hole model for a star tracker capturing line-of-sight measurements. The measurement model for the star tracker is

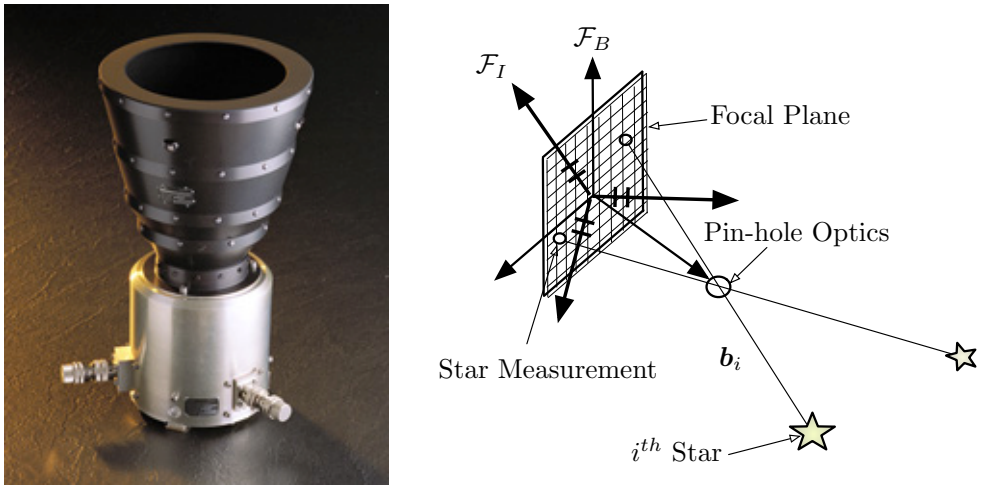

A B

Figure 3-1. Description of a typical star tracker. A) Star tracker hardware [76]. B) Star tracker measurement.

$$ {}^{I}\tilde{\boldsymbol{b}}_i = R_{B/I}\,{}^{I}\boldsymbol{b}_i + \boldsymbol{\eta}_s, $$

where ${}^{B}\tilde{\boldsymbol{b}}_i$ is the measured direction of the i^{th}-star in the body frame, $R_{B/I}$ is the attitude matrix mapping inertial to body coordinates, ${}^{I}\boldsymbol{b}_i$ is the cataloged direction of the i^{th}-star

in the inertial frame, and η_s is white zero-mean Gaussian noise that corrupts the measurement. Focal plane measurements are modeled through the vector form of the collinearity equations, such that

$$ {}^{B}\boldsymbol{b}_i = \frac{1}{\sqrt{f^2 + x_i^2 + y_i^2}} \begin{bmatrix} -x_i \\ -y_i \\ f \end{bmatrix}, \qquad {}^{I}\boldsymbol{b}_i = \begin{bmatrix} b_{x,i} \\ b_{y,i} \\ b_{z,i} \end{bmatrix} $$

where f is the focal length of the sensor and (x_i, y_i) are the coordinates of a measurement on the focal plane, and $(b_{x,i}, b_{y,i}, b_{z,i})$ are the inertial coordinates of a star identified in the catalog. Due to the narrow field-of-view of a typical star tracker, attitude accuracy about the boresight direction is typically an order of magnitude larger than the transverse directions [77].

Star trackers typically operate in two modes. The first mode is the attitude acquisition or "lost-in-space" mode, where stars are associated through pattern recognition algorithms with respect to a stored star catalog of known stars, which yields ${}^{I}\boldsymbol{b}_i$. The second mode tracks the already identified stars and increases accuracy by filtering phenomenon such as star streaking using angular velocity information. For the purposes of this discussion, it is assumed that the stars have already been identified and processed. The virtual star tracker charge-coupled device (CCD) model described in References [78, 79] is used in this research and shown in Figure 3-2. The geometry is reviewed to provide a complete picture of the vector measurements originating from a star tracker.

The vectors identifying the corners of the CCD as directed from the pinhole are denoted by $\{\boldsymbol{S}_1, \ldots, \boldsymbol{S}_4\}$. These corner vectors represented in right ascension and

declination coordinates are

$$\boldsymbol{S}_1^T = \begin{bmatrix} -\sin\vartheta \\ \cos\vartheta\sin\varepsilon \\ \cos\vartheta\cos\varepsilon \end{bmatrix},\ \boldsymbol{S}_2^T = \begin{bmatrix} \sin\vartheta \\ \cos\vartheta\sin\varepsilon \\ \cos\vartheta\cos\varepsilon \end{bmatrix},\ \boldsymbol{S}_3^T = \begin{bmatrix} \sin\vartheta \\ -\cos\vartheta\sin\varepsilon \\ \cos\vartheta\cos\varepsilon \end{bmatrix},\ \boldsymbol{S}_4^T = \begin{bmatrix} -\sin\vartheta \\ -\cos\vartheta\sin\varepsilon \\ \cos\vartheta\cos\varepsilon \end{bmatrix}$$

where ϑ is the right ascension and ε is the declination. These coordinates are related to the field-of-view (FOV), denoted by ϑ_x and ϑ_y, as

$$\vartheta = \frac{\vartheta_x}{2}, \quad \cos^2\varepsilon = \frac{\cos\vartheta_x + \cos\vartheta_y}{\cos\vartheta_x + 1}$$

The normal directions to the CCD are

$$\boldsymbol{n}_{12} = \frac{\boldsymbol{S}_1 \times \boldsymbol{S}_2}{\|\boldsymbol{S}_1 \times \boldsymbol{S}_2\|},\ \boldsymbol{n}_{23} = \frac{\boldsymbol{S}_2 \times \boldsymbol{S}_3}{\|\boldsymbol{S}_2 \times \boldsymbol{S}_3\|},\ \boldsymbol{n}_{34} = \frac{\boldsymbol{S}_3 \times \boldsymbol{S}_4}{\|\boldsymbol{S}_3 \times \boldsymbol{S}_4\|},\ \boldsymbol{n}_{41} = \frac{\boldsymbol{S}_4 \times \boldsymbol{S}_1}{\|\boldsymbol{S}_4 \times \boldsymbol{S}_1\|}.$$

A star vector, $\boldsymbol{S}_k$, is measured by the sensor if all of the following conditions are satisfied:

$$\boldsymbol{S}_k^T\boldsymbol{n}_{12} < 0,\ \boldsymbol{S}_k^T\boldsymbol{n}_{23} < 0,\ \boldsymbol{S}_k^T\boldsymbol{n}_{34} < 0,\ \boldsymbol{S}_k^T\boldsymbol{n}_{41} < 0.$$

Therefore, the virtual CCD is supplied with identified stars from pattern recognition and tracking algorithms to determine if the star is consistent with the CCD geometry. Given consistency, a measurement is captured, which is subject to errors sources such as misalignments, sensor noise, and ambient light.

3.2.4 Rate Gyroscope

The rate gyroscope is a device used to measure angular rates of a rigid body with respect to an inertial frame. Gyroscopes are often referred to as “inertial” sensors, as they make use of the inertia properties of the device. However, gyroscopes do not directly produce inertial attitude information. Instead, they integrate angular rate measurements and make use of a reference initial condition to yield inertial attitude. This makes the gyroscope a powerful tool for propagating inertial attitude with high

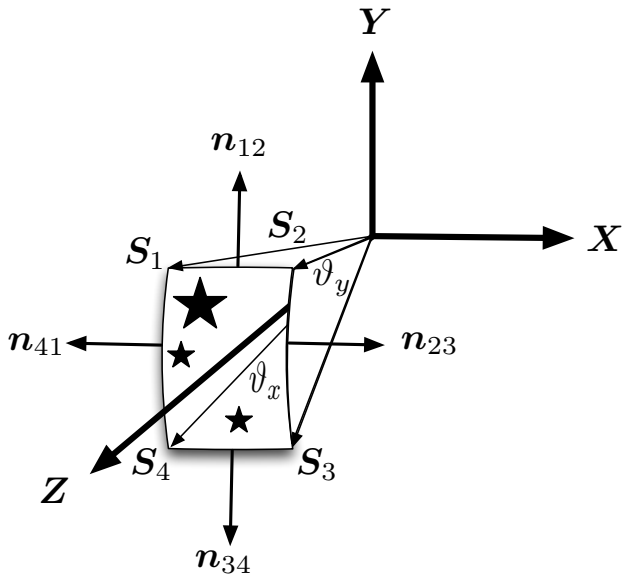

Figure 3-2. Description of the geometry of focal-plane measurements using a virtual CCD

accuracy. Farrenkopf's gyroscope model is assumed [80], which is given by

$$\omega = \tilde{\omega} - \beta - \eta_v \tag{3–1}$$

$$\dot{\beta} = \eta_u, \tag{3–2}$$

where β is the rate bias, η_v is zero-mean Gaussian white noise corruption, η_u is a zero-mean white Guassian random variable that represents random walk in the drift rate. The covariance statistics of the random variables for white noise corruption and the random walk are given by, $\sigma_v^2 I_{3\times3}$ and $\sigma_u^2 I_{3\times3}$, respectively.

3.3 Deterministic Attitude Determination

Given vector measurements originating from the sensors described in Section 3.2, the goal is to determine the spacecraft attitude relative to an inertial frame. Attitude determination is relevant in the context of resource sharing because it allows the spacecraft to initialize its attitude estimator. Adopting the terminology of Wertz [73], attitude determination is either deterministic or optimal. The deterministic solution is obtained when two non-parallel vectors are measured in one basis and are also

known in another. The TRIAD algorithm [81] is a deterministic attitude determination method, which constructs three orthonormal vectors using the familiar Gramm-Schmidt orthogonalization process known from linear algebra. Optimal attitude determination occurs when the system is overdetermined and is based in optimization theory and use the statistical properties of the sensors. An survey of several existing attitude determination algorithms is provided in Reference [82].

Deterministic attitude determination is defined when there are the minimum number of vector measurements necessary to compute the inertial attitude. Black's TRIAD algorithm solves the deterministic attitude determination problem, given two nonparallel unit vectors, ${}^{B}\boldsymbol{b}_1$ and ${}^{B}\boldsymbol{b}_2$ measured in the body and the corresponding unit vectors, ${}^{I}\boldsymbol{b}_1$ and ${}^{I}\boldsymbol{b}_2$, known in the inertial frame. The attitude matrix relates the body and inertial representations through

$$ {}^{B}\boldsymbol{b}_1 = R_{B/I}\,{}^{I}\boldsymbol{b}_1, \qquad {}^{B}\boldsymbol{b}_2 = R_{B/I}\,{}^{I}\boldsymbol{b}_2. $$

These vectors span a plane and overdetermine the system. Therefore, the TRIAD method extracts the minimum information from to the two vectors to construct three orthonormal vectors using the Gram-Schmidt orthogonalization process so that,

$$ \begin{aligned} {}^{B}\boldsymbol{b}'_1 &= {}^{B}\boldsymbol{b}_1, & {}^{B}\boldsymbol{b}'_2 &= \frac{[{}^{B}\boldsymbol{b}_1\times]\,{}^{B}\boldsymbol{b}_2}{\|[{}^{B}\boldsymbol{b}_1\times]\,{}^{B}\boldsymbol{b}_2\|}, & {}^{B}\boldsymbol{b}'_3 &= [{}^{B}\boldsymbol{b}'_1\times]\,{}^{B}\boldsymbol{b}'_2 \\ {}^{I}\boldsymbol{b}'_1 &= {}^{I}\boldsymbol{b}_1, & {}^{I}\boldsymbol{b}'_2 &= \frac{[{}^{I}\boldsymbol{b}_1\times]\,{}^{I}\boldsymbol{b}_2}{\|[{}^{I}\boldsymbol{b}_1\times]\,{}^{I}\boldsymbol{b}_2\|}, & {}^{I}\boldsymbol{b}'_3 &= [{}^{I}\boldsymbol{b}'_1\times]\,{}^{I}\boldsymbol{b}'_2. \end{aligned} $$

Using the newly defined prime vectors, the attitude from the TRIAD algorithm is given by

$$ R_{B/I} = \sum_{i=1}^{3} {}^{B}\boldsymbol{b}'_i \left({}^{I}\boldsymbol{b}'_i\right)^{T}. \tag{3–3} $$

Determining the attitude of a spacecraft from more than the minimum number of vector measurements is known as optimal attitude determination [73]. Solving for $R_{B/I}$ from vectors represented in two bases was originally posed by Wahba [83] as a batch

least squares problem with cost function given by

$$J(R_{B/I}) = \sum_{j=1}^{n} \| {}^{B}\boldsymbol{b}_j - R_{B/I}\, {}^{I}\boldsymbol{b}_j \|^2. \tag{3–4}$$

In the decades that followed the publishing of Wahba's problem, many solutions have been developed. The first major breakthrough came with the parameterization of the attitude matrix with the quaternion.

3.3.1 q-algorithm

Davenport's q-algorithm [84] provides a solution to the Wahba problem by parameterizing the attitude matrix with the Euler symmetric parameters and reducing the minimization problem to the eigenvalue-eigenvector problem. By rewriting the Wahba problem as

$$J(R_{B/I}) = \sum_{j=1}^{n} ({}^{B}\boldsymbol{b}_j - R_{B/I}\, {}^{I}\boldsymbol{b}_j)^T ({}^{B}\boldsymbol{b}_j - R_{B/I}\, {}^{I}\boldsymbol{b}_j). \tag{3–5}$$

Expanding the right-hand side of the cost function shows that the only term dependent on $R_{B/I}$ is $-2\sum_{j=1}^{n} {}^{B}\boldsymbol{b}_j{}^T R_{B/I}\, {}^{I}\boldsymbol{b}_j$. Therefore, the $R_{B/I}$ that minimizes $J(R_{B/I})$ is found by maximizing the gain function, so that

$$\underset{R_{B/I}}{\text{argmax}}\ g(R_{B/I}) = \sum_{j=1}^{n} {}^{B}\boldsymbol{b}_j{}^T R_{B/I}\, {}^{I}\boldsymbol{b}_j.$$

This problem can be shown to be equivalent to

$$\underset{R_{B/I}}{\text{argmax}}\ g(R_{B/I}) = tr(R_{B/I} V W^T),$$

where $W = \left[{}^{B}\boldsymbol{b}_1 \cdots {}^{B}\boldsymbol{b}_n \right]$ and $V = \left[{}^{I}\boldsymbol{b}_1 \cdots {}^{I}\boldsymbol{b}_n \right]$, due to the property of the trace operator. A $3x3$ matrix, B, known as the attitude profile matrix, can then be defined such that $B \triangleq WV^T$. The major breakthrough in the q-algorithm was the use of the parameterization of the attitude matrix with the Euler symmetric parameters. Using Eq. 2–7, the reduced gain function is

$$g(q) = (q_4^2 - \boldsymbol{q}^T\boldsymbol{q})\sigma + \boldsymbol{q}^T S \boldsymbol{q} + 2q_4 \boldsymbol{z}^T \boldsymbol{q}$$

where

$$\sigma \triangleq tr(B^T),\ S \triangleq B + B^T,\ \text{and } [\boldsymbol{z}\times] = B^T - B.$$

This leads to the quadratic form

$$g(q) = q^T K q, \tag{3–6}$$

where

$$K \triangleq \begin{bmatrix} S - \sigma I_{3\times 3} & \boldsymbol{z} \\ \boldsymbol{z}^T & \sigma \end{bmatrix}$$

Since K is a symmetric matrix, it has all real eigenvalues and is diagonalizable. Additionally, all eigenvalues can be shown to sum to zero.

Due to the quaternion unity constraint, this problem can be further posed as a constrained optimization problem, where

$$max\ g(q) = q^T K q$$

$$subject\ to\ q^T q - 1 = 0.$$

Using the method of Lagrange multipliers, an augmented gain function is given by

$$Kq = \lambda q, \tag{3–7}$$

which reduces to the classic eigenvalue-eigenvector problem. Substituting Kq into Eq. 3–6, yields the most important result

$$g(q) = \lambda.$$

Therefore, the optimal attitude quaternion eigenvector is associated with the maximum eigenvalue of K, such that

$$Kq_{opt} = \lambda_{max} q_{opt}.$$

Davenport used the power method [85] to determine the maximum eigenvalue, thus yielding the optimal quaternion. Other methods for solving for the maximum eigenvalue

exists, as well as other parameterizations of the attitude matrix, which have yielded fast and nearly exact solutions to the Wahba problem.

3.3.2 Other Attitude Determination Algorithms

Newer developments in attitude determination, since the breakthrough of the q-Davenport method, differ mainly in the parameterization of the attitude matrix and the associated approximations or numerical methods used to solve Wahba's problem with that parameterization. Shuster's QUaternion ESTimator (QUEST) algorithm [81, 86] was the first fast approximate solution to the Wahba problem presented in Eq. 3–4 by introducing the Gibbs vector parameterization and using $\lambda_{max} = 1$ as an initial guess for a Newton-Raphson solver to approximately determine the maximum eigenvalue of the attitude matrix. This method proved to be highly accurate approximation that rapidly converges to the optimal solution.

Other notable attitude determination techniques have been developed that span the parameterizations of attitude. The quaternion-based methods follow a similar approach to the q-algorithm but utilize other formulations for solving the eigenvector problem. Singular Value Decomposition (SVD) [87] provides an exact solution to the eigenvector problem but is computationally expensive. Other quaternion methods include, Filter QUEST [88], REQUEST [89], Estimator of the Optimal Quaternion (ESOQ) [90] and ESOQ2 [91], which provide closed-form solutions to the optimal attitude. A direct attitude matrix method was developed in Fast Optimal Attitude Matrix (FOAM) [92] that bypasses the parameterization to the quaternion altogether. EULER-2 and EULER-n [93] parameterize the attitude matrix in Wahba's problem using the axis-angle representation. In the past decade, MRPs have become more popular as an attitude representation and a solution to Wahba's problem was found by parameterization with the MRPs by Modified Rodrigues Attitude Determination (MRAD) [94]. An elegant solution was recently found, called Optimal Linear Attitude Estimator (OLAE) [95], which used the Cayley transform to transform Wahba's problem into a least squares problem

without having to solve the eigenvector problem. Most recently, the Cayley transform was applied to construct a higher-order method called the Cayley Attitude Technique [96].

There are many attitude determination techniques to choose from for resource sharing applications. Most of which seek an efficient solution to an eigenvalue-vector problem. However, the main purpose of attitude determination in this context is to initialize the attitude estimator, which is the focus of the next section.

3.4 Kalman Filter Review

Although attitude determination techniques are capable of determining the attitude directly from vector measurements, filtering the measurements can lead to significant improvements in accuracy [97]. Attitude estimation typically relies on Kalman filtering and thus a brief review of important properties of the Kalman filter are discussed.

All state information is measured or derived from measurements obtained with a sensor or from a system model. Measurements are never perfect and are subject to noise. Additionally, all models of a system are simplifications of physical reality, where unmodeled effects are termed perturbations. As a result, state information is never precisely known from measurements nor from models. State estimation is the process of determining system states from noisy measurements and perturbed models. An estimate is simply an approximation of the state given imperfect knowledge. An estimator is a mapping that takes in measurements and perturbed system dynamics and outputs an estimate of the system state. The most applied sequential estimator is the Kalman filter, which is a recursive optimal filter and one-step predictor.

Attitude resource sharing is intimately connected to the uncertainty in the attitude states of the chief and deputies. Uncertainty arises due to imperfect knowledge of a system state or process. Probability theory serves as the basis of handling uncertainty in this research. There are many methods of determining attitude based on vector

measurements. However, given knowledge of the uncertainty in the system and sensor measurements, better performance can be achieved through filtering.

Before presenting the Kalman filter equations, it is necessary to introduce several important properties of the system noise. The origin of sensor noise is similar to that of perturbations in a system dynamics model, where noise results from unmodeled effects in the sensor. Noise can either be correlated in time or uncorrelated in time, where white noise is uncorrelated in time and colored noise is correlated in time. In addition to correlation, the statistics of noise can be described by many probability density functions. All of the noise terms in this discussion will be modeled as Gaussian, as necessary for the optimality of the Kalman filter. The probability density function for a Gaussian random variable is fully described by its mean and covariance. Another property of interest is the linearity of the state evolution of the system. The Kalman filter is only optimal for linear systems, but this conflicts with the reality that most physical systems exhibit nonlinearity. Table 3-1 provides a summary of the assumptions necessary for the optimal Kalman filter.

Table 3-1. Assumptions for application of the Kalman filter

Characteristic	Assumption
Observability	The system states of interest must be observable
System Dynamics	Linear
Noise	Gaussian zero-mean probability density functions
	White noise sequences (independence in time)
	Independence of process and measurement noise

Given that all of the assumptions in Table 3-1 are true, the Kalman filter is the recursive state estimator and one-step predictor, which converges to the optimal state estimates under all meaningful metrics (e.g., mean squared error, mode, median, or variance) and achieves the Cramer-Rao lower bound [97–99].

Consider the continuous linear systems dynamics given by

$$\dot{\boldsymbol{x}}(t) = F(t)\boldsymbol{x}(t) + G(t)\boldsymbol{w}(t),$$

where $\boldsymbol{x}(t)$ is the state of the system, $F(t)$ is the state matrix, $G(t)$ is the process noise input matrix, and $\boldsymbol{w}(t)$ is the process noise. The statistics of the process noise are given by

$$E\left[\boldsymbol{w}(t)\right] = \mathbf{0},\ E\left[\boldsymbol{w}(t)\boldsymbol{w}(t)^T\right] = Q(t)\delta(t-\tau), \tag{3–8}$$

where $\delta(t-\tau)$ is the Dirac delta function and $E\left[\cdot\right]$ is the expectation operator. The linear measurement model is given by

$$\boldsymbol{y}(t) = H(t)\boldsymbol{x}(t) + \boldsymbol{v}(t),$$

where $y(t)$ are the measurements, $H(t)$ is the observation matrix, and $\boldsymbol{v}(t)$ is the white zero-mean sensor noise with statistics given by

$$E\left[\boldsymbol{v}(t)\right] = \mathbf{0},\ E\left[\boldsymbol{v}(t)\boldsymbol{v}(t)^T\right] = V(t)\delta(t-\tau). \tag{3–9}$$

Since $F(t)$ and $G(t)$ are time-varying functions, the state transition matrix (STM) is the solution to the following differential equation

$$\frac{\partial}{\partial t}\boldsymbol{\Phi}(t,t_0) = F(t)\boldsymbol{\Phi}(t,t_0), \quad \boldsymbol{\Phi}(t_0,t_0) = I_{n\times n},$$

For time invariant systems, the STM is given by

$$\boldsymbol{\Phi}(t,t_0) = e^{F(t-t_0)}.$$

For the remainder of discussions, it is assumed that the time step is sufficiently small for the STM to be accurately approximated by the matrix exponential. Additionally, the model above is for continuous linear systems, however in this research, *all systems will be assumed to be discrete as implemented on-board a spacecraft where a natural discretization occurs with the regular sampling of the rate gyroscope*.

The continuous dynamics can be discretized to yield

$$\boldsymbol{x}_{k+1} = \phi_k \boldsymbol{x}_k + \Upsilon_k \boldsymbol{w}_k, \tag{3–10}$$

where ϕ_k is the discrete state transition matrix and Υ_k is the discrete process noise matrix. Similarly, the discrete measurement model is given by

$$\boldsymbol{y}_k = H_k \boldsymbol{x}_k + \boldsymbol{v}_k, \tag{3–11}$$

where $\boldsymbol{v}_k \sim (\boldsymbol{0}, R_k)$. The discrete state transition matrix is given by

$$\boldsymbol{\Phi}_k = e^{F(t_k)\Delta t)}, \tag{3–12}$$

where

$$\Delta t = t_{k+1} - t_k. \tag{3–13}$$

However, the discrete process noise covariance matrix, $\mathcal{Q}$, requires the difficult computation of the integral given by

$$\mathcal{Q} = \int_{t_k}^{t_{k+1}} e^{F(\tau)(t_{k+1}-\tau)} G(\tau) Q(\tau) G^T(\tau) e^{F^T(\tau)(t_{k+1}-\tau)} d\tau \tag{3–14}$$

A good discussion on the discretized process noise covariance matrix is found in Reference [97], where the main numerical result comes from Reference [100]. A brief solution is provided.

First, the augmented matrix, $\mathcal{A}$, is formed by

$$\mathcal{A} = \begin{bmatrix} -F(t_k) & G(t_k)Q(t_k)G(t_k) \\ 0 & F^T(t_k) \end{bmatrix} \Delta t.$$

It was shown in Reference [100] that taking matrix exponential of $\mathcal{A}$ produces the discrete state transition matrix and process covariance matrix exactly for time invariant

systems, such that

$$e^{\mathcal{A}} = \begin{bmatrix} \mathcal{B}_{11} & \boldsymbol{\Phi}_k^{-1}\mathcal{Q} \\ 0_{n\times n} & \boldsymbol{\Phi}_k^T \end{bmatrix},$$

where $\mathcal{B}_{11}$ is not used any further. For time-varying systems, this solution is accurate for sufficiently small time steps. However, for small enough time steps the STM can be approximated with the following first-order models for the state-transition matrix given by

$$\boldsymbol{\Phi} = I_{n\times n} - F(t_k)\Delta t \tag{3–15}$$

and the process covariance matrix computed by

$$\mathcal{Q}_k = G(t_k)Q(t_k)G^T(t_k)\Delta t. \tag{3–16}$$

A rigorous derivation of the discrete Kalman filter can be found in References [98, 99]. The discrete Kalman filter contains several steps. The first step is the initialization of the filter, where the initial states and covariance are assumed based on knowledge of the problem of interest. Next the gain is computed. The Kalman gain is the driving force behind the optimality of the filter and balances uncertainty in the dynamics process and the measurement system. Next the states and covariance are updated using the computed gain which modifies the innovation to correct the predicted state from the prior information. Finally, the states and covariance are propagated (one-step prediction) to the next time step to be updated by future measurements. The final results of the Kalman filter are summarized in Table 3-2. Note, the state covariance matrix is denoted by P and defined by

$$P = E\left[\boldsymbol{x}\boldsymbol{x}^T\right]. \tag{3–17}$$

Table 3-2. Discrete Kalman filter

Initialize	$\hat{\boldsymbol{x}}(t_0) = \hat{\boldsymbol{x}}_0,\ P(t_0) = P_0$
Gain	$K_k = P_k^- H_k^T(\hat{\boldsymbol{x}}_k^-)\left[H_k(\hat{\boldsymbol{x}}_k^-)P_k^- H_k^T(\hat{\boldsymbol{x}}_k^-) + V\right]^{-1}$
Update	$P_k^+ = \left[I_n - K_k H_k(\hat{\boldsymbol{x}}_k^-)\right] P_k^-$ $\hat{\boldsymbol{x}}_k^+ = \hat{\boldsymbol{x}}_k^- + K_k\left[\tilde{\boldsymbol{y}}_k - \boldsymbol{h}_k(\hat{\boldsymbol{x}}_k^-)\right]$
Propagate	$P_{k+1}^- = \boldsymbol{\Phi}_k P_k^+ \boldsymbol{\Phi}_k^T + \mathcal{Q}_k$ $\hat{\boldsymbol{x}}_{k+1}^- = \boldsymbol{\Phi}_k \hat{\boldsymbol{x}}_k^+$

The Kalman filter is an important tool for linear systems, but the attitude system dynamics are nonlinear. Therefore, the Kalman filter cannot be directly applied. Handling this nonlinearity is the domain of the extended version of the Kalman filter.

3.5 Extended Kalman Filter

Consider the continuous nonlinear system that is affine in the process noise such that,

$$\dot{\boldsymbol{x}}(t) = f(\boldsymbol{x}(t)) + g(t)\boldsymbol{w}(t),$$

where $f(\boldsymbol{x}(t))$ is a nonlinear function of the states and $g(t)$ is a nonlinear process noise function. The measurement model is given by

$$\boldsymbol{y}(t) = h(\boldsymbol{x}(t)) + \boldsymbol{v}(t),$$

where $h(\boldsymbol{x}(t))$ is a nonlinear function of the states.

For nonlinear systems, such as the evolution of attitude for a rigid body, the Kalman filter does not produce the optimal estimate. However, there are modifications to the Kalman filter for nonlinear systems, such as the extended Kalman filter (EKF) [101, 102] and the unscented Kalman filter [48], as well as Monte Carlo-based methods [103], that seek a "pseduo-optimal" estimate. The extended Kalman filter was first applied

by Schmidt to the problem of inertial navigation in the 1960s [101], and satisfies the estimation requirements for the following developments.

Some aspects of the system nonlinearity are maintained in the extended Kalman filter, whereas other aspects require a linearization about the current state estimate – not to be confused with a linearization about the true state. A summary of the modifications to the Kalman filter is provided in Table 3-3.

Table 3-3. List of modifications to the Kalman filter for the extended Kalman filter

Step	Modification
Gain	Sensitivity matrix is formed from a linearization of the measurement function about the current state estimate
Update	The nonlinear measurement function is used in the innovation
Prediction	One-step predictor utilizes the nonlinear system dynamics
Propagation	Covariance propagation utilizes the Jacobian of the nonlinear system dynamics about the current state estimate

The extended Kalman filter follows the same steps as described for the Kalman filter, but with the modifications in Table 3-3 using the linearizations of the state matrix and observation matrix given by

$$F(t) = \frac{\partial}{\partial \boldsymbol{x}(t)} f(\boldsymbol{x}(t))|_{\hat{\boldsymbol{x}}(t)^-} \tag{3–18}$$

and

$$H(\hat{\boldsymbol{x}}_k^-) = \frac{\partial h}{\partial \boldsymbol{x}}|_{\hat{\boldsymbol{x}}_k^-}. \tag{3–19}$$

3.6 Extended Kalman Filter for Inertial Attitude Estimation

Attitude estimation has a long history, in which many of the major results were surveyed in Reference [104]. Like the differences seen in attitude determination, the structural differences in attitude estimation center around the choice of attitude parameterization. The primary challenges created by attitude states are associated with the multiplicative nature of error, attitude singularities, and enforcement of constraints. The unit quaternion is a popular parameterization for attitude estimation due to its many favorable properties (refer to Table 2-3). However, when carrying all components of the

quaternion, the unity constraint causes the state error covariance matrix to be singular. This is expected, as the states are no longer independent. If the state estimate and the true state are sufficiently close, then the attitude error state can be reduced to the 3-state attitude error vector.

In Reference [104] it was also shown that without loss of generality, the attitude EKF is assumed to make use of a rate gyroscope, which serves as a surrogate for a system dynamics model. Farrenkopf's gyroscope model is assumed, which includes a rate bias, white noise, and random walk in the drift rate. The states of interest for inertial attitude estimation are the unit quaternion, $q_{B/I}$, relating the attitude from the body to inertial frame and the gyro bias, β. In this section, the subscripts on the quaternion will be dropped, such that the attitude state is simply q. Therefore, the error state utilized in the extended Kalman filter are the attitude error vector, $\delta\boldsymbol{\alpha}$, and the bias error, $\Delta\boldsymbol{\beta}$.

The EKF requires an initialization of the quaternion estimate, $\hat{\boldsymbol{q}}$, as well as the gyroscope bias, β, and the state error covariance, P. The initial quaternion estimate should be as close as possible to the true quaternion, due to the linearization, and can be obtained from any of the attitude determination techniques described in Section 3.3. An accurate initial estimate maintains the linearity of the approximation and ensures that the filter will not diverge due to nonlinearities. The gyroscope bias can be measured on the ground prior to launch, but will typically be altered during launch and require updating. The derivation for the sensitivity matrix and discrete propagation are reviewed in the next section.

3.6.1 Sensitivity Matrix Derivation

Vector measurements take the form of

$$^{B}\tilde{\boldsymbol{b}}_i = R(q)\,{}^{I}\boldsymbol{b}_i + {}^{B}\boldsymbol{v}_i,$$

where the estimated measurement is given by

$$^{B}\hat{\boldsymbol{b}}_i^- = R(\hat{q}^-)\,{}^{I}\boldsymbol{b}_i.$$

The sensitivity is given by the difference between the unknown truth and the estimated measurement, such that

$$\begin{aligned} ^{B}\Delta\boldsymbol{b} &= {}^{B}\boldsymbol{b} - {}^{B}\hat{\boldsymbol{b}}^- \\ &= R(q)\,{}^{I}\boldsymbol{b}_i - R(\hat{q}^-)\,{}^{I}\boldsymbol{b}_i. \end{aligned}$$

From Eq. 2–2, the composition relating the true quaternion parameterized attitude matrix and the estimated state attitude matrix yields

$$R(q) = (I_{3\times 3} - [\delta\boldsymbol{\alpha}\times])\,R(\hat{q}^-).$$

The final form of the sensitivity equation for a single measurement is

$$^{B}\Delta\boldsymbol{b} = \left[\left(R(\hat{q}^-)\,{}^{I}\boldsymbol{b}_i\right)\times\right]\delta\boldsymbol{\alpha},$$

where the components of the attitude error are given by $\delta\boldsymbol{\alpha} = [e_1, e_2, e_3]^T$. Therefore, the sensitivity matrix for N vector measurements of the combined quaternion and bias state vector is

$$H_k(\hat{\boldsymbol{x}}_k^-) = \begin{bmatrix} \left[\left(R(\hat{q}^-)\,{}^{I}\boldsymbol{b}_1\right)\times\right] & 0_{3\times 3} \\ \vdots & \vdots \\ \left[\left(R(\hat{q}^-)\,{}^{I}\boldsymbol{b}_N\right)\times\right] & 0_{3\times 3} \end{bmatrix}.$$

These vector measurements have no sensitivity with respect to the bias. However, the bias is observable as a result of the coupling between the quaternion rates and the angular velocity.

3.6.2 Discrete Propagation Derivation

The last step on discrete propagation warrants further description. Using a power series approximation, the kinematic quantities are propagated by

$$\hat{\omega}_k^+ = \tilde{\omega}_k - \hat{\beta}_k^+ \tag{3–20}$$

$$\hat{\boldsymbol{q}}_{k+1}^- = \bar{\boldsymbol{\Omega}}(\hat{\omega}_k^+)\hat{\boldsymbol{q}}_k^+, \tag{3–21}$$

where

$$\bar{\boldsymbol{\Omega}}(\hat{\omega}_k^+) = \begin{bmatrix} \cos\left(\frac{1}{2}\|\hat{\omega}_k^+\|\Delta t\right) I_{3\times 3} - \left[\hat{\psi}_k^+\times\right] & \hat{\psi}_k^+ \\ -\hat{\psi}_k^{+T} & \cos\left(\frac{1}{2}\|\hat{\omega}_k^+\|\Delta t\right) \end{bmatrix}$$

and

$$\hat{\psi}_k^+ = \frac{\sin\left(\frac{1}{2}\|\hat{\omega}_k^+\|\Delta t\right)\hat{\omega}_k^+}{\|\hat{\omega}_k^+\|}.$$

The covariance is propagated by

$$P_{k+1}^- = \boldsymbol{\Phi}_k P_k^+ \boldsymbol{\Phi}_k^T + G_k Q_k G_k^T,$$

where

$$G_k = \begin{bmatrix} -I_{3\times 3} & 0_{3\times 3} \\ 0_{3\times 3} & I_{3\times 3} \end{bmatrix}$$

$$\boldsymbol{\Phi} = \begin{bmatrix} \boldsymbol{\Phi}_{11} & \boldsymbol{\Phi}_{12} \\ \boldsymbol{\Phi}_{21} & \boldsymbol{\Phi}_{22} \end{bmatrix},$$

and

$$\mathbf{\Phi}_{11} = I_{3\times3} - [\hat{\omega}\times]\frac{\{\sin(\|\hat{\omega}\|\Delta t)\}}{\|\hat{\omega}\|} + [\hat{\omega}\times][\hat{\omega}\times]\frac{\{1-\cos(\|\hat{\omega}\|\Delta t)\}}{\|\hat{\omega}\|^2}$$

$$\mathbf{\Phi}_{12} = [\hat{\omega}\times]\frac{\{1-\cos(\|\hat{\omega}\|\Delta t)\}}{\|\hat{\omega}\|^2} - I_{3\times3}\Delta t - [\hat{\omega}\times][\hat{\omega}\times]\frac{\{\|\hat{\omega}\|\Delta t - \sin(\|\hat{\omega}\|\Delta t)\}}{\|\hat{\omega}\|^3}$$

$$\mathbf{\Phi}_{21} = 0_{3\times3}$$

$$\mathbf{\Phi}_{22} = I_{3\times3},$$

and

$$Q_k = \begin{bmatrix} \left(\sigma_v^2\Delta t + \frac{1}{3}\sigma_u^2\Delta t^3\right) I_{3\times3} & -\left(\frac{1}{2}\sigma_u^2\Delta t^2\right) I_{3\times3} \\ -\left(\frac{1}{2}\sigma_u^2\Delta t^2\right) I_{3\times3} & \left(\sigma_u^2\Delta t\right) I_{3\times3} \end{bmatrix}.$$

A summary of the steps for the attitude EKF process is provided in Table 3-4.

3.6.3 Example Inertial Attitude EKF with a Magnetometer and Sun Sensors for Low Precision Pointing

An example coarse sun sensor and magnetometer-based extended Kalman filter was modeled and simulated using the initial state information given in Table 3-5, the time parameters in Table 3-6 and the initial state estimate information in Table 3-7. The spacecraft is placed in a low Earth orbit at approximately 400km altitude, where the magnetic field is strong, but also more uncertain, where the magnetometer has a standard deviation of 1°. The sun sensors are assumed to avoid eclipse throughout the simulation and have a standard deviation of 0.1°.

The sun vector model and dipole model described in Section 3.2 serve as the known inertial models for the measured vectors. Sun sensors and a magnetometer produce two vectors, which is the minimum necessary for three-axis attitude determination. The orbital period for this orbit is approximately 90 minutes. Figure 3-3 shows that due to the periodicity of the orbital motion, the sun vector and magnetic field vector periodically become nearly collinear twice per orbit, due to the symmetry of the magnetic field. When the measurements are near the collinear configuration, the error increases

Table 3-4. Inertial attitude extended Kalman filter

Initialize	$\hat{\boldsymbol{x}}(t_0) = \hat{\boldsymbol{x}}_0 = \left[\hat{q}_0^T, \hat{\beta}_0^T\right]^T$, $P(t_0) = P_0$ $\hat{q}(t_0) = \hat{q}_0$, $\hat{\beta}(t_0) = \hat{\beta}_0$
Gain	$K_k = P_k^- H_k^T(\hat{\boldsymbol{x}}_k^-)\left[H_k(\hat{\boldsymbol{x}}_k^-)P_k^- H_k^T(\hat{\boldsymbol{x}}_k^-) + V\right]^{-1}$ $H_k(\hat{\boldsymbol{x}}_k^-) = \begin{bmatrix} \left[\left(R(\hat{q}^-)^I\boldsymbol{b}_1\right)\times\right] & 0_{3\times3} \\ \vdots & \vdots \\ \left[\left(R(\hat{q}^-)^I\boldsymbol{b}_N\right)\times\right] & 0_{3\times3} \end{bmatrix}$
Update	$P_k^+ = \left[I_{3\times3} - K_k H_k(\hat{\boldsymbol{x}}_k^-)\right]P_k^-$ $\Delta\hat{\boldsymbol{x}}_k^+ = \left[\delta\hat{\alpha}_k^{+T}\ \Delta\hat{\beta}_k^{+T}\right]^T = K_k\left[\tilde{\boldsymbol{y}}_k - \boldsymbol{h}_k(\hat{\boldsymbol{x}}_k^-)\right]$ $\tilde{y}_k = \begin{bmatrix} {}^B\boldsymbol{b}_1 \\ \vdots \\ {}^B\boldsymbol{b}_N \end{bmatrix}$, $h_k(\hat{\boldsymbol{x}}_k^-) = \begin{bmatrix} R(\hat{q}^-)^I\boldsymbol{b}_1 \\ \vdots \\ R(\hat{q}^-)^I\boldsymbol{b}_N \end{bmatrix}$ $\hat{q}_k^+ = \hat{q}_k^- + \frac{1}{2}\Xi(\hat{q}_k^-)\delta\hat{\alpha}_k^+$ $\hat{\beta}_k^+ = \hat{\beta}_k^- + \Delta\hat{\beta}_k^+$
Propagate	$P_{k+1}^- = \boldsymbol{\Phi}_k P_k^+ \boldsymbol{\Phi}_k^T + G_k Q_k G_k^T$ $\hat{q}_{k+1}^- = \bar{\Omega}(\hat{\omega}_k^+)\hat{q}_k^+$ $\hat{\omega}_k^+ = \tilde{\omega}_k - \hat{\beta}_k^+$

Table 3-5. State initializations for coarse sensor inertial attitude simulations

Parameter	Value	Units
Inertia:		
J	$\mathrm{diag}\,(300, 100, 200)$	$\mathrm{kg}\cdot\mathrm{m}^2$
Initial States:		
$\boldsymbol{r}_0$	$[6778.1 \quad 0.0162 \quad 0.0080]^T$	m
$\boldsymbol{v}_0$	$[0.0000 \quad 6.6411 \quad 3.8342]^T$	m/s
q_0	$[0 \quad 1 \quad 0 \quad 0]^T$	–
ω_0	$[-0.003 \quad 0.002 \quad 0.004]^T$	rad/s

Table 3-6. Time parameters for coarse sensor inertial attitude simulations

Parameter	Value	Units
Time:		
Δt_{up}	1	*s*
Δt_{prop}	0.1	*s*
T	225	*min*

Table 3-7. State estimate initializations and sensor characteristics for coarse sensor inertial attitude simulations

Parameter	Value	Units
State Estimate:		
$\hat{q}_0$	$[0 \quad 1 \quad 0 \quad 0]^T$	–
β_0	10	deg/hr
σ_v	$10\sqrt{10} \times 10^{-7}$	$rad/s^{1/2}$
σ_u	$10\sqrt{10} \times 10^{-10}$	$rad/s^{3/2}$

as seen in Figure 3-5. Additionally, due to the angular velocity of the spacecraft shown in Figure 3-4, in this case resulting from torque-free motion, the error in each axis exhibits oscillatory behavior at the frequency of the angular velocity, as information is continuously passing between the body axes, given the slowly evolving vector measurements with the orbital motion. In these simulations, the attitude is estimated to sub-degree accuracy as evidenced by the 3-σ bounds in Figure 3-5.

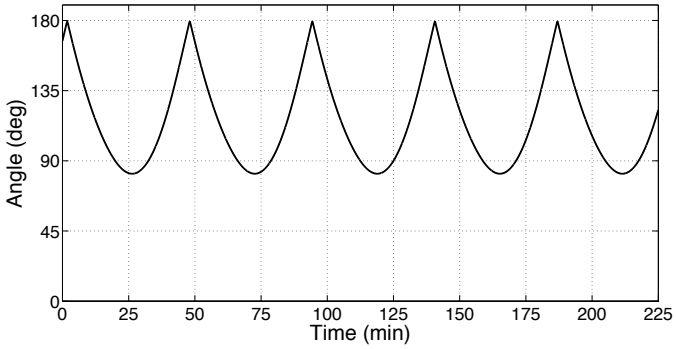

Figure 3-3. Magnetic field and sun vector collinearity for an example inertial attitude EKF with a magnetometer and sun sensors

3.6.4 Example Inertial Attitude EKF with a Star Tracker for High Precision Pointing

An example star tracker inertial attitude EKF was modeled and simulated in MATLAB [105]. These simulations make use of the star tracker model discussed in Section 3.2. The star catalog accompanying Reference [97, 106] was used with a star magnitude threshold of six. In these simulations the FOV of the star tracker is 6°, thus there is much less information available for rotations along the boresight, and less opportunity to observe stars far away from the boresight due to the narrow FOV. A

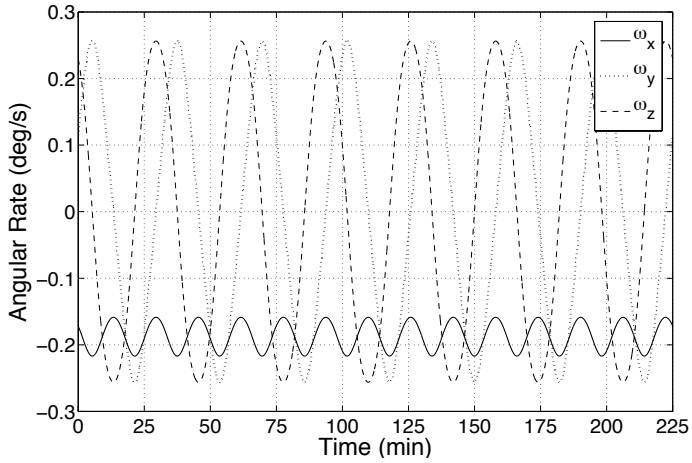

Figure 3-4. True body angular velocity for an example inertial attitude EKF with a magnetometer and sun sensors

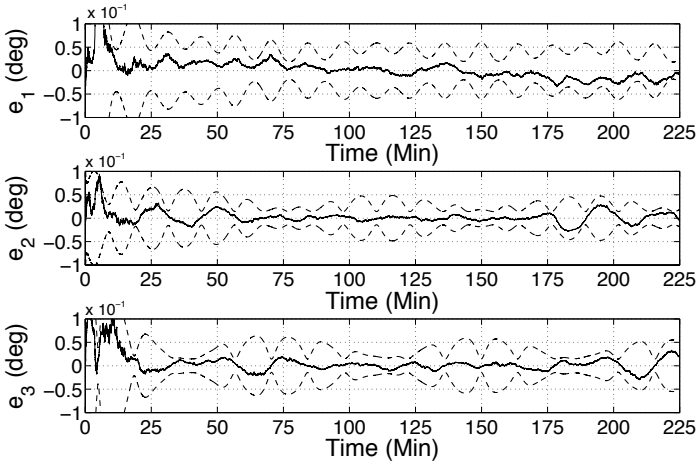

Figure 3-5. Quaternion error for an example inertial attitude EKF with a magnetometer and sun sensors

maximum of six stars were assumed to be able to be processed when measurements were taken. The star tracker model assumes that the star association problem has already been solved. The initial position and velocity states are slightly deviated from the previous example and the spacecraft states are summarized in Table 3-8. Initial state estimates are given in Table 3-9. The same time parameters listed in Table 3-6 were used in these simulations. In general, the accuracy of a star tracker will improve as the number of stars identified increases. Figure 3-6 depicts the number of stars available over the simulation, where it is assumed that the maximum number of stars

Table 3-8. State initializations for fine precision inertial attitude simulations

Parameter	Value	Units
Inertia:		
J	$\text{diag}\,(300, 100, 200)$	$\text{kg} \cdot \text{m}^2$
Initial States:		
$\boldsymbol{r}_0$	$[6778.1 \quad 0 \quad 0]^T$	km
$\boldsymbol{v}_0$	$[0 \quad 6.6412 \quad 3.8343]^T$	km/s
q_0	$[1 \quad 0 \quad 0 \quad 0]^T$	–
ω_0	$[0.001 \quad 0.001 \quad 0.001]^T$	rad/s

Table 3-9. State estimate initializations for fine precision inertial attitude simulations

Parameter	Value	Units
State Estimate:		
$\hat{q}_0$	$[1 \quad 0 \quad 0 \quad 0]^T$	–
β_0	0.1	deg/hr
σ_v	$\sqrt{10} \times 10^{-7}$	$rad/s^{1/2}$
σ_u	$\sqrt{10} \times 10^{-10}$	$rad/s^{3/2}$

is 6. From Figure 3-7, the error exhibits spikes when the number of stars is reduced. Another well known fact that is observed, is that measurements contain less attitude information about the sensor boresight than the transverse axes. That is, a line-of-sight measurement parallel with the boresight direction provides no information about the rotation about that axis. The star tracker is capable of producing highly accurate arc-second level accuracy, which is orders of magnitude better than the sun sensors and magnetometer-based attitude estimation shown in Figure 3-5. Arc-seconds will serve as the primary measure of attitude error in this work, where $1^\circ = 3600 arc - second$.

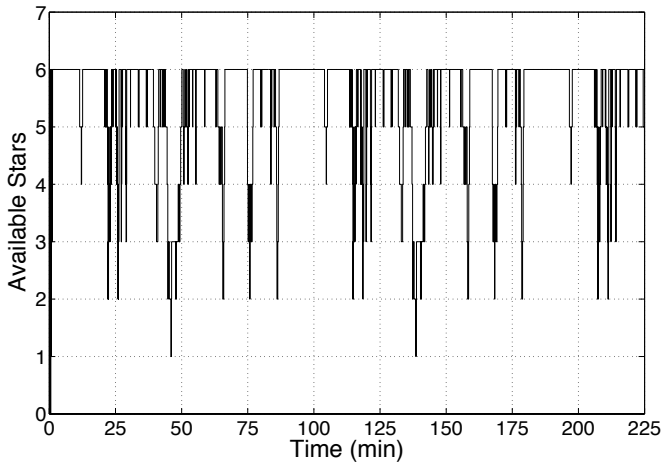

Figure 3-6. Available star vectors for an example inertial attitude EKF with a star tracker

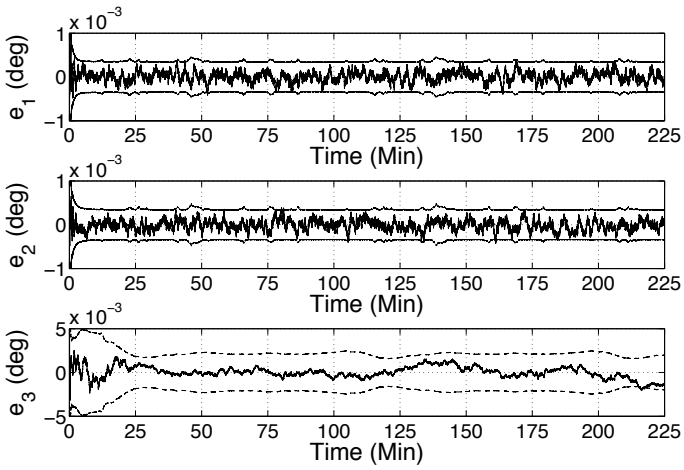

Figure 3-7. Quaternion error for an example inertial attitude EKF with a star tracker

3.7 Relative Attitude Sensors

Recall that attitude describes the orientation from one frame with respect to another. Relative attitude is concerned with the orientation of a frame fixed to a spacecraft with respect to a frame fixed to another spacecraft (or other non-inertial frame). Therefore, relative attitude sensors provide the capability to measure quantities that can be related back to relative attitude. All relative attitude sensors measure quantities that provide direction information. Examples of relative attitude sensors that provide a single direction are relative global positioning system (GPS) signals [107, 108] and various electromagnetic sensing devices such as radio frequency [26, 109]. An example of a relative attitude sensor capable of measuring multiple directions is vision-based navigation (VISNAV). This VISNAV sensor serves as the primary relative attitude sensor in this research and is discussed in more detail below.

Multi-direction relative attitude sensors are analogous to star trackers for inertial sensing. VISNAV sensors measure the direction to multiple fiducial points on an object of interest to determine relative attitude and position as shown in Figure 3-8. The chief uses detection optics and a focal-plane detector that are designed to differentiate received signals from the deputy's optical fiducials to determine multiple line-of-sight

vectors. An example system of this nature is described in Reference [110], which requires the spacecraft to be in close proximity. Due to the close proximity requirement, relative attitude and relative position are coupled.

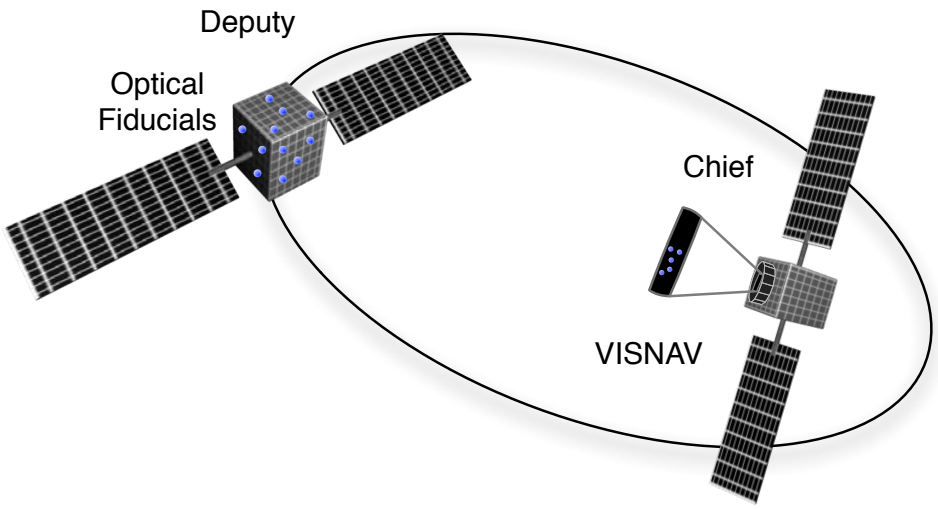

Figure 3-8. Notional depiction of a VISNAV measurement

VISNAV utilizes similar hardware to a star tracker. However, differentiating fiducials is not a pattern recognition problem like the star tracker, but instead it is a problem of physically differentiating the fiducial by the emitted signals. Given this differentiation, directions to the fiducials are captured with a focal-plane detector and modeled using the virtual CCD described in Section 3.2. Since the fiducial locations are known in deputy coordinates, knowledge of the relative position provides enough information for the line-of-sight vectors to be determined as shown in Figure 3-9. The measurement model for VISNAV sensor is

$$ {}^{C}\tilde{\boldsymbol{b}}_{D/C,i} = R_{C/D}\,{}^{D}\boldsymbol{b}_{D/C,i} + \boldsymbol{\eta}_{vis}, $$

where ${}^{C}\tilde{\boldsymbol{b}}_{D/C,i}$ is the measured direction of the i^{th}-fiducial in the chief frame, $R_{C/D}$ is the attitude matrix mapping deputy to chief coordinates, ${}^{D}\boldsymbol{b}_{D/C,i}$ is the direction of the i^{th}-fiducial in the deputy frame, and $\boldsymbol{\eta}_{vis}$ is white zero-mean Gaussian noise corrupting the measurement. Focal plane measurements are modeled through the vector form of

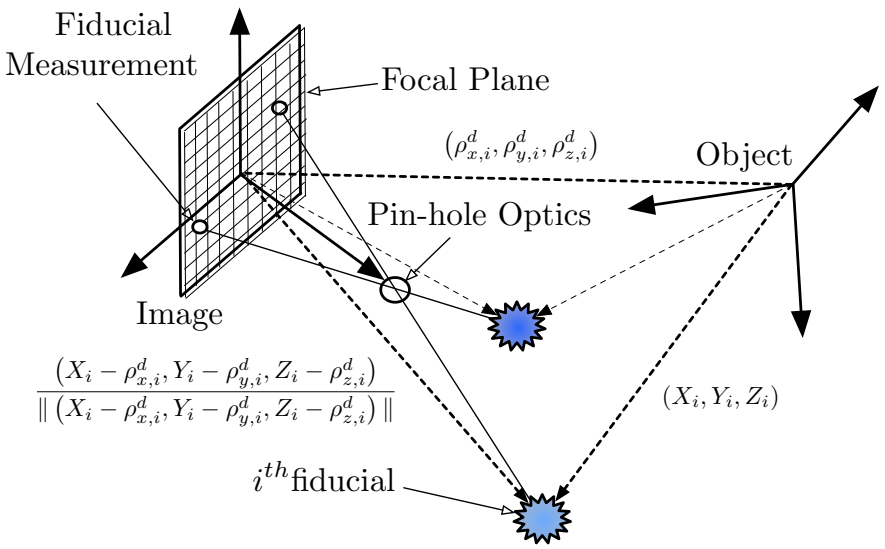

Figure 3-9. Description of the VISNAV sensor geometry

the collinearity equations, such that

$$ {}^{C}\tilde{\boldsymbol{b}}_{D/C,i} = \frac{1}{\sqrt{f^2 + x_i^2 + y_i^2}} \begin{bmatrix} -x_i \\ -y_i \\ f \end{bmatrix} $$

$$ {}^{D}\boldsymbol{b}_{D/C,i} = \frac{1}{\sqrt{(X_i - {}^{D}\rho_{x,i})^2 + (Y_i - {}^{D}\rho_{y,i})^2 + (Z_i - {}^{D}\rho_{z,i}}} \begin{bmatrix} X_i - {}^{D}\rho_{x,i} \\ Y_i - {}^{D}\rho_{y,i} \\ Z_i - {}^{D}\rho_{z,i} \end{bmatrix}, $$

where (X_i, Y_i, Z_i) are the known fiducial locations in deputy coordinates, (x_i, y_i) are the focal plane coordinates of the fiducial measurement, ${}^{D}\rho_i$ is the relative position vector between the chief and deputy, and f is the focal length of the VISNAV sensor. *The VISNAV sensor will serve as the relative attitude sensor for the remainder of this work.*

A limitation of the VISNAV sensor is that it only provides precise measurements in close proximity. As the distance between the sensor and fiducials increases, the fiducial approach a coalesced point source, which contains no attitude information. Therefore, utilization of this sensor is limited to close-proximity applications, such as

distributing-sensing formation-flying missions. It is also assumed that adaptive optics are implemented to alter the focal length of the VISNAV sensor and the intensity of light emitted from the fiducials as a function of range.

3.8 Deterministic Relative Attitude Determination

In the general case, where relative position is unknown, several methods have been devised to determine relative position and attitude simultaneously from the VISNAV measurements. The first approach uses a Gaussian Least Squares Differential Correction (GLSDC) process [110] to iteratively determine relative position and attitude. This method suffers from sensitivity to initial condition errors and is less computationally than other methods. The next approach bypasses attitude determination and utilizes filtering to directly converge upon the states [111]. However, although this method is robust to errors in initial conditions, it requires convergence before a suitable relative attitude estimate is obtained.

Two methods for relative attitude and position determination were presented in Reference [112]. The first method, Linear Algebra Resection Approach (LARA), creates a homogeneous system of equations and finds the solution to the relative attitude and position problem as the left eigenvector associated with the minimum singular value of the homogeneous equations. Through a null-space argument, this case imposes a restriction that at minimum, 6 fiducials must be visible. This is prohibitive in application. The second approach, First Attitude Free Approach (FAFA), recasts the combined relative position and attitude problem into a nonlinear system of equations parameterized solely by the relative position. The resulting equation is an 8^{th}-order polynomial with roots yielding the relative position. After isolating the real solutions of this polynomial, the relative attitude is solved for using any of the many attitude-only determination techniques, such as QUEST or OLAE. Although this technique is fairly robust, it still requires numerical iteration. The final approach utilizes position triangulation to determine distances to the fiducials [113]. These distances then provide

enough information to determine attitude independently of position. Finally, the attitude estimate is used to determine the relative position.

Contrary to the general case of relative attitude and position determination, if relative position is already known, then the Wahba problem can be solved to determine relative attitude. This will be the case that is assumed in this work, as the focus is on attitude resource sharing and not on the general case of translations and rotations.

3.9 Inertial Attitude Estimation in a Disaggregated System

For the attitude estimator for disaggregated spacecraft, the goal is to have each spacecraft in the network maintain an estimate of the inertial attitude of all spacecraft in the network, but only using local measurements. The chief is capable of measuring its inertial attitude as well as the relative attitude to the deputies. The deputies are only capable of capturing vector measurements to estimate their inertial attitude. To accomplish this, the chief utilizes an inertial sensor, such as a star tracker, and a relative sensor, such as VISNAV.

In the case of a single chief and n deputies, the state vector is

$$\boldsymbol{x} = \left[q_C^T, q_{D_1}^T, \dots, q_{D_n}^T, \boldsymbol{\beta}_C^T, \boldsymbol{\beta}_{D_1}^T, \dots, \boldsymbol{\beta}_{D_n}^T\right]^T$$

and the error state is

$$\Delta\boldsymbol{x} = \left[\delta\boldsymbol{\alpha}_C^T, \delta\boldsymbol{\alpha}_{D_1}^T, \dots, \delta\boldsymbol{\alpha}_{D_n}^T, \Delta\boldsymbol{\beta}_C^T, \Delta\boldsymbol{\beta}_{D_1}^T, \dots, \Delta\boldsymbol{\beta}_{D_n}^T\right]^T.$$

The difference with the EKF for disaggregated spacecraft with respect to the standard inertial attitude EKF is in the derivation of the sensitivity matrix and the state and covariance propagation.

3.9.1 Sensitivity Matrix Derivation

Consider the case of the chief measuring the relative attitude states of the i^{th}-deputy and its local states. It is assumed that the relative position vector between the chief and i^{th}-deputy is known and any uncertainty therein is added as process noise in the

dynamics model. Therefore, the j^{th}-vector in deputy coordinates is mapped to chief coordinates through the relative attitude matrix, such that

$$^{C}\boldsymbol{b}_{D_i/C,j} = R(q_{D_i/C})\,{}^{D}\boldsymbol{b}_{D_i/C,j}.$$

Alternatively, instead of mapping the known deputy represented vectors through the relative attitude matrix, the attitude composition law produces the equivalent forms

$$^{C}\boldsymbol{b}_{D_i/C,j} = R(q_C)R^T(q_{D_i})\,{}^{D_i}\boldsymbol{b}_{D_i/C,j}$$

and

$$^{C}\hat{\boldsymbol{b}}^{-}_{D_i/C,j} = R(\hat{q}^{-}_{C})R^T(\hat{q}^{-}_{D_i})\,{}^{D_i}\boldsymbol{b}_{D_i/C,j}.$$

The sensitivity equation is once again the difference between the true and estimated measurement, such that

$$\begin{aligned} {}^{C}\Delta\boldsymbol{b} &= {}^{C}\boldsymbol{b}_{D_i/C,j} - {}^{C}\hat{\boldsymbol{b}}^{-}_{D_i/C,j} \\ &= R(q_C)R^T(q_{D_i})\,{}^{D_i}\boldsymbol{b}_{D_i/C,j} - R(\hat{q}^{-}_{C})R^T(\hat{q}^{-}_{D_i})\,{}^{D_i}\boldsymbol{b}_{D_i/C,j}. \end{aligned}$$

From Eq. 2–2, the composition relating the true quaternion parameterized attitude matrix and the estimated state attitude matrix yields

$$R(q_C) = (I_{3\times3} - [\delta\boldsymbol{\alpha}_C\times])\,R(\hat{q}^{-}_{C})$$

and

$$R(q_{D_i}) = \left(I_{3\times3} - \left[\delta\boldsymbol{\alpha}_{D_i}\times\right]\right)R(\hat{q}^{-}_{D_i}),$$

for the chief and deputy, respectively. Therefore,

$$
\begin{aligned}
{}^{C}\Delta\boldsymbol{b} &= \left(I_{3\times3} - [\delta\boldsymbol{\alpha}_C\times]\right) R(\hat{q}_C^-)R^T(\hat{q}_{D_i}^-)\left(I_{3\times3} + \left[\delta\boldsymbol{\alpha}_{D_i}\times\right]\right) {}^{D_i}\boldsymbol{b}_{D_i/C,j} - R(\hat{q}_C^-)A^T(\hat{q}_{D_i}^-) {}^{D_i}\boldsymbol{b}_{D_i/C,j} \\
&= R(\hat{q}_C^-)R^T(\hat{q}_{D_i}^-)\left[\delta\boldsymbol{\alpha}_{D_i}\times\right] {}^{D_i}\boldsymbol{b}_{D_i/C,j} - [\delta\boldsymbol{\alpha}_C\times] R(\hat{q}_C^-)R^T(\hat{q}_{D_i}^-) {}^{D_i}\boldsymbol{b}_{D_i/C,j} \\
&\quad - [\delta\boldsymbol{\alpha}_C\times] R(\hat{q}_C^-)R^T(\hat{q}_{D_i}^-)\left[\delta\boldsymbol{\alpha}_{D_i}\times\right] {}^{D_i}\boldsymbol{b}_{D_i/C,j}. \qquad (3\text{–}22)
\end{aligned}
$$

Neglecting the higher-order terms in Eq. 3–22 results in the first order model of the sensitivity equation,

$$
{}^{C}\Delta\boldsymbol{b} = \left[\left(R(\hat{q}_C^-)R^T(\hat{q}_{D_i}^-) {}^{D_i}\boldsymbol{b}_{D_i/C,j}\right)\times\right]\delta\boldsymbol{\alpha}_C - R(\hat{q}_C^-)R^T(\hat{q}_{D_i}^-)\left[{}^{D_i}\boldsymbol{b}_{D_i/C,j}\times\right]\delta\boldsymbol{\alpha}_{D_i}. \qquad (3\text{–}23)
$$

The sensitivity matrix for a single VISNAV measurement on-board the chief is

$$
H_C(\hat{\boldsymbol{x}}^-) = \begin{bmatrix} \left[\left(R(\hat{q}_C^-)R^T(\hat{q}_{D_i}^-) {}^{D_i}\boldsymbol{b}_{D_i/C,j}\right)\times\right] & -R(\hat{q}_C^-)R^T(\hat{q}_{D_i}^-)\left[{}^{D_i}\boldsymbol{b}_{D_i/C,j}\times\right] & 0_{3\times3} & 0_{3\times3} \end{bmatrix}.
$$

The sensitivity matrix for a single VISNAV measurement on-board the chief follows directly from the two-spacecraft derivation, except that the column deputy sensitivity corresponds with the measured spacecraft. Suppose the i^{th}-deputy is measured by the VISNAV sensor, then the sensitivity matrix is

$$
H_C(\hat{\boldsymbol{x}}^-) = \begin{bmatrix} \left[\left(R(\hat{q}_C^-)R^T(\hat{q}_{D_i}^-) {}^{D_i}\boldsymbol{b}_{D_i/C,j}\right)\times\right] & 0_{3\times3(i-1)} & -R(\hat{q}_C^-)R^T(\hat{q}_{D_i}^-)\left[{}^{D_i}\boldsymbol{b}_{D_i/C,j}\times\right] & 0_{3\times3+6n-3i} \end{bmatrix}.
$$

Therefore, for N star and M fiducial measurements, the chief sensitivity matrix is

$$
H_C(\hat{\boldsymbol{x}}^-) = \begin{bmatrix} \left[\left(R(\hat{q}_C^-) {}^{C}\boldsymbol{b}_1\right)\times\right] & 0_{3\times3(i-1)} & 0_{3\times3} & 0_{3\times3+6n-3i} \\ \vdots & \vdots & \vdots & \vdots \\ \left[\left(R(\hat{q}_C^-) {}^{C}\boldsymbol{b}_N\right)\times\right] & 0_{3\times3(i-1)} & 0_{3\times3} & 0_{3\times3+6n-3i} \\ \left[\left(R(\hat{q}_C^-)R^T(\hat{q}_{D_i}^-) {}^{D_i}\boldsymbol{b}_{D_i/C,1}\right)\times\right] & 0_{3\times3(i-1)} & -R(\hat{q}_C^-)R^T(\hat{q}_{D_i}^-)\left[{}^{D_i}\boldsymbol{b}_{D_i/C,1}\times\right] & 0_{3\times3+6n-3i} \\ \vdots & \vdots & \vdots & \vdots \\ \left[\left(R(\hat{q}_C^-)R^T(\hat{q}_{D_i}^-) {}^{D_i}\boldsymbol{b}_{D_i/C,M}\right)\times\right] & 0_{3\times3(i-1)} & -R(\hat{q}_C^-)R^T(\hat{q}_{D_i}^-)\left[{}^{D_i}\boldsymbol{b}_{D_i/C,M}\times\right] & 0_{3\times3+6n-3i} \end{bmatrix}.
$$

This sensitivity matrix is no larger in rows than the two-spacecraft case. However, there can be many more columns, where the number of columns grows at a rate

of $6 + 6(n + 1)$, where n is once again the number of deputies. Most importantly, due to linearity and superposition, Murrell's algorithm can be used to process each measurement sequentially.

Similarly, the i^{th} deputy sensitivity matrix with L inertial vector measurements is

$$H_{D_i}(\hat{\boldsymbol{x}}^-) = \begin{bmatrix} 0_{3\times3} & 0_{3\times3(i-1)} & \left[\left(R(\hat{q}_{D_i}^-)^{D_i}\boldsymbol{b}_1\right)\times\right] & 0_{3\times3+6n-3i} \\ \vdots & \vdots & \vdots & \vdots \\ 0_{3\times3} & 0_{3\times3(i-1)} & \left[\left(R(\hat{q}_{D_i}^-)^{D_i}\boldsymbol{b}_L\right)\times\right] & 0_{3\times3+6n-3i} \end{bmatrix}.$$

As the deputy can only obtain local inertial measurements, the sensitivity matrix has columns of zeros for the chief state and biases.

3.9.2 Discrete Propagation Derivation

Consider the continuous-time error state dynamics to be used in a disaggregated estimation scheme for the n-deputy case, such that

$$\Delta\dot{\boldsymbol{x}}_{dc} = F_{da}\Delta\boldsymbol{x}_{dc} + G_{da}\boldsymbol{w}_{dc}$$

where

$$F_{da} = \begin{bmatrix} -[\omega_c\times] & 0_{3\times3} & -I_{3\times3} & 0_{3\times3} & 0_{3\times3} & 0_{3\times3} \\ 0_{3\times3} & -[\omega_{d,1}\times] & 0_{3\times3} & -I_{3\times3} & 0_{3\times3} & 0_{3\times3} \\ \vdots & \ddots & \ddots & \ddots & \ddots & \vdots \\ 0_{3\times3} & 0_{3\times3} & 0_{3\times3} & -[\omega_{d,n}\times] & 0_{3\times3} & -I_{3\times3} \\ 0_{3\times3} & 0_{3\times3} & 0_{3\times3} & 0_{3\times3} & 0_{3\times3} & 0_{3\times3} \\ \vdots & \vdots & \vdots & \vdots & \vdots & \vdots \\ 0_{3\times3} & 0_{3\times3} & 0_{3\times3} & 0_{3\times3} & 0_{3\times3} & 0_{3\times3} \end{bmatrix},$$

$$G_{da} = \begin{bmatrix} -I_{3\times3} & 0_{3\times3} & 0_{3\times3} & 0_{3\times3} & 0_{3\times3} & 0_{3\times3} \\ 0_{3\times3} & \ddots & 0_{3\times3} & 0_{3\times3} & 0_{3\times3} & 0_{3\times3} \\ 0_{3\times3} & 0_{3\times3} & -I_{3\times3} & 0_{3\times3} & 0_{3\times3} & 0_{3\times3} \\ 0_{3\times3} & 0_{3\times3} & 0_{3\times3} & I_{3\times3} & 0_{3\times3} & 0_{3\times3} \\ 0_{3\times3} & 0_{3\times3} & 0_{3\times3} & 0_{3\times3} & \ddots & 0_{3\times3} \\ 0_{3\times3} & 0_{3\times3} & 0_{3\times3} & 0_{3\times3} & 0_{3\times3} & I_{3\times3} \end{bmatrix},$$

The continuous-time process noise covariance matrix is given by

$$Q_{da} = \text{diag}\left(\sigma^2_{C,v} I_{3\times3}, \sigma^2_{D_1,v} I_{3\times3}, \ldots, \sigma^2_{D_n,v} I_{3\times3}, \sigma^2_{C,u} I_{3\times3}, \sigma^2_{D_1,u} I_{3\times3}, \ldots, \sigma^2_{D_n,u} I_{3\times3}\right) \tag{3–24}$$

The discrete solutions for the state transition matrix and process covariance matrix are also found through Eq. 3–15 and Eq. 3–16, respectively. Finally, each of the quaternion and bias states are propagated through Eq. 3–21 and Eq. 3–20, respectively.

The chief and deputy each individually estimate the entire state of the two spacecraft network. The chief has the potential for full observability of the system states. Whereas, the deputy only has observability over its own states (i.e., the deputy quaternion and bias). For instance, without combining information from the chief estimates, the deputies knowledge of the chief inertial attitude will always diverge. Table 3-10 summarizes the EKF to be used in the disaggregated system for attitude resource sharing. However, for the deputy to make use of the knowledge of its states from the chief, data fusion is required. A benefit of this data fusion, is that the chief also stands to gain in performance through the data fusion process. Results are developed in Chapter 4. If the time step is small enough, then the computational complexity of the propagation only increases with the order of matrix multiplication. However, if the small-time-step approximation does not hold, then the matrix exponential must be computed, which is computationally expensive for large state sizes. Therefore, this approach is only for smaller networks of spacecraft requiring resource sharing.

Table 3-10. Extended Kalman filter for inertial attitude estimation in a disaggregated system

Initialize

$$\hat{\boldsymbol{x}}(t_0) = \hat{\boldsymbol{x}}_0 = \left[q_C|_0^T, q_{D_1}|_0^T, \ldots, q_{D_n}|_0^T, \beta_C|_0^T, \beta_{D_1}|_0^T, \ldots, \beta_{D_n}|_0^T\right]^T, \; P(t_0) = P_0$$

Gain

$$K_k = P_k^- H_k^T(\hat{\boldsymbol{x}}_k^-)\left[H_k(\hat{\boldsymbol{x}}_k^-)P_k^- H_k^T(\hat{\boldsymbol{x}}_k^-) + R\right]^{-1}$$

Chief: $H_C(\hat{\boldsymbol{x}}^-) =$

$$= \begin{bmatrix} \left[\left(R(\hat{q}_C^-)\,{}^C\boldsymbol{b}_1\right)\times\right] & 0_{3\times 3(i-1)} & 0_{3\times 3} & 0_{3\times 3+6n-3i} \\ \vdots & \vdots & \vdots & \vdots \\ \left[\left(R(\hat{q}_C^-)\,{}^C\boldsymbol{b}_N\right)\times\right] & 0_{3\times 3(i-1)} & 0_{3\times 3} & 0_{3\times 3+6n-3i} \\ \left[\left(R(\hat{q}_C^-)R^T(\hat{q}_{D_i}^-)\,{}^{D_i}\boldsymbol{b}_{D_i/C,1}\right)\times\right] & 0_{3\times 3(i-1)} & -R(\hat{q}_C^-)R^T(\hat{q}_{D_i}^-)\left[{}^{D_i}\boldsymbol{b}_{D_i/C,1}\times\right] & 0_{3\times 3+6n-3i} \\ \vdots & \vdots & \vdots & \vdots \\ \left[\left(R(\hat{q}_C^-)R^T(\hat{q}_{D_i}^-)\,{}^{D_i}\boldsymbol{b}_{D_i/C,M}\right)\times\right] & 0_{3\times 3(i-1)} & -R(\hat{q}_C^-)R^T(\hat{q}_{D_i}^-)\left[{}^{D_i}\boldsymbol{b}_{D_i/C,M}\times\right] & 0_{3\times 3+6n-3i} \end{bmatrix}$$

Deputies: $H_{D_i}(\hat{\boldsymbol{x}}^-) = \begin{bmatrix} 0_{3\times 3} & 0_{3\times 3(i-1)} & \left[\left(R(\hat{q}_{D_i}^-)\,{}^{D_i}\boldsymbol{b}_1\right)\times\right] & 0_{3\times 3+6n-3i} \\ \vdots & \vdots & \vdots & \vdots \\ 0_{3\times 3} & 0_{3\times 3(i-1)} & \left[\left(R(\hat{q}_{D_i}^-)\,{}^{D_i}\boldsymbol{b}_L\right)\times\right] & 0_{3\times 3+6n-3i} \end{bmatrix}$

Update

$$P_k^+ = \left[I_{6n\times 6n} - K_k H_k(\hat{\boldsymbol{x}}_k^-)\right]P_k^-$$

$$\Delta\boldsymbol{x}^+ = \left[\delta\boldsymbol{\alpha}_C^{+T}, \delta\boldsymbol{\alpha}_{D_1}^{+T}, \ldots, \delta\boldsymbol{\alpha}_{D_n}^{+T}, \Delta\boldsymbol{\beta}_C^{+T}, \Delta\boldsymbol{\beta}_{D_1}^{+T}, \ldots, \Delta\boldsymbol{\beta}_{D_n}^{+T}\right]^T = K_k\left[\tilde{y}_k - h_k(\hat{\boldsymbol{x}}^-)\right]$$

Chief: $\tilde{y}_C = \begin{bmatrix} {}^C\boldsymbol{b}_1 \\ \vdots \\ {}^C\boldsymbol{b}_N \\ {}^C\boldsymbol{b}_{D_i/C,1} \\ \vdots \\ {}^C\boldsymbol{b}_{D_i/C,M} \end{bmatrix}$, $h_C(\hat{\boldsymbol{x}}^-) = \begin{bmatrix} R(\hat{q}_C^-)\,{}^C\boldsymbol{b}_1 \\ \vdots \\ R(\hat{q}_C^-)\,{}^C\boldsymbol{b}_N \\ R(\hat{q}_C^-)R^T(\hat{q}_{D_i}^-)\,{}^{D_i}\boldsymbol{b}_{D_i/C,1} \\ \vdots \\ R(\hat{q}_C^-)R^T(\hat{q}_{D_i}^-)\,{}^{D_i}\boldsymbol{b}_{D_i/C,M} \end{bmatrix}$

$\hat{q}_C^+|_k = \hat{q}_C^-|_k + \frac{1}{2}\Xi(\hat{q}_C^-|_k)\delta\hat{\boldsymbol{\alpha}}_C^+|_k$, $\hat{\beta}_C^+|_k = \hat{\beta}_C^-|_k + \Delta\hat{\beta}_C^+|_k$

Deputies: $\tilde{y}_{D_i} = \begin{bmatrix} {}^{D_i}\boldsymbol{b}_1 \\ \vdots \\ {}^{D_i}\boldsymbol{b}_L \end{bmatrix}$, $h_{D_i}(\hat{\boldsymbol{x}}^-) = \begin{bmatrix} R(\hat{q}_{D_i}^-)\,{}^{D_i}\boldsymbol{b}_1 \\ \vdots \\ R(\hat{q}_{D_i}^-)\,{}^{D_i}\boldsymbol{b}_L \end{bmatrix}$

$\hat{q}_{D_i}^+|_k = \hat{q}_{D_i}^-|_k + \frac{1}{2}\Xi(\hat{q}_{D_i}^-|_k)\delta\hat{\boldsymbol{\alpha}}_{D_i}^+|_k$, $\hat{\beta}_{D_i}^+|_k = \hat{\beta}_{D_i}^-|_k + \Delta\hat{\beta}_{D_i}^+|_k$

Propagate

$$P_{k+1}^- = \boldsymbol{\Phi}_k P_k^+ \boldsymbol{\Phi}_k^T + Q_k$$

Chief:

$\hat{q}_C^-|_{k+1} = \bar{\Omega}(\hat{\omega}_C^+|_k)\hat{q}_C^+|_k$

$\hat{\omega}_C^+|_k = \tilde{\omega}_C|_k - \hat{\beta}_C^+|_k$

Deputies:

$\hat{q}_{D_i}^-|_{k+1} = \bar{\Omega}(\hat{\omega}_{D_i}^+|_k)\hat{q}_{D_i}^+|_k$

$\hat{\omega}_{D_i}^+|_k = \tilde{\omega}_{D_i}|_k - \hat{\beta}_{D_i}^+|_k$

3.9.3 Notes on Disaggregated Attitude Estimation

The disaggregated approach requires that the gyro measurements be shared over a wireless link at the regular sampling interval for discrete propagation. However, in Reference [104] it was noted that although the largest numerical burden in the attitude Kalman filter occurs with the computation of the transition matrix and the contribution of the process noise to the state covariance matrix, this computation can take place at much larger time scales than the state propagation. Therefore, each deputy can locally propagate their states at the frequency of their local gyro updates without being burdened so heavily by the process noise computations.

The approach taken in this section should only be used for smaller formation flying networks, where communication is available when required. Modifications will be necessary to the formulation if larger networks and irregular communication is expected.

3.10 Summary

Inertial and relative attitude determination and estimation were surveyed. Inertial attitude is determined by solving the Wahba problem. There are many solutions to this problem, such as the popular QUEST algorithm. However, other methods such as ESOQ-2 and OLAE have been shown to provide faster computational solutions. Due to the nonlinear nature of attitude estimation, the Extended Kalman Filter for quaternion kinematics was surveyed. Next, relative attitude determination was surveyed. Due to the coupled nature of relative attitude and position, relative attitude determination is more complex than inertial attitude determination. However, closed-form solutions do exist. In the last part, the EKF for disaggregated spacecraft was developed. To the author's knowledge, this is the first derivation and application of relative attitude sensors used to directly estimate the inertial states of multiple spacecraft. These equations have application to spacecraft seeking improved inertial attitude estimates through attitude resource sharing. The multiple estimates originating from the EKF for the disaggregated system are the inputs for data fusion algorithms.

CHAPTER 4
ATTITUDE DATA FUSION

Data fusion has been developed to optimally combine multiple state estimates in disaggregated systems, where the states have typically been Euclidean in error. More recently, results have been developed for attitude data fusion, which account for the multiplicative nature of attitude compositions. This chapter reviews existing results in data fusion for Euclidean and attitude states. Contributions are made in the parameterization of attitude for data fusion and particularly in the characterization of error created by using a minimal attitude parameterization for fast attitude data fusion.

This chapter is divided into three parts. In the first part it is shown that many existing data fusion algorithms can be represented in terms of the fusion error, which is the error between the individual state estimates and the fused state. Based on the fusion error representation, it is shown that existing Euclidean state data fusion laws can be generalized to attitude states through the loss function perspective with the attitude error vector serving as the fusion error state. The second part derives a form of the attitude error vector using the vectorial attitude parameterizations and discusses the benefits of these minimal attitude parameterizations for data fusion. The third part investigates the vectorial shadow parameterizations and local error representations for fast and accurate attitude data fusion.

4.1 Data Fusion Overview

In the discussions that follow, resource sharing is assumed to be represented with a star graph where the chief spacecraft is connected to each of the deputy spacecraft, but the deputies are only linked to the chief. This configuration is shown in Figure 4-1. This type of connectivity is justified by the fact that better inertial attitude estimation is sought through resource sharing, and thus the only additional knowledge provided to the deputies is garnered through the relative attitude link on the chief and the improved knowledge of the chiefs garnered from the deputies. There could be multiple chiefs, but

this case is not considered, although it only requires a minor extension to the EKF for disaggregated systems formulation presented in Chapter 3.

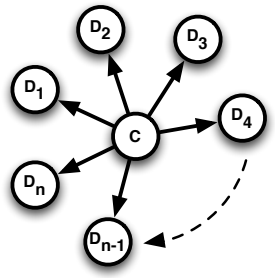

Figure 4-1. Star graph representation for attitude resource sharing

Given a star graph network, there are several important characteristics that dictate the algorithms and performance of resource sharing. A summary of important characteristics for data fusion is given in [114]. A taxonomy for fusion characteristics for the resource sharing problem is shown in Table 4-1. This is not meant to be an exhaustive list, as aspects such as imperfect, conflicting, and spurious data will not be considered. However, these properties can be extended to the present discussion.

Table 4-1. Resource sharing data fusion and system architecture taxonomy

Characteristic	Description	Options
Processing Framework	location of data fusion	*Centralized, Decentralized*
Data Correlation	state estimate dependency	*Correlated, Uncorrelated*
Connectivity	graph structure of network	*Full, Star*
Temporal structure	variation in the graph edges	*Dynamic, Static*
Directivity	one-way or two-way communication	*Symmetric, Asymmetric*
Data processing	form of information sources	*Pre-processed, Raw data*

Of these characteristics, the data fusion problem considered in this research is the decentralized star graph with correlated states, static graph edges, symmetric communication, and pre-processed information. It should be noted, that although the communications network is static, the relative attitude connectivity is time varying and based on the tasking.

4.2 Data Fusion Review

Data fusion is a problem that has arisen due to interest in multi-sensor systems, either on-board a single platform or distributed across a network of platforms. Data

fusion exploits the known dependency in the information sources, as is the case with Kalman filtering [98], or seeks an optimal combination of information to produce a best estimate when information dependency is uncertain, as is the case with covariance intersection [47, 48]. To generate a fused estimate, data fusion algorithms optimize the combination of multi-sensor information by minimizing a cost function, which is some measure of the error between the state estimates and the fused state. For non-attitude applications with unconstrained states, the fusion error is a measure of the Euclidean distance. However, attitude belongs to the space of special orthogonal matrices, $SO(3)$, and thus a measure of error through the Euclidean distance is not appropriate.

The author has observed that the properties of the data fusion algorithm are inherited from the attitude parameterization. Recent advances in attitude data fusion algorithms have made use of the unit quaternion [46, 115, 116] and the modified Rodrigues parameters (MRPs) [117, 118] to parameterize the attitude error vector. However, both of these parameterizations pose difficulties in the data fusion solution. The unit quaternion parameterization is constrained, which must be handled in the data fusion optimization explicitly through the use of Lagrange multipliers. Solving the constrained optimization problem adds additional numerical complexity for low-dimensional systems and becomes burdensome for high-dimensional systems. Alternatively, the MRP parameterization, which is from a larger class of minimal attitude parameterizations known as the vectorial attitude parameterizations, is unconstrained but has singularities at $\pm 2\pi$ requires a singularity avoidance algorithm. A singularity avoidance method that transforms the global MRP data fusion problem to a local representation, where a solution is ensured to be singularity free has been proposed in [118]. After the data fusion occurs, the solution is then transformed back to the global MRP parameterization, where it is then further transformed back to the original parameterization utilized in the attitude estimation or control algorithms. To improve upon this prior art in attitude data fusion, recent results in the minimal vectorial attitude

parameterization are applied to the parameterization of the attitude error vector. Due to the periodic invariance of attitude, the data fusion parameterization only requires singularities not be present for $\phi \in [-2\pi, +2\pi]$. The vectorial parameterizations are known to produce parameters with two distinct singularity classes. Of these two classes, one permits a shadow parameterization, which are used to produce an unconstrained, globally nonsingular parameterization of the attitude error vector. Additionally, it is shown that the parameterization determines the accuracy of the data fusion process.

4.3 Data Fusion and the Error State

One classic data fusion problem is that of linear systems with two independent Gaussian information sources – typically, a dynamic process model and a measurement model. The optimal weighted combination of the independent dynamics process and measurement models is generated by the Kalman filter. However, when the information sources are known to be dependent or the correlation is unknown, the Kalman filter can no longer be directly applied [119]. This class of problem is encountered in multi-sensor systems and a variety of data fusion algorithms have been created to generate consistent estimates that are optimal in the sense of some relevant cost function. The solution to both of these data fusion problems are a function of the Euclidean distance between the state estimates and the fused state.

4.3.1 Euclidean Fusion Error State

Consider the set of pairs, $(\hat{\boldsymbol{x}}_i, P_i)$, that describes the mean and covariance of multiple sources of a system state. The objective of any data fusion system is to optimally combine the state estimates, $\hat{\boldsymbol{x}}_i$ to generate a new fused state, $\hat{\boldsymbol{x}}_f$, such that

$$\hat{\boldsymbol{x}}_f = f_x\left(\hat{\boldsymbol{x}}_1,\ \ldots,\ \hat{\boldsymbol{x}}_n\right),$$

with approximate covariance of the fused state given by

$$P_f = f_P\left(P_1,\ \ldots,\ P_n\right).$$

Here, the function, f_x, is the state fusion law and f_P is the covariance approximation law. The covariance approximation must be consistent to ensure that it never underestimates the uncertainty in the system, which could lead to divergence. Therefore, the goal of data fusion is to optimally and consistently combine multiple sources of information. In terms of the second moment, consistency is satisfied when

$$P_f - \bar{P}_f \geq 0,$$

which designates the difference is a positive semi-definite matrix, and $\bar{P}_f$ is the actual covariance of the fused state and P_f is an approximation for the fused state covariance that is consistent with any cross correlation between the state estimates. Clearly, a consistent fused state covariance exists if the cross-correlation is known. Furthermore, consider the class of data fusion laws that can be rewritten in terms of the fusion error, such that

$$\mathbf{0} = f_x\left(\Delta\hat{\boldsymbol{x}}_1, \ldots, \Delta\hat{\boldsymbol{x}}_n\right), \tag{4–1}$$

where $\Delta\hat{\boldsymbol{x}}_i = \hat{\boldsymbol{x}} - \hat{\boldsymbol{x}}_i \in \mathbb{R}^n$ and $\hat{\boldsymbol{x}}$ is any possible value of the fused state. For this class of problems, the fusion law is recast as the minimization of a loss function, J, such that

$$\hat{\boldsymbol{x}}_f = \arg\min_{\hat{\boldsymbol{x}}} J\left(\Delta\hat{\boldsymbol{x}}_1, \ldots, \Delta\hat{\boldsymbol{x}}_n\right).$$

The first-order optimality condition for this optimization problem is

$$\mathbf{0} = \frac{dJ\left(\Delta\hat{\boldsymbol{x}}_1, \ldots, \Delta\hat{\boldsymbol{x}}_n\right)}{d\hat{\boldsymbol{x}}}.$$

From the chain rule of differentiation, the optimality condition is

$$\mathbf{0} = \sum_{i=1}^{n} \left(\frac{\partial \Delta\hat{\boldsymbol{x}}_i^T}{\partial \hat{\boldsymbol{x}}}\right) \frac{\partial J\left(\Delta\hat{\boldsymbol{x}}_1, \ldots, \Delta\hat{\boldsymbol{x}}_n\right)}{\partial \Delta\hat{\boldsymbol{x}}_i}.$$

However, the data fusion Jacobian formed from the partial derivatives of the fusion error state with respect to the fusion state is the identity matrix, and thus the optimality

condition is

$$\mathbf{0} = \sum_{i=1}^{n} \frac{\partial J\left(\Delta\hat{\boldsymbol{x}}_1, \ldots, \Delta\hat{\boldsymbol{x}}_n\right)}{\partial \Delta\hat{\boldsymbol{x}}_i}.$$

For $\hat{\boldsymbol{x}} \in \mathbb{R}^n$, the original fusion law is recaptured from this minimization. However, for states that parameterize $SO(3)$, the fusion law is altered based on the derivative of the error state with respect to the attitude parameterization.

4.3.2 Attitude Fusion Error State

In order to apply data fusion algorithms to states parameterized in $SO(3)$, the attitude error state must be well understood. A general discussion of attitude error was discussed in Chapter 2 and is now specialized in the context of data fusion. The attitude fusion error state is representative of the rotation from the individual attitude state estimates to the fused attitude state. From Eulers rotation theorem which states a rotation about a point is always equivalent to a rotation about a line through the point [54], $SO(3)$ can be parameterized by an axis and the angle of rotation about that axis, which is expressed through the Euler-Rodrigues formula given in Eq. 2–4.

The attitude error vector is derived from the attitude composition law as described in Eq. 2–1. For a general composition of attitudes,

$$R' = \delta R R,$$

where the original attitude, R, is transformed by δR, to produce the final attitude R'. Since $\{R, \delta R, R'\} \in SO(3)$ and $RR^T = I_{3\times 3}$, then

$$\delta R = R' R^T. \tag{4–2}$$

Of interest, is a vector form of the composition law. For transformations associated with small angular displacements, the Euler-Rodrigues formula becomes

$$\delta R = I_{3\times 3} - [\Delta\phi \boldsymbol{n}\times] + \mathcal{O}\left(\|\Delta\phi \boldsymbol{n}\|^2\right).$$

When $\Delta\phi$ is sufficiently small, higher order terms can be neglected and

$$\delta R = I_{3\times 3} - [\delta\boldsymbol{\alpha}\times].$$

Therefore, the attitude error vector is

$$[\delta\boldsymbol{\alpha}\times] = I_{3\times 3} - R'R^T. \tag{4–3}$$

The attitude error vector can then be defined through the axis and angle by

$$\delta\boldsymbol{\alpha} = \Delta\phi\boldsymbol{n}.$$

Clearly, the attitude error vector is parameterization independent as it is a function of the composition of $RR' \in SO(3)$. Therefore, the choice of parameterization of the attitude error vector will define the suitability for data fusion.

Let $\boldsymbol{s} \in \mathbb{R}^3$ be any minimal attitude parameterization of R. Now, applying the attitude error vector to the fusion error state formulated in Section 4.3, yields

$$\hat{\boldsymbol{s}}_f = \arg\min_{\hat{\boldsymbol{s}}} J\left(\delta\hat{\boldsymbol{\alpha}}_1, \ldots, \delta\hat{\boldsymbol{\alpha}}_n\right). \tag{4–4}$$

The loss function approach to attitude data fusion was first introduced to extend application of the covariance intersection law to attitude states [115]. The loss function perspective for Euclidean states produces the same fused state as the original fusion law. However, for minimal attitude parameterizations that are follow from the Euler-Rodrigues formula, $(\phi, \boldsymbol{n})$ and $(-\phi, -\boldsymbol{n})$ represent the same attitude. Differentiating the quadratic loss function ensures that the fused attitude is invariant to this non-unique choice.

Following the derivation of the Euclidean states, the first-order optimality condition for attitude loss function minimization is

$$\mathbf{0} = \frac{dJ\left(\delta\hat{\boldsymbol{\alpha}}_1, \ldots, \delta\hat{\boldsymbol{\alpha}}_n\right)}{d\hat{\boldsymbol{s}}}.$$

From the chain rule of differentiation, the optimality condition is

$$\mathbf{0} = \sum_{i=1}^{n} \left(\frac{\partial \delta \hat{\boldsymbol{\alpha}}_i^T}{\partial \hat{\mathbf{s}}} \right) \frac{\partial J\left(\delta \hat{\boldsymbol{\alpha}}_1, \ldots, \delta \hat{\boldsymbol{\alpha}}_n\right)}{\partial \delta \hat{\boldsymbol{\alpha}}_i}. \tag{4–5}$$

Unlike the case for Euclidean states, the data fusion Jacobian will not, in general, be the identity matrix. Therefore, both the data fusion Jacobian and representation of the error state modify the data fusion law with respect to the original formulation for Euclidean states. These modifications are parameterization dependent and have an impact on the characteristics and accuracy of the resulting attitude fusion law. That is, the accuracy of the attitude error vector approximation will influence the error in the fusion law.

In summary, this section demonstrated that the loss function approach as originally developed for the covariance intersection algorithm with quaternion parameterization [115] and later applied to the MRP parameterization [117, 118], applies to any data fusion law and attitude parameterization, given that the fusion law can be written in terms of the fusion error, as described in Eq. 4–1. Section 4.4 demonstrates how typical data fusion algorithms can be rewritten in terms of the fusion error and then adapted to attitude error states utilizing any parameterization of the attitude error vector.

4.4 Unknown Cross-Correlation Data Fusion Algorithms

The problem of data fusion with unknown correlation is common in decentralized multi-sensor systems where information is shared across the network. Two algorithms for data fusion with unknown cross-correlation will be extended to attitude problems via the loss function and the fusion error. The first is the covariance intersection (CI) fusion law, which has already been written in terms of the loss function of the attitude error vector in [115] and related to the work on quaternion averaging [120]. The second is the ellipsoid intersection (EI) fusion law, which offers a less conservative approach to data fusion with respect to the covariance intersection algorithm, where consistency has been demonstrated in simulation [121–123].

4.4.1 Covariance Intersection

Consider the set of state estimate pairs $(\hat{\boldsymbol{x}}_i, P_i)$, which describe the first and second moments of the random variable, $\boldsymbol{x}$, with an arbitrary probability density function. The covariance intersection (CI) fusion law yields a fused estimate, which is a convex combination of the state estimates. Figure 4-2 represents the a notional example of the covariance intersection results for a two-dimensional system. Figure 4-2A shows the fused state covariance ellipse for the 1-σ bound on the state error centered at zero for the original state estimates and covariance intersection solution, denoted by $\mathcal{E}_{0,P_1}$, $\mathcal{E}_{0,P_2}$, and $\mathcal{E}_{0,P_{CI}}$, respectively. with minimum cost as well as a suboptimal choice of weightings. As expected, the fused state covariance ellipse lies outside of the original state estimate covariance ellipses. Figure 4-2B demonstrates how the CI fused state is a compromise between the original state estimates.

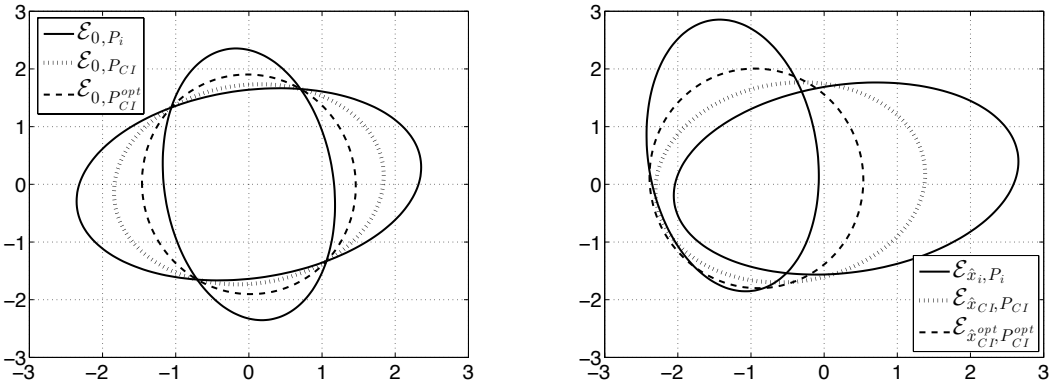

Figure 4-2. Notional covariance intersection uncertainty ellipse comparison A) Covariance intersection (centered at zero). B) Covariance intersection (centered at mean).

The CI data fusion method is general for n sensors and is given by the fusion law

$$\hat{\boldsymbol{x}}_{CI} = P_{CI} \sum_{i=1}^{n} \gamma_i P_i^{-1} \hat{\boldsymbol{x}}_i$$

and covariance approximation law

$$P_{CI}^{-1} = \sum_{i=1}^{n} \gamma_i P_i^{-1}.$$

The weightings, γ_i, must sum to one, where any convex combination satisfies the covariance intersection fusion law, as demonstrated by the dotted line in Fig. 4-2A. Alternatively, the dashed line in Fig. 4-2A represents a more appropriate choice of weightings as evidenced by the smaller size in comparison to the arbitrary CI estimate. In this case, the weightings are optimally determined with respect to a minimization criterion, typically the trace or determinant of the information form of the fused covariance, to produce a fused result that is consistent with all possible cross-correlations between the state estimates.

The state fusion law is rewritten in terms of the fusion error as

$$\mathbf{0} = \sum_{i=1}^{n} \gamma_i P_i^{-1} \Delta\hat{\boldsymbol{x}}_i,$$

which is the result of minimizing

$$J_{CI}(\Delta\hat{\boldsymbol{x}}_1, \dots, \boldsymbol{x}_n) = \sum_{i=1}^{n} \gamma_i \Delta\hat{\boldsymbol{x}}_i^T P_i^{-1} \Delta\hat{\boldsymbol{x}}_i.$$

Adapting this loss function to attitude yields,

$$J_{CI}(\delta\hat{\boldsymbol{\alpha}}_1, \dots, \delta\hat{\boldsymbol{\alpha}}_n) = \sum_{i=1}^{n} \gamma_i \delta\hat{\boldsymbol{\alpha}}_i^T P_i^{-1} \delta\hat{\boldsymbol{\alpha}}_i, \tag{4–6}$$

with the corresponding optimality condition,

$$\mathbf{0} = \sum_{i=1}^{n} \gamma_i \left(\frac{\partial \delta\hat{\boldsymbol{\alpha}}_i^T}{\partial \hat{\boldsymbol{s}}} \right) P_i^{-1} \delta\hat{\boldsymbol{\alpha}}_i. \tag{4–7}$$

The choice of the unit quaternion or MRPs, as has already been applied to CI, only change the parameterization Jacobian and attitude error vector form described in Eq. 4–5. It is important to note that Eq. 4–7 is general for any attitude parameterization applied to the CI fusion law. This fact is utilized in the example presented in Section 4.8.2.

4.4.2 Ellipsoid Intersection

Unlike the CI fusion law, which presumes a form for the fusion law with no regard to the mutual information (read: correlation), the Ellipsoidal intersection (EI) fusion law explicitly characterizes mutual information before deriving the fused state. In this form, the state estimates are decomposed into exclusive and mutual information, such that the unknown mutual information covariance is determined as the maximum possible correlation belonging to the enclosure of the union of the state estimate covariances, as shown in Fig. 4-3. Therefore, by construction, the approximate fused covariance matrix for the EI fusion law will always be less than or equal to the size of that derived from the CI fusion law.

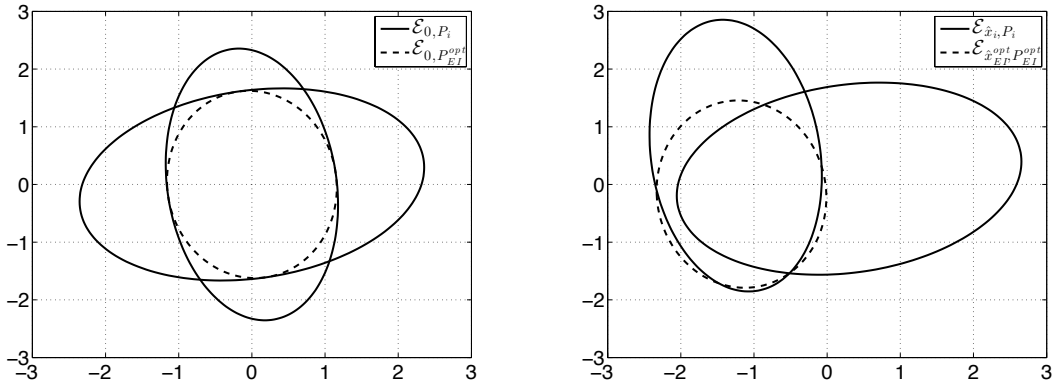

Figure 4-3. Notional ellipsoidal intersection uncertainty ellipse comparison A) Ellipsoidal intersection (centered at zero). B) Ellipsoidal intersection (centered at mean).

The derivation of the EI fusion law follows from the discussion above, which yields

$$\hat{\boldsymbol{x}}_{EI} = P_{EI}\left(\sum_{i=1}^{2} P_i^{-1}\hat{\boldsymbol{x}}_i - \Gamma^{-1}\gamma\right) \tag{4–8}$$

$$P_{EI}^{-1} = \left(P_1^{-1} + P_2^{-1} - \Gamma^{-1}\right),$$

where γ and Γ are the mutual mean and covariance, respectively. Since the mutual mean and covariance are unknown, consistency is assured if the largest possible

correlation is considered. This is the essence of the EI fusion law. The maximum mutual information covariance is found through the following convex optimization problem,

$$\Gamma = \arg \max_{\Upsilon \in \mathbb{R}^{n\times n}} \sum_{i=1}^{n} \lambda_q(\Upsilon)$$

$$\text{subject to } \mathcal{E}_{0,P_1} \cup \mathcal{E}_{0,P_2} \subseteq \mathcal{E}_{0,\Upsilon},$$

where $\mathcal{E}_{0,P_i}$ are the covariance ellipsoids of the state estimates and $\mathcal{E}_{0,\Upsilon}$ is the covariance ellipsoid for the unknown mutual information between the state estimates and the mutual mean. This is analytically found by solving for the joint diagonalization of P_1 and P_2 to produce $P_1 = I_{n\times n}$ and $P_2 = D_2$ through the eigen-decomposition on $D_1^{-\frac{1}{2}} S_1^{-1}(P_1 + P_2) S_1 D_1^{-\frac{1}{2}}$. Clearly this transformation on P_1 yields $I_{n\times n}$. The eigen-decomposition of the transformation on P_2 is

$$D_1^{-\frac{1}{2}} S_1^{-1} P_2 S_1 D_1^{-\frac{1}{2}} = S_2 D_2 S_2^T.$$

Thus, the maximum mutual information is found analytically through

$$\Gamma = S_1 D_1^{\frac{1}{2}} S_2 D_\Gamma S_2^T D_1^{-\frac{1}{2}} S_1^T, \tag{4–9}$$

where

$$D_\Gamma = \begin{cases} \max\left([D_2]_{ij}, 1\right), & \text{if } i = j \\ 0, & \text{if } i \neq j \end{cases}$$

The mutual mean is potentially singular by construction, but can be avoided with the following approximation

$$\gamma = \left(P_{EI}^{-1} - \Gamma^{-1} + 2\eta I_{n\times n}\right)^{-1} \left[\left(P_{EI}^{-1} - P_2^{-1} + \eta I_{n\times n}\right)\hat{\boldsymbol{x}}_1 + \left(P_{EI}^{-1} - P_1^{-1} + \eta I_{n\times n}\right)\hat{\boldsymbol{x}}_2\right], \tag{4–10}$$

where $\eta = 0$ if any eigenvalue of P_j, resulting from the joint diagonalization of P_i and P_j yielding $P_i = I$, has magnitude slightly larger than one, or else $\eta = \zeta$, where ζ is some small perturbation [123].

Given the EI fusion law and following the development of the error state loss function, the EI fusion state is found by minimizing the following loss function

$$J_{EI}(\Delta\boldsymbol{x}_1, \Delta\boldsymbol{x}_2, \Delta\boldsymbol{x}_\gamma) = \frac{1}{2}\sum_{i=1}^{2} \Delta\boldsymbol{x}_i^T P_i^{-1} \Delta\boldsymbol{x}_i - \frac{1}{2}\Delta\boldsymbol{x}_\gamma^T \Gamma^{-1} \Delta\boldsymbol{x}_\gamma,$$

where $\Delta\boldsymbol{x}_i \triangleq \hat{\boldsymbol{x}}_{EI} - \boldsymbol{x}_i$ and $\Delta\boldsymbol{x}_\gamma \triangleq \hat{\boldsymbol{x}}_{EI} - \gamma$. As was the case with the CI fusion law, it is important to view the system from this perspective, as attitude compositions are not purely additive. For attitude states, the loss function becomes

$$J_{EI}(\delta\hat{\boldsymbol{\alpha}}_1, \delta\hat{\boldsymbol{\alpha}}_2, \delta\hat{\boldsymbol{\alpha}}_\gamma) = \frac{1}{2}\sum_{i=1}^{2} \delta\hat{\boldsymbol{\alpha}}_i^T P_i^{-1} \delta\hat{\boldsymbol{\alpha}}_i - \frac{1}{2}\delta\hat{\boldsymbol{\alpha}}_\gamma^T \Gamma^{-1} \delta\hat{\boldsymbol{\alpha}}_\gamma.$$

The optimality condition for the EI fusion law is

$$\mathbf{0} = \sum_{i=1}^{2} \left(\frac{\partial \delta\hat{\boldsymbol{\alpha}}_i^T}{\partial \hat{\boldsymbol{s}}}\right) P_i^{-1} \delta\hat{\boldsymbol{\alpha}}_i - \left(\frac{\partial \delta\hat{\boldsymbol{\alpha}}_\gamma^T}{\partial \hat{\boldsymbol{s}}}\right) \Gamma^{-1} \delta\hat{\boldsymbol{\alpha}}_\gamma \tag{4–11}$$

Therefore, the EI fusion law for attitude states can be determined by first finding the maximum mutual information through Eq. 4–9 and Eq. 4–10, and then making use of the optimality condition in Eq. 4–11 to algebraically solve for the EI optimal fused state.

4.4.3 Summary of Data Fusion Laws for Attitude States

Modification of existing data fusion laws that were originally derived for Euclidean states has demonstrated the applicability of these same fusion laws for states that parameterize $SO(3)$. The CI and EI fusion laws, were shown to have the appropriate form to be viewed from the loss function perspective. Next, Section 4.5 will review the quaternion parameterization for data fusion and the challenges associated with its redundancy. Then, the vectorial parameterization of the attitude error vector and the generation of the vectorial parameterization Jacobian are discussed in Section 4.6 in regard to their application to data fusion.

4.5 Review of the Unit Quaternion for Data Fusion

The Euler-Rodrigues symmetric parameters are described by the unit quaternion, $\boldsymbol{q} = \left[\boldsymbol{q}_v^T, q_4\right]^T$, and defined by the axis and angle of rotation through

$$\boldsymbol{q}_v = \sin\frac{\phi}{2}\boldsymbol{n}$$
$$q_4 = \cos\frac{\phi}{2},$$

where $\boldsymbol{q}_v$ and q_4 are the vector and scalar portion of the quaternion, respectively. The unit quaternion parameterization for attitude is given by

$$R(\boldsymbol{q}) = \left(q_4^2 - \boldsymbol{q}_v^T\boldsymbol{q}_v\right) I_{3\times 3} - 2q_4\left[\boldsymbol{q}_v\times\right] + 2\boldsymbol{q}_v\boldsymbol{q}_v^T.$$

The unit quaternion is a popular attitude parameterization due to it being globally-singularity free with the bilinear kinematics

$$\dot{\boldsymbol{q}} = \frac{1}{2}\Xi(\boldsymbol{q})\omega = \frac{1}{2}\Omega(\omega)\boldsymbol{q}$$

where

$$\Xi(\boldsymbol{q}) = \begin{bmatrix} q_4 I_{3\times 3} + \left[\boldsymbol{q}_v\times\right] \\ -\boldsymbol{q}_v^T \end{bmatrix}$$
$$\Omega(\omega) = \begin{bmatrix} -\left[\omega\times\right] & \omega \\ -\omega^T & 0 \end{bmatrix}.$$

However, a major drawback of the unit quaternion for data fusion is that it requires the constraint,

$$q_4^2 + \boldsymbol{q}_v^T\boldsymbol{q}_v = 1,$$

be satisfied. The attitude matrix parameterized by the unit quaternion and associated quaternion kinematics maintain the constraint by construction and are only subject to numerical precision errors, which can be managed through brute-force normalization.

Recall the general optimization problem for attitude data fusion in Eq. 4–4. When $\delta\boldsymbol{\alpha}$ is formulated with a constrained attitude parameterization, the optimization problem must be modified to satisfy the equality constraints. The new optimization problem is given by

$$\begin{aligned} &\text{minimize } J\left(\delta\hat{\boldsymbol{\alpha}}_1, \ldots, \delta\hat{\boldsymbol{\alpha}}_n\right) \\ &\text{subject to } g(\boldsymbol{s}) - c = 0, \end{aligned} \tag{4–12}$$

where g is the constraint function and c is the constraint value. This optimization problem can be solved through the method of Lagrange multipliers [124]. Various algorithms for solving the constrained optimization problem with the method of Lagrange multipliers have been implemented for the quaternion data fusion problem [115, 116]. However, the addition of the unity constraint adds algorithmic and numerical complexity with respect to the unconstrained optimization problem. This motivates the use of minimal attitude parameterizations for attitude data fusion.

4.6 Vectorial Attitude Parameterization

The parameterization of the attitude error vector dictates the characteristics of the attitude data fusion problem as a consequence of Eq. 4–5. The unit quaternion parameterization requires that a single constraint be satisfied, which generates additional complexity with respect to an unconstrained optimization problem. It is well known that all minimal attitude parameterizations are unconstrained, but also singular for particular attitudes. Singularities can manifest through either of geometric or kinematic origin. Geometric singularities are a result of the description of attitude, in which certain orientations cause the parameters to increase to infinity. Kinematic singularities are a result of the motion of attitude, in which small changes in angular velocity correspond to a escape of the parameterization derivative to infinity in finite time, and vice versa. Both of these singularity types can cause issues for data fusion.

For systems with unconstrained rotational motion, the presence of kinematical singularities poses difficulties for attitude control, estimation, and data fusion. Due to the singularities present in all minimal attitude parameterizations, the constrained unit quaternion parameterization performs well for attitude control [125–127] and estimation [103, 104]. In this research it is assumed that the unit quaternion is used for control and estimation. Alternatively, it is known that certain minimal attitude parameterizations, such as the MRPs and higher order Rodrigues parameters (HORPs), can also be used to produce global singularity-free kinematics by making use of the shadow parameterizations [62, 63]. Furthermore, data fusion only requires the attitude parameterization be free of kinematical singularities for the range of rotations, $\phi \in [-2\pi,\ +2\pi]$, due to the periodic invariance of attitude. However, data fusion need not utilize the same parameterization as that which is utilized in the estimation and control algorithms, as the quaternions produce a constrained optimization problem for data fusion. To circumvent this problem, vectorial parameterizations of the attitude error vector are investigated to generate fast and accurate attitude data fusion laws.

4.7 Parameterized Attitude Error Vector

The vectorial attitude parameterizations and their kinematics discussed in Section 4.6 are now used to derive the attitude error vectors. The attitude composition law provides a measure of change in attitude from one configuration to another. Parameterizing the attitude composition law with the general vectorial parameterization yields

$$\delta R\left(\delta\boldsymbol{\alpha}\right) = R\left(\boldsymbol{r}'\right) R^{T}\left(\boldsymbol{r}\right). \tag{4–13}$$

Therefore, given two attitudes, represented by $\boldsymbol{r}'$ and $\boldsymbol{r}$, the attitude error on $SO(3)$ is exactly given by Eq. 4–13. Although this expression is exact, the goal is to develop a parameterized attitude error representation as required by the data fusion optimality condition in Eq. 4–5. When the principal rotations are small, the attitude error vector

can be represented accurately by a linear model for Eq. 4–13. Small rotations are a valid assumption, as attitude estimation is assumed to produce estimates satisfying the small-angle assumption – even with coarse attitude sensors.

4.7.1 First-Order Model of Attitude Error Vector

Recall that the attitude error vector defined in Eq. 4–3 is parameterization independent. One approach to formulating the attitude error vector is through sequential compositions on $SO(3)$ when parameterized through the general attitude $\boldsymbol{s}$ on $\mathbb{R}^3$. To simplify expressions, higher-order terms are neglected when the attitude error vector is assumed to be small. Alternatively, consider the general nonlinear kinematics given in Eq. 2–13, which are derived through infinitesimal rotations. A Taylor series expansion with respect to time yields

$$\boldsymbol{r}(t) = \boldsymbol{r}(t_0) + \dot{\boldsymbol{r}}(t_0)\Delta t + \frac{1}{2!}\ddot{\boldsymbol{r}}(t_0)\Delta t^2 + \cdots .$$

For small time steps and using Eq. 2–13, a linear model is

$$\boldsymbol{r}(t) = \boldsymbol{r}(t_0) + G(\boldsymbol{r}(t_0))\boldsymbol{\omega}(t_0)\Delta t.$$

If over the time step Δt, the condition, $\delta\boldsymbol{\alpha}(t_0) = \boldsymbol{\omega}(t_0)\Delta t$, is locally satisfied, then the Taylor series approximation is given by

$$\boldsymbol{r}(t) = \boldsymbol{r}(t_0) + G(\boldsymbol{r}(t_0))\delta\boldsymbol{\alpha}(t_0).$$

Therefore, the truncated approximation for the attitude error vector is

$$\delta\boldsymbol{\alpha}(t_0) = G^{-1}(\boldsymbol{r}(t_0))\left(\boldsymbol{r}(t) - \boldsymbol{r}(t_0)\right).$$

Making use of the inverse kinematic form and removing the time index, the approximate model is

$$\delta\boldsymbol{\alpha} = H(\boldsymbol{r})\left(\boldsymbol{r}' - \boldsymbol{r}\right). \tag{4–14}$$

This approximation will serve as the representation of the attitude error vector for data fusion.

4.7.2 Data Fusion Jacobian

The inverse kinematics are now shown to be intimately tied to attitude data fusion. An exact definition of the parameterization Jacobian is related to the angular velocity, where one relevant definition of the angular velocity is

$$\boldsymbol{\omega} = \frac{d\delta\boldsymbol{\alpha}}{dt},$$

where the corresponding differential relationship is

$$d\delta\boldsymbol{\alpha} = \boldsymbol{\omega} dt.$$

Similarly, the parameterization time-derivative is defined by

$$\dot{\boldsymbol{r}} = \frac{d\boldsymbol{r}}{dt},$$

which has the differential relationship

$$d\boldsymbol{r} = \dot{\boldsymbol{r}} dt.$$

It should be noted that these are exact differential relationships. Therefore, the forward and inverse kinematics, as represented through differentials, are

$$d\boldsymbol{r} = G(\boldsymbol{r}) d\delta\boldsymbol{\alpha},$$

and

$$d\delta\boldsymbol{\alpha} = H(\boldsymbol{r}) d\boldsymbol{r},$$

respectively, and thus,

$$\frac{d\delta\boldsymbol{\alpha}}{d\boldsymbol{r}} = H(\boldsymbol{r}).$$

As a result, the Jacobian required by the data fusion optimality condition in Eq. 4–5, is simply the transpose of its inverse kinematical Jacobian. That is,

$$\frac{d\delta\boldsymbol{\alpha}^T}{d\boldsymbol{r}} = H^T(\boldsymbol{r}).$$

The inverse kinematic Jacobian is singular for all minimal vectorial attitude parameterizations. What is important, is that for the Class II parameterizations (which, recalling from Chapter 2, are bestowed with a shadow set), the kinematical singularities can be avoided.

4.7.3 Attitude Error Vector Approximation Accuracy

Choice of parameterization of the attitude error vector should avoid geometric singularities associated with conversion between the unit quaternions and kinematic singularities associated with changes in the parameterization. In Reference [64] it was shown that the accuracy of propagation for the vectorial attitude parameterizations is related to the kinematical condition number, κ, which relates errors in angular velocity to errors in the time-derivative of the parameterization. Furthermore, it was shown that the MRPs have the lowest kinematical condition number when switching between the shadow parameterization and thus are the most accurate vectorial attitude parameterization for propagation.

The general change in attitude was defined in Eq. 4–2. For data fusion, the attitude error vector defined for small rotations is provided for general compositions in Eq. 4–3. For the vectorial parameterizations, the first-order approximation of the attitude error vector was derived in Eq. 4–14. The accuracy of the first-order approximation of the attitude error vector is characterized by the difference in the true value of the attitude error matrix with respect to the attitude matrix parameterized by the approximate attitude error vector, over the range $\phi \in [-2\pi, +2\pi]$. An appropriate measure in the difference is

the Euclidean distance, $\mathcal{J}$, such that the error is defined by

$$\mathcal{J} = \|\delta R(\boldsymbol{r}, \boldsymbol{r}') - R(\delta \boldsymbol{r})\|_f \tag{4–15}$$

where $\|\cdot\|_f$ represents the Frobenius matrix norm. The quantity $\delta \boldsymbol{r}$ is related to $\delta \boldsymbol{\alpha}$ though a scaling. For instance, for the MRPs, the scaling is four, whereas for the FRPs this scaling is eight. The choice of attitude parameterization is based on the objective to minimize this additive error, however other objective functions such as the multiplicative eigenangle error exhibit the same trends. As a result, parameterizations that exhibit linear behavior for $\phi \in [-2\pi, +2\pi]$ are ideal for data fusion. Consider the case of the classical Rodrigues parameters (CRPs), $\boldsymbol{\rho}$, and respective higher orders of the Rodrigues parameters, such as the third-order Rodrigues parameters (TRPs) and fourth-order Rodrigues parameters (FRPs), $\boldsymbol{\tau}$. Figure 4-4A demonstrates that the higher order Rodrigues parameters increase in linearity with the order of the parameterization. This fact of linearity follows directly from the repeated half angle formulation of the higher-order Rodrigues parameters, where the tangent function is nearly linear for small angles. In the limit, the higher-order Rodrigues parameters represent the principal rotation vector, which is an exactly linear function of ϕ, by definition. To compare the

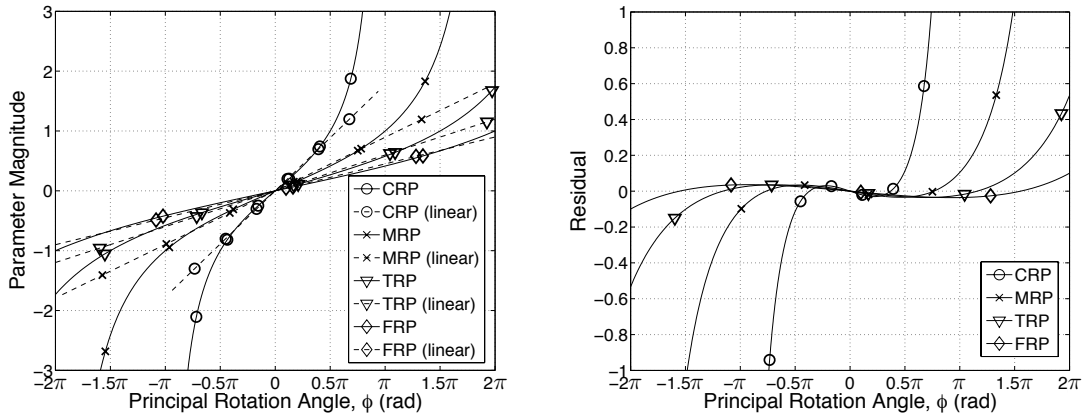

A B

Figure 4-4. Linearity of several orders of the higher-order Rodrigues parameters A) Linear model comparison. B) Linear model residual.

linearity of the parameterizations, a least squares minimization was performed to fit a first-order model using data points originating from half of the nonsingular range of the set. A residual is defined as the difference between the parameterization and the first-order model. From Fig. 4-4B, the residual shows that each order of the Rodrigues parameter begins to exhibit decay to singularity at the principal rotation associated with half of the singularity angle. For example, the CRPs begin to diverge at $\pm\pi/2$, the MRPs at $\pm\pi$, and so on. However, the shadow parameterizations offer relief from these nonlinearities for $m \geq 2$. By making use of the switching surface $\cos\phi/2 = 0$ (i.e., $q_4 = 0$) to switch between the shadow parameterizations, the vectorial attitude parameterization will exhibit the most linear relationship possible for that set. This is due to the symmetry of the parameter about $\phi = 0$, such that the aforementioned switching surface ensures the symmetric set is furthest from singularity. This implies that the principal rotation remains as small as possible for that parameterization. Figure 4-5 shows the effects of principal rotation angle and attitude error angle on the linear approximation when switching between the shadow parameterizations for the attitude error vector for the modified Rodrigues parameters and the fourth-order Rodrigues parameters. The MRPs represent the state-of-the-art for unconstrained attitude data fusion. In this graph, the attitude error angle is depicted by a positive constant principal rotation angle offset, $\Delta\phi$, such that

$$\boldsymbol{\sigma} = \tan\frac{\phi}{4}\boldsymbol{n}$$
$$\boldsymbol{\sigma}' = \tan\frac{\phi + \Delta\phi}{4}\boldsymbol{n}$$

and

$$\boldsymbol{\tau} = \tan\frac{\phi}{8}\boldsymbol{n}$$
$$\boldsymbol{\tau}' = \tan\frac{\phi + \Delta\phi}{8}\boldsymbol{n}.$$

The exact error composition on $SO(3)$, $\delta R(\boldsymbol{r})$, is computed through Eq.4–13 with the parameterized attitude matrix found in Table 2-1. The first-order approximation of the composition is computed through Eq. 4–14 using the parameterized inverse kinematical Jacobian in Table 2-2. Note, the ordinate in Fig. 4-5 is scaled logarithmically, due to the investigation of multiple orders of magnitude for the attitude error angle (in radians). The curves for $\phi \in [-\pi, +\pi]$ are generated using the listed parameters and their shadows are used for $\phi \in (-2\pi, -\pi) \cup (+\pi, +2\pi)$. The first observation from Fig. 4-5 is that since

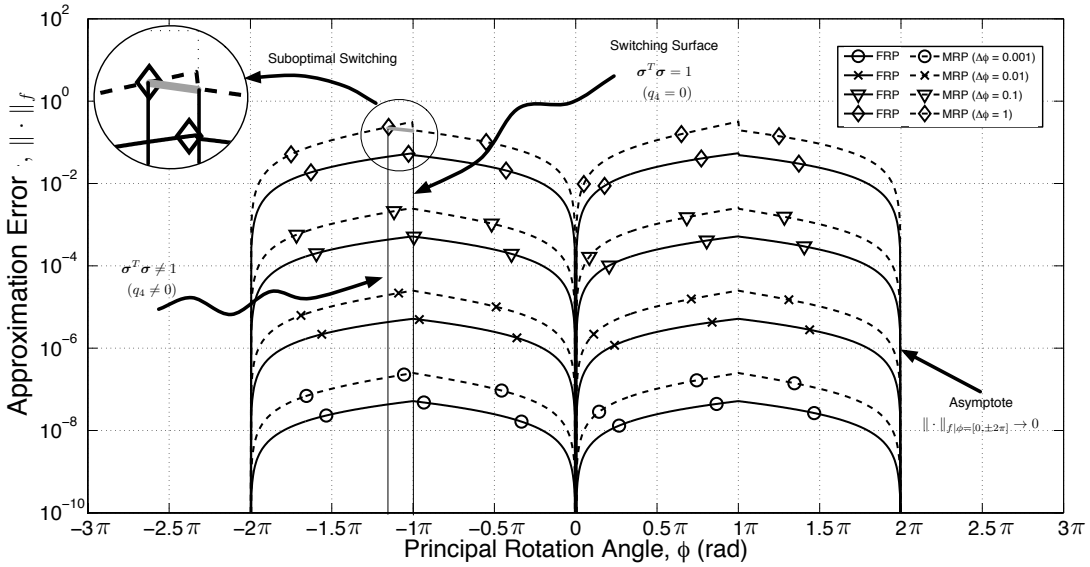

Figure 4-5. Attitude error vector approximation accuracy for the MRPs and FRPs

both the MRPs and FRPs permit a shadow parameterization, both sets have errors that asymptotically approach zero at $\phi = \{0, \pm 2\pi\}$. This is expected, as the shadow parameterization is well defined when the original set is ill-conditioned.

The next observation is that the switching condition, $q_4 = 0$, provides a very robust law for description of the attitude error vector. This fact is illustrated by the peak in error observed at $\phi = \pm\pi$. Since the peak occurs at the intersection of the parameterization with its shadow set, the error is minimal with this switching condition. That is, any other switching point would result in a larger peak error at this intersection. However, as the order of the attitude error increases, the switching law described by $q_4 = 0$ is suboptimal,

as illustrated by the jump discontinuity in the error at $\phi = \pi$ for $\Delta\phi = \{1\}$ radians. The gray line in the magnified circled region in Fig. 4-5 demonstrates that at large angle errors, the switching condition could be adjusted to reduce the error in the approximation. However, large errors invalidate the linearization small angle assumption used in the formulation of standard data fusion and state estimation algorithms. In these cases, modifications to the switching law will improve the error, but more importantly the data fusion and estimation algorithms must be reformulated to account for the nonlinearity in the attitude dynamics process. The fact remains that for small errors, the switching law $q_4 = 0$ is very accurate and robust and thus preferred for data fusion under typical conditions.

The final and particularly powerful observation is that the FRPs produce an attitude error vector which is nearly an order of magnitude more accurate than the MRPs at the peak error associated with $\pm\pi$. Both the MRPs and FRPs are subject to small polynomial error sources as indicated by their respective attitude matrix parameterizations. The higher-order polynomial for the FRPs approximates a linear function in ϕ as evidenced by Fig. 4-4. This improvement in accuracy is consistent for all orders of attitude error (see the legend in Fig. 4-5). It is important to note that as the attitude error grows, the linear approximation error begins to approach the order of the attitude error itself. Whereas, for small attitude errors, the linear approximation is several orders of magnitude smaller, and only has a small affect on the fusion process. However, from an accuracy standpoint, for all cases the FRPs are a preferable parameterization for data fusion in comparison to the MRPs. It is expected that as the order of halving in the tangent increases for the higher-order Rodrigues parameters, that the linear approximation will be more accurate for $\phi \in [-2\pi, +2\pi]$. However, there may be increasing numerical complexity as the order increases. In the limit, the Cayley transform produces the rotation vector, which is completely linear in ϕ. However, the kinematics are ill-conditioned at $\phi = 0$. These observations are illustrative of the benefit

of using the higher-order Rodrigues parameters for the attitude error vector, with the caveat that a trade-off does exist with respect to numerical complexity.

4.7.4 Unit Quaternion Transformation

Section 4.7.3 showed that minimal attitude parameterizations are suited for data fusion as they are unconstrained and can be made to be highly linear for $\phi \in [-2\pi, +2\pi]$. However, the unit quaternion still has large utility for control and estimation. This section provides the details for converting to and from the unit quaternion. Particularly, if the state estimates originate from the unit quaternion, then when using the vectorial parameterization for data fusion, it is necessary to transform back and forth between the vectorial attitude parameterizations and the unit quaternion. Table 4-2 provides a summary the forward and inverse transformations.

Table 4-2. Transformations for vectorial attitude parameterizations and the unit quaternion

Name	$\boldsymbol{r}$	$\boldsymbol{r}(\boldsymbol{q})$	$\boldsymbol{q}_v(\boldsymbol{r})$	$q_4(\boldsymbol{r})$
EOPs	ϕ	$2\tan^{-1}\frac{\boldsymbol{q}_v}{q_4}$	$\frac{\sin\frac{\phi}{2}}{\phi}\phi$	$\cos\frac{\phi}{2}$
CRPs	$\boldsymbol{\rho}$	$\frac{\boldsymbol{q}_v}{q_4}$	$\frac{1}{\left(1+\rho^2\right)^{\frac{1}{2}}}\boldsymbol{\rho}$	$\frac{1}{\left(1+\rho^2\right)^{\frac{1}{2}}}$
MRPs	$\boldsymbol{\sigma}$	$\frac{\boldsymbol{q}_v}{1+q_4}$	$\frac{2}{\left(1+\sigma^2\right)}\boldsymbol{\sigma}$	$\frac{\left(1-\sigma^2\right)}{\left(1+\sigma^2\right)}$
FRPs	$\boldsymbol{\tau}$	$\frac{\boldsymbol{q}_v}{1+q_4+\sqrt{1+q_4}}$	$\frac{4\left(1-\tau^2\right)}{\left(1+\tau^2\right)^2}\boldsymbol{\tau}$	$\frac{\left(1-6\tau^2+\tau^4\right)}{\left(1+\tau^2\right)^2}$
OPs	$\boldsymbol{\eta}$	$\boldsymbol{q}_v$	$\boldsymbol{\eta}$	$\left(1-\eta^2\right)^{\frac{1}{2}}$
LPs	$\boldsymbol{\lambda}$	$\frac{2}{(1+q_4)^{\frac{1}{2}}}\boldsymbol{q}_v$	$2\left(1-\lambda^2\right)^{\frac{1}{2}}\boldsymbol{\lambda}$	$1-2\lambda^2$

4.8 Minimal Attitude Parameterization Data Fusion

Class II vectorial attitude parameterizations are minimal, unconstrained, and nonsingular when paired with their shadow parameterizations. These properties make them ideal for parameterization of the attitude fusion error vector. In this part, a general approach to attitude data fusion using the shadow parameterization switching law is presented. These results are then discussed with respect to the CI and EI fusion laws introduced earlier in Sections 4.4.

4.8.1 Shadow Switching Data Fusion Process

It is assumed that the data fusion process begins with quaternion estimates and that Class II vectorial parameterizations are utilized for the fusion process to avoid solving for the constrained optimization. Since the Class II parameters have shadows, denoted by $\boldsymbol{r}^S$, singularity avoidance can thus be accomplished by switching to the shadow set using a switching law.

Insight into the switching law can be gained from an understanding of MRP-based attitude control. The MRP switching condition for attitude control is typically chosen to be $\boldsymbol{\sigma}^T\boldsymbol{\sigma} = 1$ [62]. This condition is equivalent to switching at the unit sphere where $\boldsymbol{\sigma} = -\boldsymbol{\sigma}^S$. The implication of this switching law is that the attitude parameterization is always bounded by unit magnitude, which is desirable for tuning the resulting controller. However, in general the switching surface takes the form

$$\boldsymbol{\sigma}^T\boldsymbol{\sigma} = c_\sigma, \tag{4–16}$$

where c_σ is an arbitrary real constant. Just like the case for control laws, the fusion law for the vectorial attitude parameterizations is based on the desire to bound the norm of $\boldsymbol{r}$, which results in an analogous switching condition to that of MRP-based attitude control. However, the boundedness in this case ensures that data fusion will be numerically stable, such that small changes in the parameterization are indeed reflective of small angle changes in the attitude.

Assuming that the parameterization for estimation and control is the unit quaternion, the data fusion switching condition for the MRPs in Eq. 4–16 is equivalent to the switching surface on the unit quaternion,

$$q_4 = c_q,$$

where c_q is an arbitrary real constant. Switching at the unit sphere for the MRP, given by $c_\sigma = 1$, is equivalent to the quaternion switching surface at $c_q = 0$. Therefore, the choice

for vectorial attitude parameterization, $\boldsymbol{r}$, of the fusion attitude error vector is given by

$$\boldsymbol{r} = \begin{cases} \boldsymbol{r}, & \text{if } q_4 \geq 0 \\ \boldsymbol{r}^S, & \text{if } q_4 < 0 \end{cases},$$

which is unconstrained and globally nonsingular. Additionally, this choice of c_q ensures the data fusion will occur at the maximum distance from singularity, where the distance is defined through attitude composition. The implications are that this switching condition will produce the most accurate representation for data fusion, as the parameterization will remain the most linear as demonstrated in Fig. 4-5.

From the above discussion, a summary of the vectorial parameterizations fusion law with shadow parameterization switching is provided in the following algorithm: Algorithm 1 provides an unconstrained global nonsingular data fusion process which

Algorithm 1 Vectorial attitude parameterization data fusion with shadow switching

procedure GENERAL FUSION PROCESS($\hat{q}_i$)
    Construct the set of quaternion estimates, $\hat{q}_i$, to be fused and ensure that quaternion vector portions point in the same direction
    Transform the quaternion state estimates to the vectorial parameterization by arbitrarily testing the first quaternion estimate in the set using the following switching condition:
    if $\hat{q}_{4,i} \geq 0$ **then**
        transform all quaternion estimates to their respective vectorial estimate, $\hat{\boldsymbol{r}}$ using the $\boldsymbol{r}(q)$ column in Table 4-2
    else if $\hat{q}_{4,i} < 0$ **then**
        transform all quaternion estimates to their respective shadow vectorial estimate, $\hat{\boldsymbol{r}}^S$, using Eq. 2–11
    end if
    Solve for the fused state from the optimality condition in Eq. 4–5, which for the CI and EI algorithms are computed through Eq. 4–7 and Eq. 4–11, respectively.
    Transform the fused state back to the unit quaternion parameterization using the $\boldsymbol{q}(\boldsymbol{r})$ and $q_4(\boldsymbol{r})$ columns in Table 4-2
end procedure

can be applied to the unknown correlation CI and EI algorithms. In fact, this process is general to any attitude data fusion law satisfying the loss function form in Eq. 4–1. An example of this process utilizing the FRPs applied to the CI fusion law is discussed in the next section.

4.8.2 Example: FRP Covariance Intersection with Shadow Switching

Recall the form of the loss function for the covariance intersection algorithm, Eq. 4–6 and the attitude error vector parameterized by the FRPs given in Table 2-2. Using these definitions, the FRP parameterized covariance intersection loss function is

$$J_{CI}(\tau_{CI}) = \sum_{i=1}^{n} \gamma_i \left(\tau_{CI} - \hat{\tau}_i\right)^T H^T(\hat{\tau}_i) P_i^{-1} H(\hat{\tau}_i) \left(\tau_{CI} - \hat{\tau}_i\right).$$

Following from Eq. 4–7, the CI FRP optimality condition is

$$0 = \sum_{i=1}^{n} \gamma_i H^T(\hat{\tau}_i) P_i^{-1} H(\hat{\tau}_i) \left(\tau_{CI} - \hat{\tau}_i\right)^T.$$

Solving the linear system of equations for $\hat{\tau}_{CI}$, yields the fused attitude given by

$$\tau_{CI} = \left(\sum_{i=1}^{n} \gamma_i H^T(\hat{\tau}_i) P_i^{-1} H(\hat{\tau}_i) \right)^{-1} \sum_{i=1}^{n} \gamma_i H^T(\hat{\tau}_i) P_i^{-1} H(\hat{\tau}_i) \hat{\tau}_i.$$

The required inverse is for a 3×3 matrix and is guaranteed to exist. Existence follows since P_i^{-1} exists by construction, the similarity transform, $H^T(\hat{\tau}_i) P_i^{-1} H(\hat{\tau}_i)$, produces the same eigenvalues as P_i^{-1}, and the matrix to invert results from a convex combination of $H^T(\hat{\tau}_i) P_i^{-1} H(\hat{\tau}_i)$ with $\sum_{i=1}^{n} \gamma_i = 1$.

4.9 Vectorial Attitude Data Fusion with the Local Error Approach

An alternative to the shadow switching method is the local error approach developed in Reference [118]. This method has the benefits of built-in singularity avoidance as well as superb kinematic conditioning. The local error is the result of computing the error quaternion with respect to a reference quaternion. Following the notation of Reference [118], the derivation is for the local error is summarized. Let the quaternion estimate be denoted by $\hat{\boldsymbol{q}}_i$, the reference quaternion as $\bar{\boldsymbol{q}}$, and the fused quaternion as $\boldsymbol{q}_f$. The fused quaternion can be related to the quaternion estimates by a small quaternion error, $\delta\boldsymbol{q}$, such that

$$\boldsymbol{q}_f = \delta\boldsymbol{q}_i \otimes \hat{\boldsymbol{q}}_i. \tag{4–17}$$

An alternative definition of the fused quaternion is to use deviations from the reference trajectory, $\delta\bar{\boldsymbol{q}}$, such that

$$\boldsymbol{q}_f = \delta\bar{\boldsymbol{q}} \otimes \bar{\boldsymbol{q}}. \tag{4–18}$$

The reference trajectory and quaternion estimate are related by

$$\bar{\boldsymbol{q}} = \Delta\boldsymbol{q}_i \otimes \hat{\boldsymbol{q}}_i$$

and thus

$$\Delta\boldsymbol{q}_i = \bar{\boldsymbol{q}} \otimes \hat{\boldsymbol{q}}_i^{-1}, \tag{4–19}$$

where $\Delta\boldsymbol{q}_i$ is once again small. Combining the definitions of Eq. 4–17, Eq. 4–18, and Eq. 4–19, the errors are related by

$$\delta\bar{\boldsymbol{q}} = \delta\boldsymbol{q}_i \otimes \Delta\boldsymbol{q}_i^{-1}$$

and through attitude compositions

$$\delta\boldsymbol{q}_i = \delta\bar{\boldsymbol{q}} \otimes \Delta\boldsymbol{q}_i. \tag{4–20}$$

Now defining the vectorial parameterization of the quantities in Eq. 4–20, the first-order model of the attitude error vector using the local error approach is

$$\delta\boldsymbol{\alpha}_i = H(\boldsymbol{r}_{\Delta\boldsymbol{q}_i})(\boldsymbol{r}_{\delta\bar{\boldsymbol{q}}} - \boldsymbol{r}_{\Delta\boldsymbol{q}_i}),$$

where $\boldsymbol{r}_{\Delta\boldsymbol{q}_i}$ is the vectorial parameterization of $\Delta\boldsymbol{q}_i$ and $\boldsymbol{r}_{\delta\bar{\boldsymbol{q}}}$ is the vectorial parameterization os $\delta\bar{\boldsymbol{q}}$. Algorithm 2 summarizes the data fusion method using the local error approach.

Figure 4-6 depicts the approximation error centered about the identity state out to $5\pi/180rad$. The FRPs still produce an order of magnitude improvement over the MRPs using the local error approach. However, even at $5\pi/180rad$ error, the approximation error is multiple orders of magnitude lower than the fusion error. Therefore, the local

Algorithm 2 Vectorial attitude parameterization local error data fusion algorithm

1: **procedure** GENERAL LOCAL ERROR DATA FUSION PROCESS($\hat{\boldsymbol{q}}_i$)
2: Construct the set of quaternion estimates, $\hat{\boldsymbol{q}}_i$, to be fused and ensure that quaternion vector portions point in the same direction
3: Construct the set of local quaternion error state estimates with respect to a reference quaternion using Eq. 4–19
4: Transform the local quaternion error state estimates to the vectorial parameterization
5: Solve for the fused state from the optimality condition in Eq. 4–5, which for CI and EI algorithms are computed through Eq. 4–7 and Eq. 4–11, respectively
6: Transform the fused local error state to the local quaternion error using the $\boldsymbol{q}_v(\boldsymbol{r})$ and $q_4(\boldsymbol{r})$ columns in Table 4-2
7: Transform the fused local quaternion error state back to an absolute fused quaternion using the inverse of the reference quaternion
8: **end procedure**

error approach is approximately equal no matter the minimal parameterization. Based on this observation, it can be argued that in fact the CRPs should be utilized as the best parameterization for minimal data fusion, as they are more computationally efficient than the MRPs and FRPs. The local error representation ensures that the CRPs will stay far away from their singularity at $\pm\pi$.

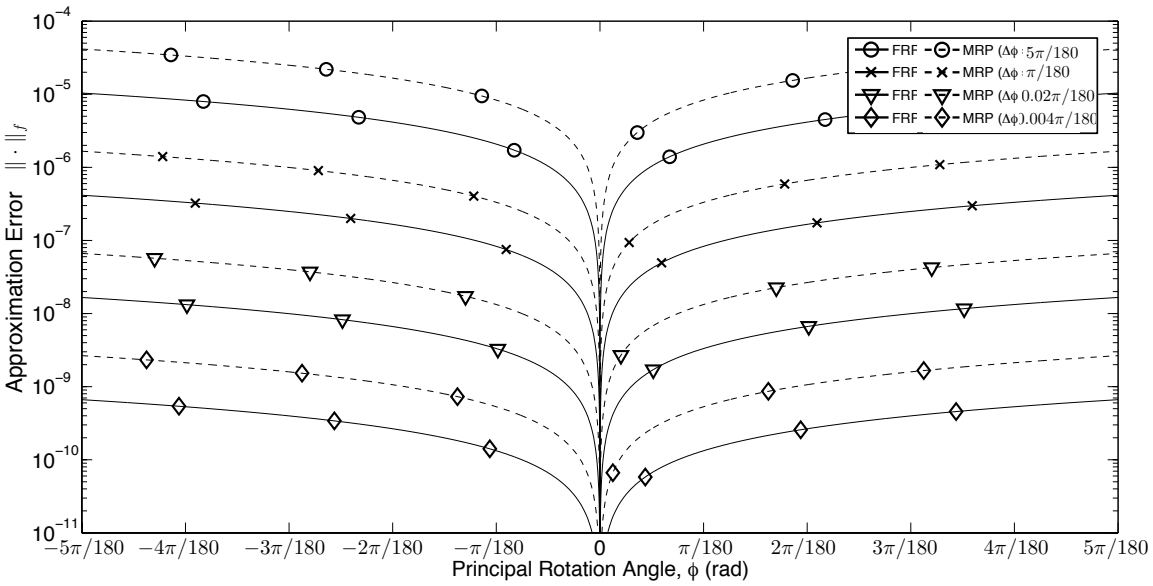

Figure 4-6. Attitude error vector approximation accuracy for the MRPs and FRPs using the local error representation

Taking into account the robustness of the local-error approach to the attitude parameterization, Figure 4-7 demonstrates that although the CRPs are an order

of magnitude worse than the MRPs and two orders of magnitude worse than the FRPs, due to the local error representation, they are still more than adequate for precision attitude applications and add only negligible error for coarse attitude estimation. However, the choice is with the designer of the to balance the accuracy of the parameterization vs the computational expense.

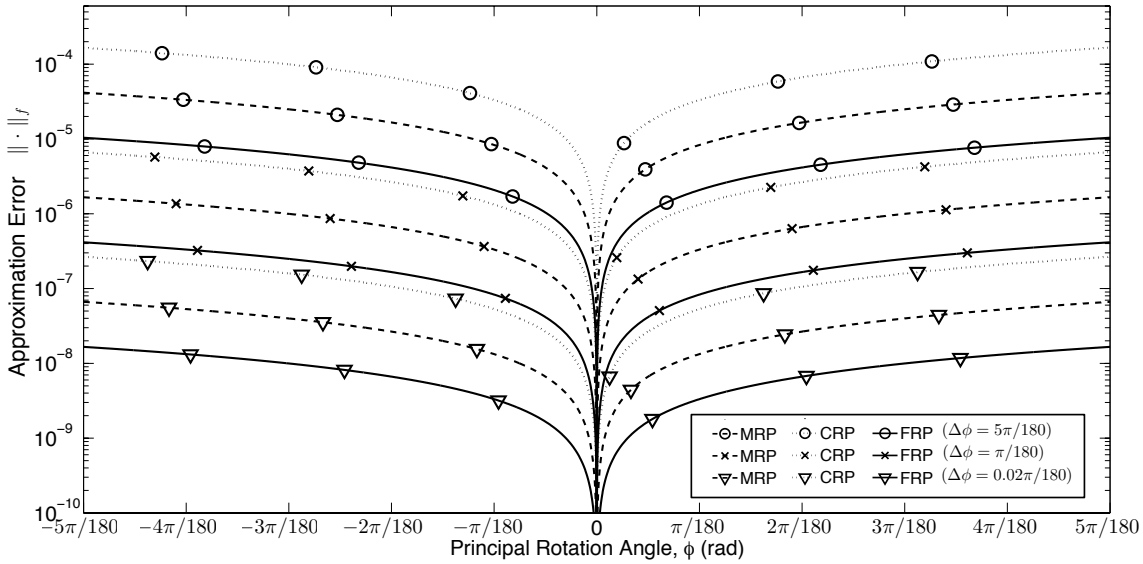

Figure 4-7. Attitude error vector approximation accuracy with the CRPs using the local error representation

Intuitively, the reference quaternion should be chosen to minimize the distance with respect to the identity quaternion. This choice ensures that whichever minimal parameterization is chosen will be the highest accuracy for that parameterization. This leads directly to the quaternion averaging solution mentioned in Reference [118]. However, using the local error approach makes the solution very insensitive to the choice of the reference trajectory, and as a result the reference trajectory can be chosen to be any of the state estimates without a noticeable loss in performance.

4.10 Comments on Attitude Data Fusion

Throughout this research, several new observations were made in the study of attitude data fusion. Several notes related to attitude parameterizations and fusion laws are provided in the following subsections.

4.10.1 A Note on MRP Singularities and Shadow Switching

In Reference [117], singularity avoidance was described for a global MRP approach using a similar switching condition as was described in this section. Additionally, a local MRP approach was presented and further expounded upon in Reference [118], which did not require use of the shadow parameterizations. In Reference [117], both of these methods were shown to be more numerically efficient than existing quaternion data fusion laws. Additionally, the global switching law was demonstrated to be more numerically efficient than the local MRP singularity avoidance method. This efficiency difference is a result of the local error approach necessitating additional transformations to and from the original attitude parameterization as well as the potential need for quaternion averaging to ensure the fusion error remains small.

Although the global MRP switching was shown to be more efficient in Reference [117], it is stated in Reference [118] that data fusion near the unit sphere will cause issues with a global MRP data fusion routine utilizing shadow switching. In particular, it is stated that additive corrections to the fused attitude may result in an erroneous switching of the MRP to its shadow parameterization. Although it is true for all conditions other than on the unit sphere, that when the MRP is inside the unit sphere the shadow MRP is outside the unit sphere, it is not true that the MRP always remains inside of the unit sphere. By continuity, the MRP will be greater than one for all $\phi > \pi$ and unbounded at the singularity existing at $\pm 2\pi$. MRP continuity near the quaternion unit sphere is shown in Fig. 4-8, where the arrows point in the direction of change with increasing ϕ, such that as $\boldsymbol{q}$ moves to $\boldsymbol{q}'$, $\boldsymbol{\sigma}$ moves to $\boldsymbol{\sigma}'$. The equivalent antipodal attitude of $-\boldsymbol{q}$ moves to $-\boldsymbol{q}'$, as $\boldsymbol{\sigma}^S$ moves to $\boldsymbol{\sigma}^{S\prime}$. Both the MRP and the shadow move continuously through the perimeter of the unit sphere along the projection plane. Thus, when the MRP is located on the unit sphere at $q_i = +1$ then the shadow MRP is also on the unit sphere, but at $q_i = -1$, where the converse of this statement is also true. Therefore, assuming that all of the vector portions of the quaternions point in the same direction, the MRP could only

erroneously be fused as a shadow MRP if the state estimate and the fused state have a fusion error of 2π. This is a clear violation of the small angle assumption that was used in the construction of the MRP composition law and attitude error vector description. As a result, the MRP switching law provides a globally nonsingular approach to data fusion. These same arguments hold for the other Class II vectorial attitude parameterizations.

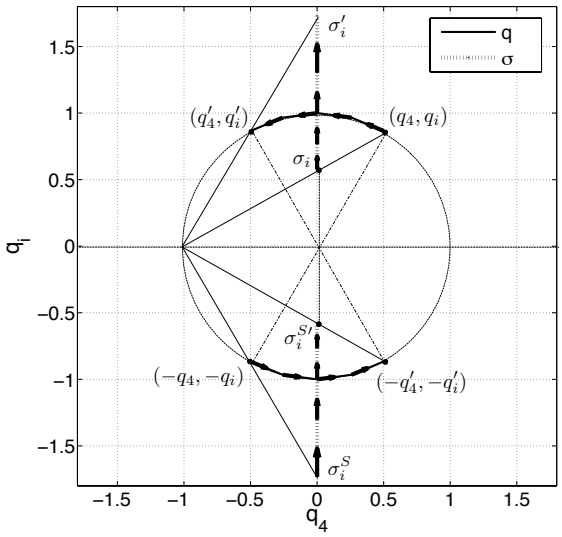

Figure 4-8. Justification for data fusion at the quaternion unit sphere using the shadow parameterizations

4.10.2 A Note on the Minimization Criterion for the CI Attitude Fusion Law

The CI fusion law is equivalent to a one-dimensional minimization problem, where the minimization criterion is typically chosen to be the trace or determinant of the information form of the approximate fused covariance matrix. This minimization criterion is thus problem dependent. The focus of this study is for attitude data fusion, and thus the performance metric for attitude estimation and data fusion is the pointing accuracy.

One definition for the pointing accuracy is

$$J_{pointing} = \sqrt{e^2},$$

where e is the error of the estimate with respect to the true state. In simulation, the performance of the data fusion law can be evaluated with respect to a truth model to

determine the true error in the system. However, the state error cannot be directly characterized for physical systems unless the state is known exactly, which in that case precludes the need for data fusion and estimation. Therefore, a good surrogate for the pointing accuracy of unbiased estimates is the state-error covariance matrix, which corresponds to uncertainty bounds on the error of the state estimate with respect to the unknown truth. From this alternative definition, the pointing accuracy is given by

$$J_{pointing} = \sqrt{tr(P_{CI})}.$$

Since the square root is monotonic, the trace is an equivalent minimization criterion to the square root of the trace. As such, the goal of data fusion should be to minimize the trace of the fused covariance matrix. Thus, there is an equivalence with the application-specific data fusion performance and the minimization criterion of the covariance intersection algorithm. In Reference [115], the trace was shown empirically to be the optimal CI minimization criterion for attitude applications. However, the CI minimization criterion follows directly from the fact that the evaluation criterion for attitude is the pointing accuracy, which was just shown to be equivalent to minimizing the trace of the state-error covariance matrix. This informal proof demonstrates that for attitude applications, one should always minimize the trace for the CI fusion law.

4.10.3 A Note on Covariance Intersection and Ellipsoidal Intersection

On the surface, it would appear that a drawback for utilizing the EI fusion law is that it is only applicable to the fusion of two states, whereas the CI fusion law can be computed for any number of state estimates. However, sequential fusion with the EI fusion law can be accomplished, where the states are iteratively fused together in sequence. This same methodology has been implemented for the CI fusion law and shown numerical and optimality improvements [128].

4.10.4 A Note on Attitude Data Fusion with Appended State Vectors

For most attitude estimation applications, other parameters are typically jointly estimated alongside the attitude. The results developed in this chapter demonstrate an improved approach to parameterizing the attitude error vector for fusing attitude information. However, all of these results are equally valid for cases with appended state vectors that are inclusive of Euclidean states, such as biases and misalignments.

4.11 Two Star Tracker Data Fusion Example

Consider the case of two star trackers outfitted on one spacecraft. The first star tracker is assumed to be aligned with the spacecraft body z-axis and the second star tracker is aligned with the body x-axis. Both star trackers are equal in capability. Each star tracker processes their local measurements and develops an estimate for the spacecraft's attitude. The simulation parameters for the star tracker example in Section 3.6.4 are used in these simulations for the initial state and state estimate parameters. Figure 4-9 provides the error results for the star tracker simulations. The error for the first star tracker is shown in Figure 4-9A, where it is verified that rotations about the boresight, parallel to the body z-axis, have the largest error. Similarly, for the second star tracker, Figure 4-9B exhibits the same behavior, but the boresight is parallel to the body x-axis. Using the FRP data fusion law, Figure 4-9C demonstrates the benefits of data fusion with the state estimates are of similar accuracy. In this case, the fused attitude combines the excellent error performance of the x-axis using the first star-tracker and the z-axis using the second star tracker.

The performance improvements are further shown in Figure 4-10, which shows a comparison in pointing error when using either of the star trackers individually versus the fused pointing error. The fused state estimate is much less sensitive to sensor effects originating from either sensor, as typically the other sensor will provide any information that is unavailable at a particular instance in time.

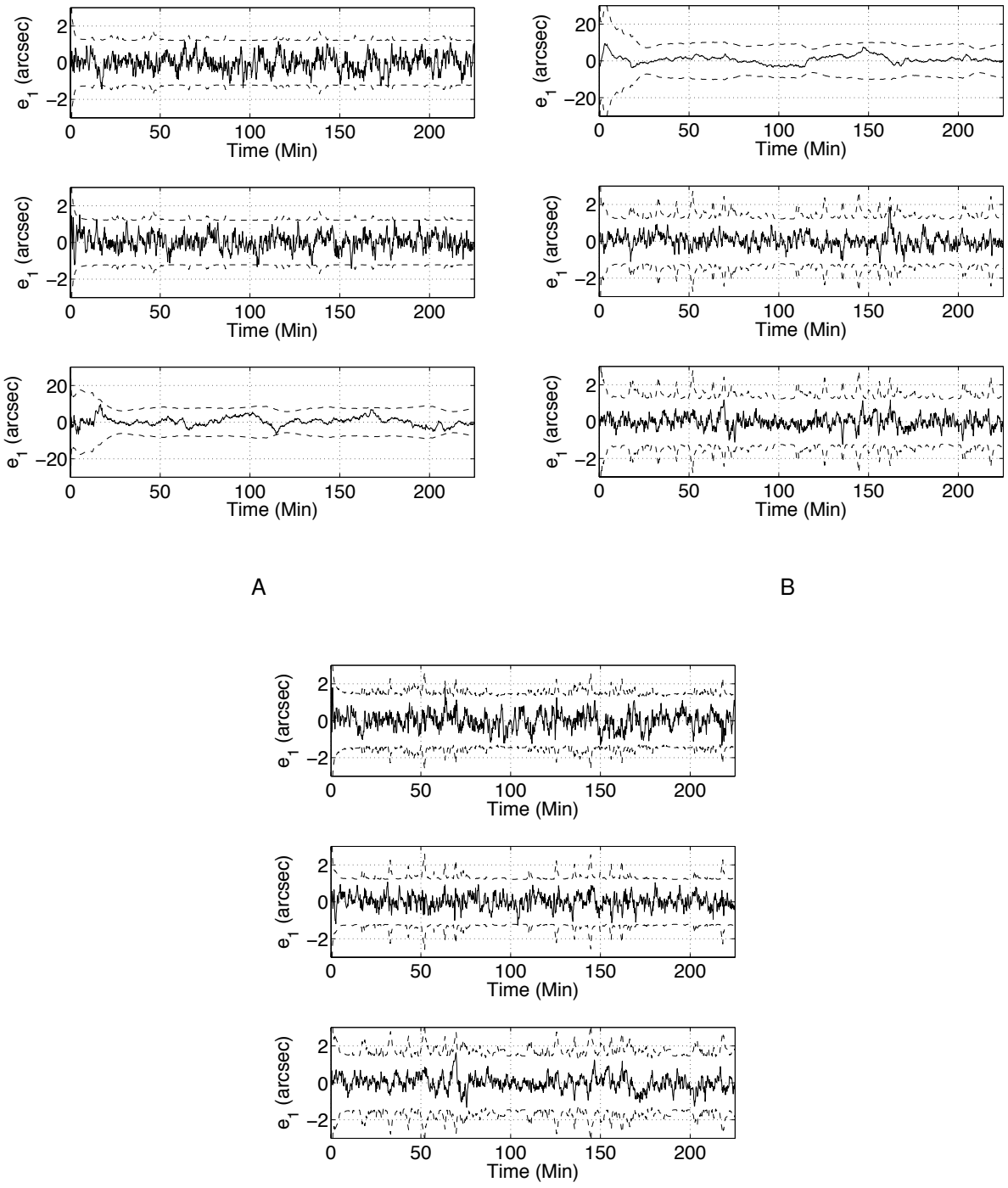

Figure 4-9. Example two star tracker data fusion using the FRPs and shadow parameters. A) Star tracker 1 error without data fusion. B) Star tracker 2 error without data fusion. C) Fused star tracker error.

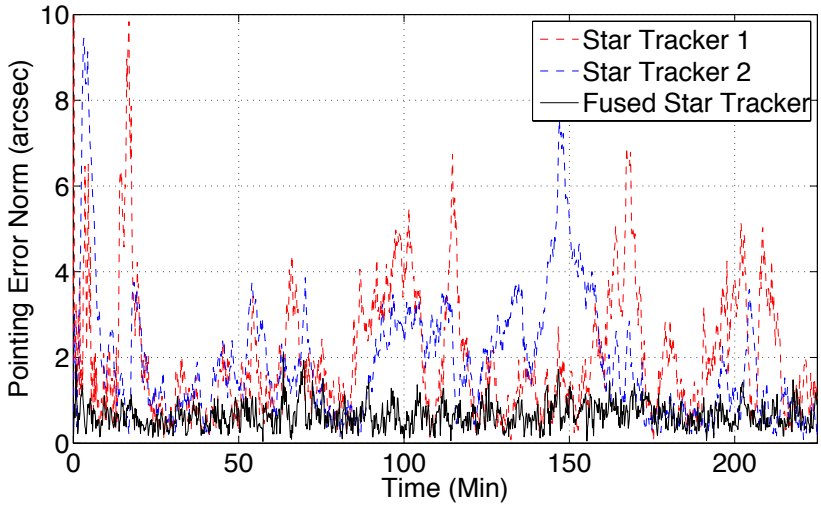

Figure 4-10. Pointing error comparison of two star trackers with and without data fusion

Figure 4-11A demonstrates the approximation error that exits with the MRPs during the converging phase of the filter. During convergence, the error is still high and the approximation error actually causes the fused estimate to be larger in error than either of the individual state estimates. However, when using the local error representation as is done in Figure 4-11B, the effect of the approximation is mitigated and the fused state exhibits the benefits of the data fusion process.

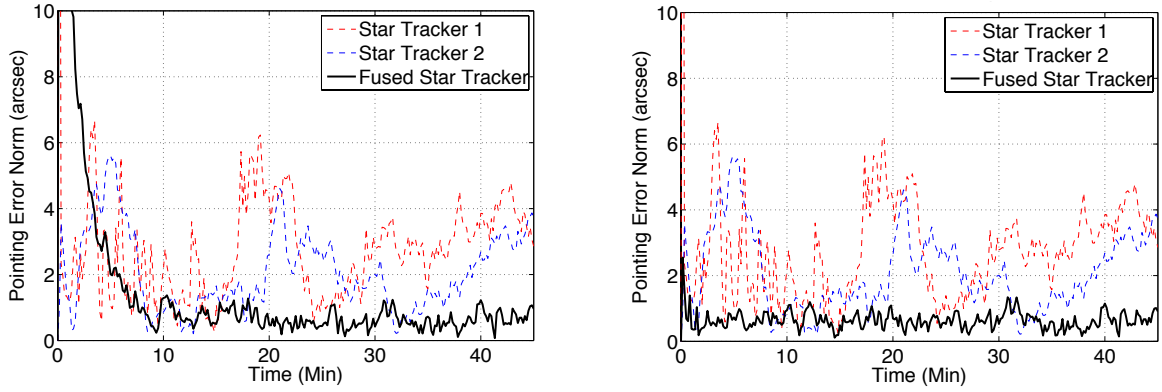

Figure 4-11. Comparison of star tracker data fusion with MRP shadow parameter and local error representation. A) MRP fusion with shadow switching B) MRP fusion with local error representation

4.12 Summary

A general framework for extending Euclidean state data fusion laws to attitude states was presented in this Chapter. The vectorial attitude parameterizations served as a framework for generating minimal unconstrained attitude data fusion laws. First-order approximations of the attitude error vector were shown to be more accurate for higher-order Rodrigues parameters with respect to the modified Rodrigues parameters and classical Rodrigues parameters. It is interesting to note that when the HORPs were developed, Tsiotras stated, “It still remains, however, to determine the applicability of these higher order parameters in realistic attitude problems” [63]. This chapter has shown that the HORPs are a highly accurate parameterization for minimal attitude data fusion.

Given the description of the attitude error vector accuracy, two methods were investigated for attitude data fusion. The first method makes use of the shadow set for the Class II vectorial parameterizations to provide an unconstrained global nonsingular parameterization for data fusion. However, it is noted that the attitude error vector accuracy is highest when centered around the null attitude state. Therefore, the local error representation was adopted to improve the accuracy for data fusion. Based on the results of the local-error, for infinitesimal rotations, data fusion is invariant to the minimal attitude parameterization, as all sets are infinitesimally linear. Even for relatively large attitude errors (several degrees), the attitude error vector linear approximation error is orders of magnitude less than the fusion error. Therefore, the CRPs are the parameter of choice for fast attitude data fusion. If a small improvement in accuracy is desired (fractions of a percent), then higher-order parameterizations can be used.

Recalling the first thesis statement on data fusion in Section 1.4, this chapter presented facts were to extend existing data fusion methods on Euclidean state spaces can be extended to the attitude state spaces. It was also seen that by choice the combination of choosing an appropriate minimal attitude parameterization, along with

the local error representation, leads to a family of fast unconstrained global nonsingular attitude data fusion laws.

CHAPTER 5
STOCHASTIC GREEDY SENSOR TASKING

This chapter is concerned with how to most effectively task the chief to capture and share relative attitude measurements with respect to the deputies to minimize the attitude error of the deputies. First the sensor tasking problem is introduced, which is followed by the introduction of fixed and greedy tasking algorithms. Metrics are then investigated for the greedy tasking approach. Simulations are performed to the fixed tasking algorithm with the greedy tasking algorithm. In addition, several metrics are compared, and Monte Carlo analysis is used to provide a statistical comparison of the tasking metrics.

5.1 Sensor Tasking Overview

In a deterministic setting, a tasking problem typically involves the solution to a traveling salesman problem, where using the analogy, a salesman must visit a prescribed set of houses in the shortest path. There are many solutions to this problem, one of the most well known and classic approaches being the Hungarian Algorithm [129]. The traveling salesman problem suffers from the curse of dimensionality and often requires heuristics and problem dependent algorithm modifications for larger networks.

Unlike the traveling salesman problem, the sensor tasking problem takes on a modified structure, where each target may need to be visited more than once and the edge weightings are based on the performance metric of interest, which may be stochastic in nature. Therefore, sensor tasking requires a modified solution approach. In the desired solution, the sensor follows a path of least resistance to distribute measurements or information to a set of deputies, while minimizing fuel and time. However, the objectives of uncertainty minimization and traditional control objective minimizations are confounded. In the event that the objective is to minimize the pointing error in the system, the controller actions are based on sensing objectives. If the objective is to minimize fuel and time, the control is only as good as the certainty in the

state estimates. Therefore, the control and tasking objectives are inseparable. Optimal solutions to problems with this structure are computationally expensive and suffer from the curse of dimensionality.

Others have investigated similar problems. An information-based approach to sensor tasking for decentralized control of vehicles constrained to planar motion and tasked with information gathering was developed in Reference [130]. The performance objective of the sensor tasking problem was evaluated by information measures. One question that is addressed in this chapter is, “are information-theoretic measures appropriate for attitude sensor tasking?” The work in Reference [130] was concerned with systems where information changes continuously with the dynamic states of a network of vehicles, such that a continuous control input on the vehicle causes a continuous information change. Sensor tasking for attitude resource sharing is also concerned with the problem of information gathering. However, in the framework under study, information is only gained when the relative attitude sensor is capturing measurements, which can require significant time steps to slew to the sharing orientation. Therefore, for a small look-ahead time, relative attitude may not be available during the slew, and thus no new information is gathered.

Optimal sensor tasking using information metrics has also been applied to space-based sensors for the planar translational motion problem [131]. Tasking was based on constraints with regard to range and field-of-view, and applied to the space situational awareness. The tasking solution involved solving a discrete-time linear programming problem. However, this decision-making did not consider the sensor dynamics and coupling between the sensor states and the observations. Another planar example used information metrics and applied them to a myopic (read: greedy) tasking for space situational awareness (SSA) [132, 133]. Finally, an information receding horizon approach to suboptimal sensor tasking was developed and demonstrated for one-dimensional harmonic oscillators [134, 135]. Stochastic optimal control theory was

used to pose the tasking problem as a partially observable Markov decision process (POMDP), in which stochastic simulation was used along with a stochastic relaxation of the deterministic tasking control. However, the method of Reference [134, 135] relies on the assumption that information gains occur within the horizon of the control.

It was previously reported that the attitude uncertainty could be used for multi-objective attitude resource sharing in a two-spacecraft scenario [136], where the spacecraft motion has six degrees-of-freedom. The full six degrees-of-freedom case causes additional complexity with respect to the planar solutions described in the aforementioned references. This chapter extends the results of Reference [136] to improve pointing performance for a general network of spacecraft in full 6-DOF motion by sharing attitude measurements based on greedy tasking algorithms. For the disaggregated system considered in this work, the chief decision is based on the deputy uncertainties.

5.2 Tasking Problem Statement

Consider a chief spacecraft, denoted by $\mathscr{C}$, which is capable of measuring the relative attitude of a deputy, denoted by $\mathscr{D}$, but only when within the FOV of the relative attitude sensor. In the case when the deputies lack inertial sensing, the information from the chief is the sole source of inertial attitude knowledge. When the deputies have inertial sensors, the shared resources may be used to improve the local state estimate through data fusion as demonstrated in section 4.11. All spacecraft are equipped with rate gyros for improved precision attitude propagation.

The structure of the sensor tasking problem results in two coupled control problems, which are cascaded in an inner-outer loop framework. The inner control loop is a discrete tasking control. The outer control loop is a continuous control input to command the actuators to track a deputy to measure relative attitude. This is a control for sensing problem. If optimality is sought in the infinite horizon (or some finite horizon), the effect of the two control inputs is obfuscated by the coupling of estimation and control. Estimation and control are inseparable due to the cascading of the control loops and

their respective control objectives. The problem is then to design the tasking control and dynamics control under these conditions.

In addition to the challenge of separation, optimal sensor tasking for continuous dynamical systems with a sensing objective suffer from the curse of dimensionality, as the number of paths in the dynamic programming problem grows unbounded with the number of time steps and nodes in the sensor network.

5.3 Tasking Solution Methodology

In order to mitigate the issues with lack of separability in estimation and control and the curse of dimensionality, a greedy sensor tasking approach is pursued in this chapter. Greedy approaches are also referred to as myopic, as the logic behind these approaches is near-sighted and only considers information immediately available for making decisions [137]. Greedy logic only requires the current state of the system and thus separates estimation and control for the tasking problem, where the discrete inner tasking control loop feeds the outer dynamics control loop with the task. The outer control loop results in tracking problem with control input designed to satisfy the inner control loop task. Figure 5-1 shows the control loop in block diagram form with the greedy approach. Given the Greedy tasking, a real-time feedback control law can be

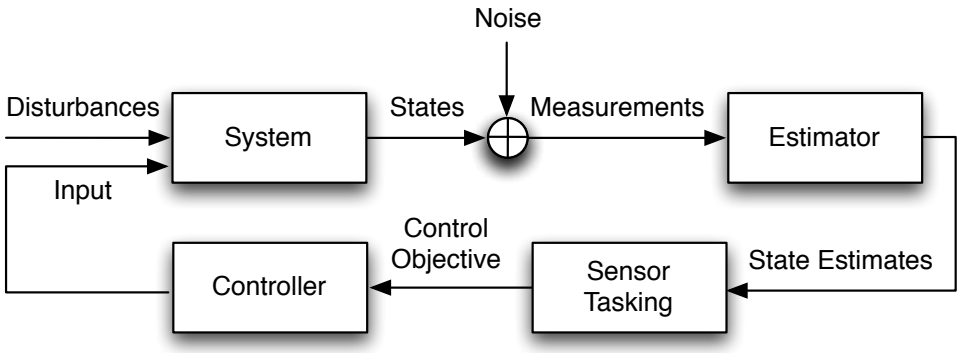

Figure 5-1. Stochastic tasking greedy control problem

used for guiding the chief spacecraft from one task to another and the estimators for all spacecraft can be updated and propagated recursively. Finally, certainty equivalence

holds and deterministic control laws can be used instead of stochastically synthesized controllers.

Figure 5-2 demonstrates the proposed method for attitude resource sharing in a disaggregated attitude determination system. The first step is to construct the instantaneous network of spacecraft that are within the sensor constraints. Next, the current states of each spacecraft are updated based on their available measurements. The deputies then communicate their current state uncertainty back to the chief for decision-making. Based on the provided information, the sensor generates a tasking queue and chooses the highest priority task in the queue to pursue for resource sharing. In order to share measurements, the chief spacecraft must reorient to point the boresight of the relative attitude sensor along the relative position vector, in which the desired quaternion kinematics for resource sharing were derived in Section 2.7.2. Once the chief spacecraft is reoriented to the sharing configuration, measurements are captured and attitude resources are shared over the communication link between the deputy and chief. This process is repeated throughout the mission.

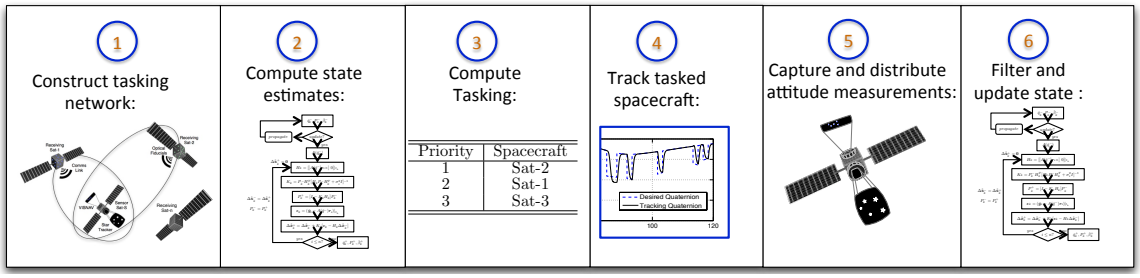

Figure 5-2. Resource sharing process

5.4 Resource Sharing Assumption on Dynamics Time Constants

The time constant for filter divergence is assumed to be much larger than the time constant for the attitude controller. These time constants are directly related to the gyro precision and actuator sizing. This assumption ensures that a deputy without inertial sensing will not diverge between the time it takes the chief to slew to point the relative

attitude sensor at the deputy. If the deputy has an inertial sensor, this assumption is unnecessary.

5.5 Tasking

Sensor management solutions are classified as fixed, greedy, or optimal. Fixed strategies predefine a tasking order, thus ensuring regular resource sharing for all deputies. However, a fixed-strategy cannot adapt to unexpected changes in system conditions – potentially leading to poor system performance. Optimal tasking is at the other extreme, where a performance index is optimized over a time horizon to generate a schedule for the sensor to provide measurements to the deputies. However, due to the inner control loop required to reorient the chief spacecraft pursue a task, estimation and control are inseparable. Therefore, optimal tasking is computationally challenging and not pursued in this research. In between these two tasking extremes is the Greedy strategy, which makes use of the current knowledge of the system – naturally separating estimation and control. The potential advantage over the fixed strategy is that performance is considered, and the system can adapt to changes based on the current information.

5.5.1 Baseline Tasking

This section describes an example fixed-tasking algorithm that is utilized as a baseline. The strategy is referred to as the Round-robin strategy and is summarized in Algorithm 3. Round-robin tasking is initialized by the set of deputies, $\mathscr{D}$, the chief node, $\mathscr{C}$, and the communication range, $\boldsymbol{D}$. In this flow, first the set of available deputies in the network, $\mathscr{D}_D$, are determined based on the deputies in range of communication with the chief, where the column matrix of communication range for the network is designated by $\boldsymbol{D}$ and the current range of the $j^{th} - \textit{deputy}$ is ρ. Next, the current states are updated based on their current information available to the chief and each deputy. For this fixed policy, the chief sequentially cycles through the available deputies. It is assumed that in order to proceed with the next task, the sensor must first satisfy the current task. This

requires that the sensor generates a tracking trajectory based on known relative state kinematics and tracks the trajectory until the relative sensor is aligned with the relative position vector and within the range constraint, $\boldsymbol{D}$. When these conditions are met, the chief measures the relative attitude of the tasked deputy and provides its sensor measurements to the deputy for integration into the deputy estimator.

Algorithm 3 Fixed-cycle resource sharing

procedure ROUND-ROBIN TASKING($P_0, \mathscr{D}, \mathscr{C}, \boldsymbol{D}$)
    Construct tasking set, $\mathscr{D}_D = \{\mathscr{D}_j | \rho_j < \boldsymbol{D}(j)\}, \forall j$
    Choose target cyclically, $\mathscr{D}^* = \begin{cases} j+1, & j \leq n \\ 1, & j > n \end{cases}$, where $\mathscr{D}^* \in \mathscr{D}_D$
    Generate tracking trajectory q_i^*, for $\mathscr{C}$ to share with the tasked spacecraft, $\mathscr{D}^*$
    Track trajectory
    if Tracking Error $\leq$ relative sensor constraint **then**
        Update $\hat{\boldsymbol{x}}_i^-|_k$ to $\hat{\boldsymbol{x}}_i^+|_k$ and $P_i^-|_k$ to $P_i^+|_k$
        Fuse states, if necessary
        Propagate states, $\hat{\boldsymbol{x}}_i^-|_{k+1}$ and $P_i^-|_{k+1}$
        Goto Construct tasking set
    else
        Fuse states, if necessary
        Propagate states, $\hat{\boldsymbol{x}}_i^-|_{k+1}$ and $P_i^-|_{k+1}$
        Goto Track trajectory
    end if
end procedure

5.5.2 Greedy Tasking

An alternative to the Round-robin strategy, and the focus of this chapter, is to maximize a performance metric based on the current state uncertainty of the deputies. For attitude-intensive missions, the uncertainty of interest is the pointing precision. Therefore, the goal is minimize the attitude state-error covariance. For linear Gaussian systems, the probability distribution describing the state error is fully captured by its mean and covariance. Additionally, for unbiased estimators, the mean state error is zero. Therefore, a complete description of the state error uncertainty is embedded in the state-error covariance matrix.

The greedy algorithm utilizes the same initialization as the Round-robin algorithm and is equivalent to the fixed-strategy until the tasking decision is made. To make a tasking decision, the chief gathers information on the deputy uncertainties, which is assumed to be fully described by the state error covariance matrix, $P_i^-|_k$. The chief then generates a tasking priority. Following the choice of a task, the chief tracks the tasked deputy until the deputy until a relative attitude measurement is available. With the availability of a measurement, the deputy incorporates this new information into its state estimate. The greedy tasking is described in Algorithm 4. This algorithm states

Algorithm 4 Uncertainty-based resource sharing

procedure GREEDY TASKING(P_0, $\mathscr{D}$, $\mathscr{C}$, $\boldsymbol{D}$)
    Construct tasking set, $\mathscr{D}_D = \{\mathscr{D}_j | \rho_j < \boldsymbol{D}(j)\}$
    From attitude estimator compute state mean and covariance, $\hat{\boldsymbol{x}}_i^-|_k$, $P_i^-|_k$
    Compute uncertainty-based metric, $J_j = f(P_j^-|_k)$
    Choose next target such that, $\mathscr{D}^* = \arg\max_{j \in N} J_j$, where $\mathscr{D}^* \in \mathscr{D}_D$
    Generate tracking trajectory q_i^*, for $\mathscr{C}$ to share with the tasked spacecraft, $\mathscr{D}^*$
    Track trajectory
    if Tracking Error $\leq$ relative sensor constraint **then**
        Update $\hat{\boldsymbol{x}}_i^-|_k$ to $\hat{\boldsymbol{x}}_i^+|_k$ and $P_i^-|_k$ to $P_i^+|_k$
        Fuse states, if necessary
        Propagate states, $\hat{\boldsymbol{x}}_i^-|_{k+1}$ and $P_i^-|_{k+1}$
        Goto Construct tasking set
    else
        Fuse states, if necessary
        Propagate states, $\hat{\boldsymbol{x}}_i^-|_{k+1}$ and $P_i^-|_{k+1}$
        Goto Track trajectory
    end if
end procedure

that the chief will share resources with the most uncertain deputy and reorient to provide it with measurements. Once the information contained in the measurement is shared and an update occurs, the uncertainty in that deputy will be reduced. If the uncertainty is sufficiently reduced, the chief will be tasked with a different deputy. Therefore, the sensor tasking adapts based on the information gained from acquiring measurements and the information lost due to covariance propagation.

The algorithm as it stands, places equal weighting on the uncertainty of each spacecraft. However, if one spacecraft requires higher precision attitude knowledge, any of these algorithms can be modified to incorporate a convex weighting relationship in the tasking decision. The greedy tasking algorithm does not specify a performance metric. Section 5.6 overviews several performance metrics that characterize the state uncertainty.

5.6 Performance Metrics

There are several properties of interest when tasking the chief to capture relative attitude measurements of the deputies. Ideally, a tasking algorithm will drive the error in the system to its minimum and consume as little fuel and time as possible. However, lack of separation and control make decisions based on fuel consumption and time difficult to pursue. Therefore, only instantaneous states are available. Particularly, state estimation provides a measure of the instantaneous uncertainty in the system. A logical strategy then, is for the chief to provide measurements to the deputy with the highest need at the present time. Defining the highest need based on the uncertainty motivates a characterization of state uncertainty size.

The covariance matrix is a measure of the variance or spread in uncertainty described by the probability density function of a random variable. Since the random variable of interest is the error state of the system, the covariance matrix will provide a comparative measure of uncertainty for all deputy attitude estimates; as they are all centered at zero (assumed to be unbiased) with their respective variances. The higher the variance, the less certain the deputy state knowledge. This implies that deputies need for additional information is greatest. Therefore, higher variances correspond to lower precision in the attitude knowledge.

The goal is to choose a metric that best captures the uncertainty of each spacecraft, so that the chief spacecraft will prioritize its tasking to reduce the pointing error in the maximum uncertainty deputy. In this section, the size of the covariance matrix

is considered. There are several possibilities that exist for characterizing the size of the uncertainty described by a probability density function. Norms provide a measure of distance for vector spaces, which is specifically applicable to the vector space of matrices defined over $\mathbb{R}^{m\times n}$. This section describes several metrics that are a function of the covariance matrix. These metrics populate the uncertainty function, $f(P_j^-|_k)$, int the greedy tasking described in Algorithm 4.

Consider two elements, A and B, which are members of a set. A metric defines the distance, d, between those two elements. More formally, a metric satisfies the following properties [138]:

1. Positivity: $d(A,B) \geq 0$, and $d(A,B) = 0 \Leftrightarrow A = B$,
2. Symmetry: $d(A,B) = d(B,A)$,
3. Triangle inequality: $d(A,B) + d(A,C) \geq d(B,C)$.

5.6.1 Trace

The trace of a symmetric positive definite matrix A, denoted as $tr(A)$, is the sum of the diagonal elements of A and satisfies all conditions of a metric. When A is the state-error covariance matrix, $P_j^-|_k$, the trace sums the small error angle covariance in all three rotational degrees of freedom. Therefore

$$f(P_j^-|_k) = tr(P_j^-|_k) \tag{5–1}$$

provides a measure of the instantaneous total attitude uncertainty of a spacecraft.

5.6.2 Matrix Norms

Alternatively, matrix norms provide a measure of distance, where all norms on a vector space are metrics. Norms are denoted by $\|\cdot\|$. Consider an $n \times m$ matrix, A, with the following properties [85, 139]:

1. Positivity: $\|A\| \geq 0$ for $A \neq 0$ and $\|A\| = 0 \Leftrightarrow A = 0$
2. Scalar homogeneity: $\|\alpha A\| \leq |\alpha|\|A\|$

3. Triangle inequality: $\|A + B\| \leq \|A\| + \|B\|$

Additionally, the norm of a matrix will assume the property of sub-multiplicativity; that is,

$$\|AB\| \leq \|A\|\|B\|. \tag{5–2}$$

Norms are non-unique, but are equivalent in convergence for finite dimensional vector spaces. Although equivalent in convergence, each norm provides a different measure of size and thus can provide different measures of uncertainty. Three norms will be explored.

The 1-norm is the maximum absolute value column sum of a matrix. Applied to a state-error covariance matrix, the 1-norm provides a measure of the maximum total error contributed by a single direction.

$$f(P_j^-|_k) = \|P_j^-|_k\|_1 = \max_j \sum_{i=1}^{n} |a_{ij}|. \tag{5–3}$$

Due to symmetry of the state-error covariance matrix, the maximum absolute value row sum, known as the ∞-norm, is equal to the 1-norm and can be used interchangeably in this application.

The 2-norm is the square root of the maximum eigenvalue of the matrix, $P_j^-|_k^T P_j^-|_k$; that is

$$f(P_j^-|_k) = \|P_j^-|_k\|_2 = \sqrt{\lambda_{max}(P_j^-|_k^T P_j^-|_k)}. \tag{5–4}$$

This norm provides another measure of the maximum error direction, but due to the product required by the determinant incorporates a multiplicative error effect.

Unlike the 1- and 2-norms, the Frobenius norm,

$$f(P_j^-|_k) = \|P_j^-|_k\|_F = \sqrt{tr(P_j^-|_k P_j^-|_k^T)}, \tag{5–5}$$

provides a measure of Euclidean distance for all terms in the state-error covariance matrix relative to zero. Therefore, all terms are weighted equally when determining the

size of the matrix. For the resource sharing problem, this norm states that each direction and cross correlation term is equally important, and thus is measure of the total error in the system. However, when relating the Frobenius norm to pointing, weight is given to the cross-correlation terms, although they do not directly impact the attitude accuracy.

5.6.3 Differential Entropy

In attitude estimation, information is continuously gained and lost in a cycle corresponding to measurement updates and propagation, respectively. Given knowledge of the underlying probability distribution describing the random variable for the state error, an important question is "how much information is contained in that random variable?" Information theory, originally developed to understand communication link efficiency, is finding many uses in modern engineering applications. In this context, information theory is utilized to generate a metric for the state-error covariance matrix size.

Information theory was introduced by Shannon [140] as a mathematical formulation for communication link efficiency. Shannon formulated data transmission as a Markov process and developed the quantity entropy, H, to describe how much information is generated or lost by that process. Entropy was constructed with the following properties [141]:

1. H_{max} is the maximum entropy, which occurs with the sure event
2. $H = 0$ occurs when all events are equally possible (i.e., uniform density)
3. $H(x, y) \leq H(x) + H(y)$ (i.e., the triangle inequality holds)

Consider a discrete random variable, X, with probability mass function, $p(x)$. The entropy satisfies the above properties and is defined as

$$H(X) = -\sum_{x} p(x) \log p(x). \tag{5–6}$$

Shannon entropy describes the compactness of a random variable.

For continuous random variables, the Shannon entropy is referred to as differential entropy [141] and is defined as

$$\mathcal{H}(X) = -\int_X f(x) log f(x) dx. \tag{5–7}$$

For Gaussian random variables, the differential entropy is

$$f(P_j^-|_k) = \mathcal{H}(P_j^-|_k) = \frac{1}{2} log\left[(2\pi e)^n det(P_j^-|_k)\right], \tag{5–8}$$

where *det*( ) denotes the determinant. Differential entropy provides a measure of the volume of the smallest set containing most of the probability contained in a probability density function. Therefore, the uniform distribution will have a maximum entropy, because all values in the support set contain the same information. Whereas, the sure event has minimum entropy. For all distributions between those two bounds, entropy provides a measure of spread in the probability density function. As a result, the differential entropy, as a function of the state-error covariance matrix, provides a natural measure of uncertainty – albeit, it is not technically a metric.

5.7 Simulations

To test the tasking algorithms and performance metrics, a simulation framework was constructed using the MATLAB software [105]. Models were constructed for the orbital and attitude motion of multiple spacecraft flying in formation. Specifically, simulations were conducted on a network consisting of four spacecraft, flying with unconstrained 6-DOF motion. This network is comprised of a single chief spacecraft and three deputies. The deputies are provided with varying fidelity rate gyros to demonstrate the utility of the developed algorithms, such that deputy-1 is provided with the worst gyro, with increasing precision up to deputy-3 – having a gyro that is equivalent to the chief spacecraft. Algorithm 3 was used as baseline for comparison to the Greedy approach described in Algorithm 4.

5.7.1 Perfect Relative Attitude Sensor Assumption

In order to isolate the affects of the sensor tasking algorithms and limit the number of variable parameters, it is assumed for the simulations that follow, that the relative attitude knowledge is perfect. This simplification, eliminates the effects of estimation and data fusion in a disaggregated system, and isolates the tasking performance. Using this assumption, the shared star tracker measurements are transformed using the exact relative attitude matrix, such that

$$^{D_i}\tilde{\boldsymbol{b}}_j = R^T(q_{C/D})\,{}^{C}\boldsymbol{b}_j + R^T(q_{C/D})\,{}^{C}\upsilon_i,\ j = 1, 2, ..., N.$$

In this setting, measurements are shared directly to the deputies and utilized as if they originated on-board the deputies. It should be emphasized that this assumption is only in place to avoid confounding effects with relative attitude and data fusion. Also note, this assumption will be relaxed in the full resource sharing simulations presented in Chapter 6.

5.7.2 Simulation Initialization

Using the simulation testbed, the four-spacecraft scenario was investigated, with inertial motion of the chief and relative motion of the deputies listed in Table 5-1.

Table 5-2 lists the control parameters for the Lyapunov controller derived in Section 2.7.4 and specifically to populate the gains in the resulting controller in Eq. 2–22. The saturation limit is indicative of the limit expected for the size of the spacecraft. Simulations were performed for 225 minutes to ensure that the estimators converged and performance was based on the steady-state behavior. The gyros operate at a sampling frequency of 10 Hz and the star tracker on the chief is sampled every second.

In order to demonstrate the performance of the algorithms discussed, each spacecraft was provided with a different gyro performance specification, as the gyro performance specifications control the information loss process in the attitude estimators

Table 5-1. State initializations for tasking simulations

Spacecraft:		
J_s, J_1, J_2, J_3	$\text{diag}\,(300, 100, 200)$	$\text{kg} \cdot \text{m}^2$
Chief Initial States:		
$\boldsymbol{r}_C\|_0$	$[6778.1 \quad 0 \quad 0]^T$	km
$\boldsymbol{v}_C\|_0$	$[0 \quad 6.6412 \quad 3.8343]^T$	km/s
$q_C\|_0$	$[1 \quad 0 \quad 0 \quad 0]^T$	–
$\omega_C\|_0$	$[0.001 \quad 0.001 \quad 0.001]^T$	rad/s
Deputy-1 Initial States:		
$\rho_{D_1}\|_0$	$[5 \quad -10 \quad 15]^T$	m
$\dot{\rho}_{D_1}\|_0$	$[-0.0100 \quad -0.0113 \quad 0]^T$	m/s
$q_{D_1}\|_0$	$[0 \quad 1 \quad 0 \quad 0]^T$	–
$\omega_C\|_0$	$[-0.003 \quad 0.002 \quad 0.004]^T$	rad/s
Deputy-2 Initial States:		
$\rho_{D_2}\|_0$	$[-10 \quad 5 \quad 25]^T$	m
$\dot{\rho}_{D_2}\|_0$	$[-0.0200 \quad 0.0226 \quad 0.0100]^T$	m/s
$q_{D_2}\|_0$	$[0 \quad 0 \quad 1 \quad 0]^T$	–
$\omega_{D_2}\|_0$	$[0.001 \quad 0.003 \quad -0.003]^T$	rad/s
Deputy-3 Initial States:		
$\rho_{D_3}\|_0$	$[-15 \quad -10 \quad 30]^T$	m
$\dot{\rho}_{D_3}\|_0$	$[0.0100 \quad 0.0339 \quad -0.0200]^T$	m/s
$q_{D_3}\|_0$	$[0 \quad 0 \quad 0 \quad 1]^T$	–
$\omega_{D_3}\|_0$	$[0.002 \quad -0.001 \quad 0.003]^T$	rad/s

Table 5-2. Control and time parameters for tasking simulations

Parameter	Value	Units
Time:		
Δt_{up}	1	*s*
Δt_{prop}	0.1	*s*
T	225	*min*
Controller:		
u_{max}	5	*Nm*
K	$\text{diag}(20, 6.667, 13.333)$	–
C	$\text{diag}(140, 46.667, 93.333)$	–

presented in Chapter 3. The chief spacecraft propagates with a state-of-the-art gyro. Deputy-3 utilizes an equivalent gyro to the chief, whereas deputy-2 propagates with a lower performance gyro and deputy-1 propagates with the most biased and noisy sensor. Table 5-3 provides details on the specific characteristics of the sensors and Table 5-4 details the state estimate initialization. It should be noted that the chief is assumed to slew at a rate slow enough for the accuracy of the sensor to hold, even during the tasking maneuvers. Additionally, the field-of-view on the perfect relative

attitude sensor is simulated with both a small and large field-of-view in the resulting simulations.

Table 5-3. Sensor characteristics for tasking simulations

Parameter	Value	Units
Chief Star Tracker:		
FOV_{star}	6	deg
σ_{star}	1.67×10^{-3}	deg
Chief VISNAV:		
FOV_{vis}	Varying	deg
σ_{vis}	1.67×10^{-3}	deg
Chief Gyro: $\sigma_{C,v}$	$\sqrt{10} \times 10^{-7}$	$rad/s^{1/2}$
$\sigma_{C,u}$	$\sqrt{10} \times 10^{-10}$	$rad/s^{3/2}$
Deputy-1 Gyro:		
$\sigma_{D_1,v}$	$10\sqrt{10} \times 10^{-7}$	$rad/s^{1/2}$
$\sigma_{D_1,u}$	$10\sqrt{10} \times 10^{-10}$	$rad/s^{3/2}$
Deputy-2 Gyro:		
$\sigma_{D_2,v}$	$5\sqrt{10} \times 10^{-7}$	$rad/s^{1/2}$
$\sigma_{D_2,u}$	$5\sqrt{10} \times 10^{-10}$	$rad/s^{3/2}$
Deputy-3 Gyro:		
$\sigma_{D_3,v}$	$\sqrt{10} \times 10^{-7}$	$rad/s^{1/2}$
$\sigma_{D_3,u}$	$\sqrt{10} \times 10^{-10}$	$rad/s^{3/2}$

Table 5-4. State estimate initializations for tasking simulations

Parameter	Value	Units
Chief Estimate:		
$\hat{q}_C\|_0$	$[1 \quad 0 \quad 0 \quad 0]^T$	–
$\beta_C\|_0$	0.1	deg/hr
Deputy-1 Estimate:		
$\hat{q}_{D_1}\|_0$	$[0 \quad 1 \quad 0 \quad 0]^T$	–
$\beta_{D_1}\|_0$	10	deg/hr
Deputy-2 Estimate:		
$\hat{q}_{D_2}\|_0$	$[0 \quad 0 \quad 1 \quad 0]^T$	–
$\beta_{D_2}\|_0$	5	deg/hr
Deputy-3 Estimate:		
$\hat{q}_{D_3}\|_0$	$[0 \quad 0 \quad 0 \quad 1]^T$	–
$\beta_{D_3}\|_0$	1	deg/hr

5.7.3 Single-run Results

The relative motion of the three deputies with respect to the chief follows from the CWH equations and in shown in Figure 5-3. A three-dimensional view is shown in Figure 5-3A, followed by orthographic projections in Figure 5-3B-5-3D. These figures demonstrate that the relative motion is bounded and that the spacecraft are flying in proximity for utilization of a VISNAV-like relative attitude sensor. The boundedness also implies that the communication link is persistent.

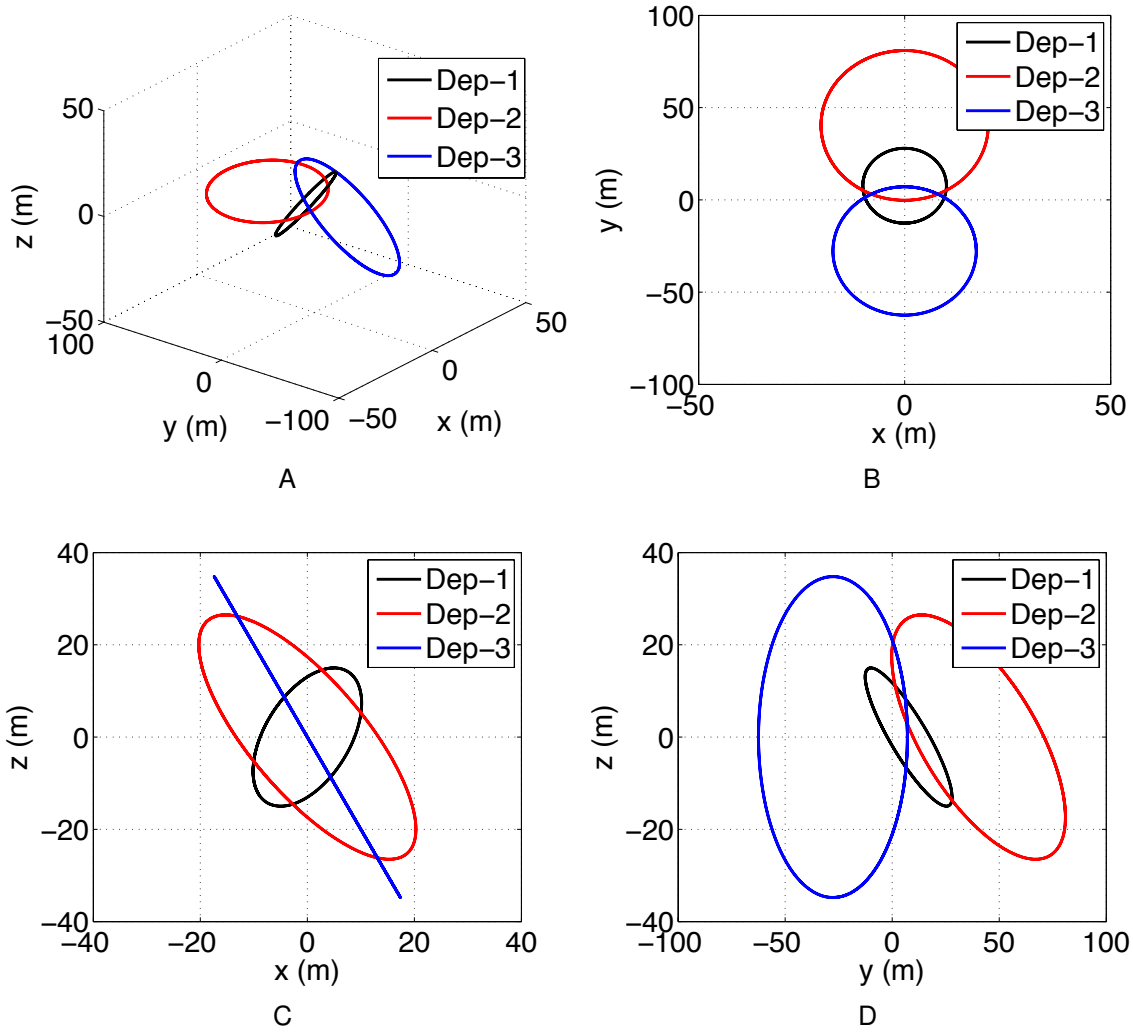

Figure 5-3. Relative position in the Hill frame. A) Three-dimensional B) X-Y projection. C) X-Z projection. D) Y-Z projection

Figure 5-4 shows an attitude precision comparison of the Round-robin strategy to the uncertainty-based greedy algorithms with varying performance metric for a single 225 minute simulation. Also recall that one second of arc is equal 1600^{th} of a degree. Each bar represents the root-mean-square (RMS) error over the simulation duration, which was computed for each algorithm and their associated metrics. The bars are divided in the pointing error contributed by the small rotations about each body axis. The RMS was computed for the time period beginning after each estimator has converged – in this case, chosen as 10 min. In these simulations a 10°-FOV sensor is assumed.

The weighted trace metric greedy allows the system designer to give more priority to a specific deputy. In the weighted case, Deputy-1 was assumed to require more precision than deputy-2 and deputy-3 with weighting $W_1 = 0.5$, $W_2 = 0.25$, and $W_3 = 0.25$. That is, deputy-1 was weighted twice as much as the other spacecraft. From Figure 5-4, the

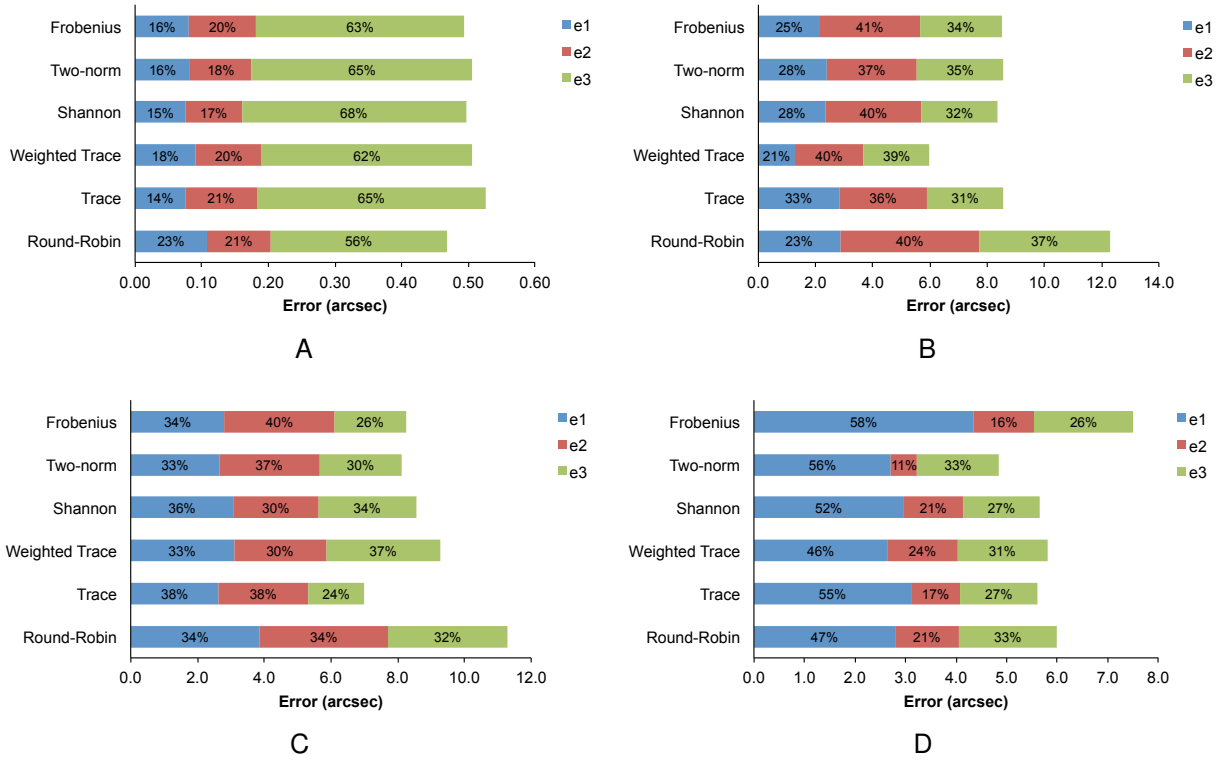

Figure 5-4. RMS error tasking performance comparison (relative sensor 10° FOV). A) Chief. B) Deputy-1. C) Deputy-2. D) Deputy-3.

chief attitude error is an order of magnitude greater than the deputies. This is a direct result of the sparsity of measurements available to the deputies in comparison to the chief; that is, the chief measurements are divided amongst the deputies. Furthermore, the slew between tasks results in no resource sharing in that time period.

Figure 5-4A shows that the chief is dominated by error rotations about the boresight direction of the relative attitude sensor. This results from the fact that direction measurements provide no information about rotations about a vector parallel to that direction. This same behavior is not observed in the bar graphs describing the deputies

in Figures 5-4B-5-4D. This is a result of the relative attitude mapping between the chief and the deputies, where the boresight direction on the chief is mapped to a time-varying direction on the deputy. The deputies motion are periodic due to the torque-free motion assumed in their simulation. This periodicity results in the observed distribution of uncertainty.

When comparing the tasking performance, the chief is mostly insensitive to the tasking algorithm and performance metric. However, there are some indirect dynamic affects from the varying attitude trajectories, which result from the tasking algorithms. The attitude trajectory directly impacts the star field that is observable to the star tracker at any point in time, and thus the accuracy of estimates derived from the star tracker. Another observation is that the round-robin tasking algorithm yields low performance for Deputy-1 and Deputy-2 but high performance for Deputy-3. Recall, that Deputy-3 contains the best gyro specifications, and thus loses information at a much lower rate than Deputy-1 and Deputy-2. Using a round-robin approach, Deputy-3 obtains measurements at an equal rate to the other deputies although it loses information at a lower rate. However, more measurements for Deputy-3 reduced the measurements available to Deputy-1 and Deputy-2. Table 5-5 tabulates the aggregated results of the RMS pointing performance. Improvement in Deputy-3 comes at the cost of reduced performance of the other deputies when utilizing an uncertainty-based greedy approach. From these results, the trace and weighted trace metric yield the lowest aggregated uncertainty. However, these results are for one simulation and for only one field-of-view.

Table 5-5. Aggregated Tasking Performance Comparison (Relative Sensor 10° FOV) RMS Error (arcsec)

	Round-robin	Trace	Weighted Trace	Shannon	Two-norm	Frobenius
Chief	0.47	0.53	0.51	0.50	0.51	0.49
Deputy-1	12.28	8.55	5.99	8.36	8.57	8.53
Deputy-2	11.30	7.01	9.28	8.56	8.13	8.25
Deputy-3	6.00	5.61	5.80	5.66	4.85	7.50
Sum	**30.05**	**21.69**	**21.58**	**23.08**	**22.05**	**24.77**

In addition to the simulation of a 10° FOV VISNAV sensor, simulations were also performed for a 60° FOV VISNAV sensor. A larger FOV sensor results in less slewing by the chief to provide measurements. Figure 5-5 provides a comparison. The general behavior of this case is consistent with the smaller field-of-view sensor. However, there are some differences. Specifically, the best tasking metric for each deputy has changed. Additionally, Table 5-6 shows the performance metric producing the highest aggregate pointing performance has changed. It is important to note that these simulations assume perfect relative attitude measurements when the deputy is within the field-of-view of the relative attitude sensor on the chief. Additionally, measurements are shared instead of state estimate through data fusion. Therefore, the pointing performance observations from the metric are confounded with the dynamic effects from the slewing and the benefits of data fusion are not observed. However, based on the assumptions, a significant improvement was observed in the aggregate accuracy when using the greedy algorithm in comparison to the round-robin strategy. A Monte Carlo analysis is performed in Section 5.7.4 to compare the affects of the tasking metric, statistically.

Table 5-6. Tasking performance comparison (relative sensor with 60° FOV) RMS error (arcsec)

	Round-robin	Trace	Weighted Trace	Shannon	Two-norm	Frobenius
Chief	0.83	0.80	0.98	0.65	0.77	0.76
Deputy-1	7.17	4.59	3.63	4.84	3.86	5.16
Deputy-2	4.56	3.54	4.40	3.25	4.01	4.34
Deputy-3	1.65	3.08	3.99	2.76	3.19	2.71
Sum	**14.21**	**12.01**	**13.00**	**11.50**	**11.83**	**12.97**

5.7.4 Monte Carlo Analysis

A Monte Carlo analysis was performed to compare the uncertainty metric. One hundred samples were drawn uniformly from the underlying probability distributions. Figure 5-6 shows the time history of the attitude error of the chief and deputies for all Monte Carlo samples. The first observation is that each of the deputies exhibits oscillatory behavior in their error. These oscillations were observed to occur at the frequency of the angular velocity of the spacecraft; that is, using the parameters in

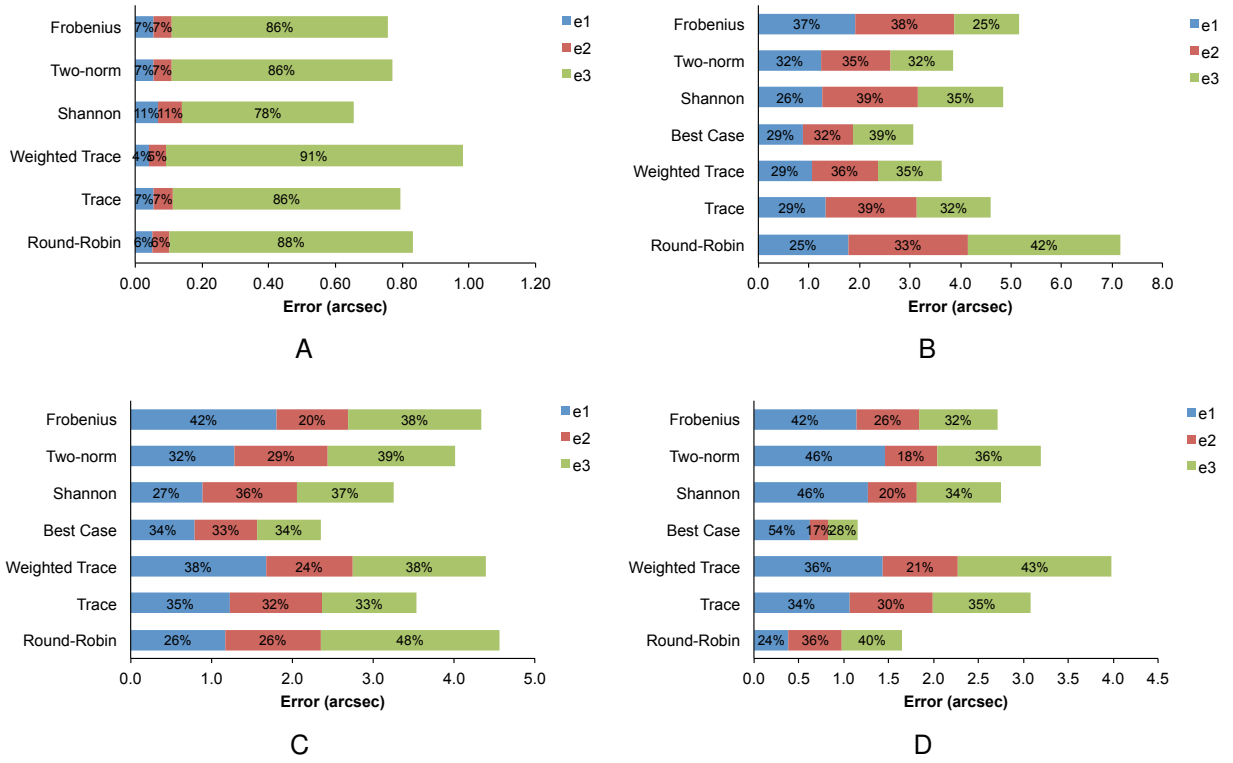

Figure 5-5. RMS error tasking performance comparison (relative eensor 60° FOV). A) Chief. B) Deputy-1. C) Deputy-2. D) Deputy-3.

Table 5-1, the norm of the angular velocity of Deputy-1 through Deputy-3, is $5.39E-3$ rad/s, $4.36E-3$ rad/s, and $3.74E-3$ rad/s, respectively. Since the attitude motion of the deputies is torque-free, angular momentum is conserved, and the norm of the angular velocity is constant throughout the simulation. Another observation is that the 3-σ bounds do in fact bound the error with approximately 99.7% confidence; that is, very few errors fall outside of the 3-σ bounds. This verifies that the filters are consistent, even when measurements are sparse, such as the case for Deputy-3 in Figure 5-6D. Finally, it can be seen that the tasking exhibits only a small variability with respect to the Monte Carlo sampling. This variability is better elucidated in the box-and-whisker plot shown in Figure 5-7. The box-and-whiskers plot visualizes the median, 25-th percentile, 75-th percentile, and minimum and maximum values of the Monte Carlo sampled data. Overlayed on this chart are the RMS error sample points from the Monte Carlo

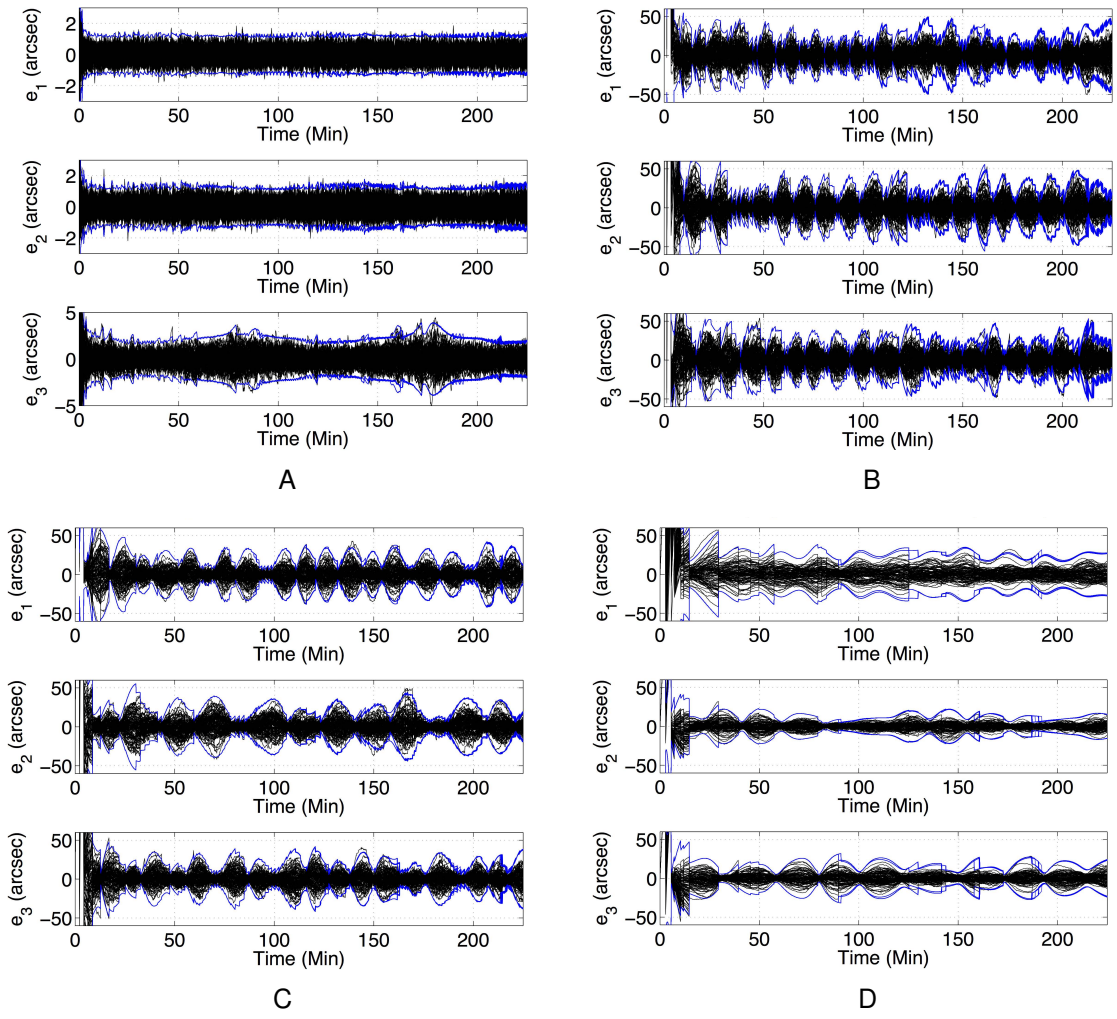

Figure 5-6. Monte Carlo attitude error trajectories for a 10° FOV relative attitude sensor using the trace metric. A) Chief. B) Deputy-1. C) Deputy-2. D) Deputy-3.

sampling, which are jittered for visualization. The mean and standard deviation are also visualized by the red line and top and bottom of the blue region, respectively. Based on this data, the one-norm metric had the lowest sample mean and variance in the RMS error. Additionally, the 10°-FOV data was more spread out than the 60°-FOV data. The relative motion is primary factor that was not removed in the experiments, but not accounted for in the tasking. The difference in performance between the 10°-FOV data and 60°-FOV data is a result of the relative translational motion of the chief with respect

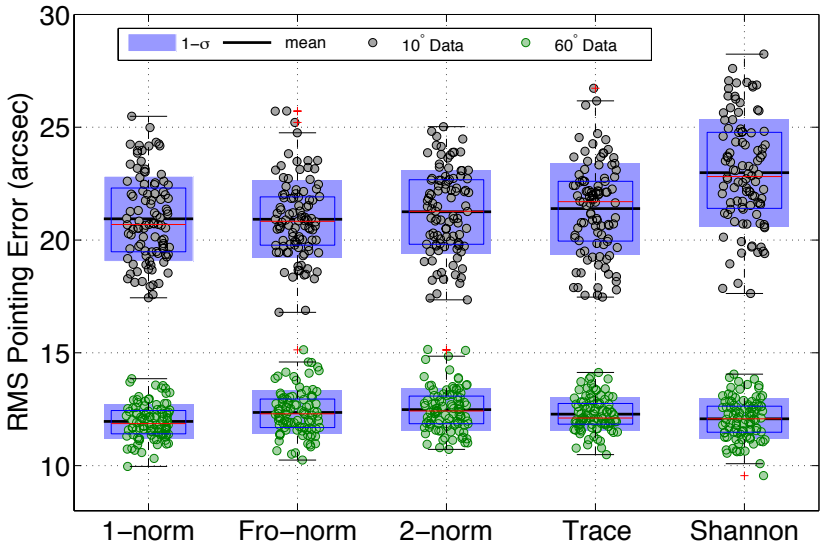

Figure 5-7. Monte Carlo sample data comparison of the RMS error

to the deputies. Therefore, modifications to the greedy tasking algorithm to account for relative translational motion may improve the performance.

5.7.5 A Note on the Trace Performance Metric

As was the case in the note on data fusion (see Section 4.10.2), without the effects of relative motion, the trace metric should provide the optimal metric for uncertainty-based tasking in attitude problems, as pointing is defined through the square root of the trace of the state-error covariance matrix. It is postulated that if the relative motion dynamic effects were not present, this would have been observed in the simulations. However, relative motion does factor into sensor tasking performance for the attitude resource sharing problem. Although the one-norm produced better results in the simulations presented, the improvements were marginal over the trace metric and may be attributed to the relative motion.

5.8 Summary

Two new methods were presented in this Chapter. The first method utilized information-guided greedy sensor tasking to overcome the issue with separation

in estimation and control. The sensor-tasking problem for a disaggregated attitude determination system was introduced. Optimal solutions to this problem were shown to suffer from coupling in estimation and control. As a solution to this problem, greedy tasking algorithms were developed. To drive the greedy algorithms, metrics based on the state-error covariance matrix were introduced. Specifically, the matrix trace, matrix norms, and differential entropy were used as a measure of the uncertainty in each spacecraft. The sensor was then tasked with providing measurements to the most uncertain spacecraft using Algorithm 4. With the Greedy tasking the system pointing error was reduced considerably over the baseline Round-robin strategy of Algorithm 3. Monte Carlo simulations were performed to determine the statistical significance in performance between the different tasking metrics. Results showed that for a particular field-of-view, all of the tasking metrics generated very similar results, but that the one-norm was marginally better than the others for the particular scenarios simulated. The main result of this chapter is that performance in attitude sensor tasking problems is confounding between the effects of relative motion.

CHAPTER 6
SPACECRAFT ATTITUDE RESOURCE SHARING SIMULATIONS

In this chapter, simulations are presented for several attitude resource sharing scenarios. These scenarios are chosen to be representative of missions that could benefit from attitude resource sharing. Simulations are divided into three parts. In the first part, resource sharing in a two spacecraft network is considered. In this case, there is no tasking decision required and the chief is assumed to always track the deputy. Resource sharing with two spacecraft demonstrates the effect of data fusion on the attitude accuracy of the chief and deputy. In the second part, resource sharing between three spacecraft is considered. In this case, the chief tracks the two deputies following a sequence resulting from the tasking algorithm. Results in this part demonstrate the combined effect of data fusion and sensor tasking. In the last part, the greedy and round-robin tasking algorithms are compared for the three spacecraft resource sharing scenarios.

6.1 Simulation Initializations

For the two and three spacecraft scenarios, the initial states and state estimates are initialized with the parameters in Table 5-1 and Table 5-4, respectively. The simulations are performed for 225 minutes, which equates to approximately 2.5 orbits in the assumed 400 km orbit of the chief. The deputies fly in bounded orbits around the chief as shown in Figure 5-3. Table 6-1 lists the sensor characteristics for the attitude sensors and rate gyroscopes.

For all simulations, attitude data fusion uses the FRP parameterization with local error representation as applied to the covariance intersection fusion law, described in Section 4.9. The first two parts assume greedy sensor tasking with the trace metric and the last part provides a comparison of results with the round-robin strategy. The following quantities will be presented to compare the performance and behavior of the resource sharing simulations:

Table 6-1. Sensor characteristics used in attitude estimate resource sharing simulations

Parameter	Value	Units
Star Tracker:		
σ_{star}	1.67×10^{-3}	*deg*
FOV_{star}	6	*deg*
VISNAV:		
σ_{vis}	1.67×10^{-3}	*deg*
FOV_{vis}	10	*deg*
Magnetometer:		
σ_{mag}	1	*deg*
Sun Sensor:		
σ_{sun}	0.1	*deg*
Chief Gyro:		
$\sigma_{C,v}$	$\sqrt{10} \times 10^{-7}$	$rad/s^{1/2}$
$\sigma_{C,u}$	$\sqrt{10} \times 10^{-10}$	$rad/s^{3/2}$
Deputy-1 Gyro:		
$\sigma_{D_1,v}$	$10\sqrt{10} \times 10^{-7}$	$rad/s^{1/2}$
$\sigma_{D_1,u}$	$10\sqrt{10} \times 10^{-10}$	$rad/s^{3/2}$
Deputy-2 Gyro:		
$\sigma_{D_2,v}$	$5\sqrt{10} \times 10^{-7}$	$rad/s^{1/2}$
$\sigma_{D_2,u}$	$5\sqrt{10} \times 10^{-10}$	$rad/s^{3/2}$
Deputy-3 Gyro:		
$\sigma_{D_3,v}$	$\sqrt{10} \times 10^{-7}$	$rad/s^{1/2}$
$\sigma_{D_3,u}$	$\sqrt{10} \times 10^{-10}$	$rad/s^{3/2}$

1. The small angle components of the attitude error vector, $\{e_1, e_2, e_3\}$, with 3-σ bounds for the chief and deputies with and without data fusion
2. Commanded tracking torque for the chief (controller from Eq. 2–22 and gains from Table 5-2)
3. Angular velocity of the chief and deputies
4. Covariance intersection weights

For all cases, the angular velocity of the two-deputies result from torque-free motion, and are provided in Figure 6-1.

6.2 Two Spacecraft Attitude Resource Sharing

With a single chief-deputy pair, resources are shared at the communication rate once the chief has acquired the sharing attitude while tracking the desired control signal described in Section 2.7.1. This case demonstrates attitude resource sharing with data fusion without tasking. The disaggregated estimation scheme and EKF equations provided in Table 3-10 are implemented for the chief-deputy pair. In this scenario, simulations are conducted for the case when the deputy has local access to coarse

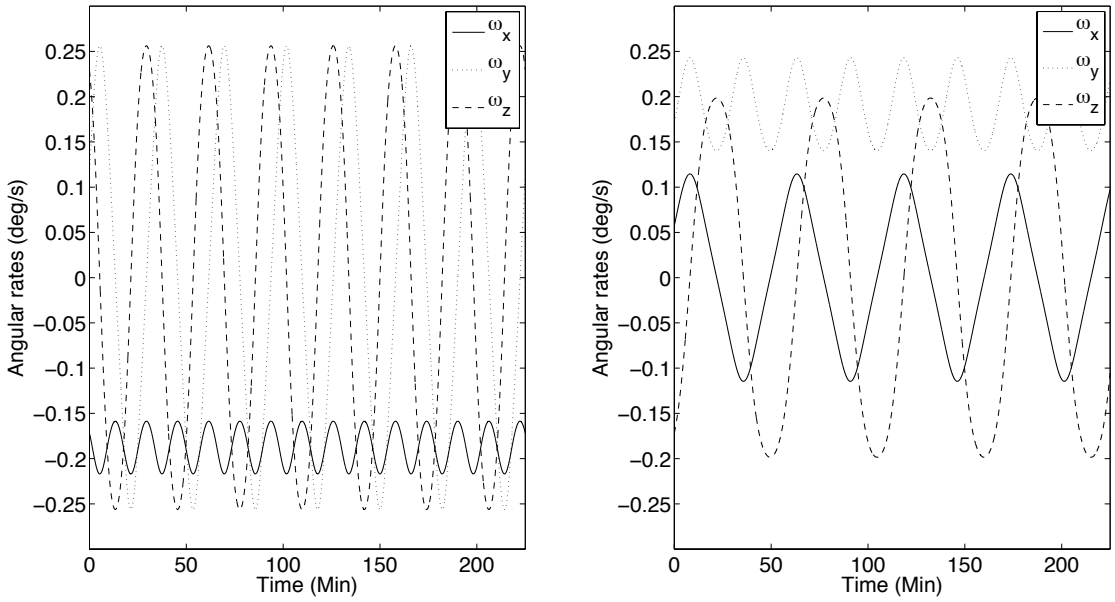

Figure 6-1. Angular velocity resulting from torque-free motion for the deputies in all simulated scenarios. A) Deputy-1. B) Deputy-2.

attitude using sun sensors and a magnetometer, and the case when is has local access to a star tracker. The chief has local access to a star tracker and VISNAV sensor with specifications listed in Table 6-1.

6.2.1 Two Spacecraft with Star Trackers Scenario

The attitude error trajectory for both spacecraft is shown in Figure 6-2. Comparing the results of the chief error in Figure 6-2A with the deputy error in Figure 6-2B, shows that without data fusion the deputy has a steady state error nearly twice as large as the chief. This is a consequence of the deputy using a noisier gyroscope than the chief. However, the incorporation of attitude resource sharing reduces the estimate error in the boresight axis of each spacecraft. This is analogous to the two star tracker case simulated at the end of Chapter 4. Since the chief always tracks the deputy, the control torque and angular velocity operate at nominal tracking levels as seen in Figure 6-3A-6-3B. Specifically, it can be seen that the period of these signals are

consistent with the chief's orbital motion, which recall was approximately 90 minutes. Since both spacecraft have the same star tracker, but different gyros, Figure 6-4 shows that in general the weightings are equal. However, there is a slight preference for the chief information.

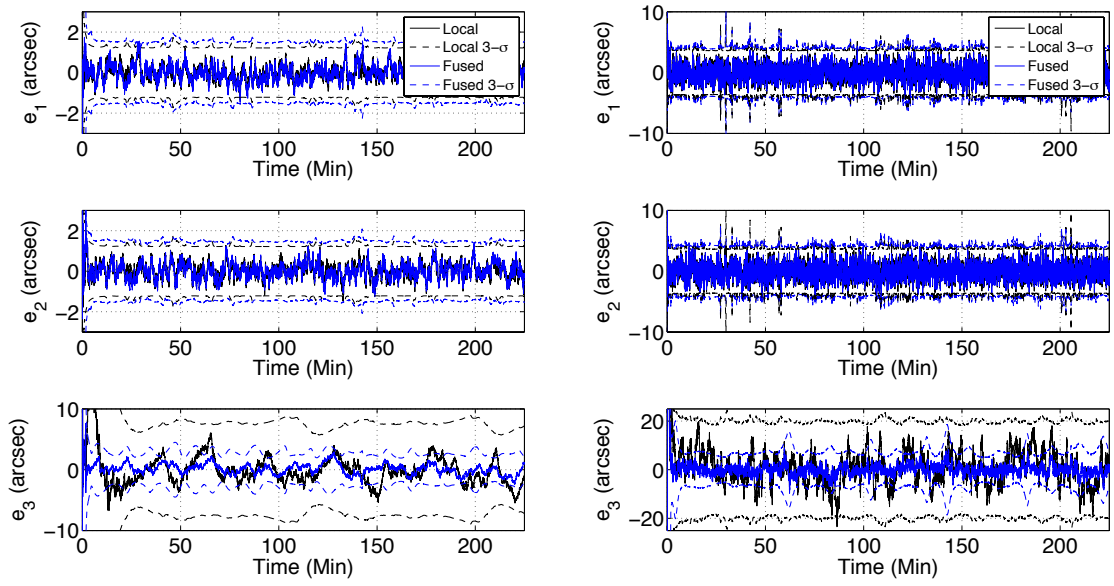

Figure 6-2. Local and fused quaternion error for the two spacecraft star tracker scenario. A) Chief. B) Deputy.

6.2.2 Two Spacecraft with Coarse Deputy Sensors Scenario

Figure 6-5 shows the attitude error in the chief and deputy for the case when data fusion is used, as well as when attitude only local data is used. Since the chief has significantly better sensing than the deputy, Figure 6-5A shows that for coarse deputy sensing, the chief's attitude error is invariant to attitude estimate resource sharing, but the deputy error is improved by orders of magnitude, as seen in Figure 6-5B. Like the two spacecraft with star trackers scenario, the chief tracks the deputy for the entirety of the simulation. As a result, Figure 6-6 shows that the control input and angular velocity are very small. In addition, the deputy never uses its local state estimate after the

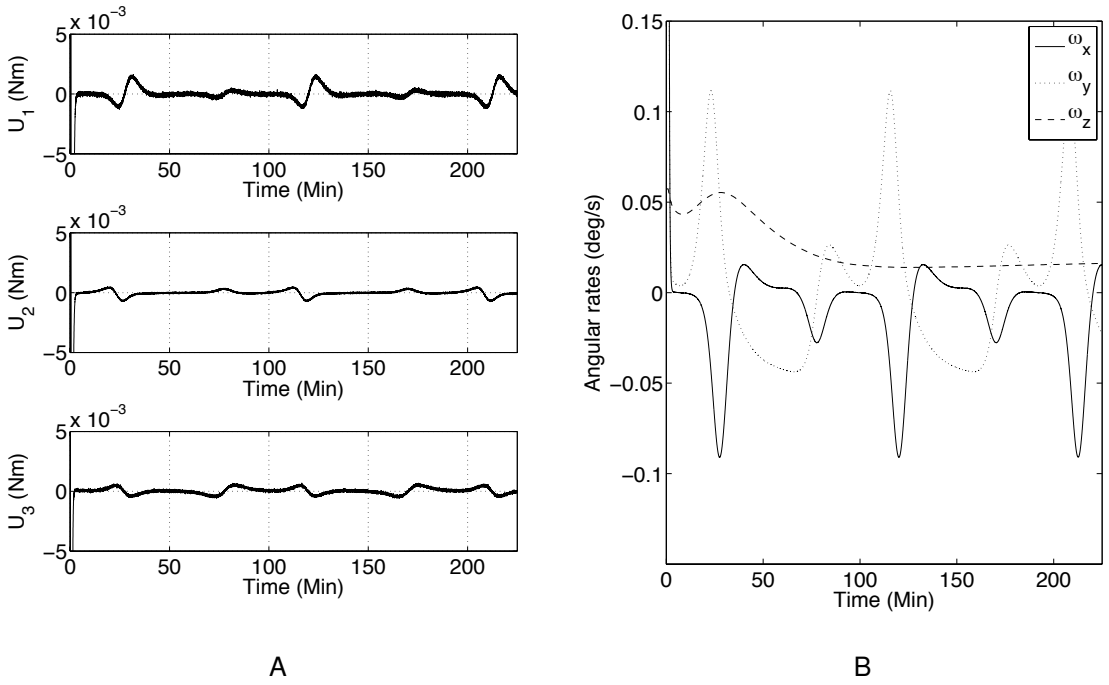

Figure 6-3. Chief attitude control for the two spacecraft star tracker scenario. A) Control torque. B) Angular velocity.

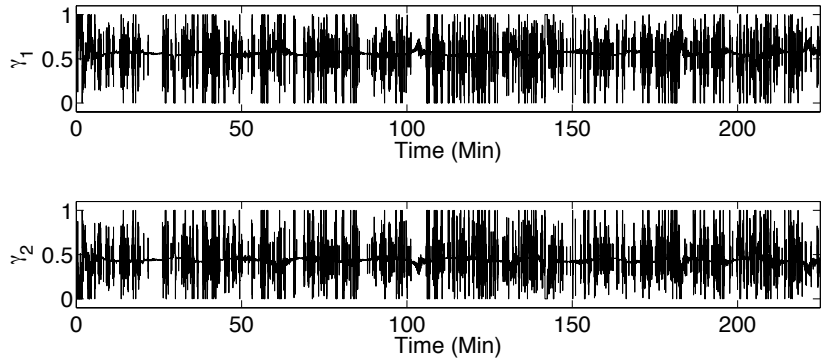

Figure 6-4. Covariance intersection weights for the two spacecraft star tracker scenario

sharing configuration is acquired by the chief, because the information from the chief is always superior to information local to the deputy. This fact is evidenced by the CI weightings in Figure 6-7.

In addition to the long-term behavior seen in the above figures, Figure 6-8 shows a plot of a transient effect in the attitude error at the onset of data fusion. At the instant

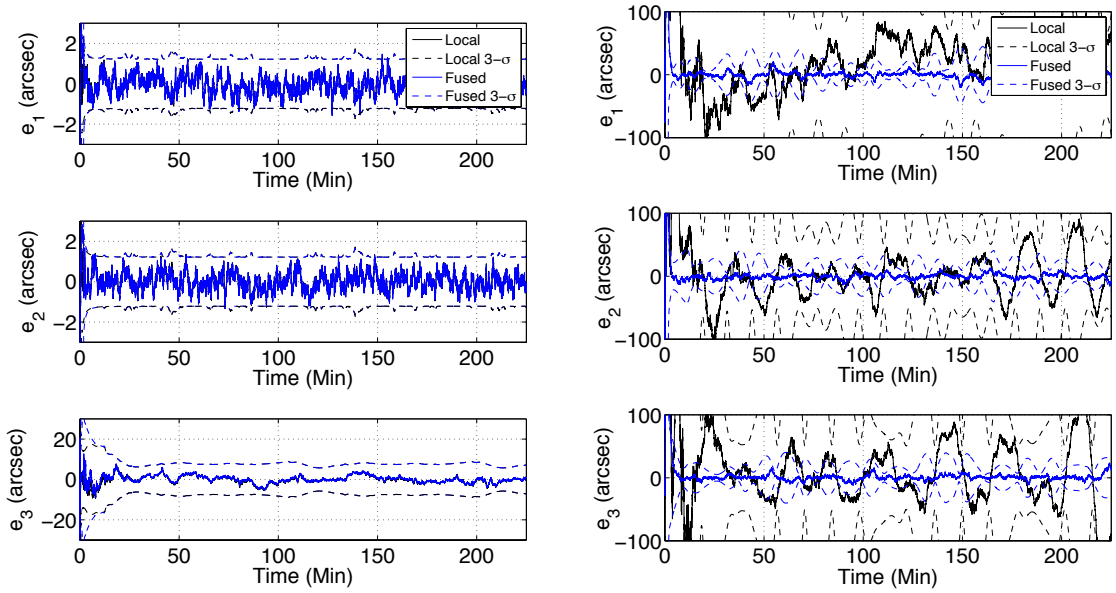

Figure 6-5. Two spacecraft local and fused quaternion error with coarse deputy attitude sensing. A) Chief. B) Deputy.

the first relative attitude measurement is available, the estimate of the deputy on the chief is very poor. However, vector measurements originating from the relative attitude sensor are highly accurate. Therefore, application of the sensitivity matrix in Eq. 3–23 at the first measurement has considerable error due to the error in $R^T(\hat{q}_D^-)$. Therefore, the Kalman gain computation is based on the sensitivity matrix with first-order errors. This causes the error to briefly grow and then decay after relative attitude measurements begin lowering the error in the deputy inertial attitude, such that the sensitivity matrix only exhibits second-order errors.

6.3 Three Spacecraft Attitude Resource Sharing

With more than one chief-deputy pair, the chief must decide which spacecraft requires an improved state estimate by capturing relative attitude measurements. These simulations implement attitude estimate resource sharing through data fusion and sensor tasking. The simulations in this section combine many of the developments

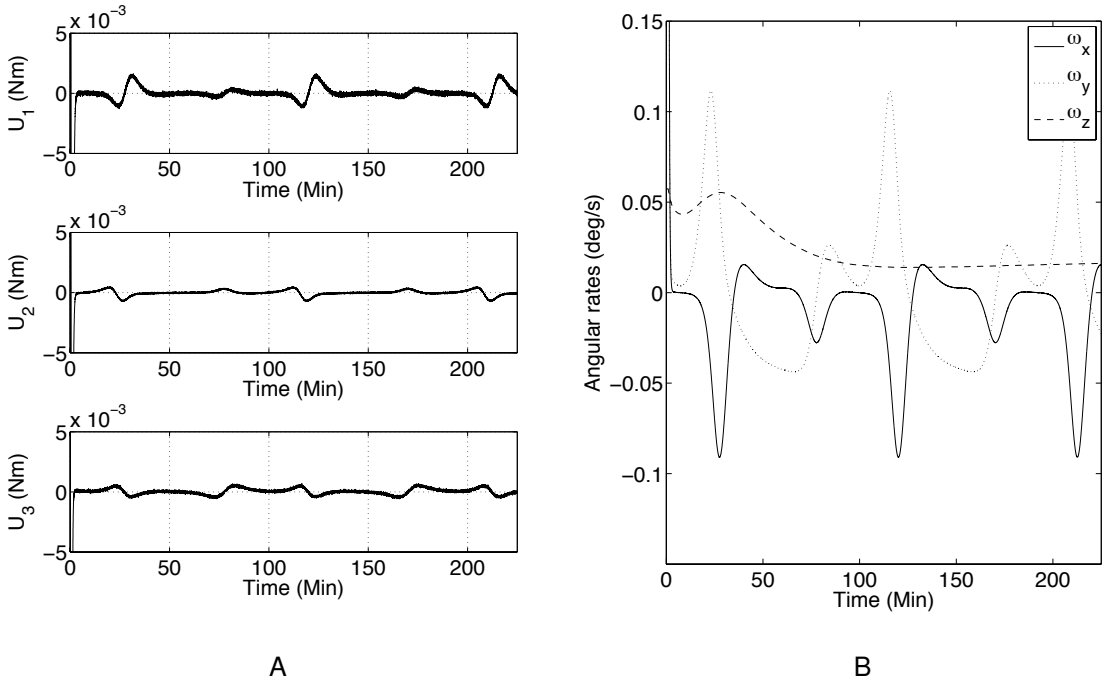

Figure 6-6. Chief attitude control for the two spacecraft coarse deputy attitude sensing scenario. A) Control torque. B) Angular velocity.

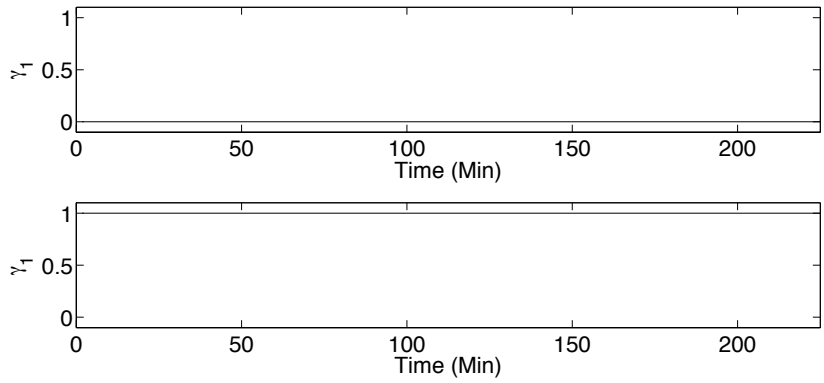

Figure 6-7. Covariance intersection weights for the two spacecraft coarse deputy attitude sensing scenario

presented in this dissertation. Specifically, the EKF for a disaggregated ADS on three spacecraft is implemented based on the general n-spacecraft extended Kalman filtering equations for disaggregated ADS provided in Section 3.9. The FRP local error covariance intersection algorithm is once again used. For tasking, the greedy tasking

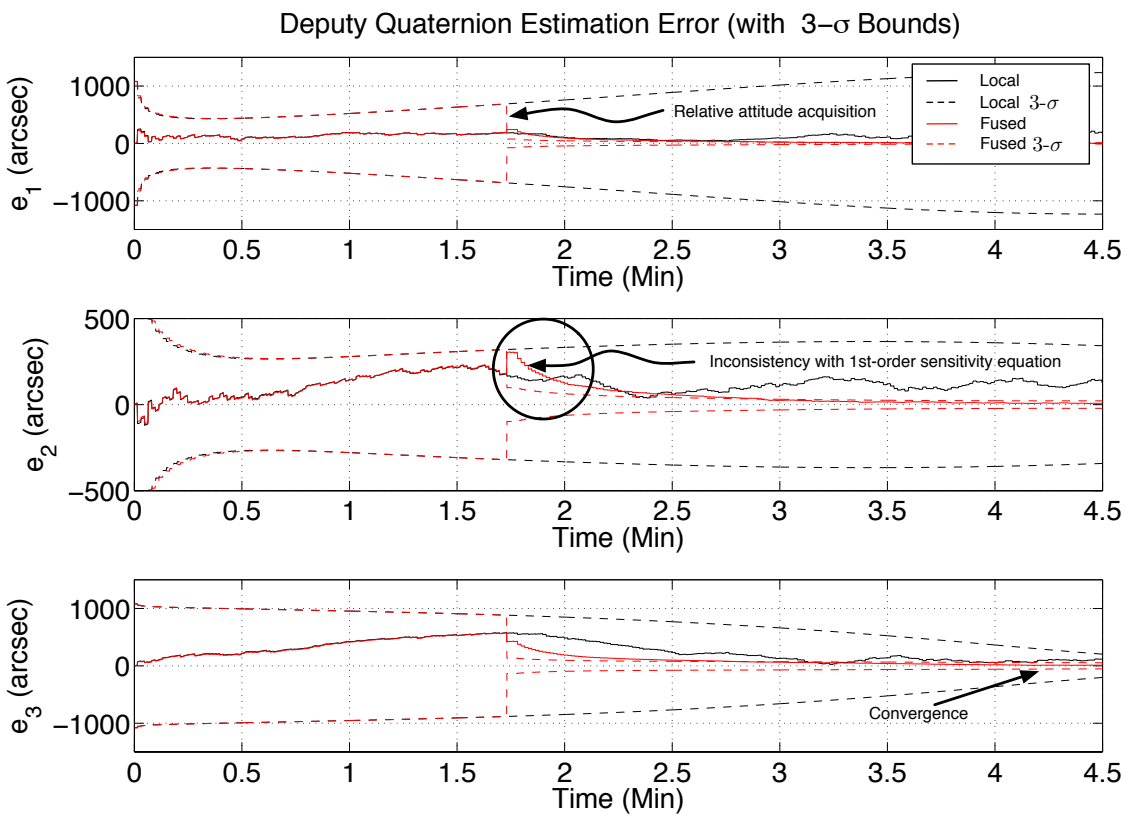

Figure 6-8. Effects observed at the onset of data fusion with precise and coarse sensors

algorithm derived for attitude measurement sharing in Chapter 5. With this framework, simulations are conducted for the case when Deputy-1 has coarse inertial attitude sensors, and the case when all spacecraft have star trackers. The chief and Deputy-2 use star trackers in both cases.

6.3.1 Three Spacecraft with Star Trackers Scenario

This case is analogous in structure to the two spacecraft with star trackers scenario, except now the chief must track both deputies based on a tasking algorithm. A juxtaposition of the attitude error for the three spacecraft is shown in Figure 6-9. Figure 6-9A shows that data fusion for the chief only reduces the error in the boresight axis when the chief has slowly evolving dynamics, which are represented by the spikes in e_3 for the local chief attitude error. The slowly evolving angular velocity of the chief

is depicted in Figure 6-10B. Recall from Figure 6-1 that Deputy-1 and Deputy-2 have comparably slow evolving attitude states. Due to these slowly evolving states, the local estimate error rotations about the boresight axis as considerably larger than for the transverse axes. However, attitude resource sharing significantly improves the errors about the boresight direction of the star trackers. Errors about the transverse axes are also reduced for both deputies, as their steady state values are higher than the information provided by the chief, due to degraded gyro specifications with respect to the chief. Figure 6-11 shows that the information from all spacecraft are used for data fusion to improve their state estimates. Therefore, resource sharing benefited all three spacecraft in the network, but especially the deputies, which had lower quality local information available without resource sharing.

6.3.2 Three Spacecraft with Coarse Deputy-1 Sensors Scenario

In the last case, the chief and Deputy-2 are equipped with star trackers, and Deputy-1 is equipped with coarse inertial attitude sensors. Figure 6-12 provides a juxtaposition of the error in each spacecraft. Much of the behavior exhibited in the three spacecraft with star trackers scenario applies to this case. However, it is observed in Figure 6-12A, that data fusion has more of an affect on the chief than in the three star tracker case. Although there is an improvement due to data fusion, the chief performance is degraded with respect to the three star tracker case. Expectedly, the error shown in Figure 6-12B for the local estimate of Deputy-1 is much greater than for the three star tracker case. In this same figure, resource sharing significantly reduces the error to comparable levels with the chief and Deputy-2. Similar behavior is shown in Figure 6-12C for Deputy-2. Since Deputy-1 has such poor local sensing, inclusive of a poor gyro, the chief is always tasked with Deputy-1, which results in the low nominal control torque and angular velocity seen in Figure 6-13. In fact, these are the exact profiles seen in the two spacecraft scenarios, since Deputy-1 is common to the simulations. Furthermore, Figure 6-14 shows that outside of early transients, the

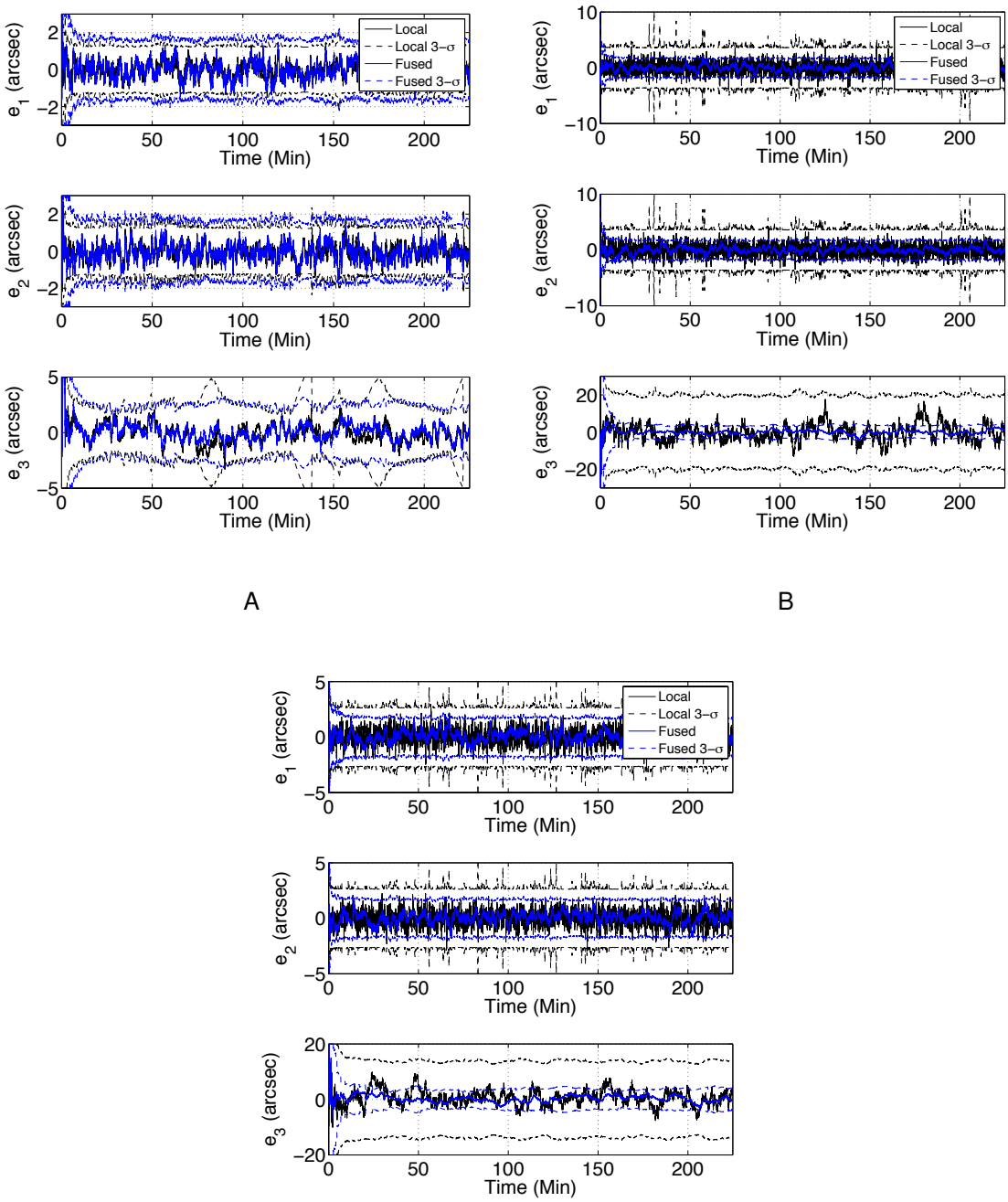

Figure 6-9. Local and fused quaternion error for the three spacecraft star tracker scenario. A) Chief. B) Deputy-1. C) Deputy-2

covariance intersection algorithm never used Deputy-1 information, instead relying on a combination of information from the chief and Deputy-2 to generate the best results.

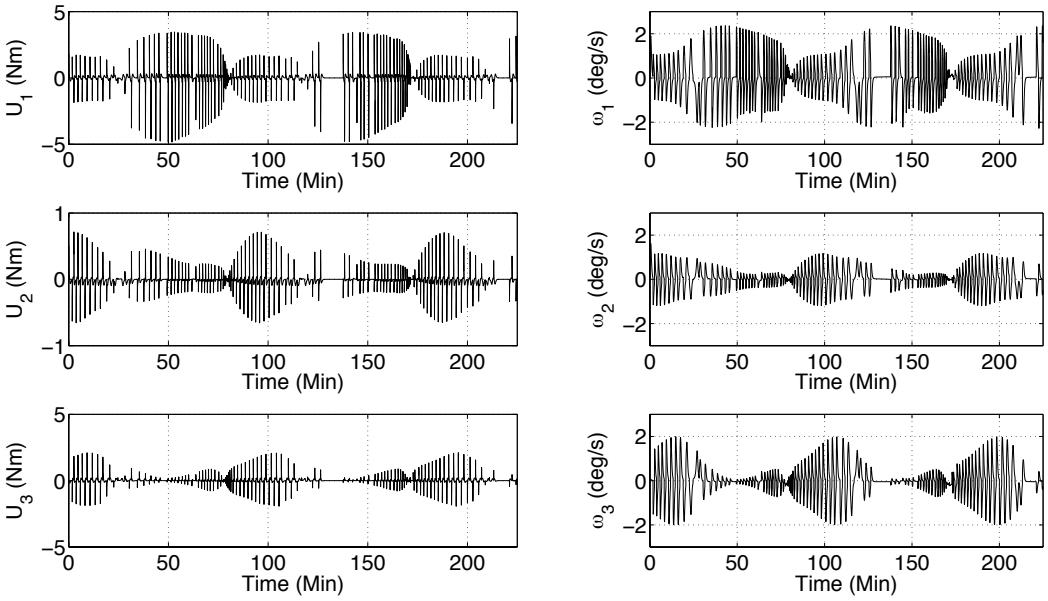

Figure 6-10. Chief attitude control for the three spacecraft star tracker scenario. A) Control torque. B) Angular velocity.

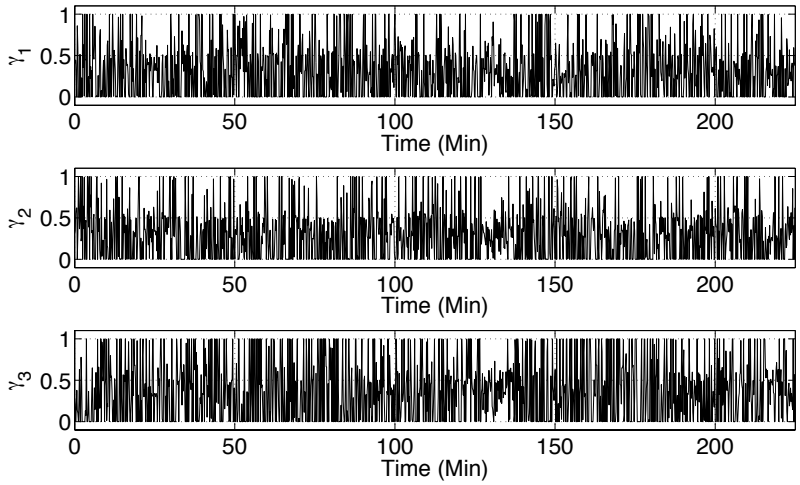

Figure 6-11. Covariance intersection weights for the three spacecraft star tracker scenario

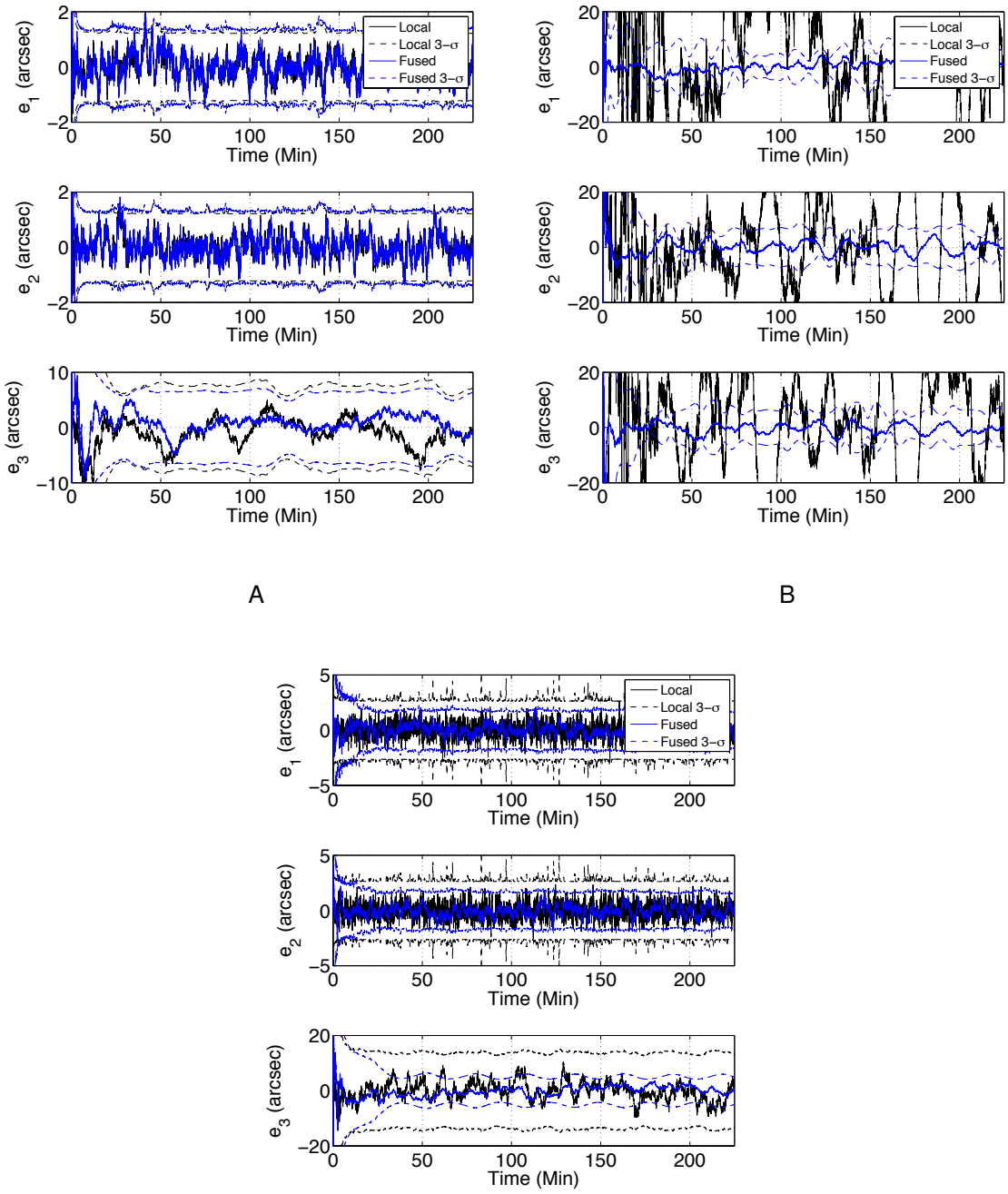

Figure 6-12. Local and fused quaternion error for the three spacecraft scenario with coarse Deputy-1 sensing. A) Chief. B) Deputy-1. C) Deputy-2

6.4 Tasking Algorithm Comparison for Attitude Estimate Resource Sharing with Data Fusion

Attitude resource sharing with data fusion does not exhibit the same behavior as measurement sharing. This section compares the performance of the three

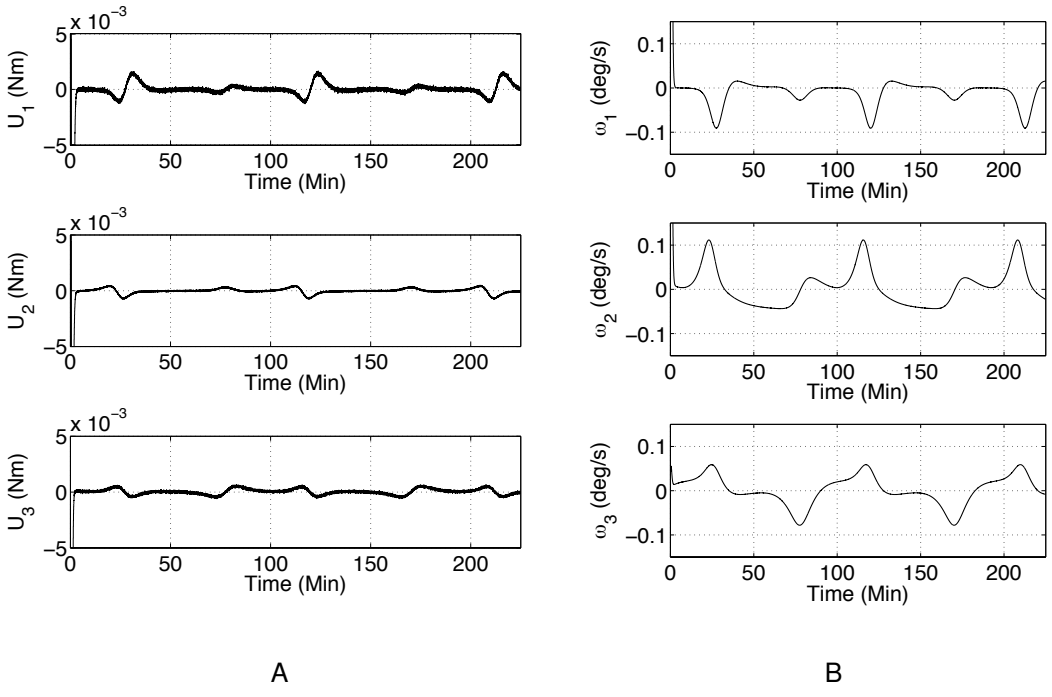

Figure 6-13. Chief attitude control for the three spacecraft scenario with coarse Deputy-1 sensing. A) Control torque. B) Angular velocity.

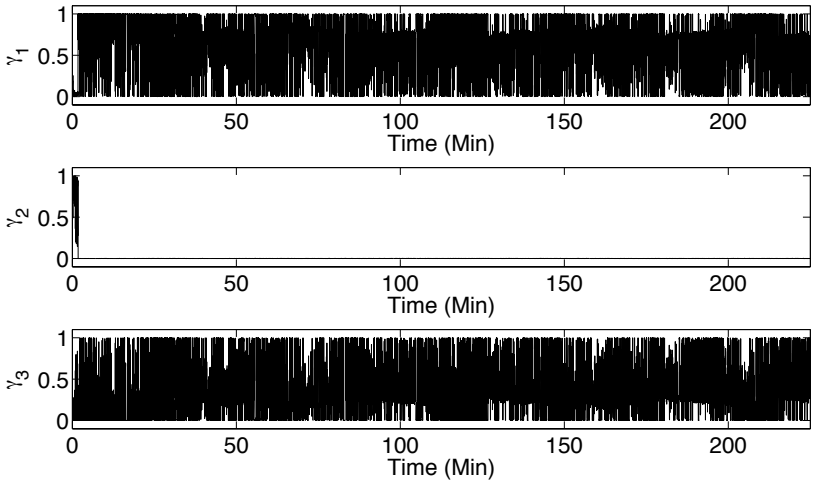

Figure 6-14. Covariance intersection weights for the three spacecraft scenario with coarse Deputy-1 sensing

spacecraft scenarios using the greedy and Round-robin tasking algorithms. Since

the two spacecraft scenarios were treated as tracking problems, they do not fit within this discussion.

As mentioned in the simulation descriptions, the three spacecraft scenarios simulated in Section 6.3 made use of the greedy tasking algorithm with the trace metric. In this section, results for the same three spacecraft scenarios are provided, but with the Round-robin tasking strategy. For the three star tracker case, a comparison of the 3-σ bound error for the local and fused state estimates is shown in Figure 6-15. By comparing Figure 6-15A and Figure 6-15B, it is seen that the resource sharing improvements are mostly insensitive to the tasking algorithm. There are some spikes that are present with the greedy tasking error of the chief that are not present in the results for the Round-robin strategy. The cause of these spikes are more evident in the case of two star trackers and a coarse attitude sensor.

The tasking algorithm impacts the attitude error the most when the resulting motion of the chief varies from rapid slewing to slow slewing. This is exactly the case encountered for the three spacecraft scenario with the chief and Deputy-2 equipped with star trackers and Deputy-1 equipped with coarse attitude sensors. Since Deputy-1 has coarse sensors and a lower precision gyro, Figure 6-13B showed that greedy tasking results in a near stationary chief, whom is only tasked with tracking Deputy-1 for relative attitude sensing. Alternatively, the Round-robin tasking strategy causes the chief to rapidly slew and track the deputies, alternating between the two after a relative attitude measurement is captured. Figure 6-17 shows the angular velocity and error for the chief using the greedy and Round-robin tasking algorithms. For periods of low angular velocity, the boresight axis error grows until the chief begins to slew at a higher rate. When the chief motion is nearly stationary, the attitude error in the boresight direction achieves a higher steady-state error. Therefore, greedy tasking, which only accounts for the state uncertainty of the deputies, does not properly account one of the primary factors affecting the system performance. The resulting control torque for the

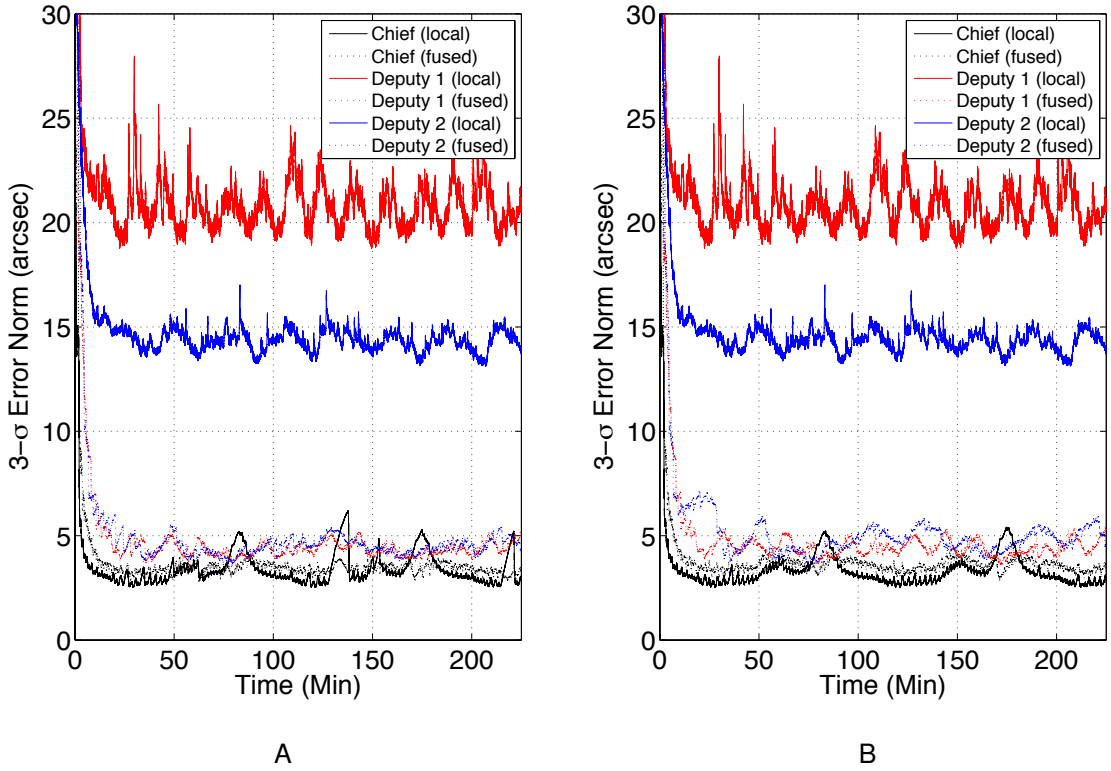

Figure 6-15. Affect of tasking algorithm choice on the error bounds of a three spacecraft scenario with fine precision sensing. A) Greedy tasking. B) Round-robin tasking.

Round-robin strategy is given in Figure 6-18. The control torque has gone from a low nominal tracking signal to aggressive slew maneuvering. Clearly, in this case, there is a trade-off between the attitude accuracy and the control torque.

6.5 Observations on Spacecraft Attitude Estimate Resource Sharing

Resource sharing in a network of spacecraft with similar attitude sensor capability improves the performance of all spacecraft when the relative attitude sensor is of similar performance to the inertial sensors. This improvement is a direct result of data fusion, which optimally combines multiple information sources to produce a best estimate. In this case, the spacecraft are less sensitive to the tasking algorithm. In these cases, greedy and Round-robin tasking will cause the spacecraft to switch constantly amongst the spacecraft and consume considerable torque as was seen in the

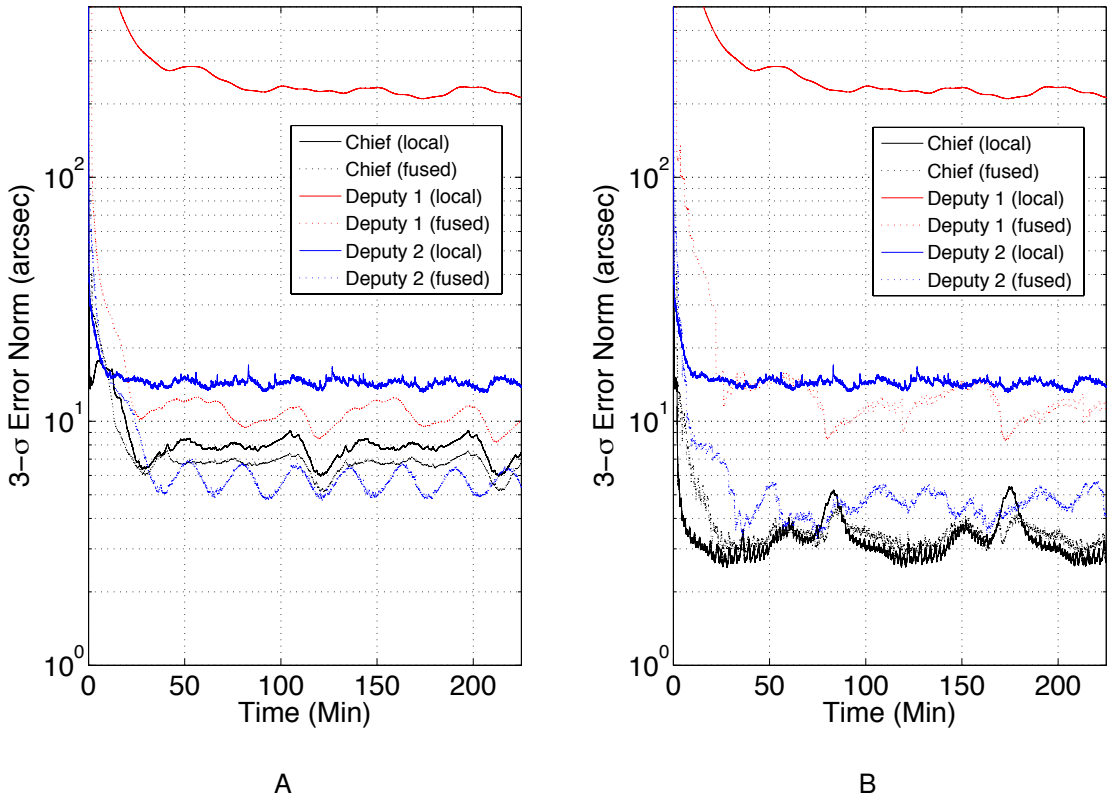

Figure 6-16. Affect of tasking algorithm choice on the error bounds of a three spacecraft scenario with coarse Deputy-2 attitude sensing. A) Greedy tasking. B) Round-robin tasking.

examples. However, the chief could instead pursue a non-sharing objective in addition to pursuing relative attitude measurements periodically. The trade-offs for the chief would be between attitude accuracy, control torque, and the amount of time pursuing other non-sharing objectives.

When the deputies are provided with dissimilar sensing capability, the tasking algorithm plays a larger role in the pointing performance of the spacecraft in the network and the deputies rely more on the shared resource. In these cases, it was seen that the chief motion was coupled with its uncertainty, which propagated to the uncertainty of the other spacecraft through data fusion. In these cases, greedy tasking reduces the amount of slewing by maintaining a fix on the deputy with the highest uncertainty, but

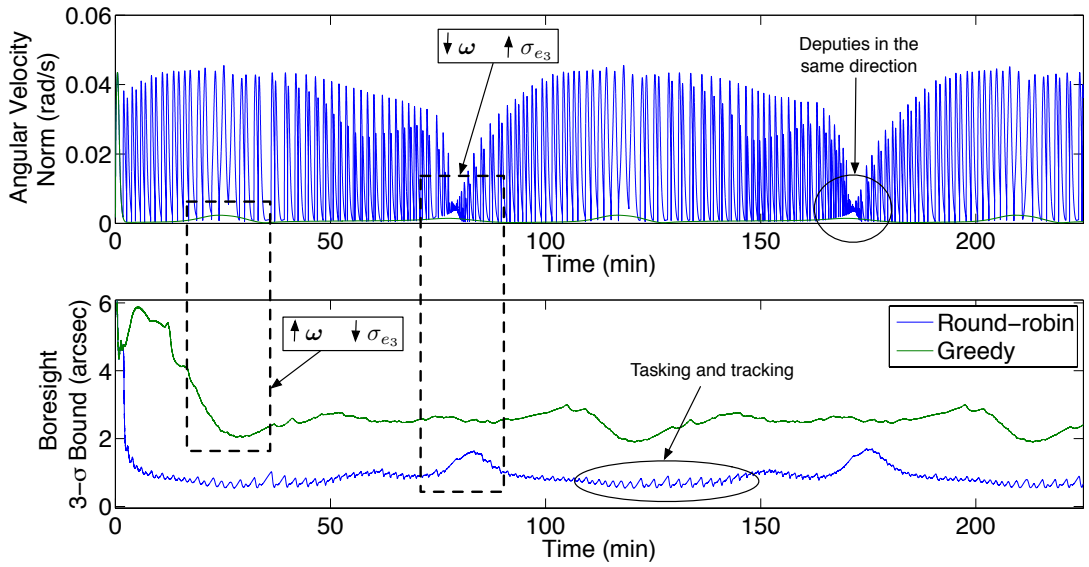

Figure 6-17. Effect of tasking on the Chief boresight attitude accuracy

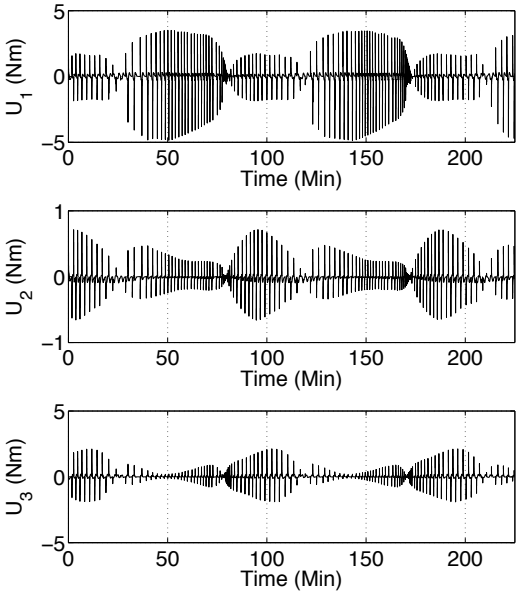

Figure 6-18. Chief attitude control for the three spacecraft scenario with coarse Deputy-1 sensing using Round-robin tasking

at the expense of some error improvements experienced by more aggressive slewing. The coupling between attitude error and slewing should be investigated further in future studies.

6.6 Summary

This chapter presented simulations on two and three spacecraft architectures, where attitude state estimates were shared between the chief and deputies using data fusion. From a performance perspective, shared state estimates using data fusion are preferred to shared state measurements, where data fusion results in better utilization of all the information available to the chief and deputies. When the deputies are equipped with inertial attitude sensors comparable to the chief, all spacecraft benefit from attitude resource sharing. However, this chapter concluded with the observation that when one deputy has less accurate attitude sensors, slewing maneuvers by the chief can affect the attitude accuracy performance of all spacecraft. Since the chief's motion is confounded with the tasking algorithm, the tasking algorithm will need to account for the dynamics explicitly. One final remark on the simulations is that the results from this chapter verified the many of the benefits of attitude resource sharing. Particularly, spacecraft equipped with low-grade attitude sensors can see large attitude improvements and spacecraft with high accuracy sensors can see performance greater than the specifications of that individual sensor allow.

CHAPTER 7
CONCLUSIONS

A new paradigm of spacecraft architectures is being investigated to provide improvements in mission flexibility, responsiveness, and threat management. This new paradigm is referred to as the disaggregated spacecraft system, where the functionalities of a traditional monolithic space asset are disaggregated across several smaller platforms consisting of a chief and multiple deputies. This research addressed some of the technical challenges associated with the disaggregation of the attitude determination system.

7.1 Revisiting the Research Questions and Thesis Statements

In Section 1.3.1 the problem was posed as to how to perform data fusion for attitude states and what attitude parameterization should be used. It was hypothesized in Section 1.4.1 that the attitude error vector could extend known data fusion laws to attitude states and that appropriate parameterization of the can produce an unconstrained global nonsingular attitude data fusion law. The developments in Chapter 4 verified these hypothesis. In addition, it was shown that the accuracy of attitude data fusion is based on the chosen attitude parameterization. The classical Rodrigues parameters (CRPs) were shown to be a fast and sufficiently accurate parameterization, whereas the higher-order Rodrigues parameters were shown to improve the accuracy but at the expense of additional computations. In most instance, the CRPs are the preferred parameterization for data fusion.

In Section 1.3.2 the problem of tasking the chief to share relative and inertial attitude measurements was posed to minimize the attitude estimation error of the deputies. It was hypothesized in Section 1.4.2 that greedy sensor tasking, as a function of deputy covariance information, could be used to distribute resources and improve the attitude accuracy of the deputies. The developments in Chapter 5 verified the hypothesis for the case when measurements are shared from the chief to the deputies. Specifically,

it was shown that greedy tasking could be used as a computationally inexpensive method to improve the accuracy of a disaggregated ADS, in comparison to fixed Round-robin tasking. In the resulting greedy tasking algorithm, metrics based on the deputy covariance information were computed by the deputies and communicated to the chief. The chief used the covariance metric in the tasking decision to share relative and inertial attitude measurements. Monte Carlo simulations showed that the greedy tasking algorithm was mostly insensitive to the covariance metric form. In Chapter 6 it was observed that greedy tasking based solely on the deputy covariance information was inefficient for shared attitude state estimates. In this case, it was seen that a coupling exists between the chief dynamics and state uncertainty. Specifically, the attitude motion causes a change in chief uncertainty that propagates to the deputies via data fusion. As a result, the baseline Round-robin strategy improved the accuracy of the deputies by exploiting this dynamic effect.

7.2 Future Work

This research made contributions in the areas of inertial attitude estimation, attitude data fusion, and sensor tasking for disaggregated attitude determination systems. The results from this research have also spawned new research directions in each of these areas.

In the area of disaggregated inertial attitude estimation, the author recommends exploration of the following topics:

- Investigate disaggregated attitude estimation that does not require each spacecraft maintain estimates of the entire network
- Investigate intermittent communication for information transfer between the chief and deputies
- Determine the factors influencing the accuracy of current relative attitude sensors (to yield measurements as precise as a star tracker)
- Investigate other relative attitude sensors such as direction measurements obtained through laser communications systems, which are not limited to the close proximity requirement of the relative attitude sensor assumed in this manuscript

In the area of attitude data fusion, the author recommends exploration of the following topics:

- Implement the attitude error state in an ellipsoidal intersection algorithm and compare the results with the covariance intersection algorithm
- Further investigate the affects of chief attitude motion on chief and deputy uncertainty, which result from the tracking controller
- Investigate the affects of relative translational motion between the chief and deputies on data fusion and state uncertainty

In the area of sensor tasking in disaggregated attitude determination systems, the author recommends exploration of the following topics:

- Investigate the affects of chief translational and rotation dynamics on the greedy tasking algorithm
- Develop the state models and cost functions to derive optimal sensor tasking algorithms for attitude resource sharing
- Develop sensor tasking algorithms that account for fuel consumption in addition to uncertainty

REFERENCES

[1] "Trends in Price Per Pound to Orbit 1990-2000," Futron Corporation, http://www.futron.com/resources.xml?page=4#tabs-1, September 2002. Online; accessed May 7, 2012.

[2] Bearden, D., "Small-Satellite Costs," *Aerospace Corporation Crosslink Magazine*, Vol. 2, No. 1, Winter 2001, pp. 32–44.

[3] Barnhart, D., Vladimirova, T., and Sweeting, M., "Satellite-on-a-Chip: A Feasibility Study," *Proceedings of the 5th Round Table on Micro/Nano Technologies for Space Workshop, Noordwijk, Netherlands, Oct 3-5*, 2005, pp. 728–735.

[4] Atchison, J. and Peck, M., "A Passive, Sun-Pointing, Millimeter-Scale Solar Sail," *Acta Astronautica*, Vol. 67, No. 1-2, 2010, pp. 108–121.

[5] Mathieu, C. and Weigel, A., "Assessing the Flexibility Provided by Fractionated Spacecraft," *AIAA Space Conference & Exposition, Long Beach, CA, Aug 30 - Sep 1*, 2005.

[6] Mathieu, C., *Assessing the Fractionated Spacecraft Concept*, Ph.D. thesis, Massachusetts Institute of Technology, 2006.

[7] Brown, O., "The Value Proposition for Fractionated Space Architectures," *AIAA Space Conference & Exposition, San Jose, CA, Sep 19-21*, No. AIAA 2006-7506, 2006.

[8] Brown, O., Eremenko, P., and Collopy, P., "Value-Centric Design Methodologies for Fractionated Spacecraft: Progress Summary from Phase 1 of the DARPA System F6 Program," *AIAA Space Conference & Exposition, Pasadena, CA, Sep 14 - 17*, 2009.

[9] Burch, R., "The Case for Disaggregation of US MILSATCOM," *Military Communications Conference (MILCOM), Baltimore, MD, Nov 7-10*, IEEE, 2011, pp. 2286–2291.

[10] Brown, O., "Fractionated Space Architectures: A Vision for Responsive Space," *4th Responsive Space Conference, Los Angeles, CA, Apr 24-27*, No. RS4-2006-1002, 2006.

[11] Guo, J., Maessen, D., and Gill, E., "Fractionated Spacecraft: The New Sprout in Distributed Space Systems," *60th International Astronautical Congress, Daejeon, Republic of Korea, Oct 12-16*, No. IAC-09-D1.1.4, October 2009.

[12] Leitner, J., "Simulating Resource Sharing in Spacecraft Clusters Using Multi-Agent Systems," *Small Satellites Systems and Services - The 4S Symposium, Funchal, Madeira, Portugal, May 31 - Jun 4*, 2010.

[13] Turner, A., "In-Space Power Transfer Bouncing the Light - Fantastic! (Presentation)," *Fractionated Spacecraft Workshop, Colorado Springs, CO, Aug 3-4*, August 2006.

[14] Jamnejad, V. and Silva, A., "Microwave Power Beaming Strategies for Fractionated Spacecraft Systems," *IEEE Aerospace Conference, Big Sky, MT, Mar 1-8*, IEEE, 2008, pp. 1–14.

[15] "Technology Readiness Level (TRL)," NASA Kennedy Space Center, http://technology.ksc.nasa.gov/sbir/sbir-phases.htm, Online; accessed July 22, 2012, trends.

[16] Schaub, H., Parker, G., and King, L., "Challenges and Prospects of Coulomb Spacecraft Formations," *The Journal of the Astronautical Sciences*, Vol. 52, No. 1-2, 2004, pp. 169–193.

[17] Kaneda, R., Yazaki, F., Sakai, S., Hashimoto, T., and Saito, H., "The Relative Position Control in Formation Flying Satellites Using Superconducting Magnets," *2nd International Symposium on Formation Flying Missions and Technologies, Washington DC, Sep 14-16*, 2004, pp. 91–96.

[18] Kwon, D., "Propellantless Formation Flight Applications Using Electromagnetic Satellite Formations," *Acta Astronautica*, Vol. 67, No. 9-10, 2010, pp. 1189–1201.

[19] Hu, M., Zeng, G., Yao, H., and Li, Z., "Electromagnetic Formation Control for Fractionated Spacecraft," *30th Chinese Control Conference, Yantai, China, Jul 22-24*, IEEE, 2011, pp. 3484–3488.

[20] O'Neill, M., *Assessing the Impacts of Fractionation on Pointing-Intensive Spacecraft*, Master's thesis, Massachusetts Institute of Technology, 2009.

[21] "Nano Star Tracker," Blue Canyon Technologies, http://bluecanyontech.com/wp-content/uploads/2012/07/BCT-Nano-Star-Tracker-datasheet-1.0.pdf, Online; accessed May 22, 2013.

[22] Van Der Horst, J. and Noble, J., "Task Allocation in Dynamic Networks of Satellites," *22nd International Joint Conferece on Artificial Intelligence in Space, Barcelona, Spain, Jul 16-22*, 2011.

[23] Stadter, P., Chacos, A., Heins, R., Moore, G., Olsen, E., Asher, M., and Bristow, J., "Confluence of Navigation, Communication, and Control in Distributed Spacecraft Systems," *IEEE Aerospace and Electronic Systems Magazine*, Vol. 17, No. 5, 2002, pp. 26–32.

[24] Blackmore, L. and Hadaegh, F., "Necessary and Sufficient Conditions for Attitude Estimation in Fractionated Spacecraft Systems," *AIAA Guidance, Navigation and Control Conference, Chicago, IL, Aug 10-13*, American Institute of Aeronautics

and Astronautics, 1801 Alexander Bell Dr., Suite 500 Reston VA 20191-4344 USA,, 2009.

[25] Fehse, W., *Automated Rendezvous and Docking of Spacecraft*, Cambridge Aerospace Series 16, Cambridge University Press, 2003.

[26] Weismuller, T. and Leinz, M., "GN&C Technology Demonstrated by the Orbital Express Autonomous Rendezvous and Capture Sensor System," *29th Annual AAS Guidance and Control Conference, Breckenridge, CO, Feb 4-8*, 2006.

[27] Obermark, J., Creamer, G., Kelm, B., Wagner, W., and Henshaw, C., "SUMO/FREND: Vision System for Autonomous Satellite Grapple," *Proceedings of SPIE Sensors and Systems for Space Applications, Orlando, FL, Apr 9*, Vol. 6555, 2007, p. 65550Y.

[28] Davis, T. and Melanson, D., "XSS-10 Micro-Satellite Flight Demonstration," *First Annual Space Systems Engineering Conference, Atlanta, GA, Nov 9*, 2005.

[29] "XSS-11 Micro-Satellite," Air Force Research Laboratory, http://www.kirtland.af.mil/shared/media/document/AFD-070404-108.pdf, December 2005. Online; accessed October 9, 2012.

[30] Howard, R. and Bryan, T., "DART AVGS Flight Results," *Proceedings of SPIE Sensors and Systems for Space Applications, Orlando, FL, Apr 9*, Vol. 6555, 2007, p. 65550L.

[31] Strandmoe, S., DePasquale, E., Escane, I., Augelli, M., Personne, G., Cavrois, B., Fau, N., Yu, M., Zink, M., Clerc, X., et al., "Automated Transfer Vehicle (ATV) Flight Control Achievements," *7th International ESA Conference on Guidance, Navigation & Control Systems, County Kerry, Ireland, Jun 2-5*, 2008.

[32] Muñoz, S., Hornbuckle, R. W., and Lightsey, E. G., "FASTRAC Early Flight Results," *Journal of Small Satellites (JoSS)*, Vol. 1, No. 02, 2012.

[33] "Orbital Express Unmated OPS," The Boeing Company, http://www.boeing.com/bds/phantom_works/orbital/oe_027.html, 2011. Online; accessed March 16, 2012.

[34] Blackwood, G., Lay, O., Deininger, W., Gudim, M., Ahmed, A., Duren, R., Noecker, C., and Barden, B., "The StarLight Mission - A Formation-Flying Stellar Interferometer," *Proceedings of SPIE the International Society for Optical Engineering*, 2002, pp. 463–480.

[35] Maghami, P. and Hyde, T., "Laser Interferometer Space Antenna Dynamics and Controls Model," *Classical and Quantum Gravity*, Vol. 20, 2003, pp. S273–S282.

[36] Teles, J., Samii, M., and Doll, C., "Overview of TDRSS," *Advances in Space Research*, Vol. 16, No. 12, 1995, pp. 67–76.

[37] Maine, K., Devieux, C., and Swan, P., "Overview of IRIDIUM Satellite Network," *IEEE Wescon Application Conference, San Francisco, CA, Nov 7-9*, IEEE, 1995, p. 483.

[38] Hinkle, A. and Washington, D., "TDRSS Concept," Goddard Space Flight Center, http://www.nasa.gov/topics/technology/features/tdrs-go.html, November 2011. Online; accessed March 15, 2012.

[39] "Iridium Global Network," Iridium Communications Inc., http://www.iridium.com//About/Newsroom/MediaLibrary.aspx, September 2011. Online; accessed March 15, 2012.

[40] Eremenko, P., "System F6: Proposer's Day Briefing," DARPA, http://www.darpa.mil/Our_Work/TTO/Programs/System_F6.aspx, October 2010. Online; accessed May 8, 2012.

[41] Lobosco, D., Cameron, G., Golding, R., and Wong, T., "The Pleiades Fractionated Space System Architecture and the Future of National Security Space," *AIAA Space Conference & Exposition, San Diego, CA, Sep 9-11*, 2008.

[42] Durrant-Whyte, H. and Bailey, T., "Simultaneous Localization and Mapping: Part I," *Robotics & Automation Magazine, IEEE*, Vol. 13, No. 2, 2006, pp. 99–110.

[43] Knuth, J. and Barooah, P., "Collaborative 3D Localization of Robots from Relative Pose Measurements Using Gradient Descent on Manifolds," *IEEE International Conference on Robotics and Automation (ICRA)*, IEEE, 2012, pp. 1101–1106.

[44] Knuth, J. and Barooah, P., "Collaborative Localization with Heterogeneous Inter-robot Measurements by Riemannian Optimization," *IEEE International Conference on Robotics and Automation*, 2013.

[45] Kim, S., Crassidis, J., Cheng, Y., Fosbury, A., and Junkins, J., "Kalman Filtering for Relative Spacecraft Attitude and Position Estimation," *Journal of Guidance, Control, and Dynamics*, Vol. 30, No. 1, 2007, pp. 133–150.

[46] Nebelecky, C., Crassidis, J., Banas, W., Cheng, Y., and Fosbury, A., "Decentralized Relative Attitude Estimation for Three-Spacecraft Formation Flying Applications," *AIAA Guidance, Navigation and Control Conference, Chicago, Illinois, Aug 10-13*, 2009.

[47] Uhlmann, J. K., "General Data Fusion for Estimates with Unknown Cross Covariances," *Society of Photo-Optical Instrumentation Engineers (SPIE) Conference Series*, Vol. 2755, 1996, pp. 536–547.

[48] Julier, S. and Uhlmann, J., "A New Extension of the Kalman Filter to Nonlinear Systems," *Signal Processing, Sensor Fusion, and Target Recognition VI*, 1997, pp. 182–193.

[49] Bar-Shalom, Y., "On the Track-to-track Correlation Problem," *IEEE Transactions on Automatic Control*, Vol. 26, No. 2, 1981, pp. 571–572.

[50] Witsenhausen, H., "Separation of Estimation and Control for Discrete Time Systems," *Proceedings of the IEEE*, Vol. 59, No. 11, 1971, pp. 1557–1566.

[51] Bar-Shalom, Y. and Tse, E., "Dual Effect, Certainty Equivalence, and Separation in Stochastic Control," *IEEE Transactions on Automatic Control*, Vol. 19, No. 5, 1974, pp. 494–500.

[52] Van de Water, H. and Willems, J., "The Certainty Equivalence Property in Stochastic Control Theory," *IEEE Transactions on Automatic Control*, Vol. 26, No. 5, 1981, pp. 1080–1087.

[53] Stengel, R., *Optimal Control and Estimation*, Dover Pubns, 1994.

[54] Whittaker, E., *A Treatise on the Analytical Dynamics of Particles and Rigid Bodies: With an Introduction to the Problem of Three Bodies*, Cambridge University Press, 1988.

[55] Vallado, D. and McClain, W., *Fundamentals of Astrodynamics & Applications*, Springer Netherlands, 3rd ed., 2007.

[56] Stuelpnagel, J., "On the Parametrization of the Three-Dimensional Rotation Group," *SIAM review*, Vol. 6, No. 4, 1964, pp. 422–430.

[57] Shuster, M., "A Survey of Attitude Representations," *The Journal of the Astronautical Sciences*, Vol. 41, 1993, pp. 439–517.

[58] Schaub, H., Junkins, J., and Schetz, J., *Analytical Mechanics of Space Systems*, Vol. 1, American Institute of Aeronautics and Astronautics, Reston, Virginia, USA, 2nd ed., 2009.

[59] Bauchau, O. A. and Trainelli, L., "The Vectorial Parameterization of Rotation," *Nonlinear Dynamics*, Vol. 32, No. 1, 2003, pp. 71–92.

[60] Chaturvedi, N., Sanyal, A., and McClamroch, N., "Rigid-Body Attitude Control," *IEEE Control Systems Magazine*, Vol. 31, No. 3, 2011, pp. 30–51.

[61] Marandi, S. and Modi, V., "A Preferred Coordinate System and the Associated Orientation Representation in Attitude Dynamics," *Acta Astronautica*, Vol. 15, No. 11, 1987, pp. 833–843.

[62] Schaub, H. and Junkins, J., "Stereographic Orientation Parameters for Attitude Dynamics: A Generalization of the Rodrigues Parameters," *The Journal of the Astronautical Sciences*, Vol. 44, No. 1, 1996, pp. 1–19.

[63] Tsiotras, P., Junkins, J., and Schaub, H., "Higher-Order Cayley Transforms with Applications to Attitude Representations," *Journal of Guidance, Control, and Dynamics*, Vol. 20, No. 3, 1997, pp. 528–534.

[64] Tanygin, S., "Attitude Parameterizations as Higher-Dimensional Map Projections," *Journal of Guidance, Control, and Dynamics*, Vol. 35, No. 1, 2012, pp. 13–24.

[65] Tanygin, S., "Projective Geometry of Attitude Parameterizations with Applications to Control," *Journal of Guidance, Control, and Dynamics*, 2013, pp. 1–11.

[66] Hughes, P. C., *Spacecraft Attitude Dynamics*, Courier Dover Publications, 2012.

[67] Clohessy, W. and Wiltshire, R., "Terminal Guidance System for Satellite Rendezvous," *Journal of the Aerospace Sciences*, Vol. 27, No. 9, 1960, pp. 653–658.

[68] Alfriend, K., Vadali, S. R., Gurfil, P., How, J., and Breger, L., *Spacecraft Formation Flying: Dynamics, Control, and Navigation*, Vol. 2, Butterworth-Heinemann, 2009.

[69] Tschauner, J. and Hempel, P., "Optimale Beschleunigeungsprogramme fur das Rendezvous-Manover," *Astronautica Acta*, Vol. 10, No. 5-6, 1964, pp. 296–307.

[70] Battin, R. H., *An Introduction to the Mathematics and Methods of Astrodynamics*, AIAA, 1999.

[71] Wie, B., Bailey, D., and Heiberg, C., "Rapid Multi-Target Acquisition and Pointing Control of Agile Spacecraft," *AIAA Guidance, Navigation, and Control Conference and Exhibit, Denver, CO, Aug 14-17*, 2000.

[72] Khalil, H. and Grizzle, J., *Nonlinear Systems*, Prentice Hall, Upper Saddle River, NJ, 3rd ed., 2002.

[73] Wertz, J., *Spacecraft Attitude Determination and Control*, Vol. 73, D. Reidel Publishing Company, 1978.

[74] Wertz, J. and Larson, W., *Space Mission Analysis and Design*, Microcosm, 3rd ed., 1999.

[75] Maus, S., Macmillan, S., McLean, S., Center, N. G. D., and Survey, B. G., *The US/UK World Magnetic Model for 2010-2015*, NOAA National Geophysical Data Center, 2010.

[76] "Star Trackers," Ball Aerospace, http://www.ballaerospace.com/page.jsp?page=104, 2011. Online; accessed May 7, 2012.

[77] Pisacane, V. L., *Fundamentals of Space Systems*, Oxford University Press, USA, 2005.

[78] Mortari, D., Bruccoleri, C., La Rosa, S., and Junkins, L., "CCD Data Processing Improvements," *5th International Conference on Dynamics and Control of Structures and Systems in Space, Cambridge, England, Jul 14-18*, 2002.

[79] Samaan, M. A., *Toward Faster and More Accurate Star Sensors Using Recursive Centroiding and Star Identification*, Ph.D. thesis, Texas A&M University, 2003.

[80] Farrenkopf, R., "Analytic Steady-state Accuracy Solutions for Two Common Spacecraft Attitude Estimators," *Journal of Guidance, Control, and Dynamics*, Vol. 1, No. 4, 1978, pp. 282–284.

[81] Shuster, M. and Oh, S., "Three-Axis Attitude Determination from Vector Observations," *Journal of Guidance, Control, and Dynamics*, Vol. 4, No. 1, 1981, pp. 70–77.

[82] Choukroun, D., *Novel Methods for Attitude Determination Using Vector Observations*, Ph.D. thesis, Israel Institute of Technology, Haifa, Israel, 2003.

[83] Wahba, G. et al., "Problem 65-1: A Least Squares Estimate of Satellite Attitude," *SIAM Review*, Vol. 7, No. 3, 1965, pp. 409.

[84] Keat, J., "Analysis of Least Squares Attitude Determination Routine DOAOP," Tech. rep., Computer Sciences Corporation, 1977.

[85] Meyer, C., *Matrix Analysis and Applied Linear Algebra*, Vol. 1, Society for Industrial & Applied Mathematics, 2000.

[86] Shuster, M., "Kalman Filtering of Spacecraft Attitude and the QUEST Model," *The Journal of the Astronautical Sciences*, Vol. 38, 1990, pp. 377–393.

[87] Markley, F., "Attitude Determination Using Vector Observations and the Singular Value Decomposition," *The Journal of the Astronautical Sciences*, Vol. 36, No. 3, 1988, pp. 245–258.

[88] Shuster, M., "A Simple Kalman Filter and Smoother for Spacecraft Attitude," *The Journal of the Astronautical Sciences*, Vol. 37, No. 1, 1989, pp. 89–106.

[89] Bar-Itzhack, I., "REQUEST: A Recursive QUEST Algorithm for Sequential Attitude Determination," *Journal of Guidance, Control, and Dynamics*, Vol. 19, No. 5, 1996, pp. 1034–1038.

[90] Mortari, D., "ESOQ: A Closed-Form Solution to the Wahba Problem," *The Journal of the Astronautical Sciences*, Vol. 45, No. 2, 1997, pp. 195–204.

[91] Mortari, D., "Second Estimator of the Optimal Quaternion," *Journal of Guidance, Control, and Dynamics*, Vol. 23, No. 5, 2000, pp. 885–887.

[92] Markley, F., "Attitude Determination Using Vector Observations: A Fast Optimal Matrix Algorithm," *The Journal of the Astronautical Sciences*, Vol. 41, No. 2, 1993, pp. 261–280.

[93] Mortari, D., "EULER-2 and EULER-N Algorithms for Attitude Determination from Vector Observations," *Space Technology*, Vol. 16, No. 5, 1996, pp. 317–322.

[94] Bruccoleri, C. and Mortari, D., "MRAD: Modified Rogrigues Vector Attitude Determination," *The Journal of the Astronautical Sciences*, Vol. 54, No. 3-4, July-December 2006, pp. 383–390.

[95] Mortari, D., Markley, F., and Singla, P., "Optimal Linear Attitude Estimators," *Journal of Guidance, Control, and Dynamics*, Vol. 30, No. 6, 2007, pp. 1619–1632.

[96] Hurtado, J., "Cayley Attitude Technique," *22nd AAS/AIAA Space Flight Mechanics Meeting, Charleston, SC, Jan 30 - Feb 2*, No. 12-120, 2012.

[97] Crassidis, J. and Junkins, J., *Optimal Estimation of Dynamic Systems*, Vol. 2, Chapman & Hall, 1st ed., 2004.

[98] Rhodes, I., "A Tutorial Introduction to Estimation and Filtering," *IEEE Transactions on Automatic Control*, Vol. 16, No. 6, 1971, pp. 688–706.

[99] Maybeck, P., *Stochastic Models, Estimation, and Control Volume 1*, Vol. 1, Academic Press, 1979.

[100] Van Loan, C., "Computing Integrals Involving the Matrix Exponential," *IEEE Transactions on Automatic Control*, Vol. 23, No. 3, 1978, pp. 395–404.

[101] Schmidt, S. F., "The Kalman Filter - Its Recognition and Development for Aerospace Applications," *Journal of Guidance, Control, and Dynamics*, Vol. 4, No. 1, 1981, pp. 4–7.

[102] Maybeck, P., *Stochastic Models, Estimation, and Control Volume 2*, Vol. 2, Academic Press, 1982.

[103] Crassidis, J., Markley, F., and Cheng, Y., "Survey of Nonlinear Attitude Estimation Methods," *Journal of Guidance, Control, and Dynamics*, Vol. 30, No. 1, 2007, pp. 12–28.

[104] Lefferts, E., Markley, F., and Shuster, M., "Kalman Filtering for Spacecraft Attitude Estimation," *Journal of Guidance, Control, and Dynamics*, Vol. 5, No. 5, 1982, pp. 417–429.

[105] MATLAB, *version 8.1.0.604 (R2013a)*, The MathWorks Inc., Natick, Massachusetts, 2013.

[106] "Star Catalog," http://www.acsu.buffalo.edu/~johnc/second_ed/chapter7/mappar.mat, October 2000. Online; accessed June 20, 2012, MATLAB .mat file.

[107] Crassidis, J. and Markley, F., "New Algorithm for Attitude Determination Using Global Positioning System Signals," *Journal of Guidance, Control, and Dynamics*, Vol. 20, No. 5, 1997, pp. 891–896.

[108] Buist, P., Teunissen, P., Verhagen, S., and Giorgi, G., "A Vectorial Bootstrapping Approach for Integrated GNSS-Based Relative Positioning and Attitude Determination of Spacecraft," *Acta Astronautica*, Vol. 68, No. 7, 2011, pp. 1113–1125.

[109] Tien, J., Purcell, G., Amaro, L., Young, L., Aung, M., Srinivasan, J., Archer, E., Vozoff, A., and Chong, Y., "Technology Validation of the Autonomous Formation Flying Sensor for Precision Formation Flying," *Proceedings of the IEEE Aerospace Conference*, Vol. 1, 2003, pp. 129–140.

[110] Junkins, J., Hughes, D., Wazni, K., and Pariyapong, V., "Vision-Based Navigation for Rendezvous, Docking, and Proximity Operations," *22nd Annual AAS Guidance and Control Conference, Breckenridge, CO, Feb 3-7*, 1999.

[111] Crassidis, J., Alonso, R., and Junkins, J., "Optimal Attitude and Position Determination From Line-of-Sight Measurements." *The Journal of the Astronautical Sciences*, Vol. 48, No. 2, 2000, pp. 391–408.

[112] Mortari, D., Rojas, J., and Junkins, J., "Attitude and Position Estimation from Vector Observations," *Proceedings of the Space Flight Mechanics Meeting Conference, Maui, Hawaii, Feb 8-12*, No. AAS 04-140, Citeseer, 2004.

[113] Tanygin, S., "Closed-Form Position Triangulation for Lost-In-Space Attitude and Position Determination," *AIAA/AAS Astrodynamics Specialist Conference, Providence, RI, Aug 16-19*, No. AIAA 2004-5388, 2004.

[114] Khaleghi, B., Khamis, A., Karray, F. O., and Razavi, S. N., "Multisensor Data Fusion: A Review of the State-of-the-art," *Information Fusion*, Vol. 14, No. 1, 2013, pp. 28–44.

[115] Crassidis, J. L., Cheng, Y., Nebelecky, C. K., and Fosbury, A. M., "Decentralized Attitude Estimation Using a Quaternion Covariance Intersection Approach," *The Journal of the Astronautical Sciences*, Vol. 57, No. 1, 2009, pp. 113.

[116] Cheng, Y., Banas, W. D., and Crassidis, J. L., "Quaternion Data Fusion," *Itzhack Y. Bar-Itzhack Memorial Symposium on Estimation, Navigation, and Spacecraft Control, Haifa, Israel, Oct 14-17*, 2012.

[117] Nebelecky, C. K., "Attitude Data Fusion Using a Modified Rodrigues Parametrization," *AIAA Guidance, Navigation, and Control Conference, Toronto, Ontario, CA, Aug 2-5*, 2010.

[118] Nebelecky, C. K., Crassidis, J. L., Fosbury, A. M., and Cheng, Y., "Efficient Covariance Intersection of Attitude Estimates Using a Local Error Representation," *Journal of Guidance, Control, and Dynamics*, Vol. 35, No. 2, 2012, pp. 692–696.

[119] Julier, S. J. and Uhlmann, J. K., *Multisensor Data Fusion*, chap. 12, CRC press, 2001, pp. 1–25.

[120] Markley, F. L., Cheng, Y., Crassidis, J. L., and Oshman, Y., "Averaging Quaternions," *Journal of Guidance, Control, and Dynamics*, Vol. 30, No. 4, 2007, pp. 1193.

[121] Sijs, J., Lazar, M., et al., "State Fusion with Unknown Correlation: Ellipsoidal Intersection," *American Control Conference, Baltimore, MD, Jun 30-Jul 2*, IEEE, 2010, pp. 3992–3997.

[122] Sijs, J. and Lazar, M., "A Distributed Kalman Filter with Global Covariance," *American Control Conference, San Francisco, CA, Jun 29 - Jul 1*, IEEE, 2011, pp. 4840–4845.

[123] Sijs, J. and Lazar, M., "State Fusion with Unknown Correlation: Ellipsoidal Intersection," *Automatica*, Vol. 48, No. 8, 2012, pp. 1874–1878.

[124] Vanderplaats, G. N., *Numerical Optimization Techniques for Engineering Design*, Vanderplaats Research & Development, Inc., Colorado Springs, CO, 4th ed., 2005.

[125] Wie, B. and Barba, P. M., "Quaternion Feedback for Spacecraft Large Angle Maneuvers," *Journal of Guidance, Control, and Dynamics*, Vol. 8, No. 3, 1985, pp. 360–365.

[126] Wen, J.-Y. and Kreutz-Delgado, K., "The Attitude Control Problem," *IEEE Transactions on Automatic Control*, Vol. 36, No. 10, 1991, pp. 1148–1162.

[127] Wie, B., Bailey, D., and Heiberg, C., "Rapid Multitarget Acquisition and Pointing Control of Agile Spacecraft," *Journal of Guidance, Control, and Dynamics*, Vol. 25, No. 1, 2002, pp. 96–104.

[128] Deng, Z., Zhang, P., Qi, W., Liu, J., and Gao, Y., "Sequential Covariance Intersection Fusion Kalman Filter," *Information Sciences*, Vol. 189, 2012, pp. 293–309.

[129] Kuhn, H., "The Hungarian Method for the Assignment Problem," *Naval Research Logistics Quarterly*, Vol. 2, No. 1-2, 1955, pp. 83–97.

[130] Grocholsky, B., *Information-Theoretic Control of Multiple Sensor Platforms*, Ph.D. thesis, University of Sydney, 2002.

[131] Erwin, R., Albuquerque, P., Jayaweera, S., and Hussein, I., "Dynamic Sensor Tasking for Space Situational Awareness," *American Control Conference, Baltimore, MD, Jun 30 - Jul 2*, IEEE, 2010, pp. 1153–1158.

[132] Williams, P., Spencer, D., and Erwin, R., "Utilizing Stability Metrics to Aid in Sensor Network Management Solutions for Satellite Tracking Problems," *22nd AAS/AIAA Space Flight Mechanics Meeting, Charleston, SC, Jan 30 - Feb 2*, No. 12-111, 2012.

[133] Williams, P., Spencer, D., and Erwin, R., "Comparison of Two Single-Step, Myopic Sensor Management Decision Processes Applied to Space Situational Awareness," *22nd AAS/AIAA Space Flight Mechanics Meeting, Charleston, SC, Jan 30 - Feb 2*, No. 12-112, 2012.

[134] Chakravorty, S. and Erwin, R., "Information Space Receding Horizon Control," *IEEE Symposium on Adaptive Dynamic Programming And Reinforcement Learning, Paris, France, Apr 11-15*, IEEE, 2011, pp. 302–309.

[135] Sunberg, Z., Chakravorty, S., and Erwin, R., "Information Space Receding Horizon Control for Multi-Agent Systems," *American Control Conference, Montreal, Canada, Jun 27-29*, 2012.

[136] Johnson, S., Lacy, S., and Fitz-Coy, N., "Autonomous Spacecraft Attitude Resource Sharing," *22nd AAS/AIAA Space Flight Mechanics Meeting, Charleston, SC, Jan 30 - Feb 2*, No. 12-124, 2012.

[137] Hero, A., *Foundations and Applications of Sensor Management*, Springer, 2008.

[138] Deza, M. and Deza, E., *Encyclopedia of Distances*, Springer, 2009.

[139] Lancaster, P. and Tismenetsky, M. T., *The Theory of Matrices: with Applications*, Academic Pr, 1985.

[140] Shannon, C., "A Mathematical Theory of Communication," *The Bell System Technical Journal*, Vol. 27, No. 3, 4, July, October 1948, pp. 379–423, 623–656.

[141] Cover, T. and Thomas, J., *Elements of Information Theory*, Wiley-interscience, 2006.

BIOGRAPHICAL SKETCH

Shawn Christopher Johnson was born in DeLand, Florida, in 1983. Growing up near the Space Coast, he gazed up to the sky to view many Space Shuttle launches and developed an excitement for all things space. With the desire to one day become an astronomer, in high school he spent the summer of 2000 at the University of Florida performing research in near-infrared astronomy as part of the Student Science Training Program under the advisement of Dr. Lauren Jones. Realizing that he enjoyed a more hands-on approach to space exploration, he opted to study aerospace engineering at the University of Florida, where he received his B.S. in the fall of 2005, along with minors in biomechanics and business administration. Shawn continued his studies at the Georgia Institute of Technology, where he earned an M.S. in aerospace engineering in the spring of 2008 as a graduate researcher in the Aerospace Systems Design Laboratory under the advisement of Dr. Dimitri Mavris. There he researched advanced design methodologies and systems engineering. Realizing that his passion still remained with space systems, he returned to the University of Florida to enter the doctoral program as a member of the Space Systems Group under the advisement of Dr. Norman G. Fitz-Coy. Along with conducting the research documented in this dissertation, he has had the pleasure of working on the University of Florida CubeSat, SwampSat.

Throughout his tenure in academia, Shawn also had the pleasure of being a teaching assistant at the University of Florida for graduate and undergraduate dynamics and controls. Outside of the classroom and lab, he interned with Regeneration Technologies, Inc. (now, RTI Biologics, Inc.) in the summer and fall of 2005, with the Georgia Tech Research Institute in the summer of 2009, and was a Space Scholar at the Air Force Research Laboratory for the summer of 2011 and 2012. Upon graduation, Shawn will join NASA's Jet Propulsion Laboratory.